GAC-MAC 2026
St. John's May 25-28

FROM SHORE TO CORE

pegnl
professional excellence.
public trust.

SC01: SURFICIAL GEOCHEMISTRY AND INDICATOR MINERAL METHODS IN MINERAL EXPLORATION

EXTENDED ABSTRACTS

Organizers: Sarah Hashmi, Roger Paulen, Jessey Rice,
Alexandre Voinot, and Lyndsay Moore

MAY 24 AND 25, 2026
GAC-MAC 2026, ST. JOHN'S,
NL Sponsored by PEG NL

The extended abstracts of the original version of this Short Course was produced for GAC–MAC 2026 held in St. John's, Newfoundland. This revised and updated version of the extended abstracts is being published by the Geological Survey of Newfoundland and Labrador as a matter of record and is available *via* the Geological Survey of Newfoundland and Labrador at no cost.

NOTE

The purchaser agrees not to provide a digital reproduction or copy of this product to a third party. Derivative products should acknowledge the source of the data.

DISCLAIMER

The Geological Survey, a division of the Department of Energy and Mines (the "authors and publishers"), retains the sole right to the original data and information found in any product produced. The authors and publishers assume no legal liability or responsibility for any alterations, changes or misrepresentations made by third parties with respect to these products or the original data. Furthermore, the Geological Survey assumes no liability with respect to digital reproductions or copies of original products or for derivative products made by third parties. Please consult with the Geological Survey in order to ensure originality and correctness of data and/or products.

Departmental website: https://www.gov.nl.ca/em
Geological Survey website: https://www.gov.nl.ca/em/mines/geoscience
Email: pub@gov.nl.ca

Recommended citation:

Hashmi, S., Paulen, R., Rice, J., Voinot, A. and Moore, L. (Editors)
2026: Surficial Geochemistry and Indicator Mineral Methods in Mineral Exploration. GAC–MAC 2026 Short Course Notes. Government of Newfoundland and Labrador, Department of Energy and Mines, Geological Survey, NFLD/3552, 252 pages.

Contents

Page

Introduction ii

Roger C. Paulen and Martin Ross Glacial dynamics, erosion, and sediment dispersal in the construction of dispersal trains 1

Jessey Rice Digging for data: Recommended till sampling methods for indicator minerals and geochemistry 25

Roger C. Paulen, Riley P.M. Mulligan, Martin Ross and Nick Eyles Field identification of past glacial flow trajectories and ice streams 41

Sarah Hashmi and Alexandre Voinot Incorporating humus sampling surveys in greenfields mineral exploration in glaciated terrain 69

Matthew I. Leybourne, James Kidder, Alexandre Voinot, Daniel Layton-Matthews and Mclean Trott Aqueous geochemistry in mineral exploration 83

Alexandre Voinot and James Kidder Isotopes in drift prospecting: Concepts, case histories, and practical workflows 107

Jonathan Tremblay and Réjean Girard Overview of the latest advances in automated mineralogy using a scanning electron microscope (SEM) 127

Cliff Stanley QA/QC concepts for mineral exploration in glaciated terranes 141

Peter Dimmell Gold grain analysis in tills: Examples from Newfoundland 153

Derek Wilton and Carol Seymour Reverse engineering indicator mineral surveys 177

Roger C. Paulen and Beth M. McClenaghan Glacial dispersal from rare earth element and critical mineral deposits 195

Réjean Girard Exploration geochemistry: From noise to anomaly! 221

Lyndsay Moore The paradox of pyrite 239

Introduction

This release is a compilation of select extended abstracts that were provided as part of the short course entitled “SC01: Surficial Geochemistry and Indicator Mineral Methods in Mineral Exploration”. This short course was held at the Geological Association of Canada–Mineralogical Association of Canada (GAC–MAC) Annual General Meeting in St. John’s, Newfoundland and Labrador, from May 25 to May 28, 2026. This short course was jointly organized by the Geological Survey of Newfoundland and Labrador (GSNL) and the Geological Survey of Canada (GSC) and covered a variety of topics on modern and updated methods in mineral exploration in glaciated terrain. The presentations addressed both conventional and unconventional approaches to surficial geochemistry applied to mineral exploration in glaciated terrain, including advanced indicator mineral methods as well as advanced mineral chemistry. The range of topics covered in this short course included a comprehensive overview of the Quaternary geology and geomorphological characteristics of glaciated terrains and their applications to mineral exploration; the incorporation of soil (till), vegetation (humus) and water into surficial sampling programs; and the use of isotope proxies in surficial sediments to discriminate between different mineralization types. Topics on indicator mineral methods encompassed new developments applied to mineral exploration, processing techniques, applied mineral chemistry, and modern methods in automated mineralogy. Case studies were an important part of the short course, highlighting commodities such as gold (examples from the island of Newfoundland), rare earth element (REE), and critical mineral mineralization (examples from Strange Lake REE deposit and Brazil Lake lithium–cesium–tantalum pegmatites). Support for this short course was provided by GSNL, GSC, Professional Engineers and Geoscientists of Newfoundland and Labrador (PEG NL) and GAC–MAC. Logistical support was provided by course volunteers Katherine Erskine, Nicolas Gomez and Heather Campbell. Joanne Rooney and Chris Pereira are thanked for organizing, editing and assembling the course materials.

Co-organizers: Sarah Hashmi (GSNL); Roger Paulen, Jessey Rice, Alexandre Voinot, and Lyndsay Moore (GSC)

Glacial Dynamics, Erosion, and Sediment Dispersal in the Construction of Dispersal Trains

Roger C. Paulen[1] and Martin Ross[2]
[1]Geological Survey of Canada, 601 Booth Street, Ottawa, ON, K1A 0E8
[2]University of Waterloo, 200 University Avenue West, Waterloo, ON, N2L 3G1

Abstract

Canada is a glaciated landscape, extensively modified by continental-scale glaciations that have deposited glacial sediments and created landforms that may potentially be covering critical mineral resources. Effective and efficient mineral exploration in glaciated terrain requires the identification of the erosional and depositional history of ice sheets that impacted the area. Drift prospecting involves the discovery of dispersal trains by geochemical or heavy mineral surveys and subsequent tracing up-ice to the source of the mineralized bedrock source(s).

Glacial erosion, sediment mixing, transport, and deposition have dispersed metal-rich debris down-ice from mineralized bedrock. These dispersal patterns may be the result of one or more phases of ice flow. Spatially, the dispersal trains are much larger exploration targets than their bedrock sources and can vary in length from a few tens of metres to >100 km. A combination of boulder tracing, till geochemistry, and indicator mineral methods can be used to detect dispersal trains and trace mineralization up-ice to its source.

Determination of former ice-flow directions is undertaken through analysis of a variety of erosional and depositional landforms and features, including streamlined and other directional landforms in drift and bedrock, striations and other small-scale erosional forms on bedrock or boulders, and in situ *measurements of pebbles, boulders, and structural features in till. Exploration success also relies on incorporating local ice-flow observations into regional ice-flow interpretations. Even when clear directional features are identified, the application of ice-flow information to drift prospecting is not always straightforward. Flow directions may change from regional ice flow that is apparently unimpeded by the terrain to topographically controlled (local) flows that exhibit strong changes in ice-flow directions around local topographic features.*

Introduction

Glacial and post-glacial sediments can be a hindrance to mineral exploration as they cover bedrock of interest and introduce additional complexity to the analysis and interpretation of geophysical data. The distribution patterns of minerals of economic interest created by ice sheets, whether they are detected as large, transported boulders, as sand-sized indicator mineral grains, or silt to clay size particles in till matrixes, has long been a successful means to prospect for mineralization buried under glacial cover. The intent of this chapter is to succinctly highlight processes and features of glacial dispersal and the application of this knowledge to mineral exploration in glaciated terrain. This chapter will focus solely on the most commonly used type of glacial sediment for drift prospecting—till—because it is a glacial sediment derived from the direct erosion of bedrock by an actively flowing glacier – *i.e.*, subglacial traction till (Evans, 2018). Glaciation in the last 2 million years has profoundly affected and shaped much of the northern hemisphere's landscape and small isolated areas in the southern hemisphere (Fig. 1). The content herein is, in part, taken from previous summaries such as McClenaghan and Paulen (2018), McClenaghan *et al.* (2023), and short course contributions by Ross (2024), Paulen *et al.* (2024a), the latter two papers were published as part of a volume from a two-day short course "Till Geochemistry and Indicator-mineral Methods for Exploration in Glaciated Terrains" offered at PDAC in 2024 (Paulen and McClenaghan, 2024) and contain considerably more information.

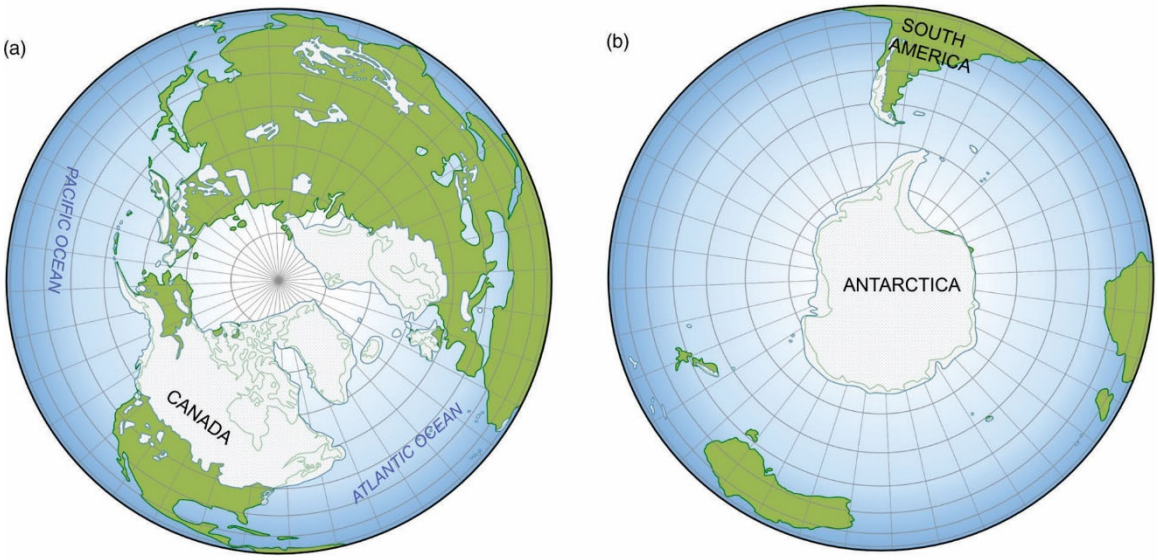


Figure 1. *Global extent of glaciation during the last glacial cycle represented by white polygons: (a) Northern Hemisphere and (b) Southern Hemisphere (modified from Ehlers and Gibbard, 2007).*

Glacial dispersal trains are three-dimensional bodies of till enriched in debris from a specific bedrock source relative to the till surrounding the train. The trains commonly have abrupt lateral edges that mark a sharp boundary between low abundances outside the dispersal train and high abundances within it (McClenaghan and Paulen, 2018). They occur at or below the till surface and are generally displaced some distance down-ice of their source (DiLabio, 1989). Conceptual models of glacial dispersal trains (*e.g.*, Miller, 1984; Stanley, 2009; McClenaghan and Paulen, 2018) typically have a buried (subsurface) up-ice component, a head, and a tail, and can be modified or offset by subsequent ice flow(s) (Fig. 2).

A relatively newly recognized consideration is the impact that ice streams have had on the glacial landscape, and how they affected glacial dispersal patterns. A basic understanding of subglacial processes, glacial dynamics, and glacial process sedimentology is requisite to understand glacial dispersal models. Reconstruction of ice flow history in any prospective region is extremely important because ice-flow indicators provide insights into glacial history and erosional vigor that have impacted glacial landscapes.

Glacial Dynamics – The Basics

Ice sheets like those in Antarctica and Greenland today, or the North American Ice Sheet Complex that covered most of Canada during the last glaciation are large ice masses that deform and flow due to gravity. Specifically, the ‘driving force’ of an ice sheet is controlled by the ice surface slope, the ice sheet thickness, the density of ice, and gravitational acceleration (Benn and Evans, 2010). An ice sheet surface is more elevated, and ice is thicker, in the interior regions than the outer regions of the ice sheet, and ice will thus flow from the higher interior regions to the lower outer regions (Fig. 3). An ice sheet can gain mass *via* snow precipitation, and it can lose mass via ice melting and calving of icebergs (if in contact with a water body). If all of this is balanced, the glacier is in equilibrium. However, if mass gain or loss is greater than the other, then the glacier will either grow in extent and thicken, or thin and shrink. In all cases, the slow transfer of mass from the interior regions to the margins will continue with ice flowing towards the outer ice sheet margins even when those margins are receding due to a negative mass balance. Some parts of an ice sheet may become stagnant, but generally, ice tends to keep flowing. The ice surface topography can shift due to changes in atmospheric circulation and precipitation, and to its internal

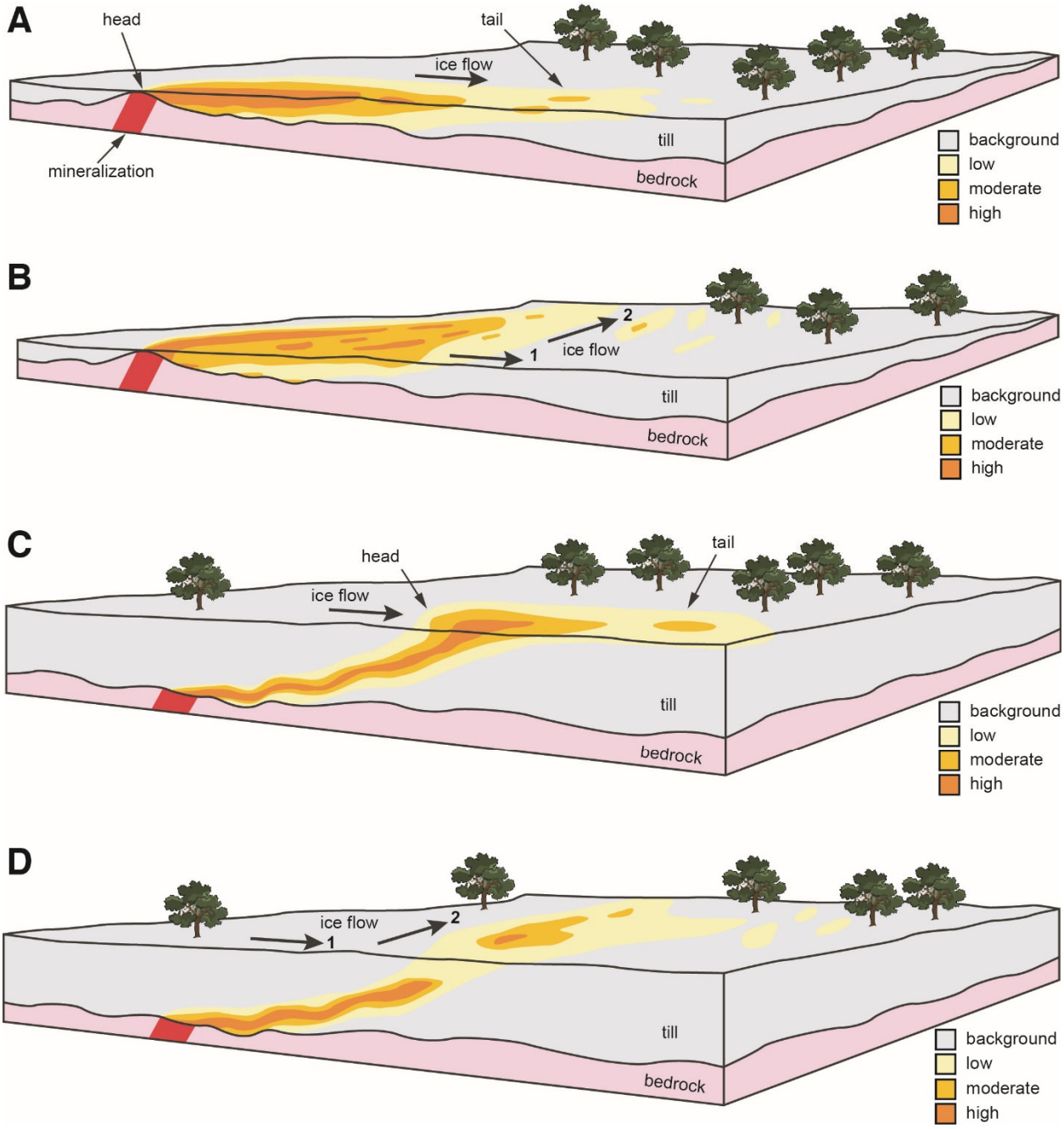


Figure 2. *Conceptual models for dispersal trains: A) Thin till cover whereby mineralized bedrock is dispersed by a single phase of ice flow, creating a dispersal train that is exposed at the surface for its entire length and trends down ice in one direction; B) Thin till cover whereby mineralized bedrock is dispersed by two phases of ice flow, creating a palimpsest dispersal train exposed at the surface and trending down ice in two directions; C) Thick till cover whereby mineralized bedrock is dispersed by a single phase of ice flow, creating a dispersal train that is buried proximal to source and exposed at the surface farther down ice, and trends down ice in one direction; D) Thick till cover whereby mineralized bedrock is dispersed by two phases of ice flow, creating a palimpsest dispersal train trending down ice in two directions. The train is buried proximal to its source and exposed at the surface further down ice. The original dispersal train created by the older ice flow '1' shown in A or C is diluted and offset by the second ice flow '2' in B and D; (modified from McClenaghan and Paulen, 2018).*

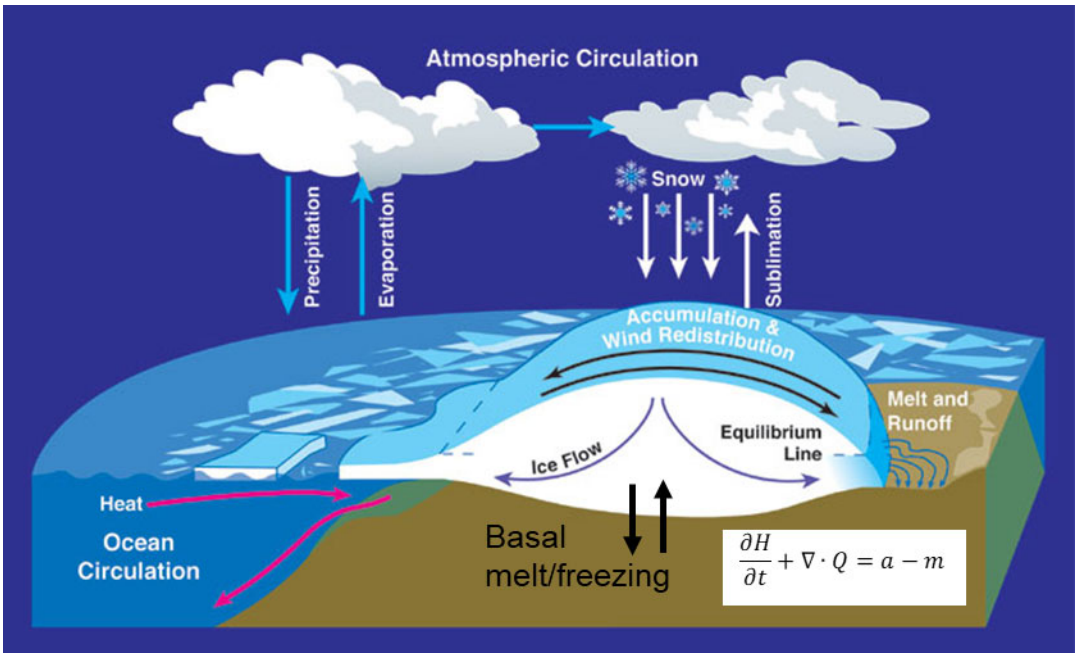


Figure 3. *Conceptual model of an ice sheet and its mass balance. H (x,y,z) is ice thickness (H>0), t is time, the flux Q is a horizontal ice flow vector, a is accumulation/ablation and m is basal melting/freezing (Hindmarsh, 2018). Modified from commons.wikimedia.org.*

dynamics. One consequence of this is a shift in the position of ice divides and orientation of regional ice flow lines (McMartin and Henderson, 2004; Rice *et al.*, 2019). Ice flow can also shift during ice thinning because the ice surface slope will increasingly adjust to the subglacial topography. It is for all these reasons that one prospective area may have experienced different ice flow directions over one or more glaciations. Tracing minerals back to their source in this context can be challenging because the minerals may have been transported by two or more ice flow phases (Parent *et al.*, 1996; Paulen *et al.*, 2013; McClenaghan and Paulen, 2018; Parent, 2023). It is thus critical to develop a good knowledge of the regional and local glacial history.

Glacial geologists are particularly interested in what is happening at the base of an ice sheet or, more specifically, at the ice-bed interface where subglacial erosion, sediment transport, and deposition take place. If the interface is below the pressure-melting point, the conditions are said to be 'cold-based', in which case basal ice flow velocity will be approaching zero (Fig. 4a). However, the ice above may still flow due to the driving stress. In contrast, if the ice-bed interface is at the PMP, a condition referred to as 'warm-based', then two things can happen: 1) ice at the base will slip on a thin water film or 2) sediments below the interface will undergo deformation (Fig. 4b). Both processes contribute to the forward motion of the ice above. Ice slip, or basal sliding typically occurs on a hard bed, such as the bedrock surface, but it can also happen locally over soft

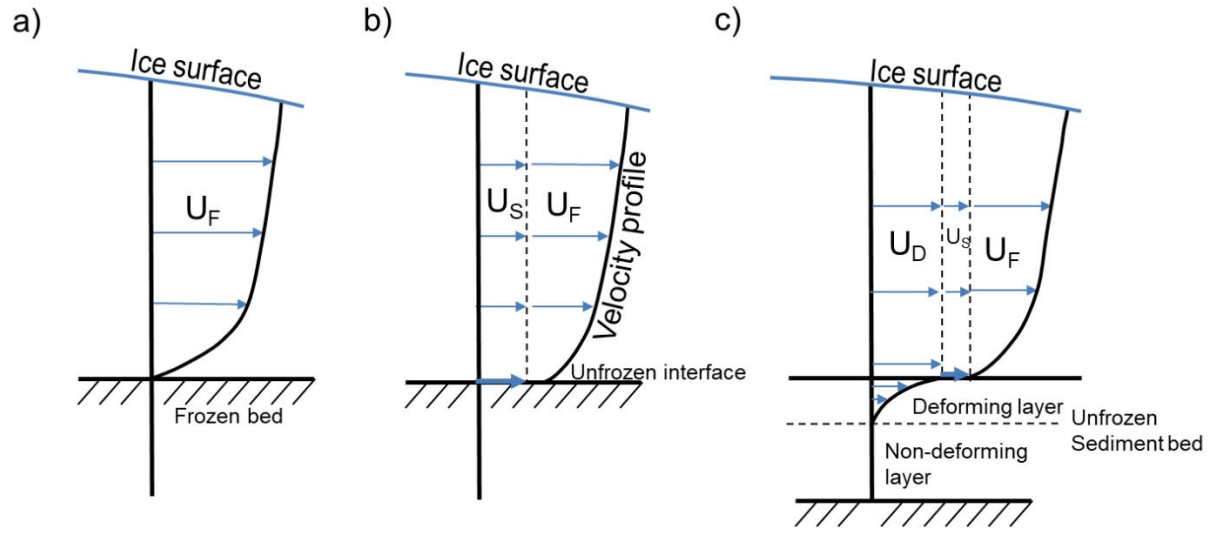


Figure 4. *Conceptual ice flow profiles for: a) internal ice flow (UF) only due to a frozen interface (cold-based ice); b) internal ice flow and basal sliding (US); c) UF, US, and subglacial deformation (UD). Modified from Boulton (1996).*

bed due to ice-bed decoupling under very low effective stress (*i.e.*, subglacial water pressures are sufficiently high to locally 'lift' the glacier from its bed). Subglacial sediment deformation will happen when the shear stress from the moving ice above exceeds the yield strength of the underlying sediment (Fig. 4c; Benn and Evans, 2010). This is more likely to happen with low-permeability mud-rich till or similar sediment and relatively low effective pressure (but not low enough for ice-bed decoupling to occur). The latter is a very important process that explains why fast flowing corridors of ice (referred to as ice streams) exist in the West Antarctic Ice Sheet despite having low driving stresses (Alley *et al.*, 1987). There is compelling evidence across the Canadian glacial landscape indicating that ice streams exerted considerable influence on LIS dynamics and subglacial sediment transport, on both hard and soft beds (Margold *et al.*, 2015, and references therein; Paulen *et al.*, 2024b).

The processes briefly described above allow for either A) the preservation under sustained cold-based ice of relict landscapes and sediments in certain glaciated regions or B) subglacial erosion, transport, and deposition of glacial sediments under warm-based conditions. Subglacial conditions also vary spatially and temporally. For example, one area may have been cold-based for some time, followed by warm-based conditions, or *vice versa*. In Canada, this created overprinting or a patchy landscape of disjointed glacial bed pieces that were formed and preserved at different times under different glacial regimes (Ross *et al.*, 2009; Trommelen *et al.*, 2012). As a result, some dispersal trains may be truncated or have complex shapes.

Glacial Erosion, Transport, and Deposition

In mineral exploration, one of the key questions when indicator minerals are found in till is: "How far up-ice did they come from?". Case studies using known sources and ice flow history provide useful information (*e.g.*, McClenaghan *et al.*, 2022), but it remains challenging when working in a new area where the mineral source(s) has yet to be found. The two main processes of bedrock erosion by sliding ice are 1) abrasion and 2) quarrying. Subglacial abrasion results from the sliding of debris-rich basal ice onto a hard bed, typically the bedrock surface. Abrasion rates are controlled by the relative hardness of the clasts protruding from the ice sole and that of bedrock, the force pressing the clasts against the hard bed (friction models), the velocity of the sliding clasts, and the debris concentration at the ice-bed interface (Iverson and Semmens, 1995; Rea, 2013). Abrasion tends to produce relatively fine-grained material (*e.g.*, sand and silt). Striations and grooves on polished bedrock surfaces are the product of abrasion (Rea, 2013).

Quarrying is initiated by the failure of jointed or fractured bedrock due to large stress gradients and fluctuating water pressures near down-ice, or lee-side bedrock steps under actively flowing ice (Hallet, 1996; Iverson, 1991, 2012; Iverson and Semmens, 1995). Subglacial cavities play a key role as they tend to form down-ice of these steps and will be part of a subglacial linked-cavity drainage system that controls the water pressure. Rock fragments of various sizes may be produced in this way and entrained by ice and incorporated into till. Most large particles from pebbles to glacial erratics (boulders and cobbles) are the product of quarrying. These particles can be further crushed and shaped by frictional processes during transport, which means that a certain proportion of the till matrix originated from larger particles produced by quarrying. Finally, a portion of the till may be derived from the erosion and entrainment of pre-existing unconsolidated sediment of potentially various origins. The origin of till particles is summarized in Fig. 5.

Particles of various sizes can be incorporated into basal ice *via* basal freeze-on and a process called 'regelation intrusion'. For the latter, ice pressing down onto sediments may temporarily melt and penetrate the sediment array and refreeze or 'regelate' in lower pressure spots (Iverson and Semmens, 1995). The sediment then becomes entrapped into basal ice and will move with it. There is a certain limit as to how thick the debris-rich basal ice layer can become through this process, but debris can also move further up into the ice *via* vertical mixing processes (*e.g.*, ice folding or

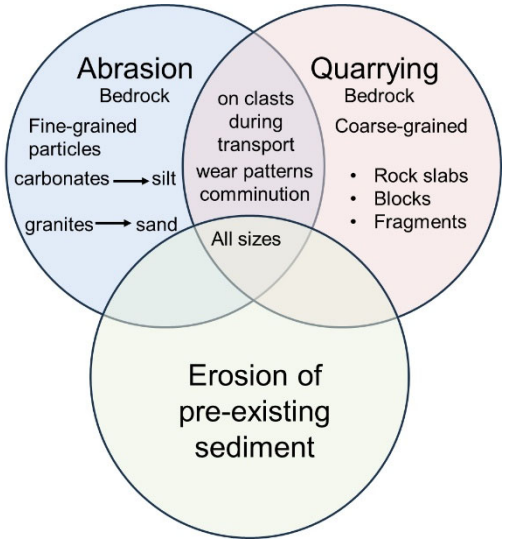


Figure 5. *Origin of sediment particles in subglacial traction till (from Ross, 2024).*

shearing) or may be released at the ice-bed interface due to basal melting (Evans, 2018). All these processes, along with ice flow velocity, control the horizontal englacial sediment flux (Hildes *et al.*, 2004; Melanson *et al.*, 2012; Evans, 2018). The debris in basal ice may be plastered onto a hard bed by pressure-melting and other mechanical, frictional processes (Benn and Evans, 2010; Evans, 2018). This process is referred to as 'lodgement'. Till emplacement and accretion is a time-transgressive process that reflects the glacial dynamics of the ice sheet that formed it, including deformation within the till itself (Evans, 2018; Menzies *et al.*, 2019).

As mentioned above, subglacial sediments at or near the ice-bed interface may also undergo deformation under certain conditions. Sediment can thus be transported in this way through rotation and other forms of particle movement. Till is deposited when deformation ceases, which occurs when the sediment strength exceeds shear stress. Due to the complexity of these processes and the multiple cycles and overprinting, subglacial till is best described as a 'subglacial traction till' (Evans *et al.*, 2006; Benn and Evans, 2010; Evans, 2018). The term subglacial traction till supersedes the familiar and older terms 'lodgement till' and 'basal till'. Subglacial traction till may occur at any depth within an unconsolidated sediment succession. It is over-consolidated, dense, matrix-supported, massive to faintly layered or jointed, and may display moderate to strong subhorizontal fissility (*e.g.*, McClenaghan *et al.*, 2023). Joint planes and fissility are generally products of sediment loading by the glacier itself and multiple generations of deformation by localized shear strain from glacier flow. Subglacial tills contain striated, faceted and bullet-shaped clasts that are typically subangular to subrounded and they can exhibit boulder pavements related to lodgement or deformation processes (Boulton, 1982; Benn and Evans, 1996; McMartin and Paulen, 2009; Paulen and McClenaghan, 2015).

Other till deposits types include meltout till, which is deposited at the base and margin of an inactive or stagnating glacier by melt-out processes. The term meltout till, or basal meltout till, supersedes the familiar, older terms 'ablation till' and 'stagnant ice moraine'. It tends to be less

consolidated than subglacial traction till, and frequently contains stratified sediment bodies, layers, or lenses related to subglacial meltwater flow, sediment dewatering, melting of buried ice or fluid injection structures (Shaw, 1982, 1983; Munro-Stasiuk, 2000; Evans *et al.*, 2006; Evans 2018).

Comminution tills are those in which the till matrix is comprised largely of crushed and pulverized bedrock that has been abraded by overriding ice (Elson, 1989; Croot and Sims, 1996). In areas of poorly consolidated sedimentary bedrock comminution of shale into aggregate pieces of various particle sizes can constitute a majority of the till matrix and clast content (*e.g.*, Paulen, 2009). Crushed and pulverized bedrock can also result from the shearing and detachment of intact blocks, which are then progressively broken down at the ice–bed interface (Hiemstra *et al.*, 2007; Bukhari *et al.*, 2021). Sheared blocks of coherent bedrock and of sediments (including till) can be incorporated into the bed of a glacier and deposited as intact blocks, stacked sequences (Paulen, 2009; Bukhari *et al.*, 2021) or as deformed or brittle sheared units. Examples of massive coherent rafted bedrock blocks range up to 100 m thickness and up to 1000 km^2 in area (*e.g.*, Stalker, 1976; Aber *et al.*, 1989; Evans *et al.*, 2021), including rafted kimberlite in the Fort à la Corne kimberlite field in central Canada (Scott-Smith *et al.*, 1996).

Other historical till subcategories and classifications include those altered by postglacial or post-depositional processes such as flow tills and supraglacial ablation tills (*e.g.*, Lawson, 1989; Hicock, 1990; Evans, 2018). These units are more correctly identified as diamictons, rather than till. Note that glacial geologists and sedimentologists use the term ‘diamicton’ to describe unconsolidated, unsorted to poorly sorted terrigenous sediment that contains a broad range of particle sizes from clay to boulders without inferring to any specific origin or depositional environment (*e.g.*, lahar sediments, debris flows, *etc.*).

Glacial Dispersal Trains

Glacial dispersal trains are the net result of glacial erosion of specific bedrock sources, transport, comminution (*i.e.,* reduction of materials to minute particles), and subglacial deposition, all of which can be complicated by multiple cycles of till re-entrainment and deposition, as subglacial dynamics fluctuate throughout glacial cycles (Paulen *et al.*, 2024c). McClenaghan and Paulen (2018) described the morphology of dispersal trains as being influenced by a number of

factors that can be grouped into four broad categories: (1) the bedrock source (composition, morphology, hardness, depth of preglacial weathering, contrast with host lithologies, topographic position, protection from glacial erosion); (2) glaciological parameters (basal ice temperature, availability of water which relates to erosion potential of the glacier, ice velocity, ice-flow trajectories); (3) transport and depositional environment (subglacially, supraglacial transport, meltout processes, *etc.*); and (4) post-depositional changes (*e.g.*, metal remobilization by hydromorphic processes, mineral weathering, downslope movement, *etc.*).

In the simplest examples, the glacial dispersal pattern is unidirectional and straightforward to interpret (*e.g.*, McClenaghan *et al.*, 2002; Batterson and Taylor, 2009; Fig. 6). However, more often there are several complicating factors that need to be considered. For instance, dispersal trains may have widely variable lengths and shapes, resulting in fan-shaped or irregular-shaped patterns, often with offset lobes re-entrained from earlier dispersal trains, a phenomena known as palimpsest dispersal (*e.g.*, Parent *et al.*, 1996; Stea and Fink, 2001; Fig. 7). Trains from multiple bedrock sources may overlap making it challenging to locate specific bedrock source areas (McClenaghan *et al.*, 2015; Plouffe *et al.*, 2016). Sometimes, the surficial expression of the dispersal pattern is completely detached from its source, whereas certain known bedrock sources lack a dispersal train altogether (*i.e.*, skip zone). Therefore, understanding the processes relating to subglacial erosion, comminution, transport, and deposition of till provide critical information for designing and interpreting till sampling surveys that support mineral exploration.

To better understand how a dispersal train is formed, the transport capacity of dispersal trains and first-order patterns of glacial erosion and deposition for a nonsteady-state ice sheet throughout the glacial cycle must be considered. In areas affected by warm-based glaciation, streamlined landform density (Hättestrand *et al.*, 1999; Rice *et al.*, 2020), elongation ratio (Hart and Smith, 1997), inheritance of terrestrial cosmogenic nuclide ratios (Fabel *et al.*, 2002; Gosse *et al.*, 2006; Margreth *et al.*, 2016), and streamlined landform characteristics (Bradwell *et al.*, 2008; Sookhan *et al.*, 2022; Eyles *et al.*, 2023) have been used to determine relative erosional vigour. The intensity of glacial erosion is an important consideration for mineral exploration as regions subjected to a higher degree of erosion can be expected to produce longer dispersal trains where the till was

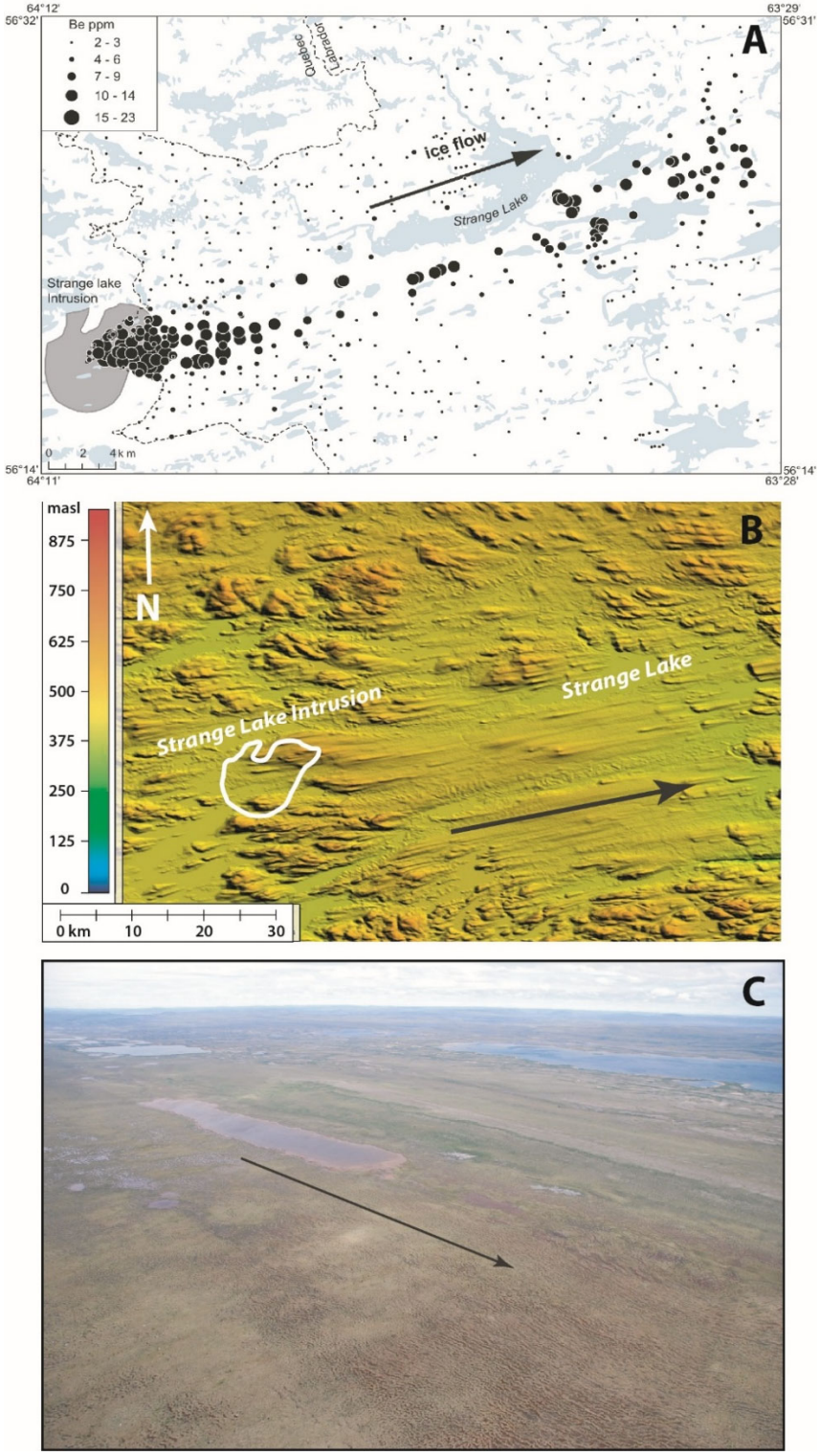


Figure 6. *The Strange Lake till dispersal train in eastern Canada: A) Ribbon-shaped glacial dispersal train of beryllium (Be) in the <0.063 mm fraction of till trending northeast from the Strange Lake rare earth element deposit. The dispersal train was formed by a single phase of ice flow towards the northeast (modified from Batterson and Taylor, 2009); B) Shuttle Radar Topographic Mission (SRTM) DEM image of the Strange Lake deposit (outlined in white) highlighting the mega-scale glacial lineations from the Kogaluk River ice stream (IS#187 of Margold* et al.*, 2015) that eroded the deposit from left to right (black arrow) and created the elongated ribbon dispersal train; C) Oblique aerial photo of the MSGLs that occur in the Strange Lake area, with landforms showing large length to width ratios, indicative of fast-flowing ice.*

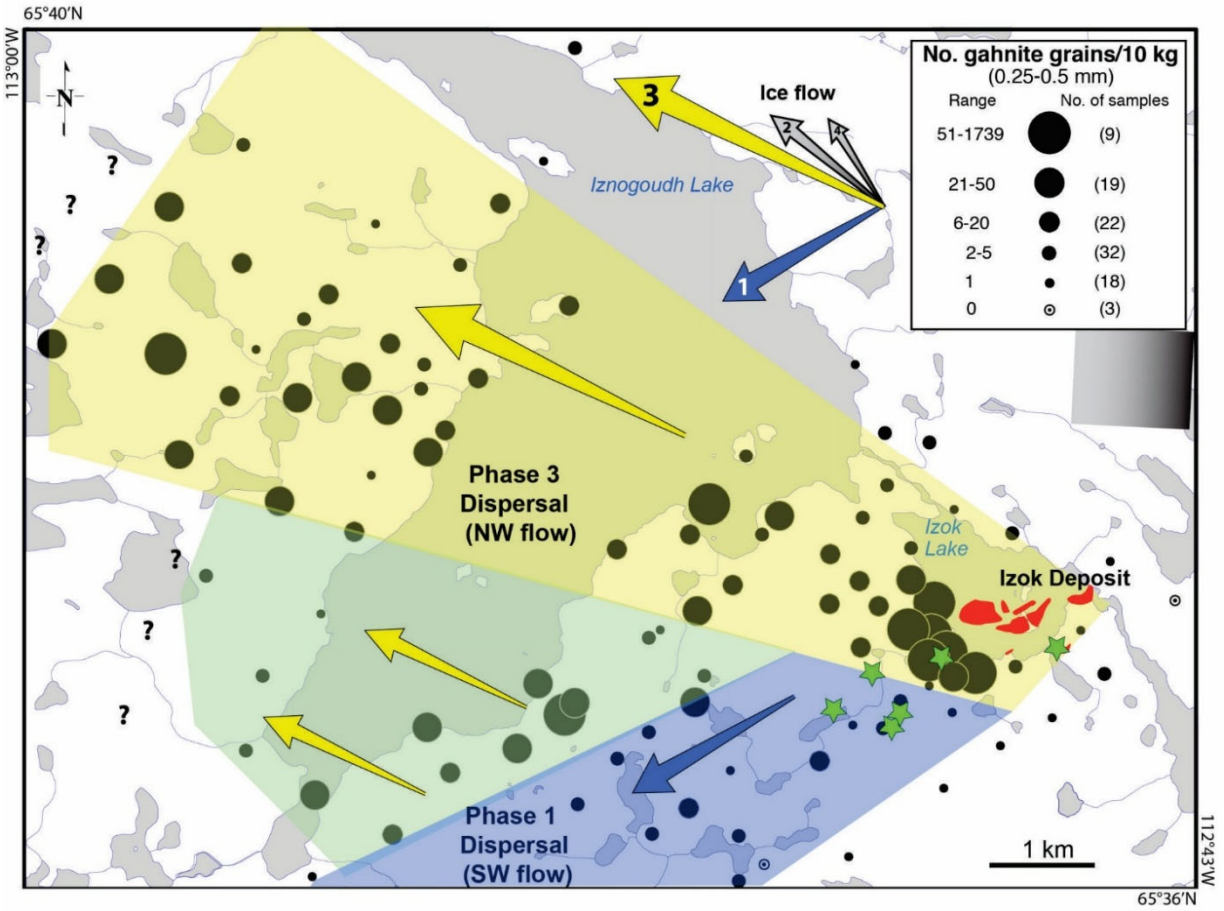


Figure 7. *Fan-shaped glacial dispersal train of gahnite abundance (in the 0.25–0.5 mm heavy mineral fraction of till normalized to a 10-kg sample mass) down ice of the Izok Lake volcanogenic massive sulphide deposit in northern Canada. The fan-shaped dispersal train was formed by two dominant phases of ice flow towards the southwest (blue polygon) and subsequent reworking by a younger ice flow towards the northwest (yellow polygon). The green polygon indicates the part of the train modified by multiple phases of ice flow (modified from McClenaghan* et al.*, 2015).*

deposited as a thin veneer (<2 m). However, in regions affected by high-intensity erosion and covered by thick till (>5 m), dispersal trains will be diluted within a short dispersal distance down ice. Palimpsest dispersal trains are uncommon in areas that were affected by higher erosion regimes. On the other hand, regions subjected to a low intensity of erosion, such as those occurring under ice divides, preserved older weathered bedrock, relict preglacial and glacial landforms, and palimpsest dispersal trains (Rice *et al.*, 2024).

Till deposits, and, in particular, glacial dispersal trains, can also be a proxy for the evolution of erosion intensity. Clasts derived from known bedrock sources within till can delimit transport distances (*e.g.*, Dreimanis and Vagners, 1971; Dredge, 1988; Kjær *et al.*, 2003; Plouffe *et al.*, 2011; Trommelen *et al.*, 2013). The magnitude of clast, mineral, or elemental dispersal signals depends on the net erosion intensity up-ice at the source, compounded with other factors such as bedrock

lithology, inherent bedrock structure (*e.g.*, bedding, jointing, and fractures), duration of glacial transport in one or more directions relative to the source area, inheritance of debris from older deposits, subsequent burial of the source, and dilution of metal-rich debris through overprinting and entrainment (Aario and Peuraniemi, 1992; Parent *et al.*, 1995; Stea and Finck, 2001; Evans *et al.*, 2006; Evans, 2018; McClenaghan *et al.*, 2018; Rice *et al.*, 2024).

Adjacent to an ice-divide, subglacial erosion intensity was probably highly variable, owing to additional factors such as initial ice buildup, ice-divide migration, and changes in mass balance with advance and retreat cycles (Kleman *et al.*, 2008; Rice *et al.*, 2024). Although, these factors are difficult to assess, erosional intensity can be estimated by interpreting the extent and thickness of till deposits, lake density, and whether subglacial landform flowsets are fragmented, rare, absent, or heavily overprinted (Rice *et al.*, 2023). The formation and distribution of large erosional landforms underneath former ice sheets are primarily governed by the subglacial thermal conditions. Glacial erosion occurs when ice sheets of a given thickness and ice flow rate reach the pressure melting point (warm-based), typically as ice flow accelerates towards the ice margins. These warm-based zones provided material for deposition for a polythermal ice sheet under steady-state conditions. There is potential for long-distance transport of subglacial debris during ice expansion and deglacial phases, but such material would have to be transported at higher velocities to remain in the migrating entrainment and transport zones of an ice sheet (Kleman *et al.*, 2008), particularly overlying soft sediment beds (Spagnolo *et al.*, 2016). The combination of a relatively short duration of an ice sheet contraction phase and inward migration of erosion zones would inhibit long-distance transport during deglaciation, except for ice-stream corridors.

Subglacial Comminution and Dispersal Models

Till is the end-product of glacial erosion, transport, comminution, and deposition and consists of two particle size modes: i) rock fragments or clasts and ii) matrix that is dominated by mineral fragments (Dreimanis and Vagners, 1971). It is important to note that dispersal patterns identified through the mapping abundance of boulders, indicator minerals, and concentrations of geochemical pathfinder elements in the till matrix may differ from one another, sometimes substantially, from one another over the same area (*cf.* McClenaghan and Paulen, 2018). Minerals in the till matrix are crushed and abraded to their terminal grain size mode which is determined

largely by the mineral's original grain size in the bedrock source, hardness, cleavage, and the cementation or metamorphic history of the mineral in its bedrock source (Shilts, 1995). In till, quartz, magnetite, feldspars, pyroxenes, and other minerals commonly dominate the sand-size fraction, carbonates and sulphides dominate the silt-size fraction, and phyllosilicates and hematite dominate the clay-sized fraction. Thus, the bulk chemical compositions of different-size fractions of till reflect the dominant minerals in each size fraction. An example from central Canada (Fig. 8) shows that concentrations of nickel vary with grain size as a result of Ni-rich serpentine that is readily abraded and crushed to clay-sized particles during subglacial transport. The result is a high signal to noise ratio in the clay-sized fraction (Shilts, 1993; Mäkinen, 1995).

Under steady state glacial flow, the concentration of dispersed debris from a particular source within a till will decrease with increasing distance down ice such that a plot of abundance *versus* distance down ice approximates a negative exponential curve (Shilts, 1976; Klassen, 1997). The transport distances of the majority of dispersal trains are relatively short (<5 km) with widely varying detectable dispersal distances down ice between boulders, sand-sized indicator minerals, or elements in the till matrix (geochemistry), sometimes up to an order of magnitude. Glacial

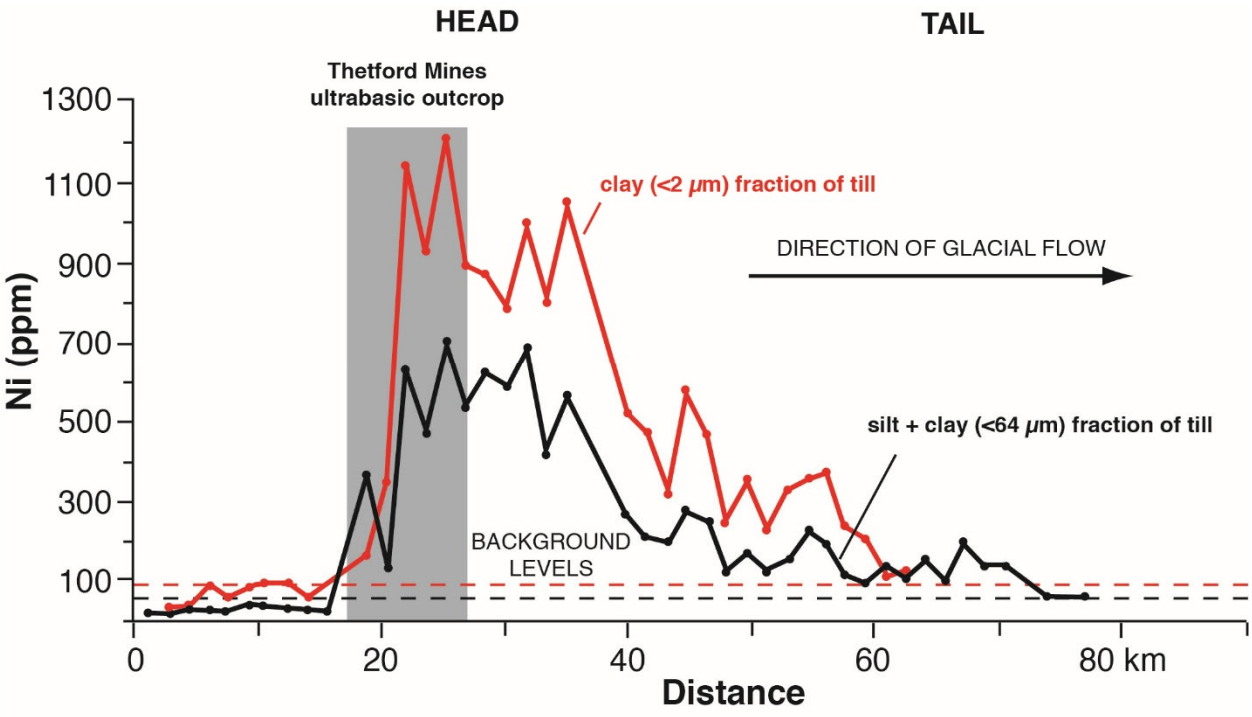


Figure 8. *Dispersal curve showing the relationship between the source, head and tail of a dispersal train, and the nature of the element abundances down ice from the source (grey shaded area) relative to size fraction analyzed. In this case nickel abundance in the silt + clay and clay-sized fractions (ppm)* versus *distance down ice in surface till in the Thelford Mines area, central Canada (modified from Shilts, 1993).*

dispersal from the Izok Lake base metal deposit in northern Canada is such an example – with sand-sized mineral gahnite dispersed more than 40 km down ice compared to silt to clay-sized geochemistry detectable only a few km down ice (McClenaghan *et al.*, 2015). Within an ice stream, the concentration gradient of dispersed debris decreases more linearly down ice and not exponentially, as the result of rapid ice flow transporting debris far from its source with little dilution (Paulen *et al.*, 2017).

Deforming conditions within till are prevalent and fluctuate in intensity throughout its deposition. As the subglacial bed deforms, mobile sediment moves as a function of the applied stress, porewater pressures, and the grain-size composition of the sediment resulting in mobilization of the sediment as a deformation 'front' (Menzies *et al.*, 2019, and references therein). A subglacial deformation time-transgressive process occurs at the interface between mobile and immobile sediment within the basal sediment package (red strike/slip symbols; Fig. 9). As a result, a dynamic balance develops between the mobilizing effect of the applied shear stress and the stabilizing effect of the normal stress. This mobilization/immobilization process happens in three dimensions and over time, separating mobile, actively moving sediment from inactive, immobile sediment. The conditions that affect where the mobile/immobile front therefore have important implications on till transportation and, ultimately, till dispersal patterns (Paulen *et al.*, 2025).

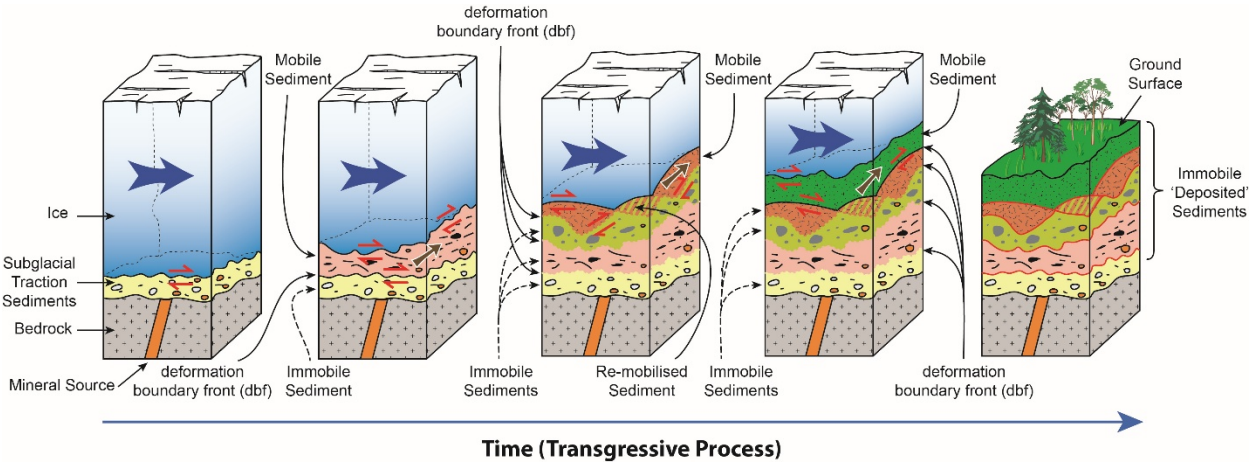


Figure 9. *Model of subglacial soft sediment deformation as a time-transgressive sequence from initial erosion and till creation, till deposition, and to final till accretion (red strike slip symbols represent the mobile/immobile sediment boundaries). After erosion of the bedrock surface and mineral source (orange polygon) by a mobile bed, a thin subglacial traction till (yellow unit) is initially deposited as an immobile bed, and effectively cuts off the mineralized source of a dispersal train from any additional erosion. Subsequently, a mobilized soft sediment subglacial layer (pink unit) flowed over the already immobilized (deposited/emplaced) till, remobilizing a small part of the metal-rich till (containing the small orange clasts, represented by small black arrows), and over time, repeats this sequence of mobilized till units that accrete as immobilized (deposited/emplaced) till, with a still active mobile till (green unit) close to the ice bed interface (modified from Menzies* et al.*, 2019).*

As the ‘deformation boundary front’ moves within the subglacial sediments, some areas of till will become remobilized under increasing stress; elsewhere, with a reduction in stress, till will be immobilized and begins to accrete. Where increasing stress occurs, tills generally become increasingly mobile, with all other factors being consistent. In contrast, reduction in stress likely results in decreasing till mobility and eventual emplacement/deposition. As till accretion occurs and the ’deformation boundary front’ migrates upward within a till sequence, re-entrainment of metal-rich till with down-ice traction and secondary accretion occurs, as a continuous time-transgressive process, and is a plausible explanation for mineral dispersal models (Miller, 1984; Stanley, 2009; McClenaghan and Paulen, 2018).

Given this understanding of subglacial deformation, entrainment, transport, and deposition, the dispersal model from existing literature that appears to be a ‘best-fit’ with observed glacial dispersal trains and glacial micromorphology is the aggradational-constant entrainment decay model (Stanley, 2009). This model shows englacial debris in ice and subglacial material (deformable bed) at the base of the glacier represented as distinct ‘cells’. Each cell contains a specific geochemical, mineralogical, or lithological composition that is portrayed as a percentage of contained metal-rich debris and is consistent with overall ice-flow mechanisms. These cells form the basal part of the glacier, including the deforming or mobile bed, deposited as a series of layers that are accreted continuously on top of each other. Each layer is composed of cells that are adjacent to each other, and material is entrained into these cells from bedrock by regelation, glacial creep, internal thrusting, or abrasion, or from subjacent cells by internal shearing (deformation) processes, and then transported upwards into overlying layers by down-ice accretion. Thus, the resultant dispersal train is formed down ice and upward through the till deposit. This migration and mixing of metal-rich and metal-poor material causes the metal-rich debris to be diluted in the till profile as down-ice dispersal continues. As a result, material originally eroded from the mineralized bedrock source is effectively dispersed by down-ice movement such that, when subsequently deposited beneath a glacier, it produces a dispersal train within the till layers (Fig. 10). Although this aggradational-constant entrainment decay model is presented in two-dimensions, it is geometrically consistent with the descriptive 3-D model described by Miller (1984), and 3-D dispersal trains that have been described in other applied till studies (*e.g.*, Kauranne, 1967; Nurmi, 1976; Ferbey and Levson, 2009; Averill, 2013, 2017; McClenaghan *et al.*, 2018; Kelley *et al.*, 2019).

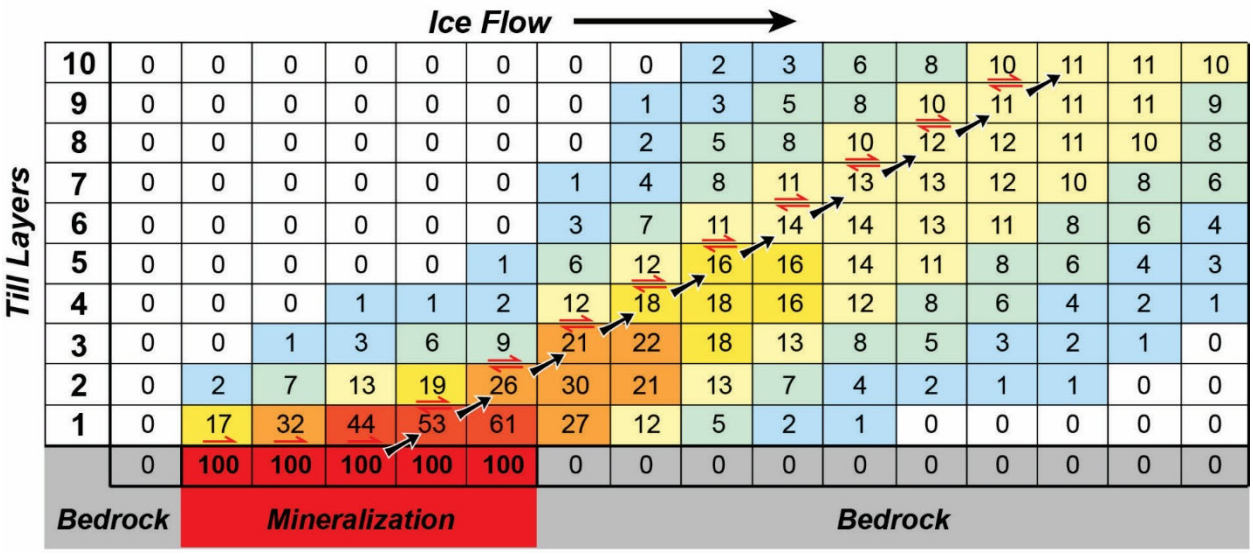


Figure 10. *Concentration (as a percentage) of metal-rich debris in till to illustrate the aggradational-constant entrainment decay model down ice from mineralized bedrock (red polygon). Mineralized bedrock is initially eroded, transported, and accreted down ice as a series of till layers. The size (length and width) of the dispersal train increases down ice, and the concentrations of metal-rich material decrease by dilution down ice. The theoretical mobile/immobile sediment boundaries and their upward propagation are shown using the same symbology as in Fig. 9 (modified from Stanley, 2009).*

Summary

Tracing indicator minerals and geochemical pathfinders from till samples back to their bedrock source is a type of inverse problem whereby the exploration geologist is trying to determine the location and prospectivity of the source rocks given the composition of glacial sediments and the overall glacial history of the area. For glacial sediment provenance, it involves mapping dispersal patterns and using their shape and ice flow information to vector towards a source area of potential interest. In some cases, it is successfully achieved using relatively limited information about the glacial geology. However, the approach is often challenging due to a variety of problems. Dispersal trains may have complex shapes, some are detached from their source, others are elusive due to being partly buried, truncated, or overprinted by other overlapping dispersal trains. Some sources also lack a dispersal train even though the area was glaciated. All those situations require more advanced understanding of glacial dynamics and glacial sediment transport, of the effect of bedrock topography, and of glacial landform formation to reduce exploration risk and increase likelihood of success. Mineral exploration is increasingly multidisciplinary, and teams trained in advanced glacial geology and glaciology, mineralogy, geochemistry, geophysics, GIS, statistics and machine learning, as well as numerical modeling can help achieve success in more challenging settings. This is the new, exciting, and promising reality of mineral exploration in glaciated terrain.

Acknowledgments

Contributions to this short course volume were made possible under the Geological Survey of Canada's (GSC) Critical Minerals Geoscience and Data Program under the 'Ice stream paradigm and search for critical minerals in Canada: exploiting the power of automated geospatial mapping techniques' research activity (2023-2027).

This short paper acknowledges the years of scientific interactions and partnerships with Canadian scientists whose footsteps we now follow. In particular, we would like to thank Beth McClenaghan (GSC Ottawa, emeritus), Ron DiLabio (GSC Ottawa, retired), Michel Parent (GSC Québec, retired) and Rod Smith (GSC Calgary) for many fruitful discussions.

References

Aario, R. and Peuraniemi, V., 1992: Glacial dispersal of till constituents in morainic landforms of different types. Geomorphology, Volume 6, pages 9–25. https://doi.org/10.1016/0169-555X(92)90044-O

Aber, J.S., Croot, D.G. and Fenton, M.M., 1989: Glaciotectonic Landforms and Structures. Kluwer, Dordrecht, Netherlands.

Alley, R.B., Blankenship, D.D., Bentley, C.R. and Rooney, S.T., 1987: Till beneath ice stream B. 3. Till deformation: evidence and implications. Journal of Geophysical Research, Volume 92, pages 8921–8929. https://doi.org/10.1029/JB092iB09p08921

Averill, S.A., 2013: Discovery and delineation of the Rainy River gold deposit using glacially dispersed gold grains sampled by deep overburden drilling: A 20 year odyssey. *In* New Frontiers for Exploration in Glaciated Terrain. *Edited by* R.C. Paulen and M.B. McClenaghan. Geological Survey of Canada, Open File 7374, pages 37–46. https://doi.org/10.4095/292686

Averill, A.A., 2017: The Blackwater gold-spessartine-pyrolusite glacial dispersal train, British Columbia, Canada: Influence of sampling depth on indicator mineralogy and geochemistry. Geochemistry: Exploration, Environment, Analysis, Volume 7, pages 43–60. https://doi.org/10.1144/geochem2015-399

Batterson, M.J. and Taylor, D.M., 2009: Geochemical re-analysis of till samples from the Strange Lake area, Labrador (NTS map sheets 14D/5 and 24A/8). Government of Newfoundland and Labrador, Department of Natural Resources, Geological Survey, Open File LAB/1479. https://www.gov.nl.ca/iet/mines/geoscience/reports-maps/docs/oflab1479/

Benn, D.I. and Evans, D.J.A., 1996: The interpretation and classification of subglacially-deformed materials. Quaternary Science Reviews, Volume 15, pages 23–52, https://doi.org/10.1016/0277-3791(95)00082-8

Benn, D.I. and Evans, D.J.A., 2010: Glaciers and Glaciation. Second Edition, Routledge, New York, 802 pages. https://doi.org/10.4324/9780203785010

Boulton, G.S., 1982: Subglacial processes and the development of glacial bedforms. *In* Research in Glacial, Glacio-Fluvial and Glacio-Lacustrine Systems. Edited by R. Davidson-Arnott, W. Nickling and B.D. Fahey. Geo Books, Norwich, pages 1–31.

Boulton, G.S., 1996: Theory of glacial erosion, transport and deposition as a consequence of subglacial sediment deformation. Journal of Glaciology, Volume 42, pages 43–62. https://doi.org/10.3189/S0022143000030525

Bradwell, T., Stoker, M. and Krabbendam, M., 2008: Megagrooves and streamlined bedrock in NW Scotland: the role of ice streams in landscape evolution. Geomorphology, Volume 97, pages 135–156. https://doi.org/10.1016/j.geomorph.2007.02.040

Bukhari, S., Eyles, N., Sookhan, S., Mulligan, R., Paulen, R., Krabben-dam, M. and Putkinen, N., 2021: Regional subglacial quarrying and abrasion below hard-bedded palaeo-ice streams crossing the Shield–Palaeozoic

boundary of central Canada: the importance of substrate control. Boreas, Volume 50, pages 781–805. https://doi.org/10.1111/bor.12522

Croot, D.G. and Sims, P.C. 1996: Early stages of till genesis: An example from Fanore, County Clare, Ireland. Boreas, Volume 25, pages 37–46. https://doi.org/10.1111/j. 1502-3885.1996.tb00833.x

DiLabio, R.N.W., 1989: Chapter 10 – Terrain geochemistry in Canada. *In* Quaternary Geology of Canada and Greenland. *Edited by* R.J. Fulton. Geological Survey of Canada, Geology of Canada, No. 1 (also Geological Society of America, The Geology of North America, Volume K1), pages 645–663. https://doi.org/10.4095/131660

Dredge, L.A., 1988: Drift carbonate on the Canadian Shield. II: carbonate dispersal and ice flow patterns in northern Manitoba. Canadian Journal of Earth Sciences, Volume 25, pages 783–787. https://doi.org/10.1139/e88-073

Dreimanis, A. and Vagners, U.J., 1971: Bimodal distribution of rock and mineral fragments in basal tills. *In* Till – A Symposium. *Edited by* R.P. Goldthwait. Ohio State University Press, USA, pages 237–250.

Ehlers, J. and Gibbard, P.L., 2007: The extent and chronology of Cenozoic global glaciation. Quaternary International, Volume 164–165, pages 6–20. https://doi.org/10.1016/j.quaint.2006.10.008

Elson, J.A. 1989. Comment on glacitectonite, defomation till and comminution till. *In* Genetic Classification of Glacigenic Deposits. *Edited by* R.P. Goldthwait and C.L. Matsch. Balkema, Rotterdam, pages 85–88.

Evans, D.J.A., 2018: Till: A Glacial Process Sedimentology. John Wiley and Sons Ltd. https://doi.org/10.1002/9781118652541

Evans, D.J.A., Phillips, E.R. and Atkinson, N., 2021: Glacitectonic rafts and their role in the generation of Quaternary subglacial bedforms and deposits. Quaternary Research, Volume 104, pages 101–135. https://doi.org/10.1017/qua.2021.11

Evans, D.J.A., Phillips, E.R., Hiemstra, J.F. and Auton, C.A., 2006: Subglacial till: formation, sedimentary characteristics and classification. Earth Science Reviews, Volume 78, pages 115–176. https://doi.org/10.1016/j.earscirev.2006.04.001

Eyles, N., Bukhari, S., Sookhan, S., Ruscica, R. and Paulen, R.C., 2023: LiDAR-based semi-automated mapping of drumlins and mega-scale glacial lineations of the Green Bay Lobe, Wisconsin, USA: Ice sheet beds as glaciotribological systems. Earth Surface Processes and Landforms. https://doi.org/10.1002/esp.5486

Fabel, D., Stroeven, A., Harbor, J., Kleman, J., Elmore, D. and Fink, D., 2002: Landscape preservation under Fennoscandian ice sheets determined from *in situ* produced ^{10}Be and ^{26}Al. Earth and Planetary Science Letters, Volume 201, pages 397–406. https://doi.org/10.1016/S0012-821X(02)00714-8

Ferbey, T. and Levson, V.M., 2009: The influence of ice flow reversals on the vertical and horizontal distribution of trace element values in tills, Huckleberry Mine area, west-central British Columbia. *In* Application of Till and Stream Sediment Heavy Mineral and Geochemical Methods to Mineral Exploration in Western and Northern Canada. *Edited by* R.C. Paulen and I. McMartin. Geological Association of Canada, Short Course Notes 18, pages 177–183. https://gac.ca/product/application-of-till-and-stream-sediment-heavy-mineral-and-geochemical-methods/

Gosse, J., Bell, T., Gray, J., Klein, J., Yang, G. and Finkel, R., 2006: Using cosmogneic isotopes to interpret the landscape record of glaciation: Nunataks in Newfoundland? *In* Glacier Science and Environmental Change. *Edited by* P. Knight. Blackwell Publishing, Malden, MA/Oxford, pages 442–446. https://doi.org/10.1002/9780470750636.ch89

Hallet, B., 1996: Glacial quarrying: A simple theoretical model. Annals of Glaciology, Volume 22, pages 1–8. https://doi.org/10.3189/1996AoG22-1-1-8

Hart, J.K. and Smith, B., 1997: Subglacial deformation associated with fast ice flow, from the Columbia Glacier, Alaska. Sedimentary Geology, Volume 111, pages 177–197. https://doi.org/10.1016/S0037-0738(97)00014-6

Hättestrand, C., Goodwillie, D. and Kleman, J., 1999: Size distribution of two cross-cutting drumlin systems in northern Sweden: A measure of selective erosion and formation time length. Annals of Glaciology Volume 28, pages 146–152. https://doi.org/10.3189/172756499781821689

Hicock, S.R., 1990: Genetic till prism. Geology, Volume 18, pages 517–519. https://doi.org/10.1130/0091-7613(1990)018<0517:GTP>2.3.CO;2

Hiemstra, J.F., Evans, D.J.A. and Ó Cofaigh, C., 2007: The role of glaciotectonic rafting and comminution in the production of subglacial tills: Examples from SW Ireland and Antarctica. Boreas, Volume 36, pages 386–399. https://doi.org/10.1080/ 03009480701213521

Hildes, D.H.D., Clarke, G.K.C., Flowers, G.E. and Marshall, S.J., 2004: Subglacial erosion and englacial sediment transport modelled for North American ice sheets. Quaternary Science Reviews, Volume 23, pages 409–430. https://doi.org/10.1016/j.quascirev.2003.06.005

Hindmarsh, R.C.A., 2018: Chapter 18 - Ice Sheet and Glacier Modelling. *In* Past Glacial Environments (Second Edition). *Edited by* J. Menzies and J.M. van der Meer. Elsevier, pages 607–663. https://doi.org/10.1016/B978-0-08-100524-8.00019-1

Iverson, N.R., 1991: Potential effects of subglacial water-pressure fluctuations on quarrying. Journal of Glaciology, Volume 37, pages 27–36. https://doi.org/10.3189/S0022143000042763

Iverson, N.R., 2012: A theory of glacial quarrying for landscape evolution models. Geology, Volume 40, pages 679–682. https://doi.org/10.1130/G33079.1

Iverson, N.R. and Semmens, D.J., 1995: Intrusion of ice into porous media by regelation: A mechanism of sediment entrainment by glaciers. Journal of Geophysical Research, Volume 100, pages 10,219–10,230. https://doi.org/10.1029/95JB00043

Kauranne, L.K., 1967: Chapter 17: Prospecting for copper by geochemical and related methods at Kotanen, Viitasaari, central Finland. *In* Geochemical Prospecting in Fennoscandia. *Edited by* A. Kvalheim. Interscience, New York, pages 255–260.

Kelley, S.E., Ross, M., Elliott, B. and Normandeau, P.X., 2019: Effect of shifting ice flow and basal topography in shaping three-dimensional dispersal patterns, Lac de Gras region, Northwest Territories, Canada. Journal of Geochemical Exploration, Volume 199, pages 105–127. https://doi.org/10.1016/j.gexplo.2019.01.012

Kjær, K.H., Houmark-Nielsen, M. and Richardt, N., 2003: Ice flow patterns and dispersal of erratics at the south-western margin of the late Scandinavian Ice Sheet: Signature of palaeo-ice streams. Boreas, Volume 32, pages 130–148. https://doi.org/10.1111/j.1502-3885.2003.tb01434.x

Klassen, R.A., 1997. Glacial history and ice flow dynamics applied to drift prospecting and geochemical exploration. *In* Proceedings of Exploration 97. *Edited by* A.G. Gubin. Fourth Decennial International Conference on Mineral Exploration, pages 221–232. https://www.911metallurgist.com/blog/wp-content/uploads/2015/10/Glacial-History-and-Ice-Flow-Dynamics-Applied-to-Drift-Prospecting-and-Geochemical-Exploration.pdf

Kleman, J., Stroeven, A.P. and Lundqvist, J., 2008: Patterns of Quaternary ice sheet erosion and deposition in Fennoscandia and a theoretical framework for explanation. Geomorphology, Volume 97, pages 73–90. https://doi.org/10.1016/j.geomorph.2007.02.049

Lawson, D.E., 1989: Glacigenic resedimentation: classification concepts and application to mass movement processes and deposits. *In* Genetic Classification of Glacigenic Deposits. *Edited by* R.P. Goldthwait and C.L. Matsch. Balkema, Rotterdam, pages 147–189.

Mäkinen, J., 1995: Effects of grinding and chemical factors on the generation and composition of the till fine fraction: an experimental study. Journal of Geochemical Exploration, Volume 54, pages 49–62. https://doi.org/10.1016/0375-6742(95)00008-D

Margold, M., Stokes, C.R. and Clark, C.D., 2015: Ice streams in the Laurentide Ice Sheet: Identification, characteristics and comparison to modern ice sheets. Earth-Science Reviews, Volume 143, pages 117–146. https://doi.org/10.1016/j.earscirev.2015.01.011

Margreth, A., Gosse, J.C. and Dyke, A.S., 2016: Quantification of subaerial and episodic subglacial erosion rates on high latitude upland plateaus: Cumberland Peninsula, Baffin Island, Arctic Canada. Quaternary Science Reviews, Volume 133, pages 108–129. https://doi.org/10.1016/j.quascirev.2015.12.017

McClenaghan, M.B. and Paulen, R.C., 2018: Mineral exploration in glaciated terrain. *In* Past Glacial Environments, Chapter 20 (Sediments, Forms and Techniques) A new and revised edition. *Edited by* J. Menzies and J.J-M. van der Meer. Elsevier, pages 689–751. https://doi.org/10.1016/B978-0-08-100524-8.00022-1

McClenaghan, M.B., Paulen, R.C., Layton-Matthews, D., Hicken, A.K. and Averill, S.A. 2015: Glacial dispersal of gahnite from the Izok Lake Zn Cu Pb Ag VMS deposit, northern Canada. Geochemistry: Exploration, Environment, Analysis, Volume 15, pages 333–349. https://doi.org/10.1144/geochem2014-317

McClenaghan, M.B., Paulen, R.C. and Oviatt, N.M., 2018: Geometry of indicator mineral and till geochemistry dispersal fans from the Pine Point Mississippi Valley-type Pb-Zn district, Northwest Territories, Canada. Journal of Geochemical Exploration, Volume 190, pages 69–86. https://doi.org/10.1016/j.gexplo.2018.02.004

McClenaghan, M.B., Paulen, R.C., Smith, I.R., Rice, J.M., Plouffe, A., McMartin, I., Campbell, J.E., Lehtonen, M., Parsasadr, M. and Beckett-Brown, C.E., 2023: Review of till geochemistry and indicator mineral methods for mineral exploration in glaciated terrain. Geochemistry: Exploration, Environment, Analysis, Volume 23, pages 1–43. https://doi.org/10.1144/geochem2023-013

McClenaghan, M.B., Spirito, W.A., Day, S.J.A., McCurdy, M.W., McNeil, R.J. and Adcock, S.W., 2022: Overview of surficial geochemistry and indicator mineral surveys and case studies from the Geological Survey of Canada's GEM Program. Geochemistry: Exploration, Environment, Analysis, Volume 22, pages 1–21. https://doi.org/10.1144/geochem2021-070

McClenaghan, M.B., Ward, B.C., Kjarsgaard, I.M., Kjarsgaard, B.A., Kerr, D.E. and Dredge, L.A., 2002: Indicator mineral and till geochemical dispersal patterns associated with the Ranch Lake kimberlite, Lac de Gras region, NW Territories, Canada. Geochemistry, Exploration, Environment, Analysis, Volume 2, pages 299–320. https://doi.org/10.1144/1467-787302-004

McMartin, I. and Henderson, P., 2004: Evidence from Keewatin (Central Nunavut) for paleo-ice divide migration. Géographie Physique et Quaternaire, Volume 58, pages 163-186. https://doi.org/10.7202/013137ar

McMartin, I. and Paulen, R.C., 2009: Ice-flow indicators and the importance of ice-flow mapping for drift prospecting. *In* Application of Till and Stream Sediment Heavy Mineral and Geochemical Methods to Mineral Exploration in Western and Northern Canada. *Edited by* R.C. Paulen and I. McMartin. Geological Association of Canada, Short Course Notes 18, pages 15–34. https:// gac.ca/product/application-of-till-and-stream-sediment-heavy-mineral-and-geochemical-methods/

Melanson, A., Bell, T. and Tarasov, L., 2013: Numerical modelling of subglacial erosion and sediment transport and its application to the North American ice sheets over the Last Glacial cycle. Quaternary Science Reviews, Volume 68, pages 154–174. https://doi.org/10.1016/j.quascirev.2013.02.017

Menzies, J., Paulen, R.C., McClenaghan, M.B., Rice, J.M., Oviatt, N.M. and Dhillin, N., 2019: Deformation 'boundary front' movements in subglacial tills - a microsedimentological perspective from till near Pine Point, NWT, Canada. The Depositional Record, Volume 5, pages 230–246. https://doi.org/10.1002/dep2.73

Miller, J.K., 1984: Model for clastic indicator trains in till. *In*: Prospecting in Areas of Glaciated Terrain 1984, Institute of Mining and Metallurgy, London, pages 69–77.

Munro-Stasiuk, M.J., 2000: Rhythmic till sedimentation: Evidence for repeated hydraulic lifting of a stagnant ice mass. Journal of Sedimentary Research, Volume 70, pages 94–106. https://doi.org/10.1306/2DC40901-0E47-11D7-8643000102C1865D

Nurmi, A., 1976: Geochemistry of the till blanket at the Talluskanava Ni-Cu ore deposit, Tervo, Central Finland. Geological Survey of Finland, Report of Investigation No. 15.

Parent, M.P., 2023: Polyphase glacial dynamics and clast dispersal patterns in glaciofluvial and glacial sediments in north-central Québec, with application to diamond exploration. *In* Surficial Geology of Northern Canada: A Summary of Geo-mapping for Energy and Minerals Program Contributions. *Edited by* I. McMartin. Geological Survey of Canada, Bulletin 611, pages 201–219. https://doi.org/10.4095/331425

Parent, M., Paradis, S.J. and Boisvert, E., 1995: Ice flow patterns and glacial transport in the eastern Hudson Bay region: Implications for the late Quaternary dynamics of the Laurentide Ice Sheet. Canadian Journal of Earth Sciences, Volume 32, pages 2057–2070. https://doi.org/10.1139/e95-159

Parent, M., Paradis, S.J. and Doiron, A., 1996: Palimpsest glacial dispersal trains and their significance for drift prospecting. Journal of Geochemical Exploration, Volume 56, pages 123–140. https://doi.org/10.1016/0375-6742(96)00011-8

Paulen, R.C., 2009: Sampling techniques in the western Canada sedimentary basin and the cordillera. *In* Application of Till and Stream Sediment Heavy Mineral and Geochemical Methods to Mineral Exploration in Western and Northern Canada. *Edited by* R.C. Paulen and I. McMartin. Geological Association of Canada, Short Course Notes 18, pages 49–74.
https://gac.ca/product/application-of-till-and-stream-sediment-heavy-mineral-and-geochemical-methods/

Paulen, R.C., Eyles, N. and Ross, M., 2024b: Glacial dispersal trains and ice streams on the Canadian Shield. *In* Till Geochemistry and Indicator Mineral Methods for Exploration in Glaciated Terrains *Edited by* R.C. Paulen and M.B. McClenaghan. Geological Survey of Canada, Open File 9210, pages 140–147.
https://doi.org/10.4095/pbmy2d03m0

Paulen, R.C. and McClenaghan, M.B., 2015: Late Wisconsin ice-flow history in the Buffalo Head Hills kimberlite field, north-central Alberta. Canadian Journal of Earth Sciences, Volume 52, pages 1–17.
https://doi.org/10.1139/cjes-2014-0109

Paulen, R.C. and McClenaghan, M.B. (eds.), 2024: Till geochemistry and indicator-mineral methods for exploration in glaciated terrains. Geological Survey of Canada, Open File 9210, 157 pages.
https://doi.org/10.4095/pbmy2d03m0

Paulen, R.C., McClenaghan, M.B. and Evans, D.J.A., 2024c: Glacial erratics and till dispersal indicators. *In* Encyclopaedia of Quaternary Science, 3rd Edition, Reference Module in Earth Systems and Environmental Sciences. *Edited by* S.A. Elias. Elsevier. https://doi.org/10.1016/B978-0-323-99931-1.00277-4

Paulen, R.C., McClenaghan, M.B. and Hicken, A.K., 2013: Regional and local ice-flow history in the vicinity of the Izok Lake Zn-Cu-Pb-Ag deposit, Nunavut. Canadian Journal of Earth Sciences, Volume 50, pages 1209–1222.
https://doi.org/10.1139/cjes-2013-0064

Paulen, R.C., Mulligan, R.P.M. and Rice, J.M., 2024a: Determination of glacial transport directions. *In* Till Geochemistry and Indicator Mineral Methods for Exploration in Glaciated Terrains. *Edited by* R.C. Paulen and M.B. McClenaghan. Geological Survey of Canada, Open File 9210, pages 10–23.
https://doi.org/10.4095/pbmy2d03m0

Paulen, R.C., Rice, J.M. and McClenaghan, M.B., 2025: Chapter 15: Till applied to exploration in glaciated terrain. *In* Micromorphology: A Practical Guide to the Microscale Analysis of Glacial Sediments and Processes. *Edited*

by E. Phillips and J. Menzies. Quaternary Research Association, London, pages 476–480. ISSN: 0264 9241. ISBN: 0 907780 296 242. https://www.qra.org.uk/bookshop/micromorphology-a-practical-guide/

Paulen, R.C., Stokes, C.R., Fortin, R., Rice, J.M., Dubé-Loubert, H. and McClenaghan, M.B., 2017: Dispersal trains produced by ice streams: An example from Strange Lake, Labrador, Canada. *In* Proceedings of Exploration 17. *Edited by* V. Tschirhart and M.D. Thomas. Sixth Decennial International Conference on Mineral Exploration, pages 871–875. https:// geochem.nrcan.gc.ca/cdogs/content/pub/pub03698_e.htm

Plouffe, A., Anderson, R.G., Gruenwald, W., Davis, W.J., Bednarski, J.M. and Paulen, R.C., 2011: Integrating ice flow history, geochronology, geology, and geophysics to trace mineralized glacial erratics to their bedrock source: An example from south-central British Columbia. Canadian Journal of Earth Sciences, Volume 48, pages 1113–1130. https://doi.org/10.1139/e10-099

Plouffe, A., Ferbey, T., Hashmi, S. and Ward, B.C., 2016: Till geochemistry and mineralogy: Vectoring towards Cu porphyry deposits in British Columbia, Canada. Geochemistry, Exploration, Environment, Analysis, Volume 16, pages 213–232. https://doi.org/10.1144/geochem2015-398

Rea, B.R., 2013: Micro- to macroscale forms. *In* Encyclopedia of Quaternary Science (Second Edition). Elsevier, pages 865–876. https://doi.org/10.1016/B978-0-444-53643-3.00076-5

Rice, J.M., Paulen, R.C., Campbell, H.E. and Ross, M., 2023: The surficial geology record of ice stream catchment dynamics and ice-divide migration in the Québec-Labrador sector of the Laurentide Ice Sheet. Quaternary Science Advances, Volume 13. https://doi.org/10.1016/j.qsa.2023.100123

Rice, J.M., Ross, M., Paulen, R.C., Kelley, S.E. and Briner, J.P., 2020: A GIS-based multi- proxy analysis of the evolution of subglacial dynamics in northeastern Québec, Canada. Earth Surface Processes and Landforms 23, pages 3155–3177. https://doi.org/10.1002/esp.4957

Rice, J.M., Ross, M., Paulen, R.C., Kelley, S.E., Briner, J.P., Neudorf, C.M. and Lian, O.B., 2019: Refining the ice flow chronology and subglacial dynamics across the migrating Labrador Divide of the Laurentide Ice Sheet with age constraints on deglaciation. Journal of Quaternary Science, Volume 34, pages 519–535. https://doi.org/10.1002/jqs.3138

Rice, J.M., Ross, M., Campbell, H.E., Paulen, R.C. and McClenaghan, M.B., 2024: Net evolution of subglacial sediment transport in the Québec–Labrador sector of the Laurentide Ice Sheet. Canadian Journal of Earth Sciences, Volume 61, pages 524–542. https://doi.org/10.1139/cjes-2023-0050

Ross, M., 2024: Glacial dynamics and glacial sediment dispersal explained. *In* Till Geochemistry and Indicator Mineral Methods for Exploration in Glaciated Terrains. *Edited by* R.C. Paulen and M.B. McClenaghan. Geological Survey of Canada, Open File 9210, pages 4–9. https://doi.org/10.4095/pbmy2d03m0

Ross, M., Campbell, J.E., Parent, M. Adams, R.S., 2009: Palaeo-ice streams and the subglacial landscape mosaic of the North American mid-continental prairies. Boreas, Volume 38, pages 421–439. https://doi.org/10.1111/j.1502-3885.2009.00082.x

Scott-Smith, B.H., Letendre, J.P. and Robison, H.R., 1996: Geology of the Sturgeon Lake 01 kimberlite block, Saskatchewan. Exploration and Mining Geology, Volume 5, pages 251–261.

Shaw, J., 1982: Melt out till in the Edmonton area, Alberta, Canada. Canadian Journal of Earth Sciences, Volume 19, pages 1548–1569. https://doi.org/10.1139/e82-134

Shaw, J., 1983: Forms associated with boulders in melt-out till. *In* Tills and Related Deposits. *Edited by* E.B. Evenson, C. Schluchter and J. Rabassa. Balkema, Rotterdam, pages 3–12.

Shilts, W.W., 1976: Glacial till and mineral exploration. *In* Glacial Till: An Interdisciplinary Study. *Edited by* R.F. Legget. Royal Society of Canada, Special Publication 12, pages 205–223.

Shilts, W.W., 1993: Geological Survey of Canada's contributions to understanding the composition of glacial sediments. Canadian Journal of Earth Sciences, Volume 30, pages 333–353. https://doi.org/10.1139/e93-026

Shilts, W.W., 1995: Geochemical partitioning in till. *In* Drift Exploration in the Canadian Cordillera. *Edited by* P.T. Bobrowsky, S.J. Sibbick, J.M. Newell and P.F. Matysek. British Columbia Ministry of Energy, Mines and Petroleum Resources, Paper 1995-2, pages 149–163. https://cmscontent.nrs.gov.bc.ca/geoscience/publicationcatalogue/Paper/BCGS_P1995-02.pdf

Sookhan, S., Eyles, N. and Bukhari, S., 2022: Drumlins and mega-scale glacial lineations as a continuum of subglacial shear marks: A LiDAR based morphometric study of streamlined surfaces on the bed of a Canadian paleo-ice stream. Quaternary Science Reviews, Volume 292. https://doi.org/10.1016/j.quascirev.2022.107679

Spagnolo, M., Phillips, E., Piotrowski, J.A., Rea, B.R., Clark, C.D., Stokes, C.R., Carr, S.J., Ely, J.C., Ribolini, A., Wysota, W. and Szuman, I., 2016: Ice stream motion facilitated by a shallow-deforming and accreting bed. Nature Communications, Volume 7. https://doi.org/10.1038/ncomms10723

Stalker, A.M., 1976: Megablocks, or the Enormous Erratics of the Albertan Prairies. Geological Survey of Canada, Paper, 76-1C, pages 185–188.

Stanley, C.R., 2009: Geochemical, mineralogical, and lithological dispersal models in glacial till: physical process constraints and application in mineral exploration. *In* Application of Till and Stream Sediment Heavy Mineral

and Geochemical Methods to Mineral Exploration in Western and Northern Canada. *Edited by* R.C. Paulen and I. McMartin. Geological Association of Canada, Short Course Notes 18, pages 35–48. https://gac.ca/product/application-of-till-and-stream-sediment-heavy-mineral-and-geochemical-methods/

Stea, R.R. and Finck, P.W., 2001: An evolutionary model of glacial dispersal and till genesis in Maritime Canada. *In* Drift Exploration in Glaciated Terrain. *Edited by* M.B. McClenaghan, P.T. Bobrowsky, G.E.M. Hall and S.J. Cook. Geological Society, London, Special Publication No. 185, pages 237–265. https://doi.org/10.1144/GSL.SP.2001.185.01.11

Trommelen, M.S., Ross, M. and Campbell, J.E., 2012: Glacial terrain zone analysis of a fragmented paleoglaciologic record, southeast Keewatin sector of the Laurentide Ice Sheet. Quaternary Science Reviews, Volume 40, pages 1–20. https://doi.org/10.1016/j.quascirev.2012.02.015

Trommelen, M.S., Ross, M. and Campbell, J.E., 2013: Inherited clast dispersal patterns: implications for palaeoglaciology of the SE Keewatin Sector of the Laurentide Ice Sheet. Boreas Volume 42, pages 693–713. https://doi.org/10.1111/j.1502-3885.2012.00308.x

Digging for Data: Recommended Till Sampling Methods for Indicator Minerals and Geochemistry

Jessey Rice
Geological Survey of Canada, 601 Booth Street, Ottawa, ON, K1A 0E8

Abstract

Collecting high-quality till samples for laboratory analysis is arguably the most crucial component of any drift-prospecting program, as both subsequent data interpretation and exploration decisions depend on the integrity of these samples. Although each till sampling survey will differ in its operational context and geological setting, the overarching objective remains consistent: to detect and trace the sources of lithological, mineralogical, or geochemical components identified within the till back to their bedrock sources. Whether applying conventional mineral exploration techniques or leveraging emerging advances such as artificial intelligence and machine learning techniques, reliable till samples remain fundamental to producing meaningful results. This chapter provides practical guidance, best practices and key considerations in survey design, compares available till-sampling methods, and evaluates their respective strengths and limitations to optimize mineral exploration outcomes.

Introduction

Till sampling is a fundamental technique for mineral exploration in glaciated terrain where glacial deposits blanket large areas of bedrock (Coker and DiLabio, 1989; Kujansuu and Saarnisto, 1990; McMartin and Campbell, 2009; Paulen, 2009; McClenaghan *et al.*, 2023). Therefore, collecting high-quality till samples is critical for every subsequent interpretation of data derived from these samples in order to reduce the likelihood of false negatives, identify potential contamination, and minimize exploration costs. Additionally, till sampling is often one of the most expensive parts of the initial exploration phase, which reinforces the importance of proper till sampling for any successful drift exploration campaign. This chapter focuses on practical sampling methods and considerations and is designed to chronologically work through key considerations at all stages of planning and carrying out a till survey, from survey design to sample submission.

The chapter summarizes the most important aspects of collecting high-quality till samples, and is meant as a complement to the more detailed and descriptive till sampling and analysis protocol manual for the Geological Survey of Canada (GSC) by McClenaghan *et al.* (2020). Additional resources for more detailed discussion in this chapter include those of Sarala (2015a, b), McClenaghan and Paulen (2018), McClenaghan *et al.* (2023), Rice and McClenaghan (2024), and Sacco (2024).

Till Survey Design

A successful till sampling program is built upon a foundation of planning and creating an appropriate till sampling design. Before any initial sample site planning is conducted, all sources of available information should be collected and evaluated and all of the proper permits and licenses should be obtained. Engaging with any local communities, stakeholders, or indigenous organizations is strongly encouraged and will provide important information for the sampling program as well. These sources should include digital elevation models such as ArcticDEM (*e.g.*, Porter *et al.*, 2018), light detection and ranging (LiDAR) imagery (*e.g.*, Johnson *et al.*, 2015; Eyles *et al.*, 2022), satellite imagery, surficial geology maps, and previous work contained in geological reports, industry assessment reports, and published literature. Essential data that should be collected from existing resources include ice-flow direction, distribution and till thickness, any secondary processes affecting till composition, and any identified stratigraphy within the region of study.

The information compiled during initial gathering of information will help define sampling strategy, optimize sample coverage, reduce redundancy (*i.e.*, reduce overlap in information between samples, maximizing the unique information given by each sample), increase the information gain from each sample by minimizing redundancy, and limit uncertainty. A number of logistical and geological factors will control the type and amount of till sampling that will be conducted under any exploration program:

i) Logistical factors: purpose of the survey, size of the survey area, sample density, budget (both time and financial), land tenure, land use restrictions, accessibility, method of transport, previous work, and sampling crew.

ii) Geological factors: nature and size of the mineralization target(s), type, thickness and distribution of till, ice-flow history of the region, environmental factors, and the geomorphology of the study area (*see* McClenaghan *et al.*, 2023).

When designing the distribution pattern of till sample sites, which is a critical step in the planning stages of the survey, three distribution patterns are most commonly used (McClenaghan *et al.*, 2020), and sometimes mixed in a single survey design depending on geological or logistical constraints.

i) *Grid sampling* (Fig. 1a) in which a specific sample density is maintained (*e.g.*, 1 sample /10 km^2). This sampling pattern is often used where ice-flow directions are not known or where multi-phased ice-flow directions are significantly different;
ii) *Parallel line sampling* in which sample spacing along lines is closer than spacing between lines (Fig. 1b), and with preferential alignment in two orthogonal directions. This sample distribution is often used perpendicular to known ice-flow directions, geophysical conductors, or known bedrock structures; and
iii) *Sporadic sampling* (Fig. 1c) where spacing is dictated by access along roads and waterways as well as the local availability of till in areas of extensive bedrock outcrop, discontinuous sediment cover, and/or thick non-till cover sediments.

Sample Site Selection

Once a till sampling survey has been designed and field logistics have been sorted, till collection can commence. In practice, one of the most challenging aspects of till sampling campaigns is correctly identifying and classifying the till collected. There are numerous processes that can deposit sediment (*i.e.*, diamicton) that visually resembles till. Till is an unsorted clay to sand-sized matrix-supported sediment that contains variable sizes, shapes, and quantities of rock fragments that have been transported directly from, or by, a glacier or ice sheet with little or no sorting by water (Dreimanis, 1989; Evans *et al.*, 2006). Subglacial traction till (historically referred to as basal till or lodgement till) is the optimal medium for mineral exploration as it is a primary derivative of bedrock and has a simpler depositional history than other media (McClenaghan *et al.*, 2023). Evans (2018) provides a detailed overview of the history of till nomenclature and con-

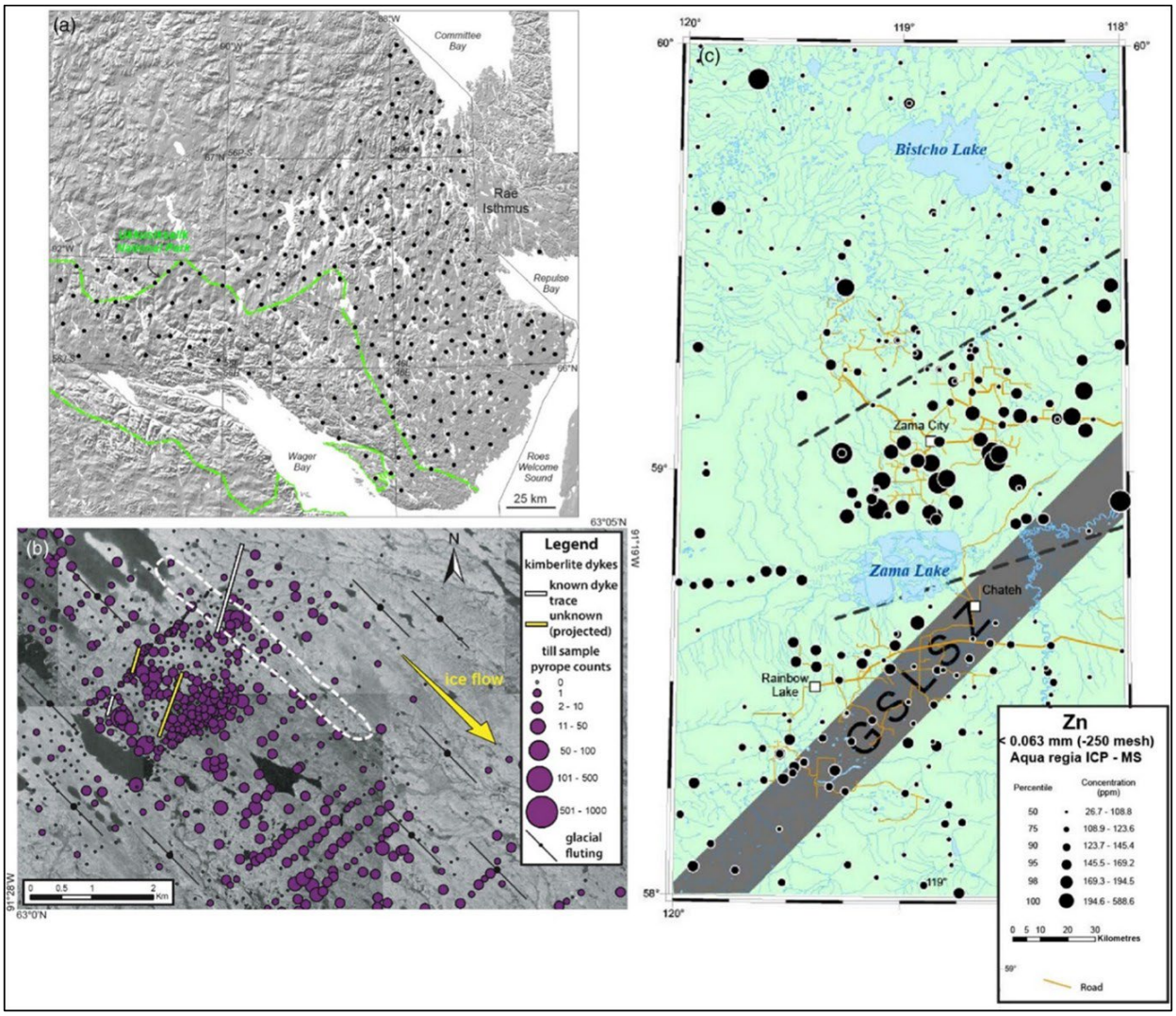


Figure 1. *Examples of different study designs: (a) a regularly spaced grid, with a preferential orthogonal alignment, for a regional-scale survey (modified from McMartin* et al.*, 2015), with some areas having more sporadic or targeted sampling design; (b) at regularly spaced intervals along lines perpendicular to the known ice-flow direction with subsequent higher density infill sampling focused on corridors of interest (modified from Strand* et al.*, 2009) with variable spacing between lines, and with some areas having more targeted or sporadic design; (c) Sporadic sampling design along roads and waterways guided by access, with the orange lines indicating roads; GSLSZ–Great Slave Lake shear zone (modified from Plouffe* et al.*, 2006).*

siderations in determining its genesis. Key characteristics that define subglacial traction tills are commonly over-consolidation, presence of deformation structures, evidence of basal shear and loading, and presence of striated and faceted clasts (Evans 2018).

The thickness of a till package/unit varies significantly by location. It is an important consideration that should be accounted for in the planning stages. However, generally, the assumption is that the till closest to the bedrock, except within paleo-ice streams where transport can be from significant distances up-ice compared to the surrounding till (*e.g.*, Dredge, 2000;

Primmer *et al.*, 2015; McClenaghan *et al.*, 2015; Paulen *et al.*, 2017), has the highest probability of being derived from the local bedrock (Fig. 2; *e.g.*, Bird and Coker, 1987). For regional-scale sampling in areas with varying glacial landforms, it is a good practice to document the glacial landforms from which the till samples are collected. Aario and Peuraniemi (1992), Proudfoot *et al.* (1995), and McClenaghan *et al.* (2020) provide overviews of selected glacial landforms, their characteristics, and the preferred location for till sampling sites on the landforms. This documentation will help to identify any biases that specific landforms could introduce, as well as highlight any multi-phase generation (*e.g.*, Stea and Brown, 1989) or modification (Eyles *et al.*, 2022) of till landforms. Considerations for till sampling in different physiographic settings are summarized by McClenaghan *et al.* (2020) and McClenaghan *et al.* (2023) and should be consulted for a more detailed explanation for each setting described (*e.g.*, mountainous terrain, rolling terrain, permafrost areas, *etc.*). The type of landscape or landform from which the samples are being collected should also be considered, as this will assist in determining the genesis and glacial transport distance. Similar to targeting till on top of bedrock, it is preferable to sample landforms that are likely composed of locally derived till. Following these considerations, sampling can generally be characterized as either surface sampling or sampling at depth, both of which are briefly summarized below.

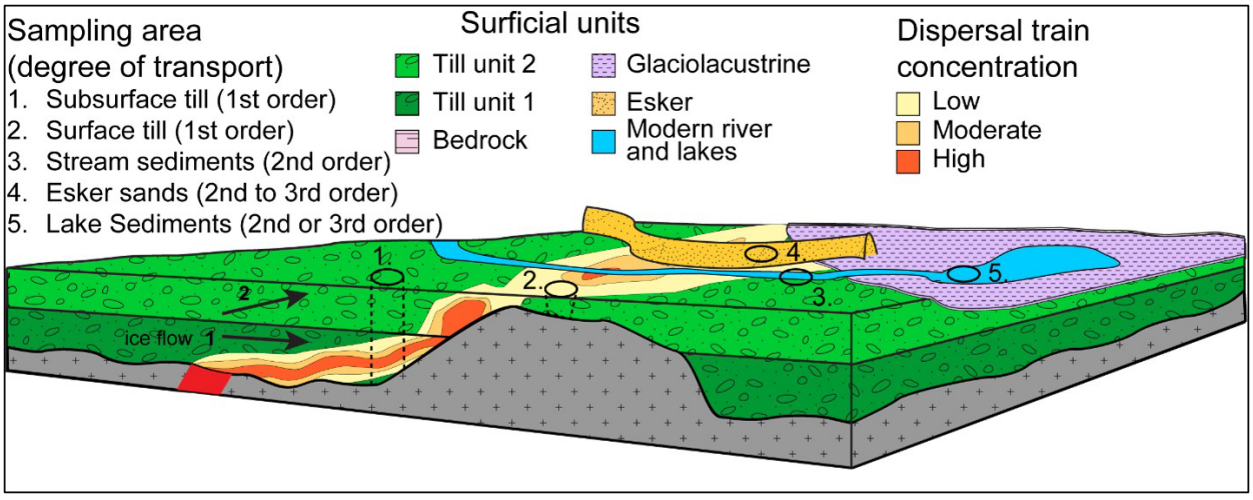


Figure 2. *Theoretical glacial terrain showing the different areas from which surficial sediments can be collected. For drift prospecting, the best practice is to collect first-order transported sediments (till). In this instance, first order means the sediment is moved directly from bedrock source by ice, with no reworking; second order means the sediment has been reworked after transport (*i.e.*, till that has been modified by meltwater and deposited in an esker); third order means again transported after that, such as a lake washing an esker and depositing sediment along the lake shore or into the lake bottom. The two black arrows represent the direction of ice flow responsible for the each respective till units. Note that no soil has developed on this hypothetical landscape.*

Sampling at Surface

During early stages of exploration (*i.e.*, reconnaissance or regional-scale), till samples are generally collected at the surface (*e.g.*, Klassen and Thompson, 1993; McMartin *et al.*, 1996; Ward *et al.*, 2011; Rice *et al.*, 2024a) or from easily accessible vertical sections along river or roads. Till sampling at depth requires substantial additional resources (*e.g.*, excavators, drills) and usually the deeper the sample, the more expensive the program will be (Sacco, 2024). No matter the depth at which till samples are collected, the C-horizon should always be targeted, as this horizon is generally minimally affected by soil development, with little alteration from weathering or hydromorphic dispersion, leaving a relatively unaltered signal of clastic glacial dispersal (McClenaghan *et al.*, 2023). This rule will largely dictate how deep samples should be collected (*e.g.*, dug through soil horizons or overlying post-glacial sediments), but the depth of sampling interval will vary between sites and it should be recorded in order to characterize compositional variations across the dataset (*e.g.*, Garrett, 1971; Brummer *et al.*, 1992).

Equipment needed for surficial sampling is outlined in McClenaghan *et al.* (2020). Prior to fieldwork, all equipment should be inspected to ensure it is in good working condition, when working in remote locations, having backups of essential equipment is recommended (*i.e.*, multiple shovels). Potential contamination from sampling equipment should also be considered prior to collection. For example, some shovels have a zinc/chromium anti-corrosion coating that can flake off and contaminate the sample and this should be removed prior to sampling, or use a steel alternative (*e.g.*, Plouffe *et al.*, 2014).

In sites free of permafrost, surface sampling commonly involves digging through the upper soil horizons to collect *in situ* C-horizon till- this could involve hand digging of sample pits, Dutch auguring, or using a small excavator to dig down to the required depth. At sites underlain by extensive permafrost, physical weathering is the dominant process in soil formation, and cryoturbation mixes soil horizons. Cryoturbation can also create frost boils, which are bare to lichen-covered, round to oval patches that contrast in colour with surrounding sediment and are often bordered by vegetation and rocks (McMartin and Campbell, 2009). Frost boils form as hydrostatic pressure in the summer-time thawed active layer pushes relatively fresh, well-homogenized, and unweathered till to the surface, creating vegetation-free centres that are ideal

for shallow sampling. Sampling depth is limited by the thickness of the active layer, which may reach ~2 m in southern continuous permafrost zones but is typically <0.5 m in more northerly regions (*e.g.*, Shilts, 1978; Dyke and Zoltai, 1980; Dredge, 2002; French, 2007). Samples should not be collected from the surface of the frost boil, but from depths where surface organics (*i.e.*, mottling) and clasts or shells of non-glacial origin are not present. Care should be taken to ensure the cryoturbated material is till and not another sediment (*i.e.*, marine or lacustrine sediments; *see* McClenaghan *et al.* (2020)).

Road cuts, ditches, river valleys, and other natural and artificial (*e.g.*, open pits) exposures offer opportunities to sample thicker till sections and observe any stratification and should be investigated during the sampling program. For more details on surficial sampling, *see* Paulen (2009), McMartin and Campbell (2009), McClenaghan *et al.* (2020, 2023) and Rice and McClenaghan (2024).

Sampling at Depth

Where till is thicker (>2 m), or when till is covered by post-glacial sediments (*i.e.*, marine sediments or glaciolacustrine sediments such as the Abitibi Greenstone Belt), the use of backhoes, portable drills, or drilling rigs will be required. In these settings, it is good practice to collect samples at different depths to characterize changes in sediment properties relating to changing stratigraphy and/or changes in ice-flow trajectory. Dispersal trains can occur at variable depths in a thick sediment package, hence sample collection at multiple depths increases the opportunities to intersect a dispersal train (Fig. 2; *e.g.*, Bird and Coker, 1987; Bajc, 1991; McClenaghan *et al.*, 2014, 2018; Kelley *et al.*, 2019). Generally, the top part of a till sequence contains material from more distal bedrock sources in comparison to the lower part of a till sequence (*e.g.*, Bond, 2001; Reyes and Clague, 2004). Having an understanding of till thickness across the area of interest will be immensely beneficial if available. Where this data is absent, ground-based geophysical methods such as ground penetrating radar or electrical resistivity tomography can be applied in representative landscape settings to image subsurface unit thicknesses and depths to bedrock (*e.g.*, Sibul *et al.*, 2017) and extrapolated across similar landscape assemblages to guide survey design and equipment selection. If feasible, drilling is used in thick-drift areas to collected till samples at depth. Smaller drills are easier to mobilize, but are limited to shallow depths (up to 10 m) and

small sample volumes, whereas larger drills reach greater depths (10s of m) and recover more material at the cost of more complex permitting, logistics, and higher expense (Sacco, 2024).

A summary of the advantages and disadvantages of sampling at depth is summarized in Table 1. The following references provide overviews of sampling equipment that can be used to collect till samples in thin and thick till settings: Coker and DiLabio (1989), Averill (1990), Hirvas and Nenonen (1990), Coker (1991), Kauranne *et al.* (1992), Salminen (1992), Plouffe (1995), Levson (2001), McMartin and McClenaghan (2001), McMartin and Campbell (2009), Paulen (2009), Sarala (2005, 2015a), McClenaghan *et al.* (2020, 2023), Sacco *et al.* (2022, 2023), and Sacco (2024).

Sample Size

Matrix Geochemistry

The size of the till sample will be determined by the type of analysis to be conducted and the grain size composition of the till matrix. The recommended sample mass for till matrix geochem-

Table 1. A summary of the different advantages and disadvantages of sampling at depth

Depth	Optimal Range	Drill type	Best use	Limitations
Shallow	2 m up to 10 m	• Cobra (hammer) • Talon (Rotary percussion) – good for high clasts content • Sipre (rotary)	• Near surface • Infill sampling • High-resolution sampling • Highly portable can be carried in remote regions • Inexpensive	• Difficulty in sediments with high clast content • Geochemical sampling only
Intermediate	5–20 m	• Semi-portable • Track or vehicle mounted drills • *e.g.*: Geoprobe 6011DT, Shock Auger	• Profile sampling • Semi-versatile sampling locations • Good for sampling geochemistry and indicator minerals	• Some smaller augers impeded by cobbles and boulders • Require road access or helicopter transport • Variable cost, higher than surface sampling
Deep	>20 m	• Large drill rigs • Reverse Circulation (RC) • Rotasonic drills	• Good for advanced projects • Drilling to bedrock • Good for geochemistry and indicator mineral sampling	• RC drilling destroys stratigraphy • Higher cross contamination • Typically require roads; can be helicopter slung • Most expensive

istry is 2–3 kg (Fig. 3A). Because geochemical analysis is carried out on the silt-plus-clay fraction (<0.063 mm), tills with a coarse sandy matrix or abundant clasts yield less analyzable material per kilogram, and larger samples should be collected. This is especially true in areas underlain by quartzite or sandstone (*e.g.*, Athabasca and Thelon basins), where till is typically very sandy and quartz-rich. If additional physical determinations (*e.g.*, grain size, colour, carbon content) or archiving are required, an additional ~1 kg should be collected for silty-clayey tills, and proportionally more for sandier tills. Large, obvious clasts (>2 cm) should not be included when filling the geochemical sample bag. It is good practice to have a portable scale (*i.e.*, fish scale) to ensure consistent collection weight.

Heavy Minerals

Heavy mineral samples should be collected from the same hole as the geochemical samples but collected in separate bags to allow for direct shipping to separate analytical laboratories. How much sample material to collect for heavy mineral separation and identification is largely dependent on the matrix texture of the till (*i.e.*, dominant grain size of the till matrix). In regions where the till matrix is silty to sandy (*e.g.*, Canadian Shield), 10–20 kg of till should be collected (Fig. 3A). In regions where the till is clay-rich (*e.g.*, Western Canada Sedimentary Basin), 20–40 kg of till should be collected (Fig. 3B). For clay-rich till, a larger amount of sample material is required to recover sufficient sand-size material for heavy mineral analysis. Pebbles picked from the till during sampling, or separated during subsequent sample processing in a lab, should be retained for lithological examination, which can aid in provenance determination (*e.g.*, Rice *et al.*, 2024b). As previously mentioned, the type of subsurface till sampling method used may dictate the type of analysis that can be completed (Fig. 3C).

Field Data and Notes

Although logistical and geological constraints mentioned above will dictate the methodology and tools used for till collection, the choice of field gear and methods of data collection are also important considerations for any till sampling campaign. Nowadays, field computers, tablets, or smaller handheld devices are used to capture field data. However, notebooks and handheld GPS



Figure 3. *Different types of till samples: A) A small (2–3 kg) sample for geochemistry and a larger (10–15 kg) sample for indicator mineral separation and identification; B) In regions with more silt-clay rich matrix, larger (20–40 kg) indicator mineral samples may be required to ensure recovery of a sufficient volume of sand-sized mineral grains; C) Stoney compact traction till recovered at depth as drill core using drilling methods is of sufficient size to allow geochemical and heavy mineral sampling.*

devices are essential. The sample location may also be recorded on an air photo, paper topographic map, or in a field notebook. Drones equipped with high-resolution cameras can assist with the identification of appropriate sample site locations, although a license to operate a drone may be required. Photographs should be taken of each sample site to record the sampling method, associated glacial landforms, nearby anthropogenic influences, sample depth, sampled material, and local vegetation.

Regional factors should also be considered when developing a sampling design, determining the type of data to collect, and ultimately interpreting the results. Reviewing reports from previous regional till-sampling programs is an effective starting point, particularly in areas characterized by thick Quaternary sequences and significant recycling of till in the Hudson Bay lowlands (Trommelen and Ross, 2010; Trommelen *et al.*, 2013), diverse glacial landsystems in the Arctic Islands (Utting *et al.*, 2007; Tremblay *et al.*, 2020), in mountainous terrains from the Cordillera (Bond and Plouffe, 2003; Ferbey *et al.*, 2016) or in zones with multiples ice flow directions (Brushett and Smith, 2018; Lamarche *et al.*, 2018). A suggested list of the minimum field data to record for till samples collected for heavy mineral and geochemical analyses is included in McClenaghan *et al.* (2020, 2023).

Quality Assurance and Quality Controls in the Field

Quality assurance and quality control (QA/QC) preparation begins at the planning stages of the sampling survey to ensure an appropriate portion of the budget will be assigned to include field duplicate samples, laboratory duplicates, blank samples, and standards. A significant source of variability in till geochemical or mineralogy data can be due to poorly defined field protocols (*e.g.*, Hoffman and Woods, 1991), therefore, having a strong QA/QC plan in place is essential. Normally, the analytical laboratory will have their own QA/QC procedures which adds some redundancy to the methodology and should be evaluated independently.

Tools used for sample collection must be thoroughly cleaned between sample sites by rinsing the tools in water. If water is not available, a hard plastic bristle brush and a clean cloth could be used to ensure that no material adheres to the sampling tools between sites. Metal flakes or shavings may break off drill bits, machinery, picks, or shovels and end up contaminating the

sample. It is good practice to monitor tools for their wear, to know the metallic composition of sampling tools, and to never wear hand jewellery during sample collection (Kontas, 1991).

Field duplicates should be collected from a second hole or from sediments exposed in a section up to 5 m away from the original sample site to assess homogeneity and variability. Ideally, the amount collected for a geochemical duplicate sample should be two times larger (*e.g.*, 4 kg) than the routine sample size (*e.g.*, 2 kg) because it will be split to create a laboratory duplicate (blind) after the entire field duplicate sample has been prepared in the laboratory for geochemical analysis. The field duplicate sample should not be homogenized with the original sample. The original and field duplicate samples should be collected using separate bags that are labelled with unique sample numbers. For a detailed description of the QA/QC protocols used by the GSC samples, refer to McClenaghan *et al.* (2020) and for their evaluations, *see* Reimann et al. (2008), Garrett (2013), Brouard *et al.* (2025) and Stanley (*this volume*).

Conclusions

This paper synthesizes the current best practices and methods for till sampling for geochemical and indicator minerals and serves as a summary of papers by Sarala (2015a) and McClenaghan *et al.* (2020, 2023, 2024), which contain more detailed descriptions of till sampling methods for different sampling environments. Although planning a till sampling program demands careful attention to logistical and geological constraints, early research and a well-planned survey design can set a solid framework for drift prospecting ventures. Given the increased use of more complex data manipulation methods, which produce highly abstract outputs that may obscure the direct relationship between interpretations and the original observations, such as principal component analysis and machine learning, demonstrating the reliability of data will increasingly become essential. Ultimately, till sampling aims to collect sediment that best reflects the integrated source bedrock composition of a spatially constrained up-ice source area, making it one of the most valuable tools available during the early stages of mineral exploration.

Acknowledgments

Special thanks to Beth McClenaghan for her contributions to previous publications from which this volume has been summarized; this chapter would not have been possible without her guidance.

Roger Paulen, Isabelle McMartin, Janet Campbell, and Alain Plouffe are thanked for their various photographs and figures used during the preparation of this chapter. Dr. Tommy Tremblay and Ezana Yohannes are thanked for their feedback and comments on the manuscript. Dr. Sarah Hashmi is thanked for her editorial guidance of this chapter and organization of the short course during which this chapter was presented. This summary of till sampling methods and protocols in glaciated terrain was largely derived from an output of the GSC's Geomapping for Energy and Minerals Program (GEM GeoNorth), under the Geological Evolution and Mineral Potential of the Hopedale Block sub-activity.

References

Aario, R. and Peuraniemi, V., 1992: Glacial dispersal of till constituents in morainic landforms of different types. Geomorphology, Volume 6, pages 9–25. https://doi.org/10.1016/0169-555X(92)90044-O

Averill, S.A., 1990: Drilling and sample process methods for deep till geochemistry surveys: making the right choices. *In* Application de la géologie du Quaternaire à l'exploration minérale, Association Professionnelle des géologues et des géophysiciens du Québec, pages 139–173.

Bajc, A.F., 1991: Till sampling survey, Fort Frances area, results and interpretation; Ontario Geological Survey, Study 56. https://www.geologyontario.mines.gov.on.ca/persistent-linking?publication=S056

Bird, D.J. and Coker, W.B., 1987: Quaternary stratigraphy and geochemistry at the Owl Creek gold mine, Timmins, Ontario, Canada. Journal of Geochemical Exploration, Volume 28, pages 267–284. https://doi.org/10.1016/0375-6742(87)90052-5

Bond, J.D., 2001: Quaternary geology and till geochemistry of the Anvil district (parts of 105K/2, 3, 5, 6 and 7), central Yukon Territory. Exploration and Geological Services Division, Yukon, Indian and Northern Affairs Canada, Bulletin 11.

Bond, J.D. and Plouffe, A., 2003: Yukon Targeted Geoscience Initiative, Part 2: Glacial history, till geochemistry and new mineral exploration targets in Glenlyon and eastern Carmacks map areas, central Yukon. *In* Yukon Exploration and Geology 2002. *Edited by* D.S. Emond and L.L. Lewis. Exploration and Geological Services Division, Yukon Region, Indian and Northern Affairs Canada, pages 109–134.

Brouard, E. and Godbout, P.M., 2025: Quality assurance and quality control of till compositional data using Python. Geological Survey of Canada, Open File 9309, 21 pages. https://doi.org/10.4095/ps1ht4x4vg

Brummer, J.J., MacFadyen, D.A. and Pegg, C.C., 1992: Discovery of kimberlites in the Kirkland Lake area, northern Ontario, Canada. Part II: Kimberlite discoveries, sampling, diamond content, ages and emplacement. Exploration and Mining Geology, Volume 1, pages 351–370.

Brushett, D.M. and Smith, C.G., 2018: Till geochemical data for the eastern Cobequid Highlands, Nova Scotia. Nova Scotia Department of Natural Resources, Open File Report ME 2018-003, 110 pages.

Coker, W.B., 1991: Overburden geochemistry in mineral exploration. *In* Exploration Geochemistry Workshop. *Edited by* J.M. Franklin, J.M. Duke, W.W. Shilts, W.B. Coker, P.W.B. Friske, Y.T. Maurice, S.B. Ballantyne, C.E. Dunn, G.E.M. Hall and R.G. Garrett. Geological Survey of Canada, Open File 2390, pages 3-1 to 3-60. https://doi.org/10.4095/132388

Coker, W.B. and DiLabio, R.N.W., 1989: Geochemical exploration in glaciated terrain: geochemical responses. *In* Proceedings of Exploration '87. *Edited by* G.D. Garland. Ontario Ministry of Northern Development and Mines, Special Volume 3, pages 336–383.

Dredge, L.A., 2000: Carbonate dispersal trains, secondary till plumes, and ice streams in the west Foxe Sector, Laurentide Ice Sheet. Boreas, Volume 29, pages 144–156. https://doi.org/10.1111/j.1502-3885.200.tb01207.x

Dredge, L.A., 2002: Quaternary geology of southern Melville Peninsula, Nunavut. Geological Survey of Canada, Bulletin 561. https://doi.org/10.4095/213215

Dreimanis, A., 1989: Tills: their genetic terminology and classification. *In* Genetic Classification of Glacigenic Deposits. *Edited by* R.P. Goldthwait and C.L. Matsch. A.A. Balkema, Rotterdam, pages 17–83.

Dyke, A.S. and Zoltai, S.C., 1980: Radiocarbon dated mudboils, central Canadian Arctic. *In* Current Research, Part B. Geological Survey of Canada, Scientific and Technical Notes, Paper 80-1B, pages 271–275. https://ostrnrcan-dostrncan.canada.ca/handle/1845/248083

Evans, D.J.A., 2018: Till: A Glacial Process Sedimentology. John Wiley and Sons Ltd. https://doi.org/10.1002/9781118652541

Evans, D.J.A., Phillips, E.R., Hiemstra, J.F. and Auton, C.A., 2006: Subglacial till: formation, sedimentary characteristics and classification. Earth-Science Reviews, Volume 78, pages 115–176. https://doi.org/10.1016/j.earscirev.2006.04.001

Eyles, N., Bukhari, S., Sookhan, S., Ruscica, P. and Paulen, R., 2022: LiDAR-based semi-automated mapping of drumlins and mega-scale glacial lineations of the Green Bay Lobe, Wisconsin, USA: Ice sheet beds as glaciotribological systems. Earth Surface Processes and Landforms. https://doi.org/10.1002/esp.5486

Ferbey, T., Plouffe, A. and Bustard, A.L., 2016: Geochemical, mineralogical, and textural data from tills in the Highland Valley Copper mine area, south-central British Columbia. British Columbia Ministry of Energy and Mines, British Columbia Geological Survey GeoFile 2016-11, Geological Survey of Canada Open File 8119, 20 pages. https://doi.org/10.4095/299242

French, H.M., 2007: The Periglacial Environment. John Wiley and Sons, West Sussex, England.

Garrett, R.G., 1971: The dispersion of copper and zinc in glacial overburden at the Louvem deposit, Val d'Or, Québec; *In* Geochemical Exploration, Proceedings, 3rd International Geochemical Exploration Symposium, Toronto, April 16–18. *Edited by* R.W. Boyle. Canadian Institute of Mining and Metallurgy, Special Volume 11, pages 157–158.

Garrett, R.G., 2013: The 'rgr' package for the R Open Source statistical computing and graphics environment- a tool to support geochemical data interpretation. Geochemistry: Exploration, Environment, Analysis, Volume 13, No. 4, pages 355–378. https://doi.org/10.1144/geochem2011-106

Hirvas, H. and Nenonen, K., 1990: Field methods for glacial indicator tracing. *In*: Glacial Indicator Tracing. *Edited by* R. Kujansuu and M. Saarnisto. A.A. Balkema, Rotterdam, pages 217–248.

Hoffman, S.J. and Woods, G.A., 1991: Multidisciplinary exploration of the BOG volcanogenic massive-sulphide prospect, Bathurst, New Brunswick. Canada; Journal of Geochemical Exploration, Volume 41, pages 85–101. https://doi.org/10.1016/0375-6742(91)90077-8

Johnson, M.D., Fredin, O., Ojala, A.E.K. and Peterson, G., 2015: Unraveling Scandinavian geomorphology: the LiDAR revolution. Journal of the Geological Society of Sweden, Volume 137, pages 245–251. https://doi.org/10.1080/11035897.2015.1111410

Kauranne, K., Salminen, R. and Eriksson, K., 1992: Regolith exploration geochemistry in arctic and temperate terrains. Handbook of Exploration Geochemistry, Elsevier, Amsterdam, Volume 5, eBook ISBN: 9781483291239.

Kelley, S.E., Ross, M., Elliott, B. and Normandeau, P.X., 2019: Effect of shifting ice flow and basal topography in shaping three-dimensional dispersal patterns, Lac de Gras region, Northwest Territories, Canada. Journal of Geochemical Exploration, Volume 199, pages 105–127. https://doi.org/10.1016/j.gexplo.2019.01.012

Klassen, R.A. and Thompson, F.J., 1993: Glacial history, drift composition, and mineral exploration, central Labrador. Geological Survey of Canada, Bulletin 435. https://doi.org/10.4095/183906

Kontas, E., 1991: Gold contamination of the fine fraction of till during sampling and sample preparation. Journal of Geochemical Exploration, Volume 39, pages 284–289. https://doi.org/10.1016/0375-6742(91)90017-O

Kujansuu, R. and Saarnisto, M. (ed.), 1990: Glacial Indicator Tracing. A.A. Balkema, Rotterdam.

Lamarche, O., Daubois, V. and Dubé-Loubert, H., 2018: Géologie des dépôts de surface de la région de Nemaska, Eeyou Istchee Baie-James. Ministère de l'Énergie et des Ressources naturelles, Québec, RP 2018-05, 29 pages, accompanying maps.

Levson, V.M., 2001: Regional till geochemical surveys in the Canadian Cordillera: Sample media, methods and anomaly evaluation. *In* Drift Exploration in Glaciated Terrain. *Edited by* M.B. McClenaghan, P.T. Bobrowsky, G.E.M. Hall and S. Cook. Geological Society of London, Special Publication 185, pages 45–68. https://doi.org/10.1144/GSL.SP.2001.185.01.03

McClenaghan, M.B. Parkhill, M.A., Seaman, A.A., Pronk, A.G., Averill, S.A., Rice, J.M. and Pyne, M., 2014: Indicator mineral signatures of the Sisson W-Mo deposit, New Brunswick, Part 2 till. Geological Survey of Canada, Open File 7467. https://doi.org/10.4095/293349

McClenaghan, M.B. and Paulen, R.C., 2018: Mineral Exploration in Glaciated Terrain, Chapter 20. *In* Past Glacial Environments (Sediments, Forms and Techniques) A New & Revised Edition. *Edited by* J. Menzies and J.J-M. van der Meer. Elsevier, pages 689–751. https://doi.org/10.1016/C2014-0-04002-6

McClenaghan, M.B., Paulen, R.C., Layton-Matthews, D., Hicken, A.K. and Averill, S.A., 2015: Glacial dispersal of gahnite from the Izok Lake Zn-Cu-Pb-Ag VMS deposit, northern Canada. Geochemistry: Exploration, Environment, Analysis, Volume 15, pages 333–349. https://doi.org/10.1144/geochem2014-317

McClenaghan, M.B., Paulen, R.C. and Oviatt, N.M., 2018: Geometry of indicator mineral and till geochemistry dispersal fans from the Pine Point Mississippi Valley-type Pb-Zn district, Northwest Territories, Canada. Journal of Geochemical Exploration, Volume 190, pages 69–86. https://doi.org/10.1016/j.gexplo.2018.02.004

McClenaghan, M.B., Paulen, R.C., Smith, I.R., Rice, J.M., Plouffe, A., McMartin, M., Campbell, J.E., Lehtonen, M., Parsasadr, M. and Beckett-Brown, C.E., 2023: Review of till geochemistry and indicator mineral methods for

mineral exploration in glaciated terrain. Geochemistry: Exploration, Environment, Analysis, Volume 23. https://doi.org/10.1144/geochem2023-013

McClenaghan, M.B., Spirito, W.A., Plouffe, A., McMartin, I., Campbell, J.E., Paulen, R.C., Garrett, R.G., Hall, G.E.M., Pelchat, P. and Gauthier, M.S., 2020: Geological Survey of Canada till-sampling and analytical protocols: from field to archive, 2020 update. Geological Survey of Canada, Open File 8591. https://doi.org/10.4095/326162

McMartin, I. and Campbell J.E., 2009: Near-surface till sampling protocols in shield terrain, with examples from western and northern Canada. *In* Application of Till and Stream Sediment Heavy Mineral and Geochemical Methods to Mineral Exploration in Western and Northern Canada. *Edited by* R.C. Paulen and I. McMartin. Geological Association of Canada, Short Course Notes 18, pages 75–95. ISBN: 978-1-897095-26-3

McMartin, I., Campbell, J.E., Dredge, L.A., LeCheminant, A.N., McCurdy, M.W. and Scromeda, N., 2015: Quaternary geology and till composition north of Wager Bay, Nunavut: Results from the GEM Wager Bay Surficial Geology Project. Geological Survey of Canada, Open File 7748. https://doi.org/10.4095/296419

McMartin, I., Henderson, P.J., Nielsen, E. and Campbell, J.E., 1996: Surficial geology, till and humus composition across the Shield margin, north-central Manitoba Saskatchewan: Geospatial analysis of a glaciated environment. Geological Survey of Canada, Open File 3277. https://doi.org/10.4095/207748

McMartin, I. and McClenaghan, M.B., 2001: Till geochemistry and sampling techniques in glaciated shield terrain: A review. *In* Drift Exploration in Glaciated Terrain. *Edited by* M.B. McClenaghan, P.T. Bobrowsky, G.E.M. Hall and S.J. Cook; Geological Society of London, Special Publication 185, pages 19–43. https://doi.org/10.1144/GSL.SP.2001.185.01.02

Paulen, R.C., 2009: Sampling techniques in the Western Canada Sedimentary Basin and the Cordillera. *In* Application of Till and Stream Sediment Heavy Mineral and Geochemical Methods to Mineral Exploration in Western and Northern Canada. *Edited by* R.C. Paulen and I. McMartin. Geological Association of Canada, Short Course Notes 18, pages 49–74. ISBN: 978-1-897095-26-3

Paulen, R.C., Stokes, C.R., Fortin, R., Rice, J.M., Dubé-Loubert, H. and McClenaghan, M.B., 2017: Dispersal trains produced by ice streams: An example from Strange Lake, Labrador, Canada. *In* Proceedings of Exploration 17. *Edited by* V. Tschirhart and M.D. Thomas. Sixth Decennial International Conference on Mineral Exploration, pages 871–875. https://geochem.nrcan. gc.ca/cdogs/content/pub/pub03698_e.htm

Plouffe, A., 1995: Drift-prospecting sampling methods. *In* Drift Exploration in the Canadian Cordillera, British Columbia. *Edited by* P.T. Bobrowsky, S.J. Sibbick, J.M. Newell,and P.F. Matysek. British Columbia Ministry of Energy, Mines and Petroleum Resources, Paper 1995-2, pages 43–52.

Plouffe, A., McClenaghan, M.B., Paulen, R.C., McMartin, I., Campbell, J.E. and Spirito, W.A., 2014: Quality assurance and quality control measures applied to indicator mineral studies of glacial sediments at the Geological Survey of Canada. *In* Application of Indicator Mineral Methods to Mineral Exploration. *Edited by* M.B. McClenaghan, A. Plouffe and D. Layton-Matthews. Geological Survey of Canada, Open File 7553. https://doi.org/10.4095/293858

Plouffe, A., Paulen, R.C. and Smith, I.R., 2006: Indicator mineral content and geochemistry of glacial sediments from northwest Alberta (NTS 84L, M): new opportunities for mineral exploration. Geological Survey of Canada, Open File 5121, Alberta Energy and Utilities Board, Special Report 77.

Porter, C., Morin, P., Howat, I., Noh, M.-J, Bates, B., *et al.*, 2018: ArcticDEM, version 3. Harvard Dataverse, V1. https://doi.org/10.7910/DVN/OHHUKH

Primmer, S., Bell, T. and Batterson, M., 2015: The role of ice dynamics on drift dispersal in the Newfoundland Ice Cap: preliminary investigations. *In* Current Research. Government of Newfoundland and Labrador, Department of Natural Resources, Geological Survey, Report 15-1, pages 277–285.

Proudfoot, D.N., Bobrowsky, P.T. and Meldrum, D.G., 1995: Drift exploration potential maps derived from terrain geology maps. *In* Drift Exploration in the Canadian Cordillera. *Edited by* P.T. Bobrowsky, S.J. Sibbick, J.M. Newell and P.F. Matysek. British Columbia Ministry of Energy, Mines and Petroleum Resources, Paper 1995-2, pages 43–52.

Reyes, A.V. and Clague, J.J., 2004: Stratigraphic evidence for multiple Holocene advances of Lillooet Glacier, southern Coast Mountains, British Columbia. Canadian Journal of Earth Sciences, Volume 41, pages 903–918. https://doi.org/10.1139/e04-039

Reimann, C., Filzmoser, P., Garrett, R.G. and Dutter, R., 2008: Statistical Data Analysis Explained: Applied Environmental Statistics with R. John Wiley and Sons, Chichester, 343 pages. https://doi.org/10.1002/9780470987605

Rice, J.M. and McClenaghan, M.B., 2024: Dirt detectives: Unravelling buried mineral potential with advanced till sampling techniques. *In* Till Geochemistry and Indicator Mineral Methods for Exploration in Glaciated Terrains. *Edited by* R.C. Paulen and M.B. McClenaghan. Geological Survey of Canada, Open File 9210, pages 24–34. https://doi.org/10.4095/pbmy2d03m0

Rice, J.M., Paulen, R.C., Campbell, H.E. and Ross, M., 2024a: The surficial geology record of ice stream catchment dynamics and ice-divide migration in the Québec-Labrador sector of the Laurentide Ice Sheet. Quaternary Science Advances, Volume 13. https://doi.org/10.1016/j.qsa.2023.100123

Rice, J.M., Ross, M., Campbell, H.E., Paulen, R.C. and McClenaghan, M.B., 2024b: Net evolution of subglacial sediment transport in the Québec-Labrador sector of the Laurentide Ice Sheet. Canadian Journal of Earth Sciences. https://doi.org/10.1139/cjes-2023-0050

Salminen, R., 1992: Scale of geochemical surveys, Chapter 7. *In* Regolith Exploration Geochemistry in Arctic and Temperate Terrains. *Edited by* K. Kauranne, R. Salminen and K. Eriksson. Handbook of Exploration Geochemistry, Elsevier, Amsterdam, Volume 5, pages 165–183. eBook ISBN: 9781483291239

Sacco, D. 2024: Strategic applications of shallow overburden drilling for drift prospecting. *In* Till Geochemistry and Indicator Mineral Methods for Exploration in Glaciated Terrains. *Edited by* R.C. Paulen and M.B. McClenaghan. Geological Survey of Canada, Open File 9210, pages 35–40. https://doi.org/10.4095/pbmy2d03m0

Sacco, D.A., Janzen, B. and Jackaman, W., 2022a: Mineral exploration in the Central Interior Copper-Gold Research projects area, central British Columbia (parts of NTS 093A, B, G, J, K, O): New tools for a proven approach to exploration under cover. *In* Geoscience BC Summary of Activities 2021: Minerals. Geoscience BC, Report 2022-01, pages 1–10.

Sacco, D., McGregor, C., Janzen, B., Knox, C. and Wolter, A., 2022b: Surficial geology, drift thickness and till sampling suitability maps (NTS 093A/13; 093G/01, 07, 09, 10, 16), British Columbia. Geoscience BC, Report 2022-08, scale 1:50 000.

Sarala, P., 2005: Till geochemistry in the ribbed moraine area of Peräpohjola, Finland. Applied Geochemistry, Volume 20, pages 1714–1736. https://doi.org/10.1016/j.apgeochem.2005.04.018

Sarala, P., 2015a: Surficial geochemical exploration methods, Chapter 10.1. *In* Mineral Deposits of Finland. *Edited by* W.D. Maier, R. Lahtinen and H. O'Brien. Elsevier, Amsterdam, pages 711–731.

Sarala, P., 2015b: New technologies for greenfield exploration. Geological Survey of Finland, Paper 57.

Shilts, W.W., 1978: Nature and genesis of mudboils, central Keewatin, Canada. Canadian Journal of Earth Sciences, Volume 5, pages 1053–1068. https://doi.org/10.1139/e78-113

Sibul, I., Plado, J. and Jõeleht, A., 2017: Ground-penetrating radar and electrical resistivity tomography for mapping bedrock topography and fracture zones: A case study in Viru-Nigula, NE Estonia. Estonian Journal of Earth Sciences, Volume 66, pages 142–151. https://doi.org/10.3176/earth.2017.11

Stea, R.R. and Brown, Y., 1989: Variation in drumlin orientation, form and stratigraphy relating to successive ice flows in southern and central Nova Scotia. Sedimentary Geology, Volume 62, pages 223–240. https://doi.org/10.1016/0037-0738(89)90117-6

Strand, P., Banas, A., Baumgartner, M. and Burgess, J., 2009: Tracing kimberlite indicator mineral dispersal trains: An example from the Churchill Diamond Project, Kivalliq region, Nunavut. *In* Application of Till and Stream Sediment Heavy Mineral and Geochemical Methods to Mineral Exploration in Western and Northern Canada. *Edited by* R.C. Paulen and I. McMartin. Geological Association of Canada, Short Course Notes 18, pages 167–175.

Tremblay, T., Sasseville, C. and Godbout, P.M., 2020: Geochemistry and mineralogy of glacial sediments in the Fury and Hecla area, northwestern Baffin Island, Nunavut. *In* Summary of Activities 2019. Canada-Nunavut Geoscience Office, pages 51–64.

Trommelen, M. and Ross, M., 2010: Subglacial landforms in northern Manitoba, Canada, based on remote sensing data. Journal of Maps, pages 618-638. https://doi.org/10.4113/jom.2010.1142

Trommelen, M., Ross, M. and Campbell, J.E., 2013: Inherited clast dispersal patterns: Implications for palaeoglaciology of the SE Keewatin Sector of the Laurentide Ice Sheet. Boreas, Volume 42, Issue 3, pages 693–713. https://doi.org/10.1111/j.1502-3885.2012.00308.x

Utting, D.J., Gosse, J.C., Hodgson, D.A., Trommelen, M.S., Vickers, K.J., Kelley, S.E. and Ward, B., 2007: Report on ice-flow history, deglacial chronology, and surficial geology, Foxe Peninsula, southwest Baffin Island, Nunavut. *In* Current Research. Geological Survey of Canada, Paper 2007-C2, 13 pages.

Ward, B.C., Leybourne, M.I. and Sacco, D.N., 2011: Drift prospecting within the QUEST Project area, central British Columbia (NTS 093J): Potential for porphyry copper-gold, volcanogenic massive sulphide mineralization and gold-copper veins. *In* Geoscience BC Summary of Activities 2010. Geoscience BC, Report 2011-1, pages 73–96.

Field Identification of Past Glacial Flow Trajectories and Ice Streams

Roger C. Paulen[1], Riley P.M. Mulligan[2], Martin Ross[3], and Nick Eyles[4]
[1]Geological Survey of Canada, 601 Booth Street, Ottawa, ON, K1A 0E8
[2]Ontario Geology Survey, 933 Ramsey Lake Road, Level 3, Sudbury, ON, P3E 685
[3]University of Waterloo, 200 University Avenue West, Waterloo, ON, N2L 3G1
[4]University of Toronto, Scarborough Campus, 1265 Military Trail, Scarborough, ON, M1C 1A4

Abstract

Determination of former ice-flow directions is undertaken through analysis of a variety of erosional and depositional landforms and features, including streamlined and other directional landforms in drift and bedrock, striations and other small-scale erosional forms on bedrock or boulders, and in situ *measurements of pebbles, boulders, and structural features in till. Exploration success also relies on incorporating local ice-flow observations into regional ice-flow interpretations. Even when clear directional features are identified, the application of ice-flow information to drift prospecting is not always straightforward. Flow directions may change from regional ice flow that is apparently unimpeded by the terrain to topographically controlled (local) flows that exhibit strong changes in ice-flow directions around local topographic features. Regional dispersal trains can be weakly modified, redirected, displaced, or seemingly unaffected by deviations in local topographically controlled ice flow.*

Older glacial sediments, landforms, and erosional flow indicators may also be preserved at surface, as a relict terrain, with almost no modification by subsequent ice flows, resulting in major discontinuities in regional ice-flow trends. The dynamic nature of glacial dispersal centres and the wide occurrence of ice streams, the presence of large continental glaciolacustrine basins, the occurrence of relict landscapes under ice divides, and cold-based ice all interplay with the complexity of the ice sheets that once covered large portions of the Northern Hemisphere.

Ice stream are corridors that occur within an ice sheet that flow more rapidly than the surrounding ice. The geomorphic imprint of ice streams over hard-bed, higher relief areas tends to be less obvious because of thinner till cover and an absence of diagnostic geomorphic features such as shear margin moraines. Despite the relatively thin till cover in some regions of the

Canadian Shield, the extremely high concentrations of mineralized (exotic) debris within the till 10s of kilometres down-ice from their sources is quite remarkable. Typically, under normal ice flow conditions in areas of hard-beds on the Canadian Shield, dispersal trains formed by erosive ice are diluted over relatively short distances (<5 km) down-ice. The long (10s of km) dispersal trains of till with distinct chemical and/or mineralogical compositions, coupled with obvious erosive/depositional corridors of streamlined landforms, provide a means of identifying hard-bedded ice streams elsewhere in northern Canada.

Introduction

Drift prospecting involves the identification of dispersal trains in glacial sediments and subsequent tracing to the source by following the glacial flow-path directions to the mineralized bedrock (*see* also DiLabio and Coker, 1989; DiLabio, 1990; Puranen, 1990; Bobrowsky *et al.*, 1995; McClenaghan *et al.*, 2001; Paulen and McMartin, 2009; Ferbey *et al.*, 2017; McClenaghan and Paulen, 2018). Dispersal trains are lithological, mineralogical, or geochemical indicators of economic mineralization that can be traced in glacial deposits to locate their bedrock source (e.g. Klassen, 2001). To ensure success in tracing an indicator back to its bedrock source, it is necessary to know the trajectories of ice flow that eroded the source and influenced the mineralized glacial debris during its transportation and deposition (Hirvas and Nenonen, 1990). Dispersal trains can develop over topographic barriers, cross one or more drainage basins, may be shifted and reworked due to the time-transgressive process of migrating ice-dispersal centres (ice divides), and elongated due to ice streaming, with many examples cited in the literature noted above.

Once an ore indicator is discovered in the glacial sediments, it is necessary to know precisely the direction(s) of ice flow that may have influenced its course during transport. This assessment of ice-flow directions should be carried out and confirmed based on the widest possible range of evidence, from large landform indicators down to small outcrop-scale indicators. Often, the dispersal train itself or other indicator trains documented in the area will serve to show the net direction of glacial erosion, entrainment, and deposition, as well as any unexpected patterns, such as displaced dispersal trains. Since local ice-flow directions can deviate quite markedly from regional flow patterns, observations of ice flow on a local scale are essential at or near the site of the ore indicator discovery.

Ice streams erode and disperse large amounts of glacial debris, producing well defined tracts of far-travelled and exotic glacial debris (*e.g.*, Bennett, 2003; Dyke, 2008; Ross *et al.*, 2009; Spagnolo *et al.*, 2016; Sookhan *et al.*, 2021). These fast-flowing corridors can be tens of metres to tens of kilometres wide and are identified by streamlined glacial morphology with highly attenuated landforms, or mega-scale glacial lineations (MSGLs) having length:width ratios exceeding 10:1 (Hart, 1999; Spagnolo *et al.*, 2014) and sharply delineated margins (Stokes and Clark, 1999). In hard-bedded terrain, such as the Canadian Shield, thinner till deposits may result in the absence of glacial geomorphic features and other ice stream identification criteria include strongly eroded and sculpted bedrock forms (Krabbendam *et al.*, 2016) and the long distance dispersal of exotic clasts and till (*e.g.*, Paulen *et al.*, 2017; Sookhan *et al.*, 2021).

The objective of this short course paper is to illustrate and provide criteria for the recognition of landforms and other site-specific glacial features that indicate the former ice-flow directions. We also highlight the differences between documented dispersal trains created by 'normal' (steady state) glacial flow and those created by faster flowing ice. This paper, and accompanying presentation, can only provide a broad overview of this topic and the examples presented here represent a minor portion of glacial geomorphology that is summarized in McMartin and Paulen (2009). The content herein is, in part, taken from previous summaries by Paulen *et al.* (2024a, b), those two papers were published as part of a volume from a two-day short course "Till Geochemistry and Indicator-mineral Methods for Exploration in Glaciated Terrains" offered at the PDAC conference in 2024 (Paulen and McClenaghan, 2024) and offer additional information.

It is strongly recommended that persons attempting to develop skills in ice-flow reconstruction at any scale using satellite imagery, digital elevation models (DEMs), airphoto interpretation, and/or landform analysis should read additional material such as Mollard's (1996) airphoto atlas, Sauer and Elder's (1982) accompanying guide, and Ryder (1995). In addition, reviews of ice-flow indicators and field methods for ice-flow indicator mapping are provided by Prest (1983), Kujansuu and Saarnisto (1990), Lundqvist (1990), Ryder (1995), and Benn and Evans (2010).

Glacial Landforms

In areas with little or no previous ice-flow reconstructions, preliminary information on ice-flow directions can be obtained from oriented glacial landforms visible on topographic maps, aerial photographs, satellite imagery, and digital elevation models (DEMs). Streamlined (linear) subglacial bedforms composed of glacial sediments, such as drumlins, flutings, and crag-and-tail forms consisting of elongated ridges and intervening depressions aligned parallel to the ice-flow direction, are relatively easy to identify on multiple data sources (Fig. 1A). Streamlined landforms typically occur in groups and show as a characteristic pattern of multiple ridges on airphotos (Kujansuu, 1990). These features can be enhanced by vegetation patterns that result from variations in soil thickness and water drainage between the crests of ridges and intervening troughs. This initial overview of landforms on maps and air photographs can provide a good general impression of ice-flow directions in the area, which can then be studied in detail in the field (Smith

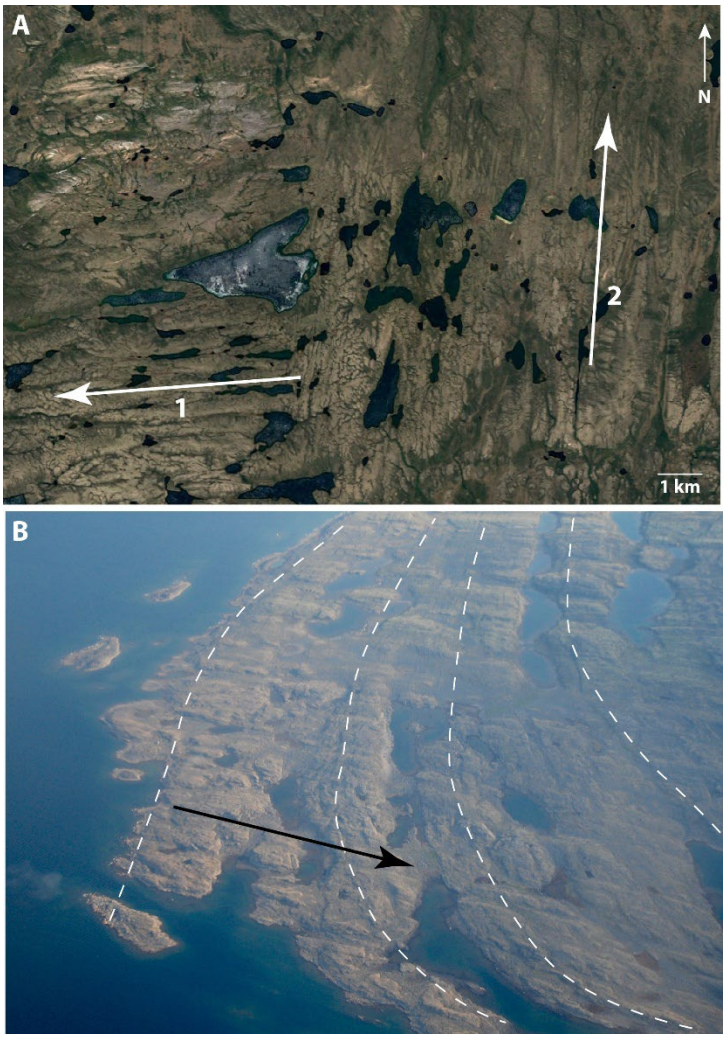


Figure 1. *A) Two sets of streamlined subglacial bedforms oriented parallel to former phases of ice flow from the Laurentide Ice Sheet towards the west (1), then north (2), on the northeast margin of Great Bear Lake, Northwest Territories (image source: Landsat 7 with 15 m resolution panchromatic band); B) Oblique aerial photograph of thin till over Canadian Shield bedrock, southwest region of Baffin Island. The terrain is dominated by the regional structure of the bedrock geology (white dashed lines) with a light overprinting from the northern Laurentide Ice Sheet (black arrow) with streamlined bedrock and small till ridges.*

and Clark, 2005). A weakness of this method is that there are sometimes extensive areas that lack oriented glacial forms entirely. In some regions, the orientation and structure of the bedrock at or near the surface can occur in a similar manner, which can prove deceptive when attempting to identify directions of ice flow from remote sensing data alone (Fig. 1B).

Streamlined landforms are also eroded into local bedrock and are used in the reconstruction of ice-flow directions. Very large bedrock forms, such as flyggbergs (Fig. 2A), usually are rare (Glasser and Warren, 1990), but under the right erosive conditions, large glacially streamlined landforms can develop in hard bedded terrain (*i.e.*, shield cratons), particularly by fast-flowing ice, or ice streams (Krabbendam *et al.*, 2016). Glacially eroded streamlined bedrock hills are commonly termed rock drumlins, and are often enhanced by mantles and streamlined 'tails' of glacial sediments (Lundqvist, 1990; McMartin and Paulen, 2009). These forms typically are asymmetrical with a thinner down-ice tail and thus indicate the direction of ice flow. Erosional crag-and-tail landforms produced by the streaming of ice around resistant bedrock obstacles, and

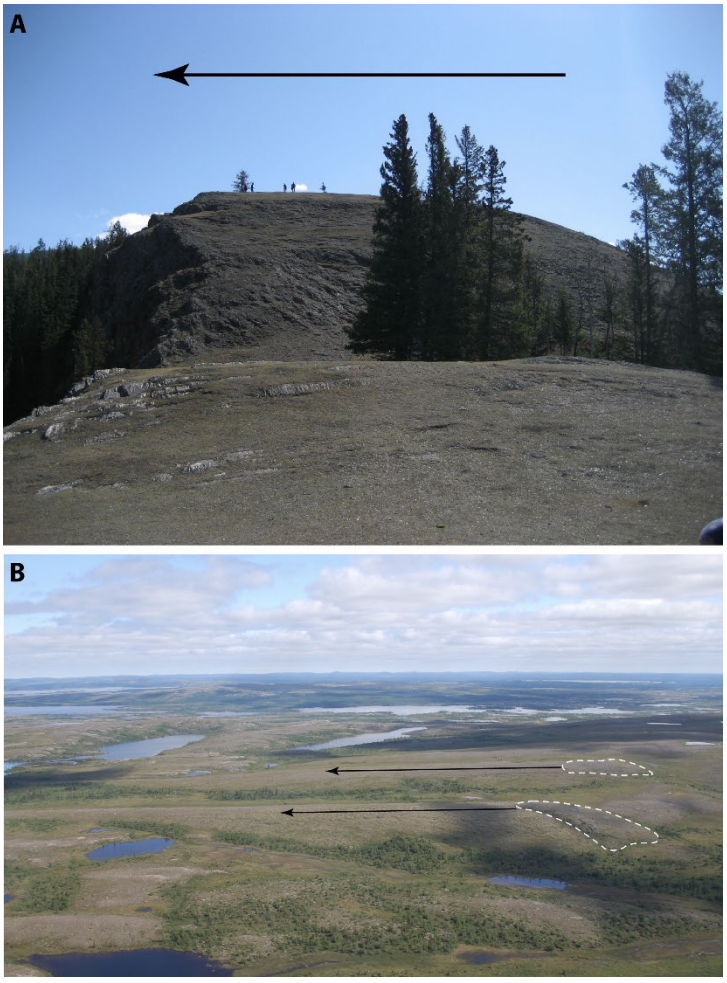


Figure 2. *Examples of bedrock-controlled glacial landforms. A) A very large glacially sculpted bedrock hill in Jasper National Park (Old Fort Point), called a 'flyggberg'. Ice flow is from right to left (arrow); note the streamlined, up-ice, or stoss side, on the right and the plucked down-ice, or lee, side on the left. There are people on top of the hill for scale; B) Outcrop knobs in northeastern Québec (outlined by white dashed lines) that have long 'tails' of till that have formed in the lee side, or down-ice to form crag-and-tail landforms. Crag-and-tail morphologies are excellent indicators of former trajectories (black arrows) of glacial erosion and depositional processes.*

subsequent protection of the tail from erosion, are distinct from depositional forms such as large flutings and cavity fills deposited in the lee of basal obstructions, but can still be used to determine regional ice-flow trends (Fig. 2B).

More commonly, relatively medium- to small-sized glacially sculpted bedrock landforms can be observed and mapped from air photos, DEMs, and on the ground. These include roches moutonnées, whalebacks, and bedrock sculpting such as stoss-and-lee forms (Fig. 3). Although these bedrock forms are mostly rounded and shaped by glacial erosion, their morphologies can be strongly influenced by the alignments of planes of weakness such as joints, bedding, and foliation or from preglacial weathering (Fig. 4).

In some areas, particularly underneath former ice divides, crosscutting and superimposed streamlined landforms can be found (*e.g.*, Stea and Brown, 1989; Clark, 1994; McMartin and Henderson, 2004; Rice *et al.*, 2024). These palimpsest streamlined landforms are interpreted to be the result of drastic changes in ice-flow directions, concomitant with adjustments in the overall shape of the ice sheet. Furthermore, the final flow phase indicated by glacial landforms may differ from dominant sediment transport paths (Fig. 5), therefore the evidence from landforms should be filled out with other investigations, such as studies of till provenance, fabric, stratigraphy, and facies, as well as detailed striation mapping (Lundqvist, 1990; McMartin and Paulen, 2009).

Glacial Erosional Outcrop Forms

In areas with a thin or moderate till cover, smaller erosional features, indistinguishable on regional imagery, are a reliable means of determining directions and history of ice flow (Rea, 2013). Grooves and striae (striations) are scratches made by rocks embedded in moving ice as they were dragged across bedrock (Fig. 6). Striae are found on smooth glacially polished surfaces; they are quite shallow and may be difficult to see on some lithologies. Striae are best preserved on fine-grained rocks that have not experienced intense post-glacial weathering. Ultramafic, mafic to intermediate volcanic rocks, limestone, quartzite, and greywacke commonly are the best lithologies to preserve striae. Striae are less common on coarse-textured intrusive rocks, medium- to high-grade metamorphic rocks, and clastic sedimentary rocks, but you can sometimes see fine polishes on quartz veins, which are relatively resistant to post-glacial erosion. Finding striations



Figure 3. *Medium- to small-sized glacially-sculpted bedrock landforms with ice-flow directions indicated by arrows. A) A stoss-and-lee outcrop above the treeline in northern Labrador; B) A stoss-and-lee sculpted outcrop on the Melville Peninsula, Nunavut (rock hammer for scale); C) A large stoss-and-lee outcrop that has been cleaned off for landscaping in central Finland; D) A house perched on a large glacially sculpted and grooved whaleback bedrock form in Hopedale, Labrador; E) A grooved and polished whaleback outcrop on the eastern shore of Georgian Bay, Ontario, which has been cleaned off for landscaping (photograph by Nick Eyles); F) A grooved and polished stoss-and-lee landform on the Labrador coastline, near Makkovic (field notebook for scale).*

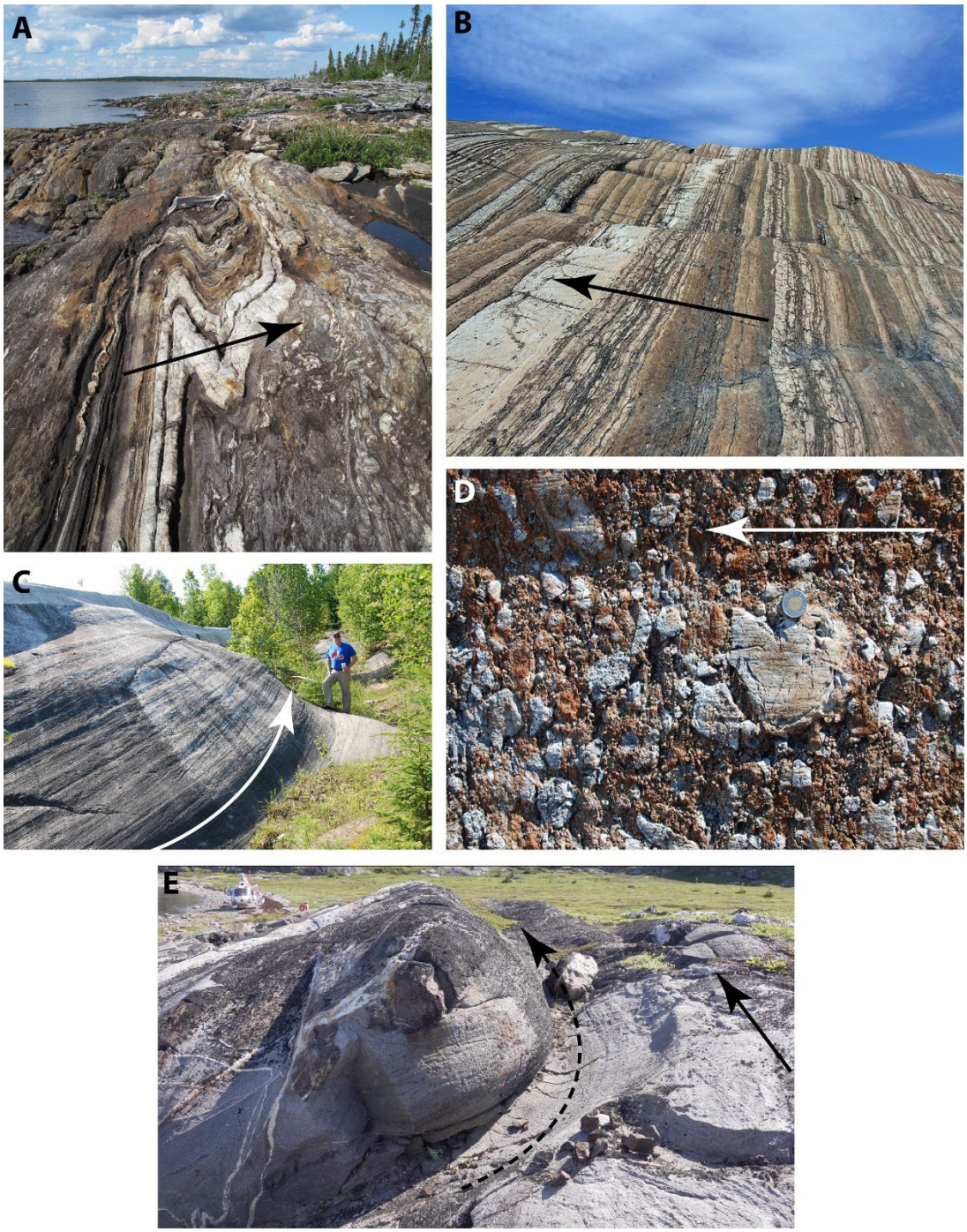


Figure 4. *Glacially eroded outcrop morphologies influenced by the bedrock geology with the ice-flow directions indicated by arrows. A) Migmatite whereby the biotite-rich melanosome layers have been differentially eroded relative to the quartz-rich leucosome layers (southern shore of the Smallwood Reservoir in Labrador, photo by Beth McClenaghan); B) Metasedimentary bedrock with differential erosion between the darker schistose layers and lighter quartzite beds (Belcher Islands, photo by Jean Veillette); C) Curvilinear glacial-erosion marks by ice preferentially eroding softer Proterozoic marble relative to the resistant volcanic and granitic bedrock (Cantley, Québec); D) An iron-altered quartzite clast conglomerate, where larger grooves can be seen in the rock matrix, and finer striations on the quartzite clasts (east of Schefferville, Labrador; Canadian two-dollar coin for scale); E) Glacial erosion has stripped off the soft regolithic material on this granitic gneiss but preserved the hard corestone, a relic of preglacial chemical weathering. Ice flow at this site is shown by the black solid arrow; note how the glacial ice was deflected around the corestone (dashed black arrow), deviating by almost 90° (coastal Labrador).*

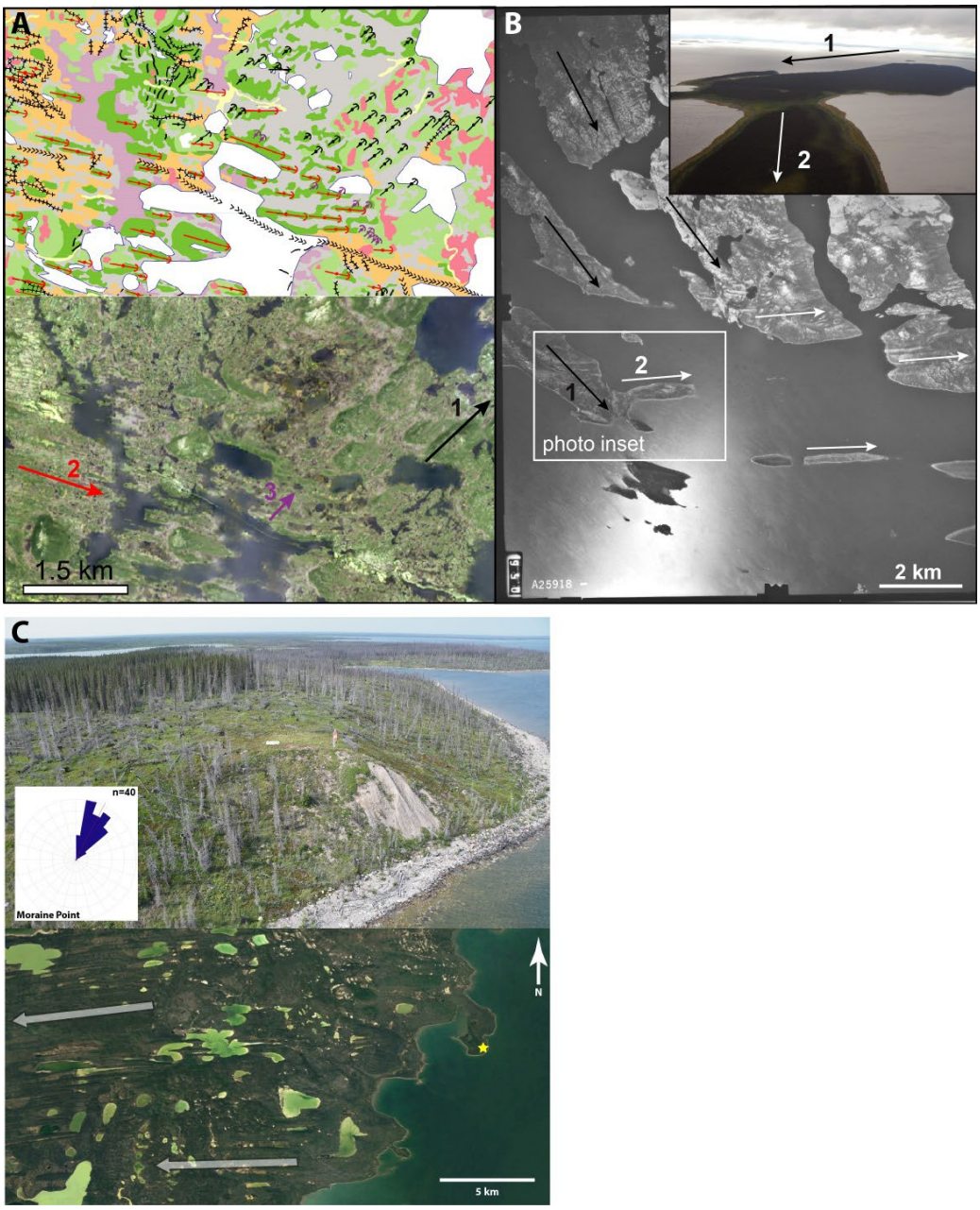


Figure 5. *Examples of palimpsest landforms and where there is a discordant trend between the general direction of glacial erosion and transport and the surface landforms, which are often megascale glacial lineations formed by erosion beneath ice streams during deglaciation. A) A localized detailed surficial map from southwest of Lac aux Goélands in northeastern Québec (Paulen* et al.*, 2022; Rice* et al.*, 2024). This region shows the complex evolution of landforms from a strong northeast ice flow (phase 1, black landforms), then a strong east ice flow (phase 2, red landforms), and a weaker deglacial northeast ice flow (phase 3, purple landforms). The few early phase 1 landforms are best preserved in areas of thin to no glacial cover, with major overprinting by phase 2 ice in regions of thicker till deposits that were subsequently modified during a late deglacial ice-flow during phase 3. The change in landscapes is also evident on satellite imagery (Landsat 8 with 15 m resolution panchromatic band); B) Examples of crosscutting landforms on a 1:50 000 scale air photo from the northwest Smallwood Reservoir, Labrador, where larger and older southeast-trending landforms (1, black arrows) have been reworked by later eastward flow (2, white arrows); note that the inset oblique aerial photo was captured facing west; C) An exposure of till at Moraine Point, on the west side of Great Slave Lake, Northwest Territories (yellow star in Landsat image). A clast fabric collected from about 4 m from surface illustrates that the till was accreted from ice flowing to the southwest, while the streamlined landforms at surface to the west strongly reworked the landscape by an eastward flowing ice stream (image source: Landsat 7 with 15 m resolution panchromatic band).*

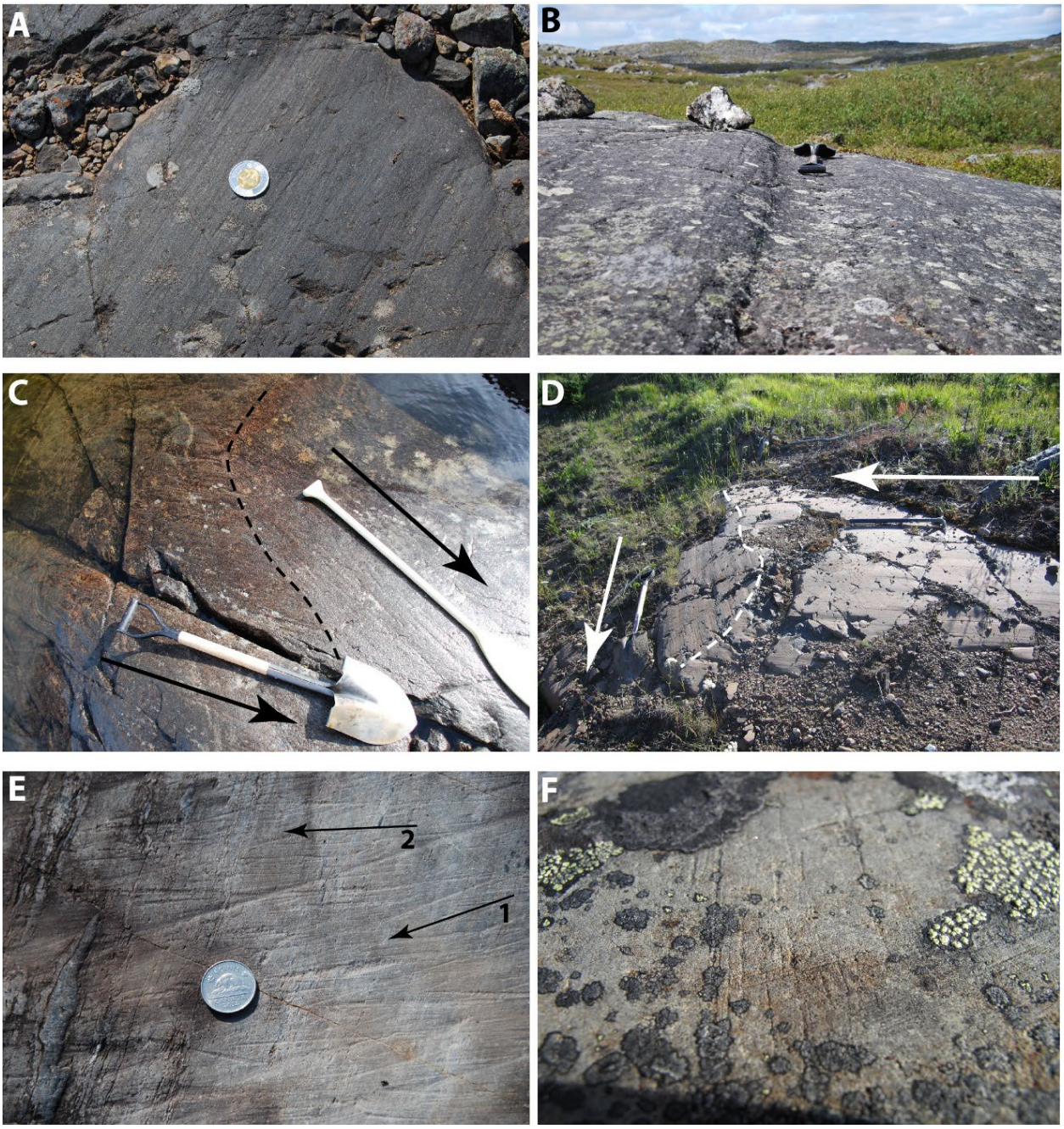


Figure 6. *Examples of striated and grooved bedrock. A) Striations preserved on a mafic metavolcanic outcrop in eastern Québec (Canadian two-dollar coin for scale); B) A large glacial groove eroded into a granitic gneiss, with shovel inside the groove for scale (eastern Northwest Territories); C) An outcrop with faceted surfaces showing an older ice flow (paddle) preserved in the lee side of the younger ice flow (shovel) in eastern Northwest Territories; the dashed line demarks the edge or intersection of the faceted surfaces; D) An outcrop with two ice-flow directions at right angles to each other, each preserved on a faceted surface in the central interior of British Columbia (photo by Crystal Huscroft, modified from Plouffe* et al.*, 2009). The older flow (shovel) is preserved in the lee side facet of the younger flow (geo-pick); E) On flat surfaces, larger grooves and finer striations help determine the relative ages of the ice-flow phases. The older larger grooves (flow 1) have been overprinted by a younger finer polish (flow 2; Canadian five-cent coin for scale); F) On flat surfaces with sets of fine crosscutting striations, it is almost impossible to determine former directions of ice flow and relative ages; this is where other indicators (*e.g.*, outcrop shape and sculpting, behaviour with the nature of the bedrock,* e.g.*, differential erosion around quartz veins or clasts, and associated landforms) are necessary.*

depends upon a variety of local circumstances, and in places where the bedrock has undergone intense structural jointing and fracturing, the exposed bedrock will not be ideal for the preservation of glacial polish. Additionally, lichen, mosses, and other plant life often obliterate the formerly polished surface of an outcrop. However, striae are easily found where bedrock has been recently exhumed, such as roadcuts and ditches. In more remote regions, some effort is often required to dig around the sculpted edges of an outcrop (Fig. 7).

As with large-scale landforms, the trend of ice flow is easily identified by striae, but determining the direction of flow is usually difficult. In some cases, the outcrop surface is sculpted and faceted into a stoss-and-lee form (Fig. 3), which provides a sense of the former ice-flow direction. An excellent directional indicator can be readily determined from striae where differential erosion or abrasion of bedrock that contains hard mineral grains or which is of inhomogeneous nature (*e.g.*, conglomerate, volcaniclastic breccia, quartz veins, *etc.*) has formed "rat-tails" (*i.e.*, miniature crag-and tail-forms) on an outcrop face. Small knobs of harder rock protrude with tails of softer rock extending down-flow (Fig. 8A–D). Other less reliable features include 'nail-head' striations, which are characterized by individual striations that broaden as the contact point between the rock being transported by the ice and the bedrock surface increases, and end abruptly as the force of friction exceeds the forces of the ice holding the rock at the base of the glacier (Fig. 8E, F). Lastly, directional ice flow can also be indicated by crescentic fractures (Fig. 9).

No Outcrop? Ice Flow Determinations from Till

In areas with little or no bedrock exposure, or bedrock with poor preservation potential (*e.g.*, younger Mesozoic of western Canada), deciphering former glacial flow paths is limited to ice-flow indicators such as drift landforms (drumlin ridges and fluted plains), rare striated boulder pavements, clast orientation fabrics, and bullet-shaped boulders.

Striated boulder pavements are usually only observed in natural sections such as those exposed along rivers or in man-made exposures such as roadcuts and borrow pits. These can form as polished armoured surfaces from glacial overriding of gravel deposits (Krüger, 1984; Paulen and McClenaghan, 2015) or as an erosional surface within a till sequence where they are typically one



Figure 7. *A few examples of how to find or reveal striations on bedrock surfaces when they are not freshly exposed in roadcuts, along lake shores, or rivers. A) At a site in western Nunavut, till is carefully scraped away from a glacially eroded bedrock surface; B) At the same site as (A) after the outcrop is cleaned, brushed away, and moistened, the glacially polished surface is revealed; C) Another example of striations preserved along the edge of a sculpted outcrop (Brunton compass for scale); D) The use of water on the outcrop surface can help immensely in observing striations and small grooves on this metasediment (Sharpie marker for scale); E) Application of water to this outcrop of glacially smoothed migmatite highlights the striations, making them easier to measure and photograph. F) Sometimes, positioning yourself to see the sunlight reflecting off the glacial polish can greatly aid seeing and measuring ice-flow direction (Brunton compass for scale).*

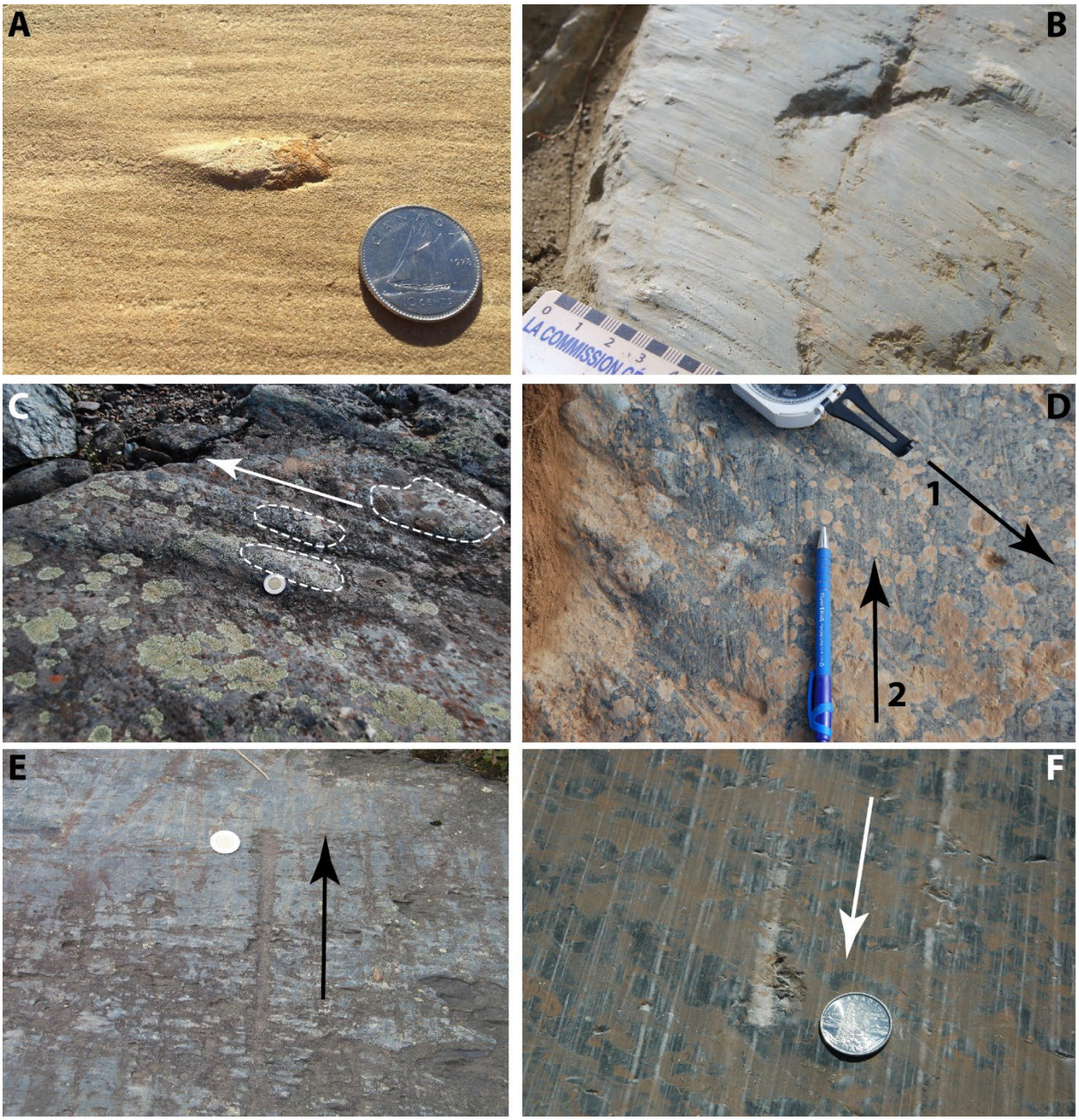


Figure 8. *Examples of directional erosional ice-flow indicators with ice-flow direction shown by arrows. A) A small rat-tail that has formed in the lee-side of a pebble within a sandstone (ice flow is from right to left; Canadian ten cent coin for scale); B) Very small rat-tails formed from quartz eyes in a metamorphosed rhyolite (ice flow is from left to right); C) Large rat-tails formed in migmatite with quartz boudins (outlined by white dashed lines) that were more resistant to glacial abrasion (Canadian two-dollar coin for scale); D) Larger rat-tails formed in a metamorphosed volcaniclastic sediment from ice flowing parallel to the Brunton compass (flow phase 1). A later ice-flow phase (2, blue pen) has overprinted finer striations on top of the rat-tails but has not obliterated the forms, which also provides an age relationship; E) Large nail-head striations gouged into metasedimentary rock; note how the striation increases in width and depth before it terminates (Canadian two-dollar coin for scale); F) Small nail-head striation formed on limestone, which helps determine direction of glacial abrasion on a very flat surface (Canadian twenty-five cent coin for scale).*

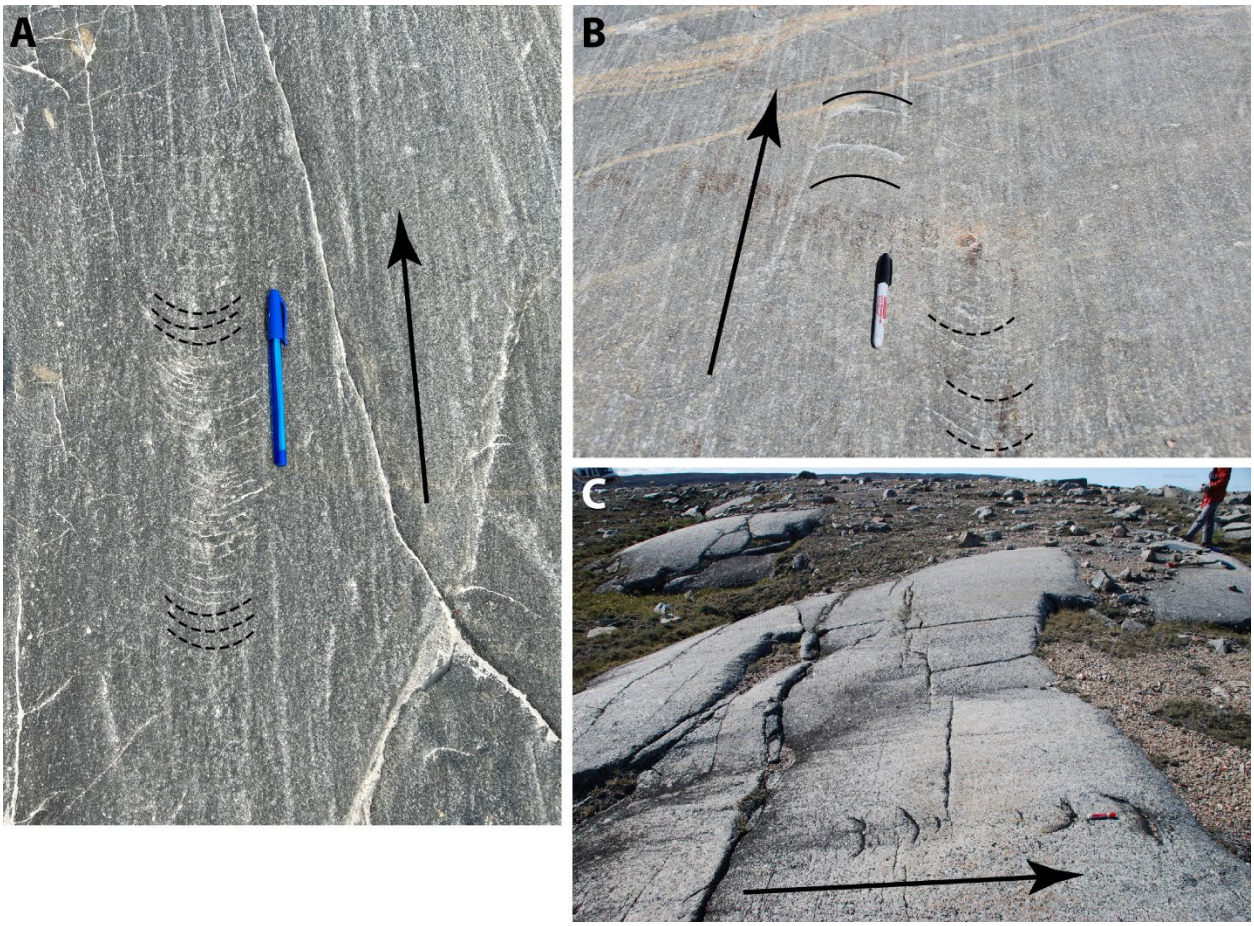


Figure 9. *Examples of directional ice-flow indicators, with the ice flow direction shown by arrows. A) Crescentic fractures (some are outlined by dashed black curves) formed into the surface of a silicified mafic xenolith; the apex of the fracture always points up-ice (pen for scale); B) A glacially striated and polished gneissic leucogranite with both crescentic fractures (dashed curves) and crescentic gouges (solid curves) (Sharpie marker for scale); C) Large crescentic gouges formed on a glacially sculpted tonalite granite. These are formed by glacial quarrying of the rock surface; the apex of the gouge always points down-ice (red whiteboard marker for scale).*

clast thick and clasts can either be in contact with each other or separated by enclosing sediment (Clark, 1991; Hicock, 1991). The clasts in these pavements are faceted (planed tops) and striated on their upper surfaces, indicating an erosive ice bed (Fig. 10). Care has to be exercised when interpreting boulder pavements, as clasts could have been faceted by earlier entrainment at the base of an ice sheet and simply reworked into a boulder pavement by successive ice flow (McMartin and Paulen, 2009).

Clast orientation analysis (*i.e.*, till fabrics) can be conducted within till deposits. Information about ice-flow direction is preserved in the arrangement of elongated clasts in till deposited under ice sheets. As tills are accreted and deform (*i.e.*, active or deforming bed), prolate clasts (*i.e.*, clasts having an a-axis or length-to-width ratio of 2:1, or greater) within the active layer tend to rotate

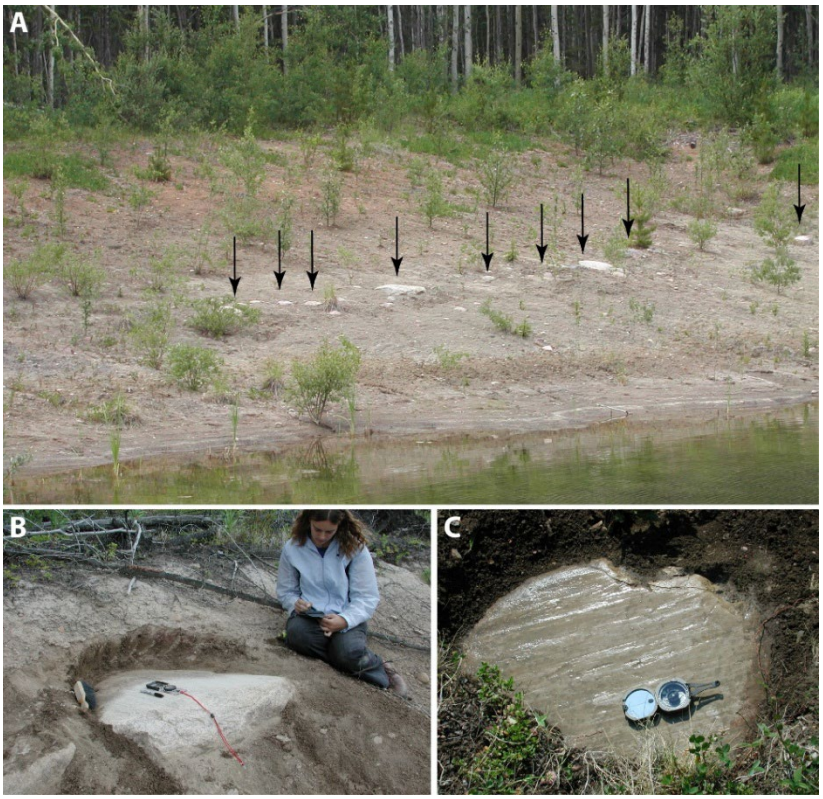


Figure 10. *Examples of where boulder pavement in till can be used as an ice-flow indicator. A) A horizon of boulders (indicated by arrows) in the wall of a roadside borrow pit; B) Ideal boulders will have faceted or planed upper surfaces created by glacial erosion of the lodged boulder; C) Striations measured from several boulders should have similar trends and, if so, represent an erosional ice-flow indicator similar to a striated outcrop (Brunton compass for scale).*

into a stable, flow-parallel position as long as the stress direction remains uniform (Larsen and Piotrowski, 2003). Once clasts become aligned, they tend to stay aligned parallel to the shear direction when exposed to high-strain rates, giving a high fabric strength (Hooyer and Iverson, 2000). However, stone-rich tills tend to have lower fabric strength because of more frequent clast collisions (Ildefonse *et al.*, 1992). This is a statistical exercise, and a minimum of 50 clast measurements is required (Benn and Lukas, 2021) to reduce statistical variance and to calculate the relative strength (eigenvalues) using an Equal Area Stereonet (Fig. 11). Careful interpretation of till fabric data is necessary as this is a statistical method, and consequently not every till fabric analysis will yield the true direction of glacial flow, or indeed any direction at all. This means that little weight can be attached to the results of a single till fabric analysis unless it is backed up by observations of other ice-flow indicators.

Conclusions based on till fabric evidence alone require a number of analyses to be made in the same area. A till clast fabric may represent an amalgam of several previous glacial flow directions involving initial transport, differential stresses at or near the glacier sole, deformation, reorient-tation during deposition, and subsequent modification by deglacial processes. Local variations in subglacial topography, ice temperature and ductility, and debris concentrations produce differing

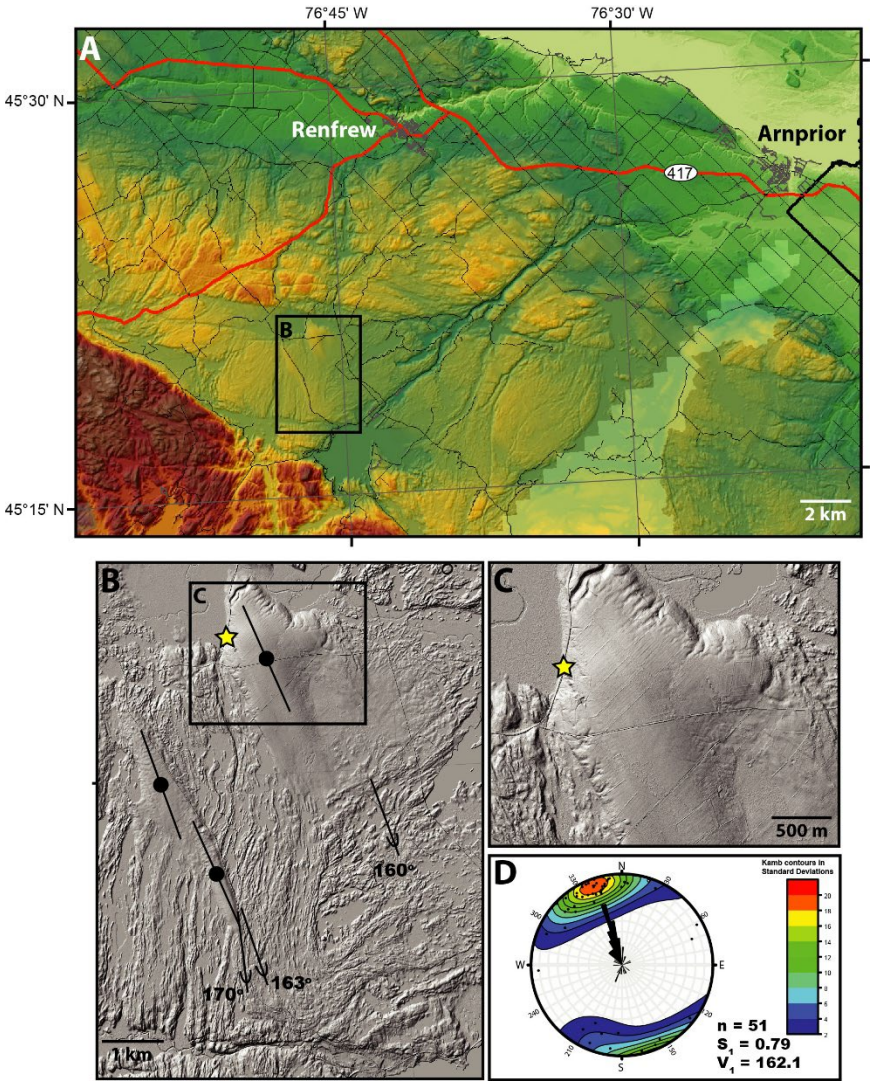


Figure 11. *An example of a till fabric site in eastern Ontario with inset maps. A) Coloured DEM (Ministry of Natural Resources and Forestry, 2018) and 0.5 m LiDAR hillshade relief maps (Ministry of Natural Resources and Forestry, 2022a, b) of Grenville Province terrain between the Ottawa-Bonnechere Graben to the northeast (Ottawa Valley) and the Madawaska Highlands to the southwest. The white sawtooth mask represents a region with no LiDAR coverage; B) A hillshade DEM showing details of streamlined landforms not readily seen on the provincial DEM. The yellow star represents a till fabric site and locations and orientations of selected striae measurements are plotted; C) A detailed hillshade image showing the till fabric site (yellow star) in a roadcut exposing till along the up-ice nose of the streamlined glacial landform; D) Results of the measured clasts plotted as both a bidirectional rose plot and an equal area stereonet projection, illustrating how the till clasts parallel the landform and the regional striation measurements seen in photograph B (rose and stereonet plots created by Stereonet; Allmendinger* et al.*, 2013; Cardozo and Allmendinger, 2013).*

stress fields, ice-flow directions, and fabric alignments (Krüger, 1970; Dreimanis, 1999). Large sculpted clasts, sometimes referred to as 'bullet-shaped boulders' (McMartin and Paulen, 2009) may have a different alignment than smaller ones, as ice and fine debris transported along the glacier's base flow around the boulders and cobbles (*cf.* Kjær and Krüger, 1998). Modification can be expected during deposition around drumlins, flutings, and crag-and-tail structures as ice flows from high-pressure regimes to low-pressure 'shadows' down-ice of the obstacle.

There are extensive discussions with detailed field methodologies and statistical analysis for till fabrics in McMartin and Paulen (2009), Paulen and McClenaghan (2015), and Benn and Lukas (2021), and references therein. To summarize, tills deposited subglacially are characterized by strong fabrics, with primary eigenvalues (E1) in excess of 0.6, aligned in the direction of glacial transport, and tertiary (E3) eigenvalues of less than 0.15. Modal plunge angles should be low, with pebbles plunging in the direction of the source (McMartin and Paulen, 2009).

Ice Streams Footprints

Numerous palaeo-ice stream footprints have been identified in areas that were covered by the Laurentide, Cordilleran, and Innuitian ice sheets in Canada (*e.g.*, Dyke and Morris, 1988; Dredge, 2000; Winsborrow *et al.*, 2004; De Angelis and Kleman, 2005, 2007; Margold *et al.*, 2015; Veillette *et al.*, 2017; Eyles *et al.*, 2018; McMartin *et al.*, 2021). Glacial dispersal trains emanating from mineralized point sources within larger palaeo-ice stream trunk flows have been identified in northern Canada (Fig. 12). The two examples below are documented hard-bedded dispersal trains created by faster flowing ice streams and highlight dispersal features different from those in the literature created by 'normal' (steady state) glacial flow (*e.g.*, McClenaghan and Paulen, 2018, and examples therein).

Strange Lake Dispersal Train

The Strange Lake glacial dispersal train in northern Québec and Labrador, is a remarkably linear ribbon defined by till geochemistry and airborne gamma-ray data that extends >60 km down-ice (northeast) from a mineralized rare earth element-rich peralkaline intrusion (Paulen *et al.*, 2017; McClenaghan *et al.*, 2019). This dispersal train formed within one of several ice streams that operated over a hard bed near the center of the Labrador Dome of the Laurentide Ice Sheet (Margold *et al.*, 2015).

In the mid-1980s, the Geological Survey of Canada and the Geological Survey of Newfoundland and Labrador carried out high-density surficial geochemical studies (1 sample site per 1.97 km^2) around the Strange Lake intrusion and associated Strange Lake Zr–Y heavy rare earth element (REE) deposit in eastern Canada. The purpose of the surveys was to determine the

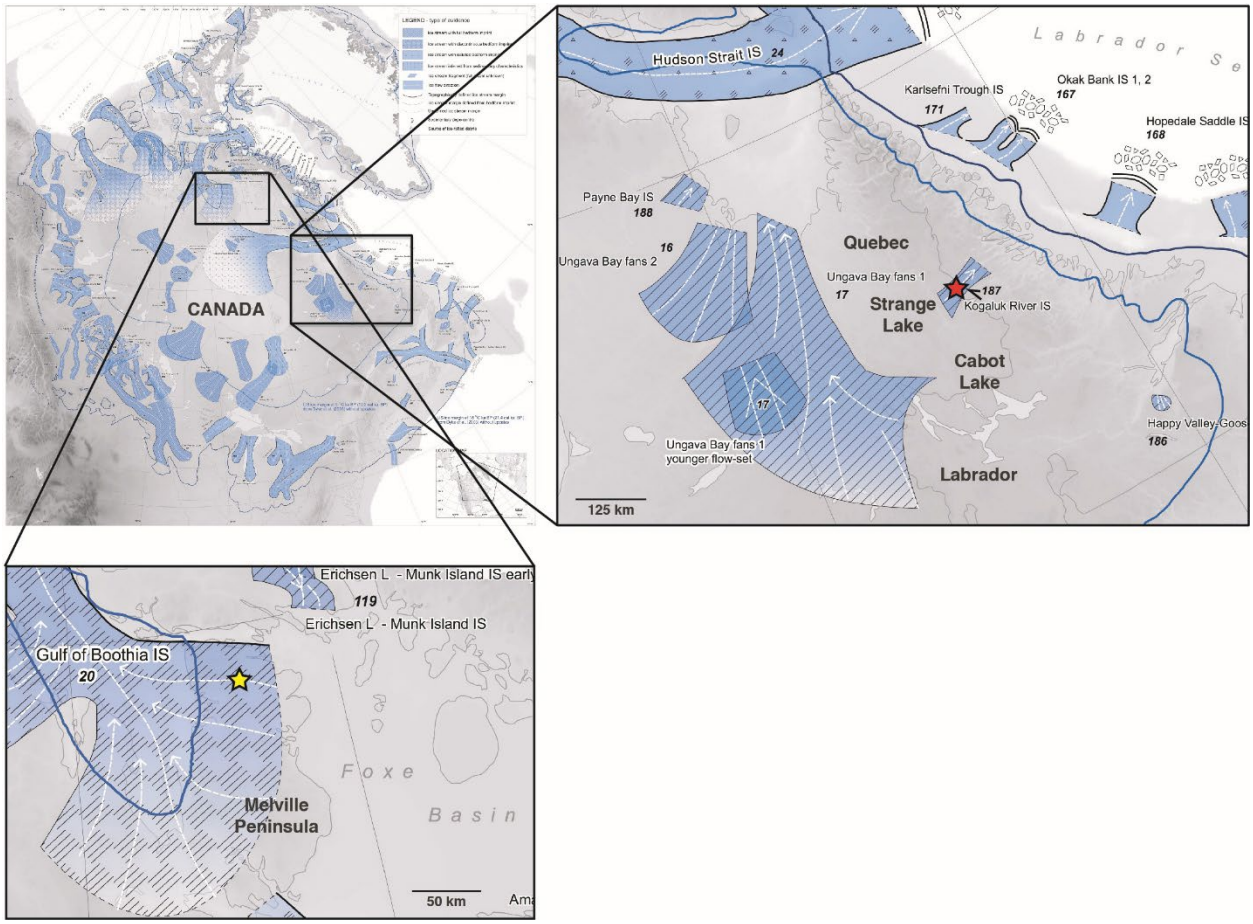


Figure 12. *Map of ice stream corridors of the Late Wisconsin Laurentide and Innuitian ice sheets (modified from Margold* et al.*, 2015). The eastern Canada inset map shows the northern Labrador coastline with the Strange Lake intrusion and deposit (red star) that is situated within the trunk of the Kogaluk River continental ice stream (IS #18). The northern Canada inset map highlights the Gulf of Boothia ice stream fan (IS #20) which consists of a number of ice stream corridors that flowed from the ice divide on the Melville Peninsula into Committee Bay. The Aviat kimberlite cluster (yellow star) is situated within one of these continental ice streams.*

ice-flow history, patterns of glacial dispersal, and the surficial geochemical signatures of the rare earth element-rich intrusion (Batterson, 1989). A glacial dispersal train trending northeast from the Strange Lake intrusion and its mineralized zones for a minimum of 50 km was defined using airborne gamma-ray spectrometry, radioactive boulders, lake sediment geochemistry, and till geochemistry (Geological Survey of Canada, 1980; McConnell and Batterson, 1987; Batterson and Taylor, 2009).

The till survey outlined an exceptional linear dispersal train, with a width comparable to the bedrock source along its entire length (Fig. 13). Single-element geochemical patterns for ore-related elements (Y, Zr, Nb, Be, La) define a ribbon-shaped dispersal train for at least 40 km down-ice from the peralkaline complex. The formation of this train was originally attributed to sustained,

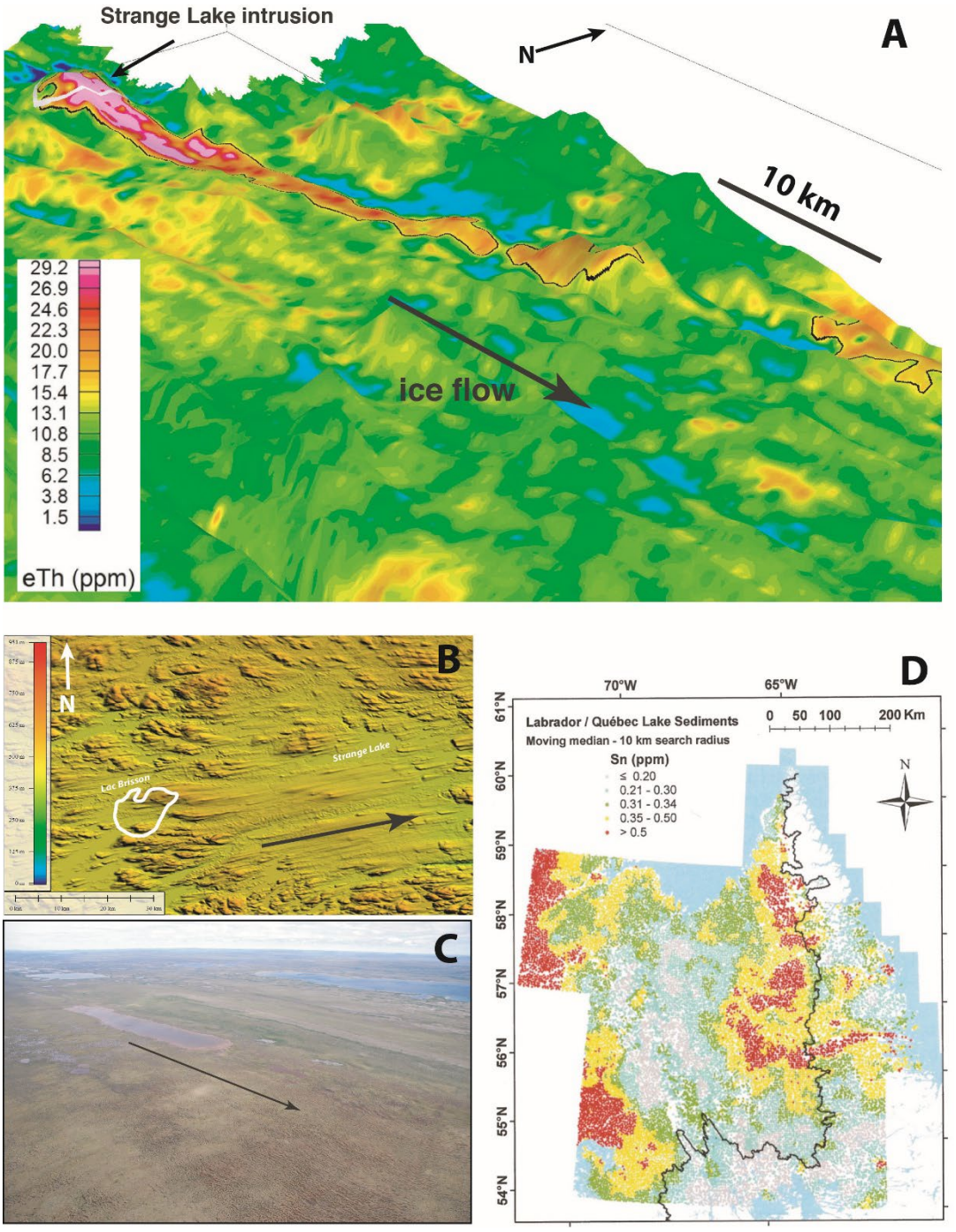


Figure 13. *A) The Strange Lake till dispersal train from airborne gamma-ray spectrometry survey data (Geological Survey of Canada, 1980), overlain on a DEM (applied with 10x vertical exaggeration) of the Strange Lake region and viewed obliquely from the southeast. The linear MSGLs dominate the landscape and mirror the ribbon-shaped dispersal train; B) Shuttle Radar Topographic Mission (SRTM) DEM image of the Strange Lake deposit (outlined in white) highlighting the mega-scale glacial lineations from the Kogaluk River ice stream that eroded the deposit from left to right (black arrow) and created the elongated ribbon dispersal train; C) Oblique aerial photo of the MSGLs in the Strange Lake area, with landforms showing large length to width ratios, indicative of fast-flowing ice; D) Plot of lake sediment geochemistry for tin (Sn; from Amor* et al.*, 2018), an element affiliated with peralkaline granitic intrusions. A long linear Sn anomaly extends from the host granite of the Strange Lake deposit and continues for more than 100 km out to the Labrador coast.*

unidirectional steady-state glacial flow (Batterson, 1989). Reanalysis of regional lake sediment geochemistry showed that this dispersal train likely extended right out to the coast (Amor *et al.*, 2018).

Surficial mapping conducted along the Ancestral Labrador Ice Divide (*see* Rice *et al.*, 2023, and references therein for overview) and heavy mineral glacial dispersal studies at Strange Lake (McClenaghan *et al.*, 2019), which included examination of the Shuttle Radar Topographic Mission (SRTM) DEM imagery of the Strange Lake deposit, highlighted that the surficial geomorphology was dominated by MSGLs, formed from fast-flowing ice. The Strange Lake intrusion and deposit, and resultant dispersal train were situated within the trunk of the Kogaluk River ice stream (Margold *et al.*, 2015) that strongly eroded the deposit and carried out mineral-rich debris to the Labrador coast.

Aviat Dispersal Train

Another example of a hard-bedded ice stream dispersal train is from the Aviat kimberlite cluster on the northern Melville Peninsula, Nunavut. A kimberlite indicator mineral-rich dispersal train (referred to as the Tremblay Corridor) extends 65 km down-ice (northwest) from a cluster of kimberlite intrusions on northern Melville Peninsula, Nunavut (Armstrong, 2009; Paulen *et al.*, 2019). This glacial dispersal train was formed by the Gulf of Boothia Ice Stream, which originated from the Foxe Dome of the Laurentide Ice Sheet (Tremblay and Paulen, 2012). Reconnaissance heavy mineral sampling surveys of till, eskers, and beaches over the northern portion of the Melville Peninsula commenced in 2001 by an exploration company as part of their diamond exploration program. Recovery of diamond indicator minerals was reported in these early samples (Armstrong, 2009). Follow-up sampling resulted in the recovery of diamond indicators with adhering kimberlite. Since the initial discovery, in excess of 80 000 line kilometres of airborne geophysics have been flown and approximately 11 000 surficial samples have been collected across the property (Armstrong *et al.*, 2008).

The combined sampling surveys revealed a kimberlite indicator mineral-rich zone in till approximately 65 km long and 10 km wide, trending 286°, which is parallel to the observed dominant glacial-flow direction (Fig. 14). This regional-scale indicator mineral train is referred to

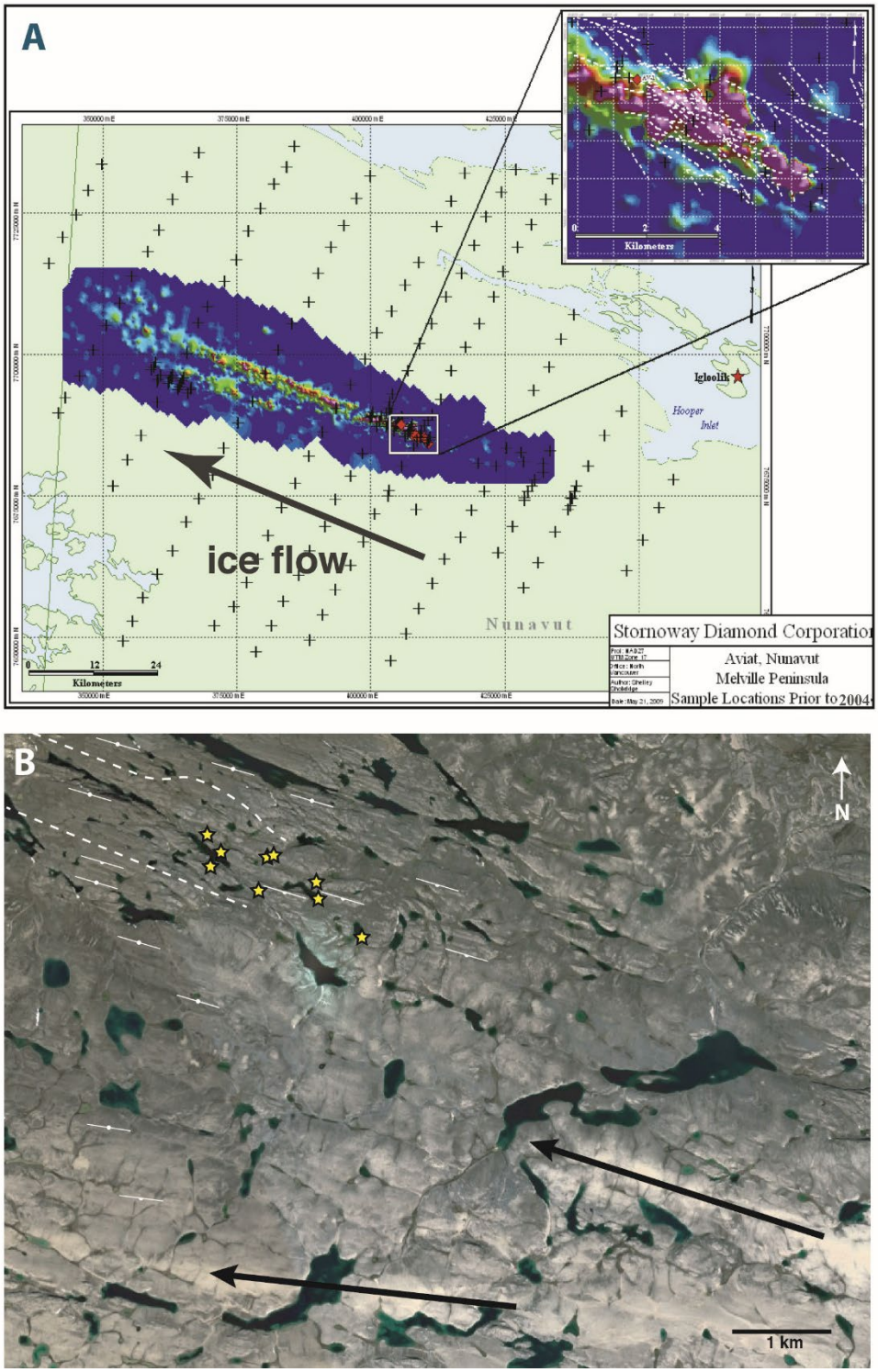


Figure 14. *A) Colour-shaded map of total kimberlite indicator mineral abundance in all surficial samples (2004–2008) over the entire Tremblay corridor, with an inset zooming on the eastern terminus of the dispersal train. The original 2004 surficial samples were used to discover the dispersal train are shown as crosses (modified from Armstrong, 2009); B) Satellite image of the Aviat cluster of kimberlites. The small yellow stars indicate outcropping kimberlites. The white dashed line is the linear dispersal train proximal to the kimberlite field. This region is the onset zone for the northern tracts of the Gulf of Boothia ice streams (*see *Fig. 1). Mega-scale glacial lineations can be seen on the landscape (shown as white fluting symbols), as well as large carbonate dispersal trains (black arrows) formed by streaming ice (image source: Landsat 7 with 15 m-resolution panchromatic band).*

as the Tremblay Corridor and all presently known kimberlites occur within a 10 km long by 3 km portion at its eastern terminus (Armstrong, 2009).

The linear nature of the dispersal train and overall indicator mineral abundances aided diamond exploration. Armstrong (2009) originally reported that the linear dispersal trains were attributed to sustained, unidirectional steady-state glacial flow, similar to the initial interpretation of the Strange Lake dispersal train. However, mapping of glacial landforms in the northern Melville Peninsula (De Angelis and Kleeman, 2005; Tremblay and Paulen, 2012) shows that the kimberlite dispersal train occurs within a region of several ice streams. These ice streams were driven by westward flow from the former spreading ice centre (the Foxe sector of the Laurentide Ice Sheet) over the Foxe basin which overrode the northern Melville Peninsula and streamed ice into the Gulf of Boothia–Lancaster Sound trough (Fig. 15).

Summary and Implications for Exploration

Recognition and identification of ice-flow indicators, regional landform analysis of remotely sensed datasets, small erosional features on bedrock surfaces, and till fabric analysis are essential components for developing an understanding of past glacial trajectories and the relative ages of discrete ice-flow phases (glacial erosion history) that collectively lead to the net glacial sediment transport recorded in dispersal trains. These notes provide a broad overview of ice-flow indicators with a focus on those most commonly used in Canada. Successful drift prospecting relies on incorporating observations of local ice-flow indicators into regional ice-flow interpretations. Local ice flows can have varying effects on the dispersion of ore indicators from regional ice flows. Often, elongated glacial landforms will indicate one dominant flow direction whereas striae and till fabric indicators reveal a more complicated glacial history. Furthermore, although the dominant direction of ice-flow indicators tends to represent the last flow stage, some bedforms, or the tills into which they are carved/formed/eroded, may have developed during older flow stages, particularly under former ice divides or in areas once covered by sluggish, non-erosive ice.

Consultation of published survey maps and reports or analysis of increasingly high-resolution regional datasets, such as satellite imagery and terrain data, provide a preliminary working model for glacial dispersal in a regional perspective or at a nearby property. However, site-specific work

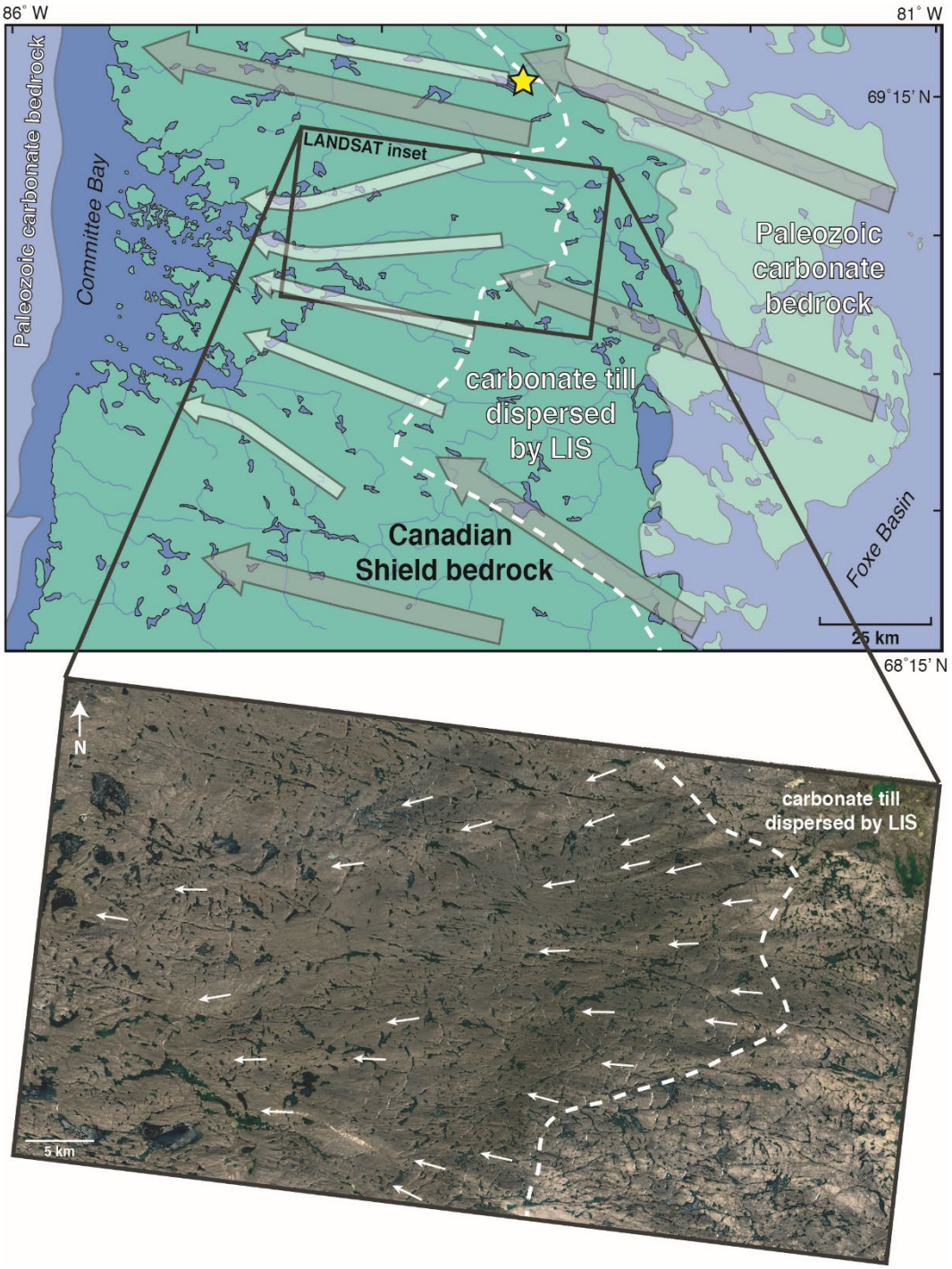


Figure 15. *The carbonate dispersal trains of central Melville Peninsula, Nunavut (*see *Dredge, 2000). During the last glacial event, the Laurentide Ice Sheet eroded Paleozoic carbonate bedrock from the Foxe Basin and eastern Melville Peninsula and deposited a light-coloured carbonate till inland over Canadian Shield bedrock (dark arrows and white dashed line; Tremblay and Paulen, 2012). During deglaciation, several ice streams formed as part of a large fan in Committee Bay (white arrows), with their onset zones at the western edge of the carbonate till zone, producing elongate ribbons, or fingers, of carbonate-rich till that extend almost 50 km to Committee Bay (yellow star is the Aviat kimberlite field). Lower inset shows a satellite image of the central Melville Peninsula, showing the elongate tracts of carbonate till ribbons (lighter tones, demarked by small arrows) created by ice streams that flowed westward to Committee Bay. The onset zones for these ice streams are in the region with regionally deposited carbonate till (image source: Landsat 7 with 15 m-resolution panchromatic band).*

is still necessary to either confirm the existing interpretations of ice-flow directions or to establish local deviations so that one prospects in all the up-ice directions, or exploration vector, of the mineralization indicators.

Dispersal trains from point sources in non-ice-stream areas of northern Canada tend to be much shorter (<10 km; *cf.* McClenaghan and Paulen, 2018). Dispersal trains created by ice streams, however, are tens of kilometres long, and their geometry, due to higher subglacial erosion and formation by faster flowing ice, tend to be linear, narrow ribbons (Paulen *et al.*, 2017; Sookhan *et al.*, 2021).

The geometry of dispersal trains and nature of till deposited by palaeo-ice streams can have significant impacts on the application of till geochemistry and indicator mineral methods to mineral exploration because their glacial transport distances can be significant (>50 km). The distally-derived till within a palaeo-ice stream footprint will reflect bedrock source(s) much farther up ice than till adjacent to ice streams, creating a mosaic of tills of different provenances at surface (*e.g.*, Ross *et al.*, 2009). When ice streams erode a point source, such as a mineral deposit, it forms a large linear exploration target. When ice streams erode non-mineralized bedrock, the resultant exotic till that is deposited masks the geochemical and mineralogical signature of the underlying bedrock. The long glacial transport distances observed by glacial sediments deposited by ice streams should be taken into consideration when collecting till samples and interpreting till geochemistry and heavy mineral patterns in these regions of Shield terrain in the northern hemisphere.

Acknowledgments

Contributions to this short course volume were made possible under the Geological Survey of Canada's (GSC) Critical Minerals Geoscience and Data Program under the 'Ice stream paradigm and search for critical minerals in Canada: exploiting the power of automated geospatial mapping techniques' research activity (2023-2027).

This short paper acknowledges the years of scientific interactions and partnerships with Canadian scientists in government and academia. In particular, we would like to thank Isabelle

McMartin (GSC Ottawa, emeritus), Beth McClenaghan (GSC Ottawa, emeritus), and Ralph Stea (Nova Scotia Department of Energy and Mines, retired) for many fruitful discussions and intense arm-waving over glacially sculpted outcrops.

References

Allmendinger, R.W., Cardozo, N.C. and Fisher, D., 2013: Structural geology algorithms: Vectors and tensors. Cambridge University Press, Cambridge, England. https://doi.org/10.2138/am.2013.607

Amor, S., McCurdy, M. and Garrett, R., 2018: Creation of an atlas of lake-sediment geochemistry of western Labrador and northeastern Québec. Geochemistry: Exploration, Environment, Analysis, Volume 19, pages 369–393. https://doi.org/10.1144/geochem2018-061

Armstrong, J.P., 2009: Kimberlite indicator mineral anomalies in a regional, local, and bedrock context: Examples from Canada. *In* Workshop B: Indicator Mineral Methods in Mineral Exploration. *Edited by* M.B. McClenaghan and L.H. Thorleifson. 24th International Applied Geochemistry Symposium, 31 May 2009, Fredericton, Canada, pages 47–53.

Armstrong, J.P., Stubley, M.P. and Chang, F.Y., 2008: Geology and exploration history of the Aviat kimberlite cluster, northern Rae Craton, Melville Peninsula, Nunavut, Canada. *In* 9th International Kimberlite Conference, Frankfurt, Extended Abstract No. 9IKC-A-00266. https://doi.org/10.29173/ikc3498

Batterson, M.J., 1989: Glacial dispersal from the Strange Lake alkalic complex, northern Labrador. *In* Drift Prospecting. *Edited by* R.N.W. DiLabio and W.B. Coker. Geological Survey of Canada, Paper 89-20, pages 31–40.

Batterson, M.J. and Taylor, D.M., 2009: Geochemical re-analysis of till samples from the Strange Lake area, Labrador (NTS map sheets 14D/5 and 24A/8). Government of Newfoundland and Labrador, Department of Natural Resources, Geological Survey, Open File LAB/1479. https://www.gov.nl.ca/iet/files/mines-geoscience-publications-openfiles-oflab1479.pdf

Benn, D.I. and Evans, D.J.A., 2010: Glaciers and Glaciation. Second Edition, Routledge, New York, 802 pages. https://doi.org/10.4324/9780203785010

Benn D.I. and Lukas, S., 2021: Macrofabric. *In* A Practical Guide to the Study of Glacial Sediments, Second Edition. *Edited by* D.J.A. Evans and D.I. Benn. Quaternary Research Association, London, pages 125–154. https://www.qra.org.uk/bookshop/a-practical-guide-to-the-study-of-glacial-sediments/

Bennett, M.R., 2003: Ice streams as the arteries of an ice sheet: their mechanics, stability and significance. Earth-Science Reviews, Volume 61, pages 309–339. https://doi.org/10.1016/S0012-8252(02)00130-7

Bobrowsky, P.T., Sibbick, S.J., Newell, J.H. and Matesek, P.F. (eds.), 1995: Drift Exploration in the Canadian Cordillera. British Columbia Ministry of Energy, Mines and Petroleum Resources, Paper 1995-2. https://cmscontent.nrs.gov.bc.ca/geoscience/publicationcatalogue/Paper/BCGS_P1995-02.pdf

Cardozo, N.C. and Allmendinger, R.W., 2013: Spherical projections with OSXStereonet. Computers and Geosciences, Volume 51, pages 193–205. https://doi.org/10.1016/j.cageo.2012.07.021

Clark, C.D., 1994: Large-scale ice-moulding: A discussion of genesis and glaciological significance. Sedimentary Geology, Volume 91, pages 253–268. https://doi.org/10.1016/0037-0738(94)90133-3

Clark, P.U., 1991: Striated clast pavements: products of deforming subglacial sediment? Geology, Volume 19, pages 530–533. https://doi.org/10.1130/0091-7613(1991)019<0530:SCPPOD>2.3.CO;2

De Angelis, H. and Kleman, J., 2005: Palaeo-ice streams in the northern Keewatin sector of the Laurentide Ice Sheet. Annals of Glaciology, Volume 42, pages 135–144. https://doi.org/10.3189/172756405781812925

De Angelis, H. and Kleman, J., 2007: Palaeo-ice streams in the Foxe/Baffin sector of the Laurentide Ice Sheet. Quaternary Science Reviews, Volume 26, pages 1313–1331. https://doi.org/10.1016/j.quascirev.2007.02.010

DiLabio, R.N.W., 1990. Glacial dispersal trains. *In* Glacial Indicator Tracing (1st Edition). *Edited by* R. Kujansuu and M. Saarnisto. CRC Press, pages 109–122.

DiLabio, R.N.W. and Coker, W.B., 1989: Drift Prospecting. Geological Survey of Canada, Paper 89-20. https://doi.org/10.4095/127357

Dredge, L.A., 2000: Carbonate dispersal trains, secondary till plumes, and ice streams in the west Foxe Sector, Laurentide Ice Sheet. Boreas, Volume 29, pages 144–156. https://doi.org/10.1111/j.1502-3885.2000.tb01207.x

Dreimanis, A., 1999: Need for three-dimensional analysis of structural elements in glacial deposits for determination of direction of glacier movement. *In* Glacial Processes, Past and Present. *Edited by* D.M. Mickelson and J.W. Attig. Geological Society of America, Special Paper 337, pages 59–67. https://doi.org/10.1130/0-8137-2337-X.59

Dyke, A.S., 2008: The Steensby Inlet ice stream in the context of the deglaciation of northern Baffin Island, eastern Arctic Canada. Earth Surface Processes and Landforms, Volume 33, pages 573–592. https://doi.org/10.1002/esp.1664

Dyke, A.S. and Morris, T.F., 1988: Drumlin fields, dispersal trains, and ice streams in Arctic Canada. Canadian Geographer / Le Géographe canadien, Volume 32, pages 86–90. https://doi.org/10.1111/j.1541-0064.1988.tb00860.x

Eyles, N., Arbelaez-Moreno, L. and Sookhan, S., 2018: Ice streams within the last Cordilleran Ice Sheet of western North America. Quaternary Science Reviews, Volume 179, pages 87–122. https://doi.org/10.1016/j.quascirev.2017.10.027

Ferbey, T., Plouffe, A. and Hicken, A.S. (ed.), 2017: Indicator Minerals in Till and Stream Sediments of the Canadian Cordillera. Geological Association of Canada, Special Paper Volume 50.

Geological Survey of Canada, 1980: Airborne gamma ray spectrometric map, Dihourse Lake. Québec–Newfoundland Geophysical Series, Map 35124(08)G. https://doi.org/10.4095/124881

Glasser, N.F. and Warren, C.R., 1990: Medium scale landforms of glacial erosion in south Greenland: Process and form. Geografiska Annaler, Series A, Physical Geography, Volume 72, pages 211–215. https://doi.org/10.2307/521149

Hart, J.K., 1999: Identifying fast ice flow from landform assemblages in the geological record: A discussion. Annals of Glaciology, Volume 28, pages 59–66. https://doi.org/10.1016/0037-0738(94)90133-3

Hicock, S.R., 1991: On subglacial stone pavements in till. Journal of Geology, Volume 99, pages 607–619. https://doi.org/10.1086/629520

Hirvas, H. and Nenonen, K., 1990: Field methods for glacial indicator tracing. *In* Glacial Indicator Tracing (1st Edition). *Edited by* R. Kujansuu and M. Saarnisto. CRC Press, pages 217–248.

Hooyer, T.S. and Iverson, N.R., 2000: Clast-fabric development in a shearing granular material: Implications for subglacial till and fault gouge. Geological Society of America, Bulletin 112, pages 683–692. https://doi.org/10.1130/0016-7606(2000)112<683:CDIASG>2.0.CO;2

Ildefonse, B., Launeau, P., Bouchez, J.L. and Fernandez, A., 1992: Effects on mechanical interactions on the development of preferred orientations: a two-dimensional experimental approach. Journal of Structural Geology, Volume 14, pages 73–83. https://doi.org/10.1016/0191-8141(92)90146-N

Kjær, K.H. and Krüger, J., 1998: Does clast size influence fabric strength? Journal of Sedimentary Petrology, Volume 68, pages 746–749. https://doi.org/10.2110/jsr.68.746

Klassen, R.A., 2001: A Quaternary geological perspective on geochemical exploration in glaciated terrain. *In* Drift Exploration in Glaciated Terrain. *Edited by* M.B. McClenaghan, P.T. Bobrowsky, G.E.M. Hall and S.J. Cook. Association of Exploration Geochemistry, Geological Society of London, Special Publication 185, pages 1–17. https://doi.org/10.1144/GSL.SP.2001.185.01

Krabbendam, M., Eyles, N., Putkinen, N., Bradwell, T. and Arbelaez-Moreno, L., 2016: Streamlined hard beds formed by palaeo-ice streams: A review. Sedimentary Geology, Volume 338, pages 24–50. https://doi.org/10.1016/j.sedgeo.2015.12.007

Krüger, J., 1970: Till fabric in relation to direction of ice movement, a study from the Fakse Banke, Denmark. Geografisk Tidsskrift, Volume 69, pages 133–170.

Krüger, J., 1984: Clasts with stoss-lee form in lodgement tills: A discussion. Journal of Glaciology, Volume 30, pages 241–243. https://doi.org/10.3189/S0022143000006006

Kujansuu, R., 1990: Glacial flow indicators in air photographs. *In* Glacial Indicator Tracing (1st Edition). *Edited by* R. Kujansuu and M. Saarnisto. CRC Press, pages 71–86.

Kujansuu, R. and Saarnisto, S.M. (ed.), 1990: Glacial Indicator Tracing (1st ed.). CRC Press. https://doi.org/10.1201/9781003079415

Larsen, N.K. and Piotrowski, J.A., 2003: Fabric pattern in a basal till succession and its significance for reconstructing subglacial processes. Journal of Sedimentary Research, Volume 73, pages 725–734. https://doi.org/10.2110/jsr.2005.024

Lundqvist, J., 1990: Glacial morphology as an indicator of the direction of glacial transport. *In* Glacial Indicator Tracing (1st Edition). *Edited by* R. Kujansuu and M. Saarnisto. CRC Press, pages 61–70.

Margold M., Stokes C.R. and Clark C.D., 2015: Ice streams in the Laurentide Ice Sheet: A new mapping inventory. Journal of Maps, Volume 11, pages 380–395. https://doi.org/10.1080/17445647.2014.912036

McClenaghan, M.B., Bobrowsky, P.T., Hall, G.E.M. and Cook, S.J. (eds.), 2001: Drift Exploration in Glaciated Terrain. Geological Society, London, Special Publication No. 185. https://doi.org/10.1144/GSL.SP.2001.185

McClenaghan, M.B. and Paulen, R.C., 2018: Mineral exploration in glaciated terrain, Chapter 20. *In* Past Glacial Environments (Sediments, Forms and Techniques) A new & Revised Edition. *Edited by* J. Menzies and J.J-M. van der Meer. Elsevier, pages 689–751. https://doi.org/10.1016/B978-0-08-100524-8.00022-1

McClenaghan, M.B., Paulen, R.C. and Kjarsgaard, I.M., 2019: Rare metal indicator minerals in bedrock and till at the Strange Lake peralkaline complex, Québec and Labrador, Canada. Canadian Journal of Earth Sciences, Volume 56, pages 857–869. https://doi.org/10.1139/cjes-2018-0299

McConnell, J.W. and Batterson, M.J., 1987: The Strange Lake Zr-Y-Nb-Be-REE deposit, Labrador: A geochemical profile in till, lake and stream sediment, and water. Journal of Geochemical Exploration, Volume 29, pages 105–127. https://doi.org/10.1016/0375-6742(87)90073-2

McMartin, I. and Henderson, P.J., 2004: Evidence from Keewatin (central Nunavut) for paleo-ice divide migration. Géographie physique et Quaternaire, Volume 58, pages 163–186. https://doi.org/10.7202/013137ar

McMartin, I., Godbout, P.-M., Campbell, J. E. Tremblay, T. and Behnia, P., 2021: A new map of glacigenic features and glacial land systems in central mainland Nunavut, Canada. Boreas, Volume 50, pages 51–75. https://doi.org/10.1111/bor.12479

McMartin, I. and Paulen, R.C., 2009: Ice-flow indicators and the importance of ice-flow mapping for drift prospecting. *In* Application of Till and Stream Sediment Heavy Mineral and Geochemical Methods to Mineral Exploration in Western and Northern Canada. *Edited by* R.C. Paulen and I. McMartin. Geological Association of Canada, Short Course Notes 18, pages 15–34.
https://gac.ca/product/application-of-till-and-stream-sediment-heavy-mineral-and-geochemical-methods/

Ministry of Natural Resources and Forestry, 2018: Provincial digital elevation model, version 3. Ministry of Natural Resources and Forestry, Provincial Mapping Unit, Peterborough, Ontario, available on Ontario GeoHub. https://ws.geoservices.lrc.gov.on.ca/arcgis5/rest/services/Elevation

Ministry of Natural Resources and Forestry, 2022a: Ontario digital terrain model (Lidar-derived) – Eastern Ontario DTM. Ministry of Natural Resources and Forestry, Provincial Mapping Unit, Peterborough, Ontario, available on Ontario GeoHub. https://ws.geoservices.lrc.gov.on.ca/arcgis5/rest/services/Elevation

Mollard, J.D., 1996: Landforms and surface materials of Canada: A stereoscopic airphoto atlas and glossary, 8th Edition. Printwest, Regina.

Paulen, R.C., Eyles, N. and Ross, M., 2024b: Glacial dispersal trains and ice streams on the Canadian Shield. *In* Till Geochemistry and Indicator Mineral Methods for Exploration in Glaciated Terrains. Edited by R.C. Paulen and M.B. McClenaghan. Geological Survey of Canada, Open File 9210, pages 140–147.
https://doi.org/10.4095/pbmy2d03m0

Paulen, R.C. and McClenaghan, M.B., 2015: Late Wisconsin ice-flow history in the Buffalo Head Hills kimberlite field, north-central Alberta. Canadian Journal of Earth Sciences, Volume 52, pages 1–17. http://dx.doi.org/10.1139/cjes-2014-0109

Paulen, R.C. and McClenaghan, M.B., 2024: Till geochemistry and indicator-mineral methods for exploration in glaciated terrains. Geological Survey of Canada, Open File 9210, 157 pages.
https://doi.org/10.4095/pbmy2d03m0

Paulen, R.C. and McMartin, I. (ed.), 2009: Application of Till and Stream Sediment Heavy Mineral and Geochemical Methods to Mineral Exploration in Western and Northern Canada. Geological Association of Canada, Short Course Notes 18.
https://gac.ca/product/application-of-till-and-stream-sediment-heavy-mineral-and-geochemical-methods/

Paulen, R.C., Mulligan, R.P.M. and Rice, J.M., 2024a: Determination of glacial transport directions. *In* Till Geochemistry and Indicator Mineral Methods for Exploration in Glaciated Terrains. *Edited by* R.C. Paulen and M.B. McClenaghan. Geological Survey of Canada, Open File 9210, pages 10–23.
https://doi.org/10.4095/pbmy2d03m0

Paulen, R.C., Rice, J.M. and Ross, M., 2022: Surficial geology, Lac aux Goélands, Québec, NTS 23 P southeast. Geological Survey of Canada, Canadian Geoscience Map 429, 1:100,000. https://doi.org/10.4095/328291

Paulen, R.C., Stokes, C.R., Fortin, R., Rice, J.M., Dubé-Loubert, H. and McClenaghan, M.B., 2017: Dispersal trains produced by ice streams: An example from Strange Lake, Labrador, Canada. *In* Proceedings of Exploration 17. *Edited by* V. Tschirhart and M.D. Thomas. Sixth Decennial International Conference on Mineral Exploration, pages 871–875. https://geochem.nrcan.gc.ca/cdogs/content/pub/pub03698_e.htm

Paulen, R.C., Stokes, C. and McClenaghan, M.B., 2019: Mineral dispersal trains as products of hard-bedded ice streams in northern Canada. 20th Congress of the International Union for Quaternary Research (INQUA), Abstract P-4840. https://virtual.oxfordabstracts.com/#/event/public/574/submission/2181

Plouffe, A., Bednarski, J.M., Huscroft, C.A. and McCuaig, S.J., 2009: Gold grain content of till in the Bonaparte Lake map area, south central British Columbia (NTS 92P). Geological Survey of Canada, Open File 6047. https://doi.org/10.4095/226247

Prest, V.K., 1983: Canada's heritage of glacial features. Geological Survey of Canada, Miscellaneous Report 28. https://doi.org/10.4095/109273

Puranen, R., 1990: Modelling of glacial transport in tills. *In* Glacial Indicator Tracing (1st Edition). *Edited by* R. Kujansuu and M. Saarnisto. CRC Press, pages 15–34.

Rea, B.R., 2013: Micro- to macroscale forms. *In* Encyclopedia of Quaternary Science (Second Edition). Edited by R. Kujansuu and M. Saarnistos. Elsevier, pages 865–876. https://doi.org/10.1016/B978-0-444-53643-3.00076-5

Rice, J.M., Paulen, R.C., Campbell, H.E. and Ross M., 2024: The surficial geology record of ice stream catchment dynamics and ice-divide migration in the Québec-Labrador sector of the Laurentide Ice Sheet. Quaternary Science Advances, Volume 13. https://doi.org/10.1016/j.qsa.2023.100123

Rice, J.M., Paulen, R.C., Ross, M., McClenaghan, M.B. and Campbell, H.E., 2023: Quaternary geology of the southern Core Zone area, Québec and Newfoundland and Labrador. *In* Surficial Geology of Northern Canada: A Summary of Geo-mapping for Energy and Minerals Program Contributions. *Edited by* I. McMartin. Geological Survey of Canada, Bulletin 611, pages 221–265. https://doi.org/10.4095/331426

Ross, M., Campbell, J.E., Parent, M. and Adams, R.S., 2009: Palaeo-ice streams and the subglacial landscape mosaic of the North American mid-continent prairies. Boreas, Volume 38, pages 421–439. https://doi.org/10.1111/j.1502-3885.2009.00082.x

Ryder, J.M., 1995: Recognition and interpretation of flow direction indicators for former glaciers and meltwater streams. *In* Drift Exploration in the Canadian Cordillera. *Edited by* P.T. Bobrowsky, S.J. Sibbick, J.H. Newell, and P.F. Matesek. British Columbia Ministry of Energy, Mines and Petroleum Resources, Paper 1995-2, pages 1–22.

Sauer, E.K. and Elder, L., 1982: Airphoto interpretation for terrain analysis. Extension Division, University of Saskatchewan, Saskatoon.

Smith M.J. and Clark, C.D., 2005: Methods for the visualization of digital elevation models for landform mapping. Earth Surface Processes and Landforms, Volume 30, pages 885–900. https://doi.org/10.1002/esp.1210

Sookhan, S., Eyles, N., Bukhari, S. and Paulen, R.C., 2021: LiDAR-based quantitative assessment of drumlin to mega-scale glacial lineation continuums and flow of the paleo Seneca-Cayuga paleo-ice stream. Quaternary Science Reviews, Volume 263. https://doi.org/10.1016/j.quascirev.2021.107003

Spagnolo, M., Clark, C.D., Ely, J.C., Stokes, C.R., Anderson, J.B., Andreassen, K., Graham, A.G.C. and King, E.C., 2014: Size, shape and spatial arrangement of mega-scaleglacial lineations from a large and diverse dataset. Earth Surface Processes and Landforms, Volume 39, pages 1432–1448. https://doi.org/10.1002/esp.3532

Spagnolo, M., Phillips, E., Piotrowski, J.A., Rea, B.R., Clark, C.D., Stokes, C.R., Carr, S.J., Ely, J.C., Ribolini, A., Wysota, W. and Szuman, I., 2016: Ice stream motion facilitated by a shallow-deforming and accreting bed. Nature Communications, Volume 7. https://doi.org/10.1038/ncomms10723

Stea, R.R. and Brown, Y., 1989: Variation in drumlin orientation, form and stratigraphy relating to successive ice flows in southern and central Nova Scotia. Sedimentary Geology, Volume 62, pages 223–240. https://doi.org/10.1016/0037-0738(89)90117-6

Stokes, C.R. and Clark, C.D., 1999: Geomorphological criteria for identifying Pleistocene ice streams. Annals of Glaciology, Volume 28, pages 67–74. https://doi.org/10.3189/172756499781821625

Tremblay, T. and Paulen, R.C., 2012: Glacial geomorphology and till geochemistry of Central Melville Peninsula, Nunavut. Geological Survey of Canada, Open File 7115. https://doi.org/10.4095/290993

Veillette, J.J., Roy, M., Paulen, R.C., Ménard, M. and St-Jacques, G., 2017: Uncovering the hidden part of a large ice stream of the Laurentide Ice Sheet, northern Ontario, Canada. Quaternary Science Reviews, Volume 155, pages 136–158. https://doi.org/10.1016/j.quascirev.2016.11.008

Winsborrow, M.C.M., Clark, C.D. and Stokes, C.R., 2004: Ice streams of the Laurentide Ice Sheet. Géographie physique et Quaternaire, Volume 58, pages 269–280. https://doi.org/10.7202/013142ar

Incorporating Humus Sampling Surveys in Greenfields Mineral Exploration in Glaciated Terrain

Sarah Hashmi[1] and Alexandre Voinot[2]
[1]Geological Survey of Newfoundland and Labrador, 50 Elizabeth Avenue,
St. John's, NL, A1A 1W5
[2]Geological Survey of Canada–Natural Resources Canada,
601 Booth Street, Ottawa, ON, K1A 0E8

Abstract

*Humus is the dark brown to black, organic layer that lies above mineral matter and below live vegetation in a podzolic soil profile. Humus is an excellent (and relatively underutilized) sampling medium in glaciated terrain as it can reflect the geochemical signature of the underlying substrate (*i.e.*, bedrock and till) and has been successfully used in delineating both precious metal (gold) and critical mineral (rare earth elements) mineralization. This extended abstract summarizes how humus can be incorporated into regional-scale greenfield sampling surveys. Two case studies from Newfoundland and Labrador are also summarized, where humus (in conjunction with till) has been successful in delineating ore and associated element anomalies for gold and rare earth element mineralization.*

Introduction and Background

Humus is the by-product of decomposition of vegetation (*i.e.*, leaves, grass, lichen, and wood debris; Fig. 1) and forms above the mineral soil horizon (Kauranne *et al.*, 1992; Fig. 2). Vegetation, such as trees and smaller plants, takes up nutrients from the underlying pedosphere, lithosphere, and groundwater, as well as the biosphere and atmosphere, *via* diffusion and absorption mechanisms (Dunn, 2007; Salminen, 2008). Sampling humus for mineral exploration works on the premise that live trees and plants can absorb and translocate trace elements from the underlying bedrock, deeper soil horizons and groundwater *via* roots, and therefore, carry the geochemical signature of the underlying substrate. As a result, if mineralization is present in the vicinity, geochemical anomalies may be observed within the decomposed plant matter.

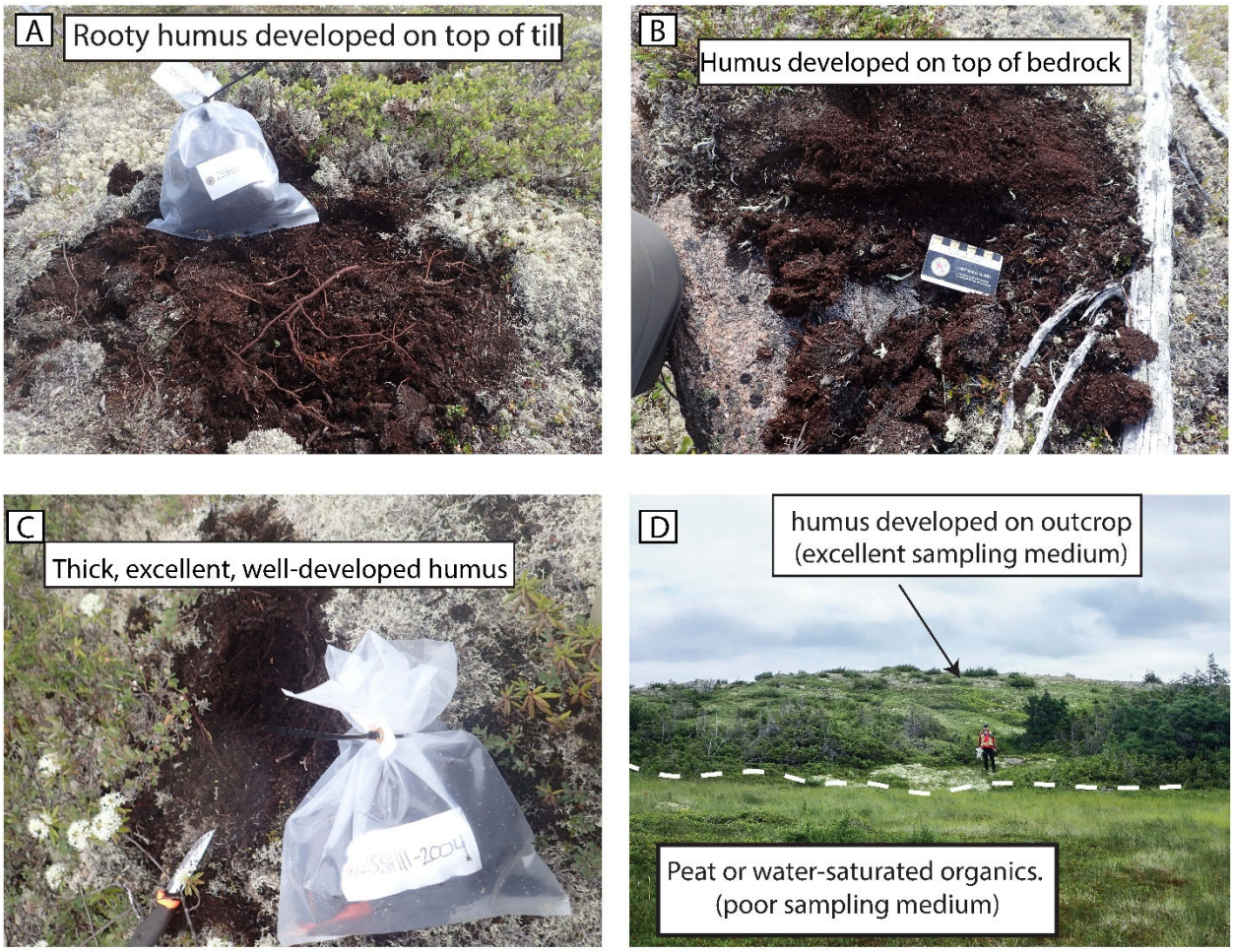


Figure 1. *A) Well-developed humus sampled over till; B, C) Well-developed humus sampled directly over bedrock; D) Unsuitable humus sampling sites include peat bog. Ideally, humus should be collected either directly over bedrock or soil horizon developed in till.*

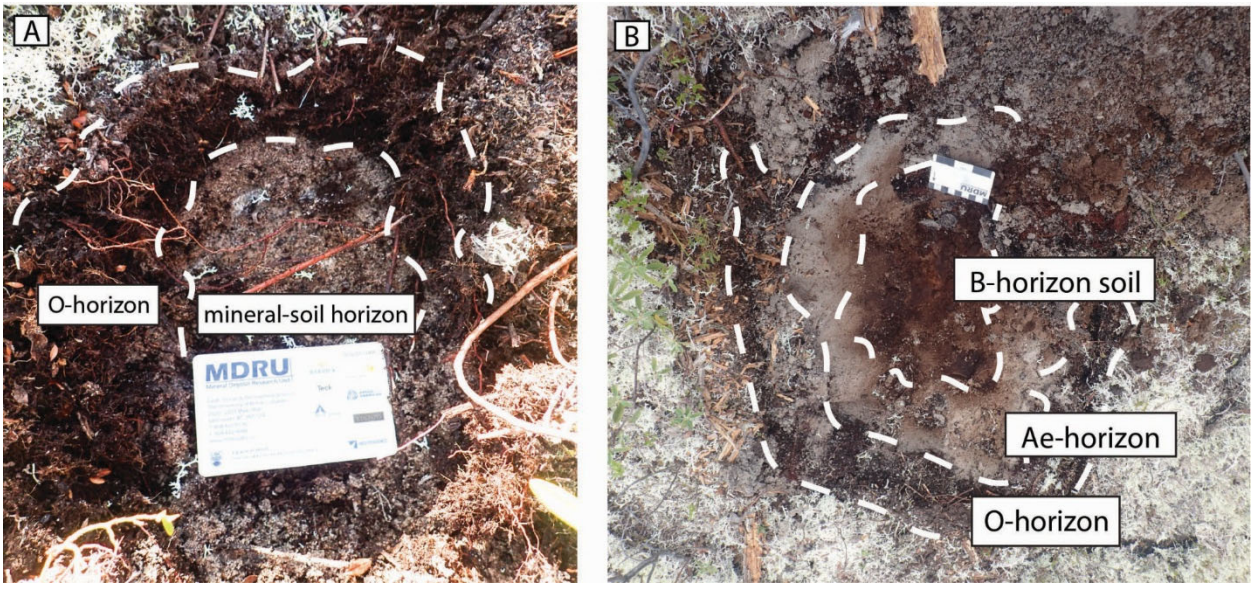


Figure 2. *A, B) Podzolic soil profiles developed in till in southeast Labrador, Canada.*

Trace elements of interest, such as major ore metal(oid)s along with their associated pathfinder elements, can be concentrated within plants due to 1) absorption from underlying metal-rich till and/or mineralized bedrock, 2) transport of key elements from deeper, buried mineralization to surface by electrochemical transport (Hamilton, 1998), 3) groundwater diffusion (Govett, 1973), 4) capillary migration (Mann *et al.*, 2005), and 5) vapor transport (Smee, 1998; Fig. 3).

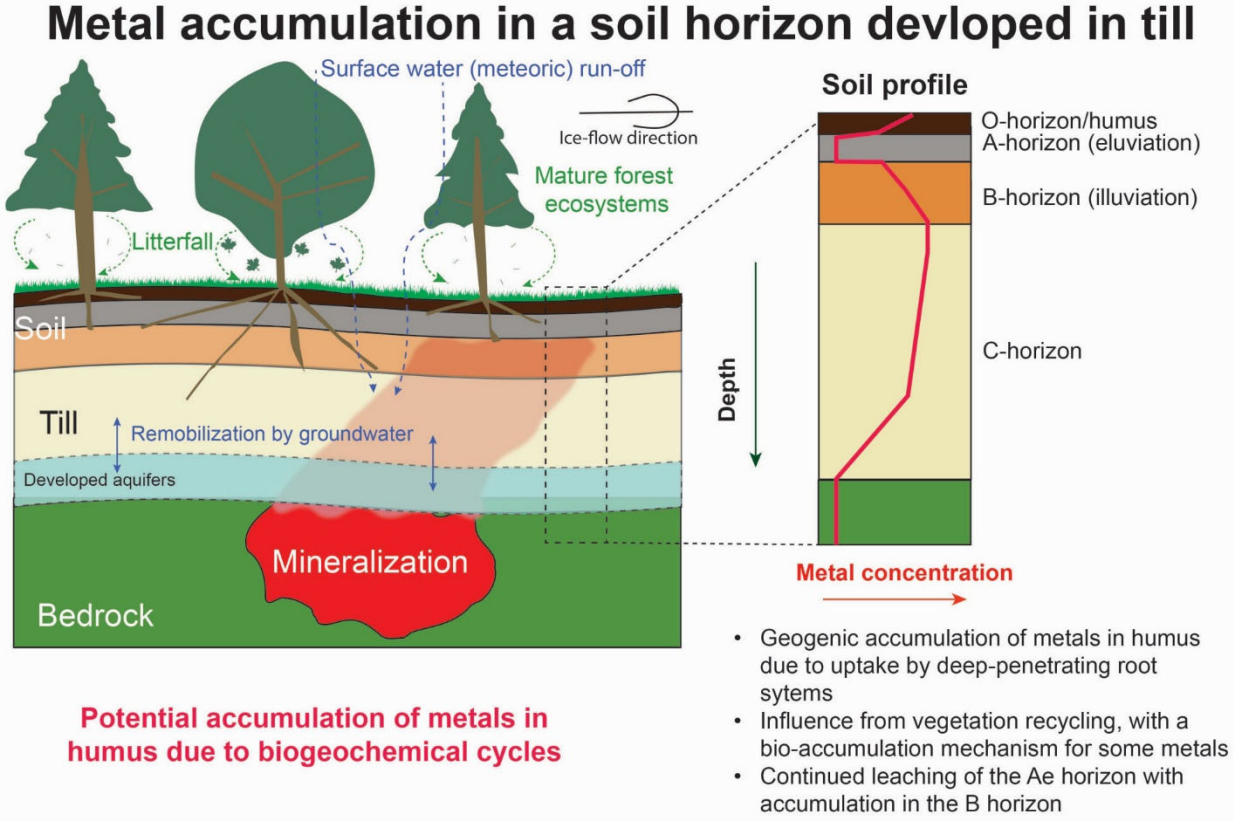


Figure 3. *A schematic showing a soil profile developed on till. Mechanical dispersion by glaciers results in the deposition of metal-rich till in B-horizon and C-horizon soil. Elevated-metal concentrations are also present in humus (O-horizon) due to biogenic and geogenic accumulation. Figure modified after Hashmi* et al. *(2026).*

Humus is an excellent sampling medium in glaciated terrain because it can carry the geochemical signature of both the underlying and surrounding bedrock units as well as till. In addition, in areas with limited till (or thick deposits of glacial sediments unsuitable for sampling), humus can be sampled directly over bedrock (Fig. 2).

Humus has been used successfully to delineate shallow to outcropping Au mineralization (Au mineralization on Glover Island; Hashmi, 2024a; Table 1), as well as deeply buried base-metal mineralization (>100 m; Restigouche Zn–Pb–Cu deposit in New Brunswick; Hall *et al.*, 2003), and U mineralization (~400 m; Phoenix U deposit in Saskatchewan; Power *et al.*, 2012).

Table 1. Select local- and regional-scale, surficial (humus and till) sampling surveys that have successfully delineated the geochemical signature of ore and pathfinder for commodities such as Au, base metals, PGEs and Li (modified after Hashmi *et al.*, 2026)

Scale of survey	Commodity	Pathfinder elements (select)	Location	Media sampled	Reference
Local	Au	Ag, As, Bi, Cu, Mo, Ni, Pb, S, Sb, Te, Zn	Jackson's Arm, NL	humus + till	Hashmi (2024a)
Local	Au	As, Bi, Co, Cd, Mo, Ni, Pb, Sb, Te, Zn	Glover island, NL	Humus + till	Hashmi (2024a)
Local	Au	As, Au, Br, Hg, Mo, Pb, Sb	Williams Property, ON	Humus + soil	Fortescue (1985)
Local (semi-detailed)	Cu, Pb, Zn	Cd, Pb (airborne)	Talbot deposit, MN	Humus + soil	van Geffen *et al.* (2012)
Local (semi-detailed)	Cu–Zn	Co, Cu, Fe, Mn, Ni, Zn	Rod deposit, Snow Lake, MN	Humus	Ferreira and Fedikow (1988)
Local (semi-detailed)	Zn, Pb, Cu	Ag, As, Cu, Hg, Pb, Sb	Restigouche Deposit, NB	Humus + soil	Hall *et al.* (2003)
Local (semi-detailed)	Li	Cs, Li, Ta	Brazil Lake, NS	Humus+ till + vegetation	MacDonald *et al.* (1992)
Local (semi-detailed)	Ni, Cu, PGE	Cu, Ni, Pd, Pt	Sudbury, ON	Humus + till	Coker *et al.* (1991)
Local (semi-detailed)	PGE	Cu, Ni, Pd, Pt	Lac des Iles Pd deposit, ON	Humus + till	Dyer and Barnett (2007)
Regional (moderate density)	REE	LREE, HREE, U, Th	Alexis River Valley area, NL, Canada	Humus + till	Hashmi (2024 c, d)

Methods

Sampling Grid and Sample Collection

For regional, low-density sampling surveys, humus should ideally be collected in conjunction with till to better characterize the geochemical signature of the surficial media. In areas with known ice-flow history, both humus and till samples should be collected perpendicularly to the direction of the major ice flow (Hashmi, 2024a), in order to intercept any potential dispersal trains containing anomalous ore or pathfinder element concentrations (Table 1; McClenaghan *et al.*, 2023; Hashmi *et al.*, 2026). Table 2 summarizes the four main types of sampling surveys and their objectives. Most greenfield sampling surveys fall within the moderate-density and semi-detailed scales (1 sample in 0.25 to 10 km^2), depending on the objectives of the sampling survey. Realistically, in relatively built-up regions (*i.e.*, regions with a road and/or trail network), humus sampling sites will be highly dependent on the accessibility, and may follow a pseudo-random sampling distribution with consideration for potential sources of contamination, such as roads or

Table 2. Sampling density guidelines for humus sampling survey, modified after Dunn (2007)

Scale	Sample density	Objective
Reconnaissance-scale	1 site per 10 km^2 or greater	Investigate geochemical provinces
Moderate density	1 site per 1 – 10 km^2	Evaluate a mineral district
Semi-detailed	1 site per 0.25–1 km^2	Delineate individual/clusters of mineral deposits
Property-scale	1 site per 25–250 m	Infill sampling around previously identified anomalies

industries (McMartin *et al.*, 1996; McClenaghan *et al.*, 1998; Bajc and Hall, 2000; Hashmi *et al.*, 2022).

The live vegetation on the surface should be removed prior to humus sampling to expose the humified layer; this can be done using a stainless-steel knife and/or a reciprocating saw. Ideally ~750–1000 g sample should be collected to account for mass loss during drying due to moisture content. It is common practice to exclude the first 2–3 cm when possible, of the humus layer from sampling to reduce the potential for airborne contamination (*e.g.*, dust). Mineral matter and charcoal (if present) should also be documented because its presence can affect the samples' geochemistry (Hashmi *et al.*, 2026). Humus samples can be collected over both bedrock and till; where possible, the sample should be collected near an outcrop to increase confidence in the source for its geochemical signature.

Sample Pre-processing

Post collection, humus samples should be thoroughly air-dried under breathable cover while on the field and then in non-reactive aluminum pans in a commercial oven in the laboratory, generally at 30 to 40°C until completely dry (usually for up to seven days). They can then be submitted for crushing and sieving. Currently, the preferred size fraction for sieving is -80 mesh (<180 μm) for major and trace element analyses (Hashmi *et al.*, 2026). Humus samples should be sieved using solder-free stainless-steel sieves (or with silicone-coated solder if possible) to reduce Sn and Pb contamination from the solder.

Pre-processing for humus samples (before digestion and analysis) can include ashing. Ashing is the decomposition of sample material (usually ~100 g aliquot of dry sieved material) at high temperatures (475°C for 24 hours; Hashmi *et al.*, 2026), that is then reduced to 2–4 g of residual

material. This technique can be highly advantageous for humus because it can preconcentrate some ultra trace metals (occurring in the parts per trillion concentration range) by a factor of 25–50. However, ashing can also result in the loss of some key elements such as As, Cd, Cr, Hg, Mo, Ni, Se or Zn as volatile compounds (Azcue and Mudroch, 1994; Enders and Lehmann, 2012).

Analytical Techniques

Generally, the most frequently used method for determining major and trace metal concentrations in humus involves an *aqua regia* digestion (1:3 nitric to hydrochloric acid) followed by analysis by inductively coupled plasma-mass spectrometry (ICP-MS; Bajc and Hall, 2000; Hashmi *et al.*, 2026; Fig. 4). *Aqua regia* is considered a partial digestion that can dissolve most organic-bound base and precious metals (McClenaghan *et al.*, 2023).

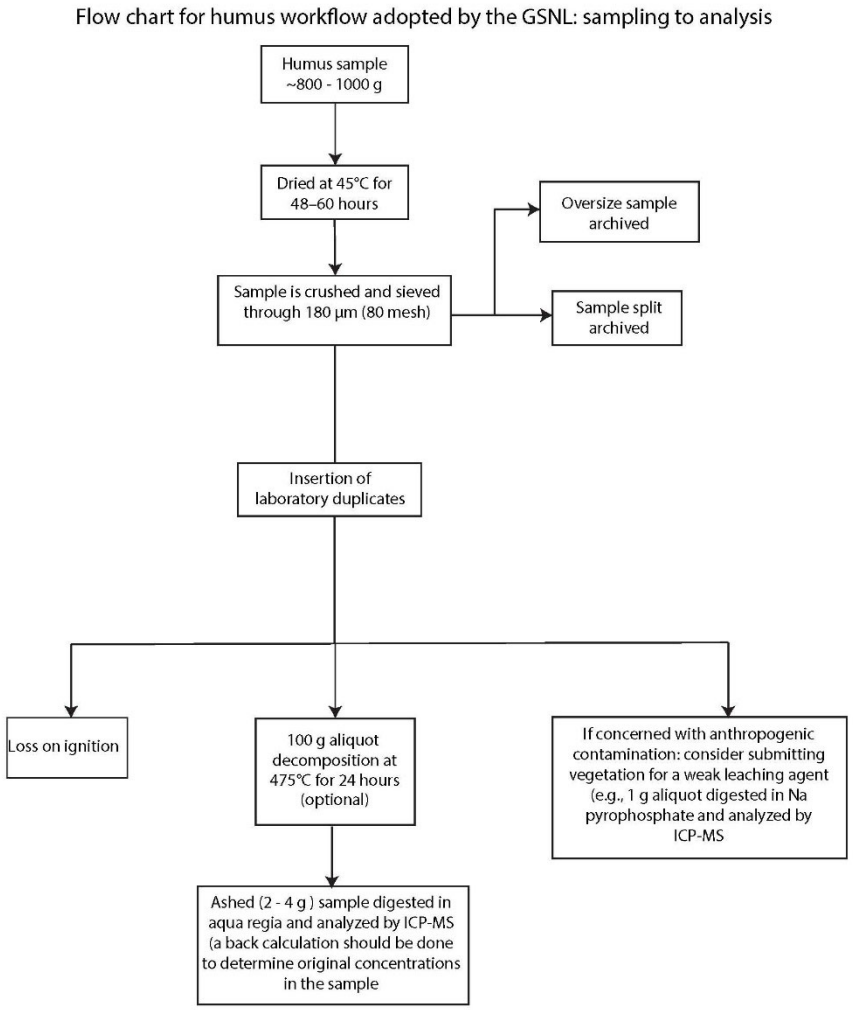


Figure 4. *Analytical workflow for humus samples processed and submitted for analyses by the Geological Survey of Newfoundland and Labrador (GSNL). Modified after Hashmi (2024a).*

Microwave digestion ICP-MS is another technique that has gained popularity as an effective method for digesting soil samples over the last few decades (Falciani *et al.*, 2000; Sastre *et al.*, 2002). Ideally, a combination of nitric and hydrofluoric acid in a closed vessel microwave digestion can provide complete dissolution of the sample, including solid silicate phases (Falciani *et al.*, 2000). For example, Sastre *et al.* (2002) tested digestion techniques to determine base metal (Cd, Cu, Pb and Zn) concentrations in standard reference materials (SRMs). The authors concluded that although for soil samples with high organic content, a nitric acid or a microwave hydrofluoric acid digestion could be used, a microwave *aqua regia* + hydrofluoric acid digestion was the optimal procedure for optimal recovery of most metals (Sastre *et al.*, 2002).

Instrumental neutron activation analysis (INAA) is also a popular method for determining element content in humus samples (Bajc, 1999; Dunn, 2007; Nyade *et al.*, 2013). Here, a ~15 g of dry solid sample is compressed and encapsulated in a sealed plastic vial and irradiated in a nuclear reactor. Instrument neutron activation analysis is beneficial for humus samples because the samples do not require digestion and the relatively large aliquot reduces nugget effect for elements such as Au. However, INAA detection limits are high relative to an ICP-MS (down to 10–100 parts-per-billion *versus* low parts-per-trillion, respectively), and the technique only offers a limited list of analytes, which does not include some key critical metals such as Li and rare earth elements (REEs).

Loss-on-ignition (LOI) can be used to determine the amount of organic carbon and other key characteristics (carbonate or interstitial water content of specific mineral phases) within humus (Sheldrick, 1984). It is typically determined by gradually heating a humus sample to temperatures ranging from 350°C to up to 1000°C (Sheldrick, 1984; Hashmi, 2024a), and therefore, can be used to estimate the amount of mineral matter present within the sample. Another way to determine the amount of organic *versus* mineral matter in a humus sample is by using a weak partial extraction method such as Na-pyrophosphate as this extraction targets the humic and fulvic components within organic matter. Sodium pyrophosphate followed by ICP-MS analyses can help determine the amount of trace metals associated with organic matter (Hall *et al.*, 1998).

Quality Control and Quality Assurance

Quality assurance measures in the field include cleaning of sampling tools (ideally with deionized water) before and after each sample to reduce cross contamination. Sample bags should be labelled clearly and photographed to ensure that sample location and identification numbers are not accidentally mixed up. Sampling crews must remove all jewelry prior to sampling, avoid smoking and wearing sunscreen on their hands (to reduce Zn contamination from the sunscreen; Hashmi *et al.*, 2026). Collection of field duplicates (one every 10 samples) will help determine site variability. In the laboratory, insertion of laboratory duplicates and certified reference materials (CRMs) will help determine repeatability, reproducibility, precision and accuracy of analyses. Most commercial laboratories will insert their own in-house CRMs as well.

Case Studies

Glover Island, Newfoundland and Labrador

A humus and till sampling program was carried out in 2022 on the island of Newfoundland around Au mineralization to determine whether humus could reflect the presence of Au mineralization in the ground, through Au content and associated pathfinders, the overlying humus, along with till. In total, 76 humus samples were collected in the Jackson's Arm, Nipper Harbour and Little Grand Lake map areas. Of these, sampling completed in the Little Grand Island region (*i.e.*, Glover Island) is summarized here, whereby Au mineralization is hosted within deformed metaconglomerate of the Basal Conglomerate Member and volcanic rocks of the Kettle Pond Formation of the Glover Group (Conliffe, 2022), as well as in altered volcanic rocks (Conliffe, 2021). A total of 31 humus and 3 till samples were collected within the vicinity of known Au mineralization. The samples were dried, crushed and sieved (*see* Hashmi, 2024a for details on the complete workflow). The <180 µm sieved humus fraction was ashed before undergoing Na-pyrophosphate extraction as well as *aqua regia*, followed by ICP-MS analyses. The geochemistry results demonstrate that elevated to highly anomalous concentrations of precious metals such as Au, Ag, Pd and Pt were present in humus samples collected over known Au mineralization, including up to 686 ppb Au, 21,000 ppb Ag (79 ppb Ag by Na-pyrophosphate), 49 ppb Pt and 15 ppb Pd (Hashmi, 2024; Fig. 5).

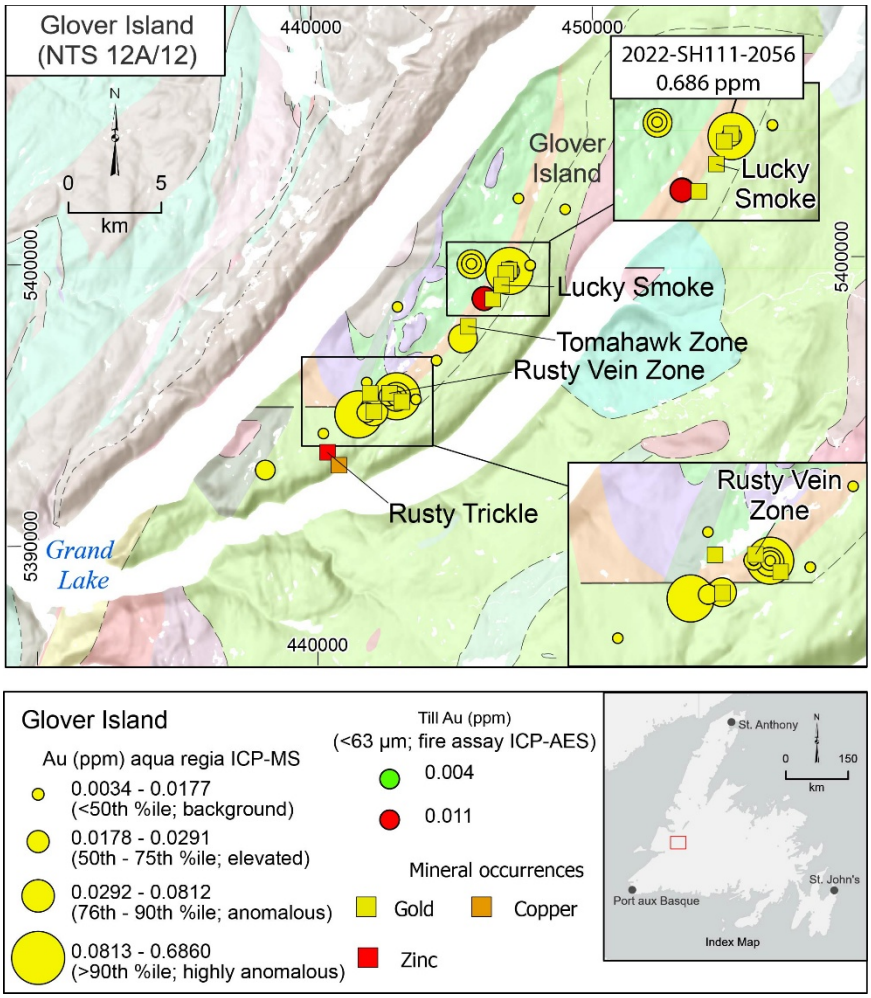


Figure 5. *Proportional dot plots showing Au concentration in humus and till on Glover Island. Figure modified after Hashmi (2024a).*

Alexis River Valley, Southeastern Labrador, Newfoundland and Labrador, Canada

A humus and till sampling survey was completed in the Alexis River Valley region (NTS map sheets 13A/10, 14 and 15) of southeastern Labrador, Newfoundland and Labrador, Canada, to target critical metal (REEs, U–Th, Ni–Cu) mineralization in the region (Hashmi, 2024b, c, d). This region is prospective for critical metals such as REEs and U (Gower, 2019; Magyarosi, 2022).

The bedrock in this region has been affected by multiple orogenic events, including the 1) Paleoproterozoic Eagle River orogenic event, 2) late Paleoproterozoic Labradorian orogenic event, and 3) the late Mesoproterozoic Grenvillian orogenic event (Gower, 2019). These orogenic events are characterized by key anorthositic intrusions in the region, including the Early Labradorian Alexis River Intrusion and the Upper Eagle River Mafic Intrusion. Mineral occurrences associated

with these intrusions include Ti (associated with the Alexis River anorthositic intrusion). Additionally, the 1.3 Ga Fox Harbour Volcanic Belt (FHVB) that hosts REE mineralization is located just outside the southeastern corner of the study area (Magyarosi, 2022). In total, 76 humus and 73 till samples were collected in the region. The humus samples were dried, milled and sieved to the <180 µm size fraction, followed by ashing and digestion by *aqua regia* and analysis by ICP-MS. Loss-on-ignition was also determined for the humus samples to determine organic content (Hashmi, 2024b, c, d). The results of the survey identified several sites with anomalous REE and U contents. The author also noted a strong spatial correlation between REE and U anomalies in both humus and till. Humus concentrations of 3.73 ppm HREE (sum of Tb, Dy, Ho, Er, Tm and Yb), relative to 84 ppm HREE in till (Fig. 6), and up to 62 ppm LREE (sum of La, Ce, Pr, Nd, Sm, Eu, Gd), relative to 817 ppm LREE in till (Fig 7), and up to 1.64 ppm U, relative to 9.45 ppm U in till (Fig. 8).

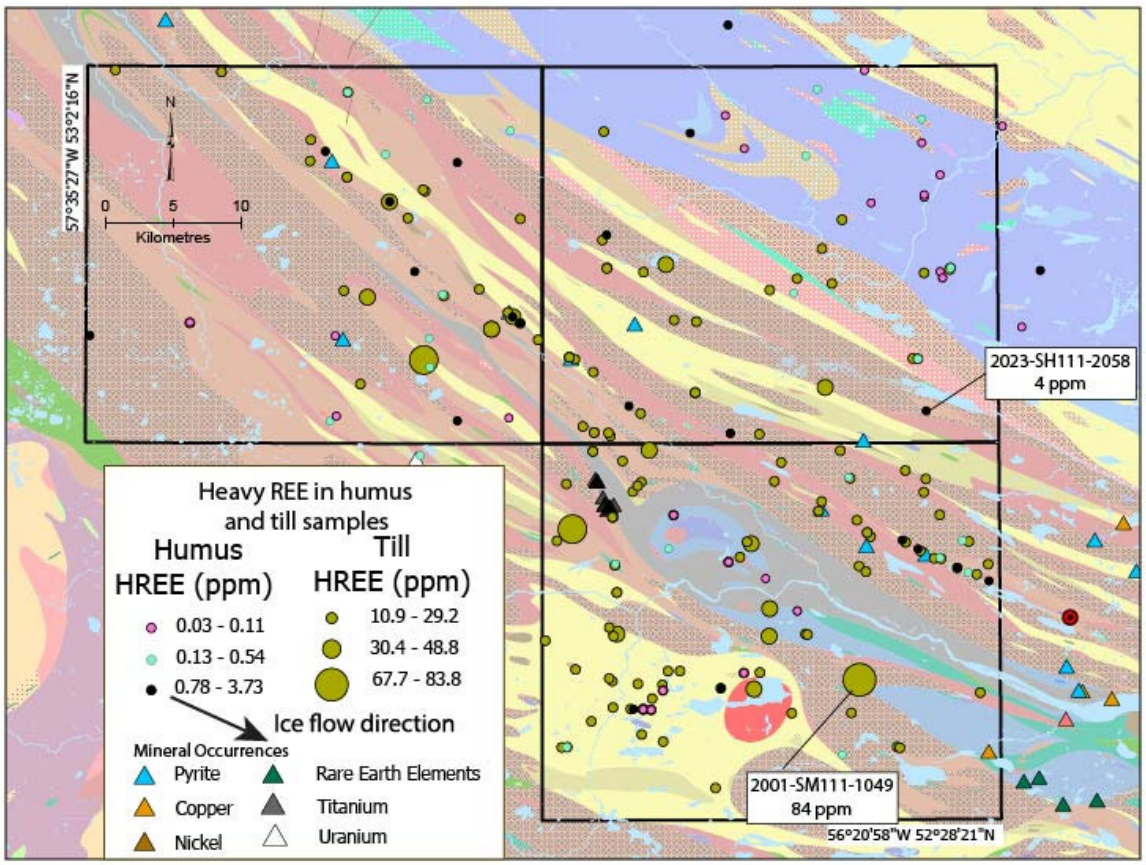


Figure 6. *Proportional dot plot shows HREE distribution in humus and till in the Alexis River Valley region. Figure modified after Hashmi* et al. *(2026).*

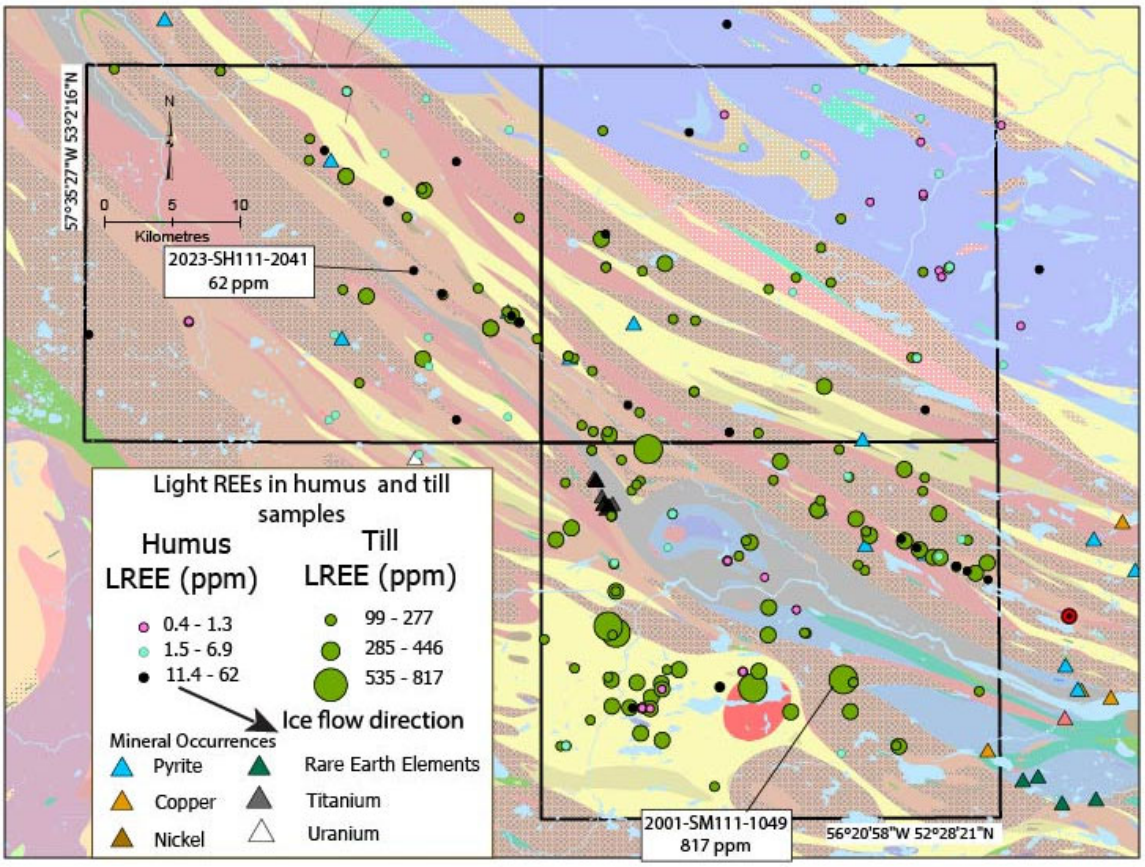


Figure 7. *Proportional dot plot shows LREE distribution in humus and till in the Alexis River Valley region in SE Labrador. Figure modified after Hashmi* et al. *(2026).*

Conclusions and Recommendations

Humus is the decomposed organic matter that lies above mineral soil and below live vegetation in a soil profile and is a well-suited sampling medium for greenfield exploration in glaciated terrain. It is easy to sample, light weight and relatively fast to collect (relative to till samples). Humus samples can be collected in conjunction with till and can be sampled over both bedrock and till and have been successfully used to explore precious and critical mineral commodities such as Au, Ag, REEs and base metals.

For greenfield exploration programs, a moderate- to high-density scale should be implemented, *i.e.*, 1 sample per 2–4 km^2, and ~750–1000 g sample should be collected to ensure that sufficient material is available for analysis after drying, crushing and sieving to <180 µm. Typically, humus samples are digested in *aqua regia* followed by ICP-MS analyses; however, closed-vessel microwave digestion paired with ICP-MS analyses is also gaining popularity as it provides

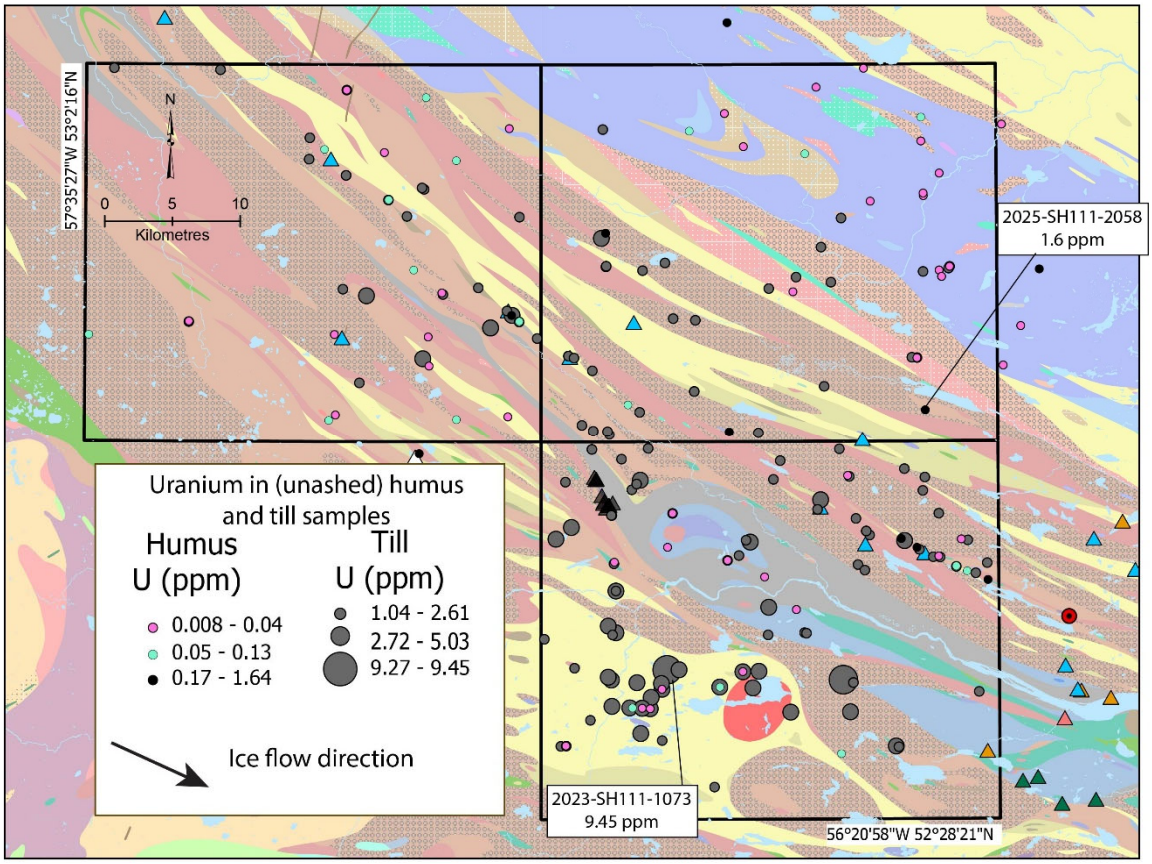


Figure 8. *Proportional dot plot shows U distribution in humus and till in the Alexis River Valley region in SE Labrador. Figure modified after Hashmi* et al. *(2026).*

complete digestion. It is useful to complete LOI on humus samples to determine the presence of mineral matter. In the presence of mineral matter, partial extractions such as Na-pyrophosphate paired with ICP-MS analyses can be used to determine the trace element content associated with organic matter as it targets only the humic and fulvic components within organic matter (compared to *aqua regia* which is a partial digestion). The case studies presented in this extended abstract demonstrate how humus can be successfully used to delineate Au mineralization on the island of Newfoundland as well as REE mineralization in southeast Labrador. In both case studies, the author determined that humus geochemistry can reflect both the geochemical anomalies within the underlying till as well as bedrock and that humus should be sampled in conjunction with till to maximize utilization of surficial media sampling for greenfield exploration in glaciated terrain.

References

Azcue, J. and Mudroch, A., 1994: Comparison of different washing, ashing, and digestion methods for the analysis of trace elements in vegetation. International Journal of Environmental Analytical Chemistry, Volume 57, pages 151–162. https://doi.org/10.1080/03067319408027420

Bajc, A.F., 1999: Results of regional humus and till sampling in the eastern part of the Shebandowan greenstone belt, northwestern Ontario. Ontario Geological Survey, Open File Report 5993, 85 pages.

Bajc, A.F. and Hall, G.E.M., 2000: Geochemical response of surficial media, north and east ranges, Sudbury basin. Ontario Geological Survey, Open File Report 6033, 265 pages.

Coker, W.B., Dunn, C.E., Hall, G.E.M., Rencz, A.N., DiLabio, R.N.W., Spirito, W.A. and Campbell, J.E., 1991: The behaviour of platinum group elements in the surficial environment at Ferguson Lake, N.W.T., Rottenstone Lake, Sask. and Sudbury, Ont., Canada. Journal of Geochemical Exploration, Volume 40, pages 165–192. https://doi.org/10.1016/0375-6742(91)90037-U

Conliffe, J., 2021: Geochemical and hyperspectral data from gold occurrences in the Glover Island and Grand Lake areas, western Newfoundland (NTS map area 12A/12). Government of Newfoundland and Labrador, Department of Industry, Energy and Technology, Geological Survey, Open File 012A/12/1845, 9 pages.

Conliffe, J., 2022: VMS-style mineralization in the Kettle Pond Formation, Glover Island NTS map areas 12A/12 and 13). *In* Current Research. Government of Newfoundland and Labrador, Department of Industry, Energy and Technology, Geological Survey, Report 22-1, pages 1–28.

Dunn, C.E., 1998: Geochemistry of humus from the southern La Ronge Domain, Saskatchewan (NTS 73P/7). Geological Survey of Canada. Open File 3345, 125 pages.

Dunn, C.E., 2007: Biogeochemistry in mineral exploration. *In* Handbook of Exploration and Environmental Geochemistry. *Edited by* C.E. Dunn. Elsevier Science B.V., pages xiii–460. https://doi.org/10.1016/S1874-2734(07)09001-8

Dyer, R.D. and Barnett, P.J., 2007: Multimedia exploration strategies for PGEs: Insights from the surficial geochemistry case studies Project, Lake Nipigon Region geoscience initiative, northwestern Ontario. Canadian Journal of Earth Sciences, Volume 44, pages 1169–1202. https://doi.org/10.1139/e07-031

Enders, A. and Lehmann, J., 2012: Comparison of wet-digestion and dry-ashing methods for total Elemental analysis of biochar. Communications in Soil Science and Plant Analysis, Volume 43, pages 1042–1052. https://doi.org/10.1080/00103624.2012.656167

Falciani, R., Novaro, E., Marchesini, M. and Gucciardi, M., 2000: Multi-element analysis of soil and sediment by ICP-MS after a microwave assisted digestion method. Journal of Analytical Atomic Spectrometry, Volume 15, pages 561–565. https://doi.org/10.1039/B000742K

Ferreira, K.J. and Fedikow, M.A.F., 1988: Preliminary results of a humus geochemical survey over the Rod Cu-Zn Deposit, Snow Lake, Manitoba. Manitoba Energy and Mines, Geological Services. Open File Report OF87-12.

Fortescue, J.A.C., 1985: A standardized approach to the study of the geochemistry of humus, Williams Property Hemlo, Thunder Bay district. Ontario Geological Survey, Geochemical Series, Map 80716.

Fortescue, J.A.C., Stahl, H. and Webb, J.R., 1986: Humus geochemistry near Barbara and Hanes lakes, Algoma District. Ontario Geological Survey, Geochemical Series, Map 80797.

Fortescue, J.A.C., Stahl, H. and Webb, J.R., 1988: Humus geochemistry in the Lac des Iles area, District of Thunder Bay. Ontario Geological Survey. Geochemical Series, Map 80800.

Govett, G.J.S., 1973: Differential secondary dispersion in transported soils and post-mineralization rocks: an electrochemical interpretation. International Geochemical Exploration Symposium, London, pages 81–91.

Gower, C.F., 2019: Regional geology of eastern Labrador (eastern Makkovik and Grenville provinces). Government of Newfoundland and Labrador, Department of Natural Resources, Geological Survey, Memoir 4 (Geofile LAB/1752), 654 pages.

Hall, G.E.M., 1998: Analytical perspective on trace element species of interest in exploration. Journal of Geochemical Exploration, Volume 61, pages 1–19. https://doi.org/10.1016/S0375-6742(97)00046-0

Hall, G.E.M., Parkhill, M.A. and Bonham-Carter, G.F., 2003: Conventional and selective leach geochemical exploration methods applied to humus and B Horizon soil overlying the Restigouche VMS Deposit, Bathurst Mining Camp, New Brunswick. *In* Massive Sulfide Deposits of the Bathurst Mining Camp, New Brunswick, and Northern Maine. *Edited by* W.D. Goodfellow, S.R. McCutcheon and J.M. Peter. Society of Economic Geology Monograph 11, pages 763–782. https://doi.org/10.5382/Mono.11.34

Hashmi, S., 2024a: Humus and till geochemistry in the vicinity of Au mineralization in Newfoundland: Results from Glover Island (NTS 12A/12 and 13), Jackson's Arm (NTS 12H/15) and Nippers Harbour (NTS 2E/13) map areas. Government of Newfoundland and Labrador, Department of Industry, Energy and Technology, Geological Survey, Open File NFLD/3458, 51 pages.

Hashmi, S., 2024b: New surficial geochemistry and indicator-mineral survey to target critical metals (base metals, PGEs, REEs, U): revisiting the Alexis River Valley region (NTS map areas 13A/10, 14 and 15) southeastern Labrador. *In* Current Research. Government of Newfoundland and Labrador, Department of Industry, Energy and Technology, Geological Survey, Report 21-1, pages 127–138.

Hashmi, S., 2024c: Humus-geochemistry data targeting critical metals (base metals, PGEs, REEs, U) in the Alexis River Valley region (NTS map areas 13A/10, 14 and 15), southeastern Labrador. Government of Newfoundland and Labrador, Department of Industry, Energy and Technology, Geological Survey, Open File 013A/0125, 9 pages.

Hashmi, S., 2024d: Till-geochemistry data targeting critical metals (base metals, PGEs, REEs, U) in the Alexis River Valley region (NTS map areas 13A/10, 14 and 15), southeastern Labrador. Government of Newfoundland and Labrador, Department of Industry, Energy and Technology, Geological Survey, Open File 013A/0126, 12 pages.

Hashmi, S., Leybourne, M.I., Hamilton, S., Layton-Matthews, D. and McClenaghan, M.B., 2022: Suitability of surficial media for Ni–Cu–PGE exploration in an established mining camp: A case study from the South Range of the Sudbury Igneous Complex, Canada. Geochemistry: Exploration, Environment, Analysis, Volume 22. https://doi.org/doi:10.1144/geochem2021-051

Hashmi, S. Voinot, A., and McClenaghan, M.B., 2026: Application of humus geochemistry to mineral exploration in glaciated terrain: A review. Geochemistry: Exploration, Environment, Analysis 2026. https://doi.org/10.1144/geochem2025-065

Kaszycki, C.A. and Hall, G.E.M., 1996: Application of phase selective and sequential extraction methodologies in surficial geochemistry. *In* EXTECH I: A Multidisciplinary Approach to Massive Sulphide Research in the Rusty Lake-Snow Lake Greenstone Belts, Manitoba. *Edited by* Bonham-Carter, G.F., Galley, A.G. and Hall, G.E.M. Geological Survey of Canada, Bulletin 426, pages 155–168.

Kauranne, L.K., 1992: Volume 5: Regolith exploration geochemistry in arctic and temperate terrains. *In* Handbook of Exploration and Environmental Geochemistry. *Edited by* L.K. Kauranne, K. Eriksson and R. Salminen.

Mann, A.W., Birrell, R.D., Fedikow, M.A.F. and Souza, H.A.F., 2005: Vertical ionic migration: mechanisms, soil anomalies, and sampling depth for mineral exploration. Geochemistry: Exploration, Environment, Analysis, Volum 5, pages, 201–210. https://doi.org/doi:10.1144/1467-7873/03-045

MacDonald, M.A., Boner, F.J. and Lombard, P.A., 1992: Multi-media detailed geochemical study of the Brazil Lake pegmatites (NTS 20P/13), Yarmouth County, Nova Scotia. Nova Scotia Department of Natural Resources, Open File Report 92-016, 159 pages.

McClenaghan, M.B., Paulen, R.C., Ayer, J.A., Trowell, N.F. and Bauke, S.D., 1998: Regional till and humus geochemistry of the Timmins-Kamiskotia area, northeastern Ontario (NTS 42A/11, 12, 13, 14). Geological Survey of Canada, Open File 3675, 287 pages.

McClenaghan, M.B., Paulen, R.C. *et al.*, 2023: Review of till geochemistry and indicator mineral methods for mineral exploration in glaciated terrain. Geochemistry: Exploration, Environment, Analysis, Volume 23. https://doi.org/doi:10.1144/geochem2023-013

McMartin, I., Henderson, P.J., Nielsen, E. and Campbell, J.E., 1996: Surficial geology, till and humus composition across the Shield margin, north-central Manitoba and Saskatchewan: Geospatial analysis of a glaciated environment. Geological Survey of Canada, Open File 3277, 300 pages.

Magyarosi, Z., 2022: Preliminary investigation of rare-earth-element mineralization, Fox Harbour volcanic belt, southeastern Labrador. *In* Current Research. Government of Newfoundland and Labrador, Department of Industry, Energy and Technology, Geological Survey, Report 22-1, pages 57–83.

Nyade, P.K., Wilton, D.H.C., Longerich, H.P., Thompson, G.M. and McNeill, P., 2013: Use of surficial geochemical methods to locate areas of buried uranium mineralization in the Jacque's Lake area of the Central Mineral Belt, Labrador, Canada. Canadian Journal of Earth Sciences, Volume 50, pages 1134–1146. https://doi.org/10.1139/cjes-2013-0032

Power, M.J., Hattori, K., Sorba, C. and Potter, E.G., 2012: Geochemical anomalies in the soil and uppermost siliciclastic units overlying the Phoenix uranium deposit, Athabasca Basin, Saskatchewan. Geological Survey of Canada, Open File 7257.

Salminen, R., 2008: Chapter 1- Field methods in regional geochemical surveys. *In* Environmental Geochemistry. *Edited by* B. De Vivo, H.E. Belkin and A. Lima. Elsevier, Amsterdam, pages 1–12. https://doi.org/10.1016/B978-0-444-53159-9.00001-2

Sheldrick, B.H. (ed.), 1984: Analytical methods manual. 1984; Research Branch, Agriculture Canada, LRRI Contribution No. 84-30. https://sis.agr.gc.ca/cansis/publications/manuals/1984-30/84-001-merged.pdf

Sastre, J., Sahuquillo, A., Vidal, M. and Rauret, G., 2002: Determination of Cd, Cu, Pb and Zn in environmental samples: Microwave-assisted total digestion *versus aqua regia* and nitric acid extraction. Analytica Chimica Acta, Volume 462, pages 59–72. https://doi.org/10.1016/S0003-2670(02)00307-0

Smee, B.W., 1998: A new theory to explain the formation of soil geochemical responses over deeply covered gold mineralization in arid environments. Journal of Geochemical Exploration, Volume 61, pages 149–172. https://www.sciencedirect.com/science/article/pii/S0375674298000077

van Geffen, P., Kyser, K.T., Oates, C.J. and Ihlenfeld, C., 2012: Till and vegetation geochemistry at the Talbot VMS Cu-Zn prospect, Manitoba, Canada: Implications for mineral exploration. Geochemistry: Exploration, Environment, Analysis, Volume 12, pages 67–88. https://doi.org/doi:10.1144/1467-7873/11-RA-066

Aqueous Geochemistry in Mineral Exploration

Matthew I. Leybourne[1], James Kidder[2], Alexandre Voinot[2],
Daniel Layton-Matthews[1], and McLean Trott[1]
[1]Queen's University, Queen's Facility for Isotope Research, Department of Geological Sciences and Geological Engineering, Kingston, ON, K7L 3N6
[2]Geological Survey of Canada, 601 Booth Street, Ottawa, ON, K1A 0E8

Abstract

Ground and surface waters remain important media for the geochemical exploration of many different styles of mineralization. Water-transported (hydromorphic) metals can develop anomalous concentrations that reveal hidden mineralization directly (dissolved phase) and through adsorption and precipitation reactions with suspended and bed-load stream sediments (labile fraction). Groundwater recharges to depth, resulting in greater likelihood of interacting with buried mineralization compared to surface geochemical methods. Advances over the past two decades in understanding water–rock interaction, metal transport and attenuation, and analytical technology have substantially enhanced the efficacy of aqueous geochemical exploration.

*Significant developments since 2007 include: (1) routine sub-parts-per-trillion (ppt) dissolved gold detection in groundwater using rigorous field protocols; (2) widespread adoption of non-traditional metal stable isotopes (Li, B, Fe, Cu, Zn, Se, Mo) as pathfinder and source-discrimination tools; (3) recognition of the role of metal nanoparticles and colloids in anomaly transport; (4) application of hydrogeochemistry to critical mineral commodities including lithium, cobalt, and rare earth elements in support of the energy transition; (5) technological advances in drilling technologies (*e.g.*, direct push) allowing for low-cost grid drilling for water; and (6) integration of machine-learning approaches for multi-element geochemical data interpretation. The most successful aqueous-phase indicators of mineralization remain those that are ore-associated and mobile in solution under prevailing pH-Eh conditions.*

Introduction

Aqueous geochemistry—encompassing ground and surface water chemistry and the labile fraction of stream sediments—has been applied successfully in mineral exploration for several

decades (Appelo and Postma, 2004; Drever, 1997). Since the synthesis of Leybourne (2007), the field has advanced substantially, driven by improvements in analytical sensitivity, new isotopic tools, and a growing body of case studies across diverse geological settings and climate zones. The central challenge identified in 2007 has intensified: most shallow, surface-exposed deposits have already been found. Discovery now depends on detecting buried mineralization beneath cover sequences that may be tens to hundreds of metres thick (Cameron *et al.*, 2004; Kidder *et al.*, 2025; Reid *et al.*, 2023). This challenge reflects the long-recognized shift from surface to covered exploration environments (Rose *et al.*, 1979).

Hydrogeochemistry has proven to be an especially powerful tool for this challenge. Because groundwaters penetrate deeply into the Earth's crust and integrate chemical signals from the rocks and ore bodies they traverse, they can generate anomalies detectable at surface even when mineralization is concealed beneath post-mineral cover, laterite, regolith, till, or transported overburden (Buskard *et al.*, 2019; Carey *et al.*, 2003; Kidder *et al.*, 2025). Case studies compiled in the most recent systematic review (Kidder *et al.*, 2025) demonstrate anomalies in stream and groundwaters detectable up to 10 km from deposit sources, and covering commodities including Cu, Au, Zn–Pb, U, Ni-PGE, and diamonds.

This paper updates the Leybourne (2007) synthesis, retaining the original structure—methods, deposit-type case studies, and sampling recommendations—and incorporates advances published through 2026. The paper also addresses critical mineral commodities (Li, REE, Co), non-traditional isotope systems, nanoparticle and colloid geochemistry, and the emerging use of data science in hydrogeochemical exploration.

Principles of Aqueous Geochemical Exploration

Anomaly Formation and Transport Mechanisms

Geochemical techniques for mineral exploration rely on the development of anomalies against the regional geochemical background. In aqueous geochemical exploration, any anomalous signature is fundamentally a result of hydromorphic (colloidal and dissolved water-transported) dispersion. These processes are consistent with classical models of solute transport and equilibrium

in natural waters (Garrels and Christ, 1965). This distinguishes waters from stream sediments, soil, and till, in which anomalies can develop through both mechanical and hydromorphic processes.

Several mechanisms transport metals from buried deposits to sampled waters. Primary oxidation of sulphide minerals—where oxygen-bearing groundwaters interact with mineralized rock—releases metals and sulphate into solution. Redox (Eh) and pH together govern the stability of dissolved metal species. Similar controls are widely documented in groundwater systems impacted by natural and mining-related geochemical gradients (Blowes *et al.*, 2014; Nordstrom, 2011). Most ore metals (Cu, Pb, Zn, Ni) are relatively immobile at near-neutral pH, whereas oxyanion-forming elements (As, Se, Mo, Re, V) remain mobile at neutral to slightly alkaline conditions and can create large distal dispersion halos (Cameron *et al.*, 2002; Leybourne and Cameron, 2008). Understanding these controls is essential for designing surveys and interpreting results (Kidder *et al.*, 2025).

Since 2007, recognition of the role of metal nanoparticles and colloids in aqueous transport has grown considerably. The importance of colloidal transport in natural waters has been widely recognized in environmental geochemistry (Filella, 2006; Lead and Wilkinson, 2006), including riverine systems where colloids dominate trace metal fluxes (Pokrovsky *et al.*, 2012). Gold, in particular, occurs in colloidal form in many natural waters, explaining solubility values that exceed predictions from classical thermodynamic models (Hough *et al.*, 2011; Leybourne *et al.*, 2000a; Reith *et al.*, 2012). Similarly, Fe- and Mn-oxyhydroxide nanoparticles scavenge trace metals from solution and may be carriers of ore-related geochemical signatures in both groundwater and surface water (Hochella *et al.*, 2019). Proper ultrafiltration (to 1 kDa or smaller) is increasingly recommended in research programmes to distinguish truly dissolved, colloidal, and particulate fractions (Zhu *et al.*, 2024).

Water–Rock Interaction and Geochemical Modelling

Mineral saturation indices and metal speciation calculations remain core tools, implemented in software such as PHREEQC (Parkhurst and Appelo, 2013), The Geochemist's Workbench (Bethke, 2008), and MINTEQA2 (Allison *et al.*, 1991). These approaches build on decades of groundwater modelling and hydrogeochemical thermodynamics (Appelo and Postma, 2004).

Important advances since 2007 include: improved thermodynamic databases, especially for trace metals in saline and high-temperature systems; kinetic rate models for sulphide oxidation and silicate weathering; and reactive-transport modelling frameworks that couple geochemistry with groundwater flow (Zhu *et al.*, 2024). These tools are now accessible to non-specialist users and have become more routinely applied in exploration-scale hydrogeochemical programmes.

Machine learning and multivariate statistical methods have become important complements to speciation modelling for interpreting large, multi-element hydrogeochemical datasets. Random forest classifiers, support vector machines, and neural network approaches have been applied to discriminate mineralized from background waters, to predict pathfinder element concentrations, and to identify geochemical anomalies (Carranza, 2011; Rodriguez-Galiano *et al.*, 2015). More broadly, machine learning methods have demonstrated strong potential for spatial prediction and anomaly detection in geochemical datasets (Cracknell and Reading, 2014; Zuo *et al.*, 2016). Deep learning approaches, while requiring large training datasets, show promise for anomaly detection at the regional scale (Xu *et al.*, 2025).

Aqueous Geochemical Exploration for Specific Deposit Types

The following sections summarise key considerations in the hydrogeochemical exploration of specific deposit types. Table 1 lists key geochemical characteristics, and Table 2 summarizes key pathfinders and methods. A lithium and critical mineral section has been added to reflect the rapidly expanding importance of these commodities.

The fundamental hydrogeochemical characteristics of VMS deposits established in the Bathurst Mining Camp studies (Leybourne *et al.*, 1998, 2002, 2003; Leybourne and Goodfellow, 2003) have been confirmed and extended in subsequent research. Zinc remains the most consistently anomalous and widely dispersed indicator in both ground and surface waters, with coincident anomalies of Pb, Cu, As, Mo, Sb, and elevated sulphate providing additional support. The strong control of pH on metal mobility—with carbonate buffering suppressing Zn and Pb concentrations and limiting dispersion—has been further documented across diverse VMS-hosting terrains. These observations are consistent with broader exploration frameworks that integrate hydrogeochemistry with indicator mineral approaches (McClenaghan, 2005).

Table 1. Major components of different deposit types

Deposit type	Major components	Minor components	Labile components	Relatively immobile components	Suitable isotopes
VMS	Fe, S, Cu, Zn, Pb	Cd, Hg, Au, As, Sb, Ba, Bi, In	Fe, S, Zn, Cu, As, Pb, Bi, In	Pb, Bi, In, Au, Ag, Ba	S, Pb, Fe, Cu, Zn
Porphyry Cu ± Mo	Cu, Mo, S	Cu, Mo, S, Fe, Se, Ag, Au, As, Re	Cu, Mo, S, Fe, Se, As, Re	Ag, Au	S, Cu, Mo
SEDEX	Fe, S, Cu, Zn, Pb	Ag, Au, Ba, Cd	Fe, S, Zn, Cu, C	Pb, Ba, Au, Ag	Pb, S, Zn
Gold (vein)	Au, Ag	As, Sb, Se, Te, S, Hg	S, Se, As, Hg, Te, Sb	Au, Ag	S, Tl
Ni–Cu–PGE	Ni, Cu, PGE	Cr, Co, S	Cu, S, PGE	Co, Ni, Cr	S, Os, Re-Os, Cu, Ni
Kimberlite (diamond)	Sr, Nb, Ba, Cr, Ni	LILE, HFSE, REE	Sr, LILE	Ba, HFSE, Nb, Cr, Ni, REE	Sr, Nd, Pb
Unconformity U	U	Se, Mo, V, Cu, Pb	U, Se, Cu, Mo	Pb, V	Pb, U-series, Tl, Mo
Li-Brine / Pegmatite	Li, B	Mg, K, Na, Rb, Cs	Li, B, Rb, Cs		Li, B, Sr

Notes: HFSE–high-field-strength elements; LILE–large ion lithophile elements; REE–rare earth elements; PGE–platinum group elements

Significant advances since 2007 include the application of non-traditional stable isotopes to VMS hydrogeochemistry. Iron isotopes ($\delta^{56}Fe$) record sulphide oxidation and Fe-oxyhydroxide precipitation, potentially fingerprinting VMS-derived iron in surface and groundwaters *(Rouxel et al.*, 2008). Zinc isotopes ($\delta^{66}Zn$) show systematic fractionation between ore minerals and secondary dispersion products, offering a new vector tool (Gagnevin *et al.*, 2012; John *et al.*, 2008). Copper isotopes ($\delta^{65}Cu$) are fractionated by supergene oxidation and may help trace Cu sources in cover sequences (Mathur *et al.*, 2009). Sulphur isotopes ($\delta^{34}S$), long used in VMS exploration, are now routinely combined with sulphate oxygen isotopes ($\delta^{18}O_{SO4}$) to constrain sulphide oxidation pathways (Kidder *et al.*, 2025; Leybourne *et al.*, 2022).

The global hydrogeochemical review of Kidder *et al.* (2025) synthesized VMS case studies across eastern and northern Canada, western Australia, Scandinavia, and the Iberian Pyrite Belt, demonstrating that the principles established at Bathurst are broadly applicable across climatic regimes, though survey design and sampling density must be adapted to local hydrology and pH buffering.

Table 2. Summary of key aqueous geochemical pathfinders for different deposit types, updated to 2025

Type of deposit	Main pathfinders	Secondary pathfinders	Analytical techniques	Key references	Notes
VMS	Zn	Low pH, Pb, SO_4, As	(TQ) ICP-MS; IC; MC-ICP-MS isotopes	Kidder *et al.* (2025); Buskard *et al.* (2020); Leybourne *et al.* (2003)	Zn/Fe-isotopes fingerprint ore; radiogenic Pb fingerprints ore *vs.* non-ore; non-traditional isotopes increasingly useful to track fluid pathways
Porphyry Cu ± Mo	Distal: Se, Re, Mo, As; Proximal: Cu	Pb, Zn, S	(TQ) ICP-MS; IC; MC-ICP-MS	Kidder *et al.* (2025); Cameron and Leybourne (2005); Leybourne and Cameron (2006)	S/Se values and Cu isotopes distinguish ore from saline regional waters
SEDEX	Zn	Ag, Au, Ba, Cd, Pb	(TQ) ICP-MS; IC; TIMS; MC-ICP-MS	Kidder *et al.* (2025); Kelley and Taylor (1997)	Sulphide-Pb isotopically distinct; Pb isotopes fingerprint ore *vs.* non-ore Pb
Gold (vein)	Au (ppt level)	Se, As, Sb	(TQ) ICP-MS (BrCl preservation); activated carbon	Reid *et al.* (2023); Gray (2001); Buskard *et al.* (2020)	ppt-level Au detection now routine; As/Sb supplementary; saline waters may suppress oxyanion pathfinders; Li isotopes show promise
Cu-Ni-PGE	Ni, Cu, Pd	As, Cr, Co, S, other PGE	(TQ) ICP-MS; IC	Hattori and Cameron (2004); Kidder *et al.* (2025)	Pd mobile as hydroxide complexes at alkaline pH; enhanced in sulphide-rich settings
Kimberlite (diamond)	Elevated pH, low Mg, high K/Mg	Ni, Co, Cr; elevated Co/Mg and Ni/Mg	(TQ) ICP-MS; IC	Sader *et al.* (2007); Kidder *et al.* (2025)	Brucite and serpentine precipitation consume Mg; Sr, REE assist in rock-type discrimination
Unconformity U	Oxidizing: U, Rn; Reducing: Se, Mo	Se, Mo, As, V, Cu, Pb	(TQ) ICP-MS; IC; TIMS; MC-ICP-MS	Dickson and Giblin (2006); Pirlo and Giblin (2004)	Radiogenic $^{207}Pb/^{204}Pb$ and $^{206}Pb/^{204}Pb$ useful; U-series isotopes promising; Tl isotopes appear to be unimpacted by secondary remobilization
Li deposits / brines	Li, B	Mg, Na, K, Rb	(TQ) ICP-MS; Li/B isotopes by MC-ICP-MS	Godfrey *et al.* (2019); Munk *et al.* (2025)	Li and B isotopes distinguish brine sources; evaporation *vs.* rock dissolution signatures; Sr isotopes fingerprint heavily differentiated/ alkaline-rich mineral phases (spodumene, leipidolite *etc.*)

Notes: ICP-MS–inductively coupled plasma-mass spectrometry (TQ = triple quadrupole); MC-ICP-MS–multi-collector ICP-MS; IC–ion chromatography; TIMS–thermal ionization mass spectrometry; BrCl–bromine chloride preservation for gold

Porphyry Copper and Related Deposits

Porphyry Cu systems remain among the best candidates for hydrogeochemical exploration, because they tend to produce large, long-lived supergene, mobile oxyanion halos (Se, Re, Mo, As) detectable for several kilometres downflow of mineralization under near-neutral oxidizing conditions. Supergene redistribution of gold has long been recognized as a function of climate, geomorphology, and redox conditions (Bowell, 1992; Webster and Mann, 1984). The Spence deposit case studies (Cameron and Leybourne, 2005; Leybourne and Cameron, 2006, 2008) established the conceptual framework that remains current: oxyanion mobility creating distal vectors, Cu restricted to proximal zones by adsorption, and stable S isotopes constraining fluid sources and detecting ore interaction.

Since 2007, copper isotopes have emerged as an important addition to the porphyry hydrogeochemical toolkit. Oxidative leaching of chalcopyrite and secondary Cu minerals produces systematic isotopic fractionation, with supergene Cu-bearing waters acquiring lighter $\delta^{65}Cu$ values than primary mineralization (Braxton and Mathur, 2011; Mathur *et al.*, 2009). These signatures can be traced in groundwaters and soil pore waters to fingerprint Cu derived from mineralization. Re isotopes ($^{187}Re/^{185}Re$) and Re–Os systematics have also been explored as tracers of Mo–Cu mineralization in groundwater, though analytical challenges remain (Kidder *et al.*, 2025).

Rhenium, being a highly mobile oxyanion (ReO_4^-) under oxidizing conditions and a specific pathfinder for Mo-bearing porphyry systems, has received increasing attention as an exploration tool. Its extreme mobility and low natural background make it a sensitive distal indicator in both surface water and groundwater (Kidder *et al.*, 2025; Leybourne and Cameron, 2008).

Sedimentary Exhalative (SEDEX) Deposits

The basic framework for SEDEX hydrogeochemistry remains as described by Leybourne (2007): Zn is the dominant and most widely dispersed indicator, with host rock carbonate buffering controlling the magnitude and extent of metal anomalies. SEDEX deposits in black shale-dominant settings with limited carbonate produce the largest and most multi-element anomalies, whereas carbonate-buffered settings restrict mobility.

Lead isotopes remain a particularly powerful tool for SEDEX exploration, as the isotopically distinctive Pb of SEDEX ore minerals can be traced in groundwaters and stream sediments even where absolute Pb concentrations are low (Kidder *et al.*, 2025). Zinc isotopes offer additional discrimination potential, given the distinctive $\delta^{66}Zn$ values of SEDEX sulphide mineralization (John *et al.*, 2008). Regional hydrogeochemical surveys over the Howard's Pass district have confirmed the utility of water chemistry for mapping sub-crop SEDEX targets.

Gold Deposits

The detection of dissolved gold in groundwater at parts-per-trillion (ppt) levels has become one of the most important advances in exploration hydrogeochemistry since 2007. Buskard *et al.* (2019) provided a comprehensive assessment of dissolved Au at ppt concentrations, establishing rigorous field sampling and analytical protocols that make routine ppt-level Au measurement feasible. Dissolved Au provides the best and most direct hydrogeochemical vector to Au mineralization. Research across the Yilgarn Craton of Western Australia has confirmed that groundwater Au anomalies directly associated with orogenic (mesothermal) Au mineralization can be detected through thick regolith cover, although anomaly footprints can be small given the low solubility of Au (Gray *et al.*, 2016; Reid *et al.*, 2023).

Thiosulphate complexing of gold under mildly oxidizing, near-neutral to alkaline conditions remains an important mechanism for Au dispersion. However, colloidal transport of Au has been increasingly recognized as significant in near-surface waters, particularly in lateritic and tropical regolith profiles (Hough *et al.*, 2011; Reith *et al.*, 2012). Ultrafiltration studies have shown that a substantial fraction of dissolved Au—previously assumed to be truly dissolved—is in fact carried by nanometre-scale colloids. This distinction has implications for the dispersion distance and anomaly morphology of Au in groundwater and for comparison with equilibrium speciation model predictions.

Arsenic and Sb remain useful secondary pathfinders for Au at neutral to near-neutral pH, but their utility is reduced in acidic sulphate waters (Buskard *et al.*, 2019; Gray, 2001). The sulphur isotopic composition of dissolved sulphate can provide a vector to Au-associated sulphide mineralization, particularly in arid regolith settings (Kidder *et al.*, 2025; Whitford *et al.*, 1997).

Preservation protocols for Au in water samples have been refined. The use of 1% bromine chloride (BrCl) acidification to preserve dissolved Au in HDPE bottles, or field preconcentration on activated carbon sachets, remain the recommended approaches (Buskard *et al.*, 2019; Kidder *et al.*, 2025; Leybourne *et al.*, 2000a).

Magmatic Cu–Ni–PGE Deposits

Hydrogeochemical exploration for magmatic Ni–Cu–PGE deposits has remained relatively limited, but key findings from the Lac des Iles case study (Hattori and Cameron, 2004) have been confirmed and the framework extended. Palladium is the most mobile PGE under oxidizing near-neutral to alkaline conditions, forming hydroxide complexes that are not strongly adsorbed to clay or Fe-oxyhydroxide surfaces. Nickel and Cu, mobilized where acidic conditions prevail from Fe-sulphide oxidation, provide closer-range vectors. The distinctive mafic-ultramafic host rocks raise groundwater pH through hydrolysis of Mg–Fe silicates, which can limit base metal mobility but enhances Pd dispersion.

Osmium concentrations and Re–Os isotopes of groundwaters and stream sediments in komatiitic Ni–Cu–PGE settings could be a fruitful avenue for exploration, although there have been no studies to date. Although analytical challenges remain, this system offers unique fingerprinting capability for komatiite-hosted sulphides distinct from any other rock type.

Kimberlite and Diamond Exploration

The aqueous geochemistry of groundwater-kimberlite interaction, established primarily through the Kirkland Lake case studies (Sader *et al.*, 2007, 2021), remains the primary framework for diamond exploration hydrogeochemistry. Elevated pH (commonly >9, reaching >12 in some cases), anomalously low Mg, and high K/Mg values in groundwaters interacting with kimberlite are robust indicators of ultramafic rock interaction. As Sader *et al.* (2007) noted, these responses occur regardless of whether the kimberlite is diamond-bearing or barren, presenting an interpretive challenge.

Unconformity-Type Uranium Deposits

Dissolved uranium remains the best hydrogeochemical indicator of unconformity-type U mineralization under oxidizing conditions, with Se, Mo, V, and Cu as supporting pathfinders. The fundamental challenge of U being immobile under reducing conditions—which may prevail in close proximity to ore—remains. U-series isotope disequilibrium ($^{234}U/^{238}U$ activity ratios) has been further developed as an indicator of recent U dissolution and transport, providing information even where total U concentrations are not highly anomalous (Dickson and Giblin, 2006).

Radon (^{222}Rn) in groundwater has received renewed attention as a near-field indicator of U mineralization, given its short half-life (~3.8 days) limiting dispersion but making it very sensitive to immediate proximity to U ore (Sukanya *et al.*, 2022). Helium isotopes, particularly the accumulation of radiogenic ^{4}He in groundwater, are increasingly applied as regional-scale tracers of fluid residence time and crustal flux in sedimentary basins (*e.g.*, Pinti *et al.*, 2022). These processes are analogous to regional groundwater evolution and residence-time controls observed in sedimentary aquifers (Edmunds and Smedley, 2000). In the Athabasca Basin, basin-scale circulation of U-bearing fluids through thick sandstone sequences provides the hydrogeological framework for transport of dissolved species (Chi *et al.*, 2019), and earlier hydrogeochemical studies demonstrate that helium forms part of groundwater anomaly suites associated with uranium mineralization (Earle and Drever, 1983).

Critical Mineral Deposits: Lithium, Cobalt, and Rare Earth Elements

The energy transition has created substantial demand for critical minerals—lithium, cobalt, nickel, manganese, rare earth elements, and others—and has motivated the application of hydrogeochemistry to exploration for these commodities (Zhu *et al.*, 2024).

Lithium exploration using water geochemistry has developed rapidly, particularly for continental brine (salar) systems. Groundwater Li concentrations and Li isotopes ($\delta^{7}Li$) provide vectors to Li-enriched brines in evaporitic basin settings (Godfrey *et al.*, 2019; Munk *et al.*, 2025). Lithium isotopes are fractionated by water-rock interaction, evaporation, and clay mineral

adsorption, producing distinctive $\delta^{7}Li$ values for different brine and rock sources. Boron isotopes ($\delta^{11}B$) provide complementary discrimination.

Cobalt is typically associated with Ni–Cu–PGE sulphide, laterite, and sediment-hosted Cu–Co deposits (*e.g.*, Ziwa *et al.*, 2020). In lateritic systems, intense ferruginous weathering of ultramafic rocks leads to redistribution and enrichment of Co in Fe–Mn oxyhydroxides (Marsh *et al.*, 2013; Newsome *et al.*, 2020). Under acidic and oxidizing conditions, dissolution of primary and secondary Co-bearing minerals can release Co^{2+} into groundwater, generating elevated concentrations proximal to mineralized zones (Ziwa *et al.*, 2020). The Katanga-style sediment-hosted Cu–Co deposits of central Africa have been explored using water chemistry tracing of Co, Cu, and associated elements in local streams and groundwaters.

Rare earth element (REE) hydrogeochemistry has expanded considerably, driven by both critical mineral exploration and environmental research. The mobility of REEs in aqueous systems is strongly influenced by complexation and colloidal transport processes (Johannesson *et al.*, 1996; Tang and Johannesson, 2010). Groundwaters near ion-adsorption clay REE deposits, the dominant global source of heavy REEs, carry distinctive REE signatures reflecting the weathering of enriched laterites (Kidder *et al.*, 2025). The negative Ce anomaly in oxidizing surface waters, generated by Ce oxidation to Ce^{4+} and precipitation, is a sensitive indicator of redox conditions and can be used diagnostically in exploration programmes (Leybourne *et al.*, 2000b). REE patterns normalized to chondrite or PAAS (Post-Archean Australian Shale) in groundwaters may be able to fingerprint mineralized *versus* barren rock types.

Discussion: Aqueous Geochemistry in Mineral Exploration

Ground and Surface Water Sampling Techniques and Strategies

The sampling methods documented in Leybourne (2007), including bailers, double-valve pumps, straddle-packer systems for groundwaters; direct collection from actively flowing streams for surface waters, remain current. Key updates include:

- Purpose-drilled groundwater sampling bores are increasingly cost-effective when the target area is defined, allowing sample density to match deposit footprint sizes (Buskard *et al.*, 2019; Kidder and Jones, 2017; Kidder *et al.*, 2025).

- Multi-parameter field probes (pH, Eh, conductivity, dissolved oxygen, temperature) have improved in quality, cost, and ease of use. In-line flow-through cell measurements at pump discharge are now standard practice in research programmes, preventing atmospheric oxidation of sensitive species.
- Field-portable X-ray fluorescence instruments have advanced but remain limited in detection capability for the most critical trace elements (Pelchat *et al.*, 2013). Laboratory-based ICP-MS with collision/reaction cell technology provides the best combination of detection limits, multi-element capability, and matrix tolerance.
- Passive sampling devices, such as diffusion samplers (peepers), DGT (diffusive gradients in thin films) (Mohammadi *et al.*, 2022), and activated carbon samplers for Au, have found application in exploration programmes where repeated sampling is impractical *(Buskard et al.*, 2019; Kidder *et al.*, 2025). DGT in particular offers a time-integrated, operationally labile metal fraction that can enhance anomaly contrast.

Stable and Radiogenic Isotopes: Advances Since 2007

Isotopic tools have advanced dramatically since 2007, driven by the wide availability of MC-ICP-MS instruments in commercial and university laboratories, automation of element purification workflows, and by rapidly declining analysis costs. Triple quadrupole ICP-MS instruments are increasingly being used for isotope ratio measurements as well. The application of isotopes in hydrogeology builds on established frameworks for tracing fluid sources and pathways (Kendall and McDonnell, 1988). The rapid expansion of many non-traditional isotope systems reflects advances in analytical precision and theoretical frameworks for isotope fractionation *(Johnson et al.*, 2004). The Kidder *et al.* (2025) review highlights isotopes as one of the most significant advances in exploration hydrogeochemistry of the past two decades.

1. Sulphur isotopes ($\delta^{34}S$ of dissolved sulphate and sulphide) remain the most practically useful stable isotope system in mineral exploration hydrogeochemistry, providing vectors to mineralization and constraining fluid sources. The $\delta^{18}O$ of dissolved sulphate ($\delta^{18}O_{SO4}$) combined with $\delta^{34}S$ constrains sulphide oxidation pathways. Oxygen and H isotopes of water continue to be invaluable for understanding groundwater recharge, flow history, and mixing. Carbon isotopes constrain carbonate dissolution and organic matter interactions.

2. Lead isotopes remain an important fingerprinting tool, particularly for VMS, SEDEX, and U deposits where ore-related Pb has distinctive $^{206}Pb/^{204}Pb$ and $^{207}Pb/^{204}Pb$ values. The lower cost and greater accessibility of quadrupole (especially triple quadrupole) ICP-MS-based Pb isotope measurements (compared to TIMS) has been realized. Strontium and Nd isotopes in groundwaters can help discriminate rock types with which the fluids have interacted, supporting kimberlite, REE, and mafic-ultramafic deposit exploration.
3. Isotopic research has expanded enormously since 2007. Iron isotopes ($\delta^{56}Fe$) record redox-controlled Fe cycling and sulphide oxidation. Copper isotopes ($\delta^{65}Cu$) are fractionated during supergene Cu enrichment and can trace Cu mineralization sources in groundwater. Zinc isotopes ($\delta^{66}Zn$) are fractionated at ore deposits and in secondary dispersion. Selenium isotopes ($\delta^{82}Se$) record redox changes and can fingerprint Se from sulphide mineralization. Lithium and boron isotopes ($\delta^{7}Li$, $\delta^{11}B$) are powerful tools for critical mineral exploration and for characterizing water-rock interaction in diverse geological settings. Molybdenum isotopes ($\delta^{98}Mo$) record redox conditions and can fingerprint ore-associated Mo in surface and groundwaters.

Metal Nanoparticles and Colloids

A major conceptual advance since 2007 has been the recognition that a significant fraction of "dissolved" metal in natural waters—including exploration samples collected with standard 0.45 μm filtration—is in fact associated with nanoparticles and colloids (Hochella *et al.*, 2019). Gold nanoparticles are now recognized as a primary form of Au in near-surface geochemical systems (Leybourne *et al.*, 2000a), explaining the apparent supersaturation relative to classical solubility models and the unexpected mobility of Au in some regolith profiles (Hough *et al.*, 2011). Iron and manganese oxyhydroxide nanoparticles transport adsorbed trace metals (including REEs, Co, As, and others) over distances that may not be predictable from classical dissolved-phase geochemistry alone.

Practical implications for exploration include the need to consider filtration cut-off in sample design (Knaack *et al.*, 2021): 0.45 μm filtration is operationally practical but includes many nanoparticles. Research programmes investigating the colloidal fraction require ultrafiltration (1–10 kDa membranes) or flow field-flow fractionation. There are still some practicality compli-

cations for mineral exploration, including the need for filtration inside a mobile fume hood and the collection of multiple aliquiots (*e.g.*, bulk along with multiple stage retentate and permeate sub-samples), however these will likely be overcome as equipment becomes smaller and more efficient. These approaches are not yet routine in commercial exploration programmes but represent a frontier likely to be adopted as analytical costs decrease and the practicality of in field filtration increases.

The Role of Microbiology

Since 2007, the role of microbial activity in controlling sulphide oxidation, metal mobilization, and metal attenuation in surficial environments has been much more thoroughly documented (Reith *et al.*, 2012; Southam and Saunders, 2005). Microorganisms catalyse the oxidative dissolution of sulphide and iron minerals, accelerating the generation of acid mine drainage and, by extension, of natural geochemical anomalies around undisturbed sulphide deposits. Sulphate-reducing bacteria influence the speciation of dissolved metals and sulphur, potentially attenuating metal dispersion. Biomineralization of secondary Au (re-precipitation of dissolved Au by bacteria in regolith) has been documented at several sites, with implications for the morphology of Au anomalies in near-surface environments. Similarly, Enders *et al.* (2006) correlated Cu leaching and supergene enrichment of the Morenci porphyry deposit (USA) to the activity of Fe oxidizing and sulphate reducing bacteria. Microbiologically mediated processes are now incorporated into reactive-transport models of ore weathering. A practical workflow for microbial water sampling can be complicated by the logistics of remote locations mineral exploration. Generally, a sampling methodology can be based around a peristaltic pump with specialized 0.22 μm filter capsules. Microbial material captured on the filter must be preserved immediately. Samples typically require deep freeze preservation which is not always possible in exploration camps. DNA preservation in field conditions can be achieved using lysis buffers (*e.g.*, Longmire's buffer) or by desiccation (*e.g.*, silica gel), both of which have been shown to maintain DNA integrity under ambient conditions (Allison, 2021; Majaneva *et al.*, 2018; Renshaw *et al.*, 2015; Wegleitner *et al.*, 2015).

Hydrology and Survey Design

Hydrological understanding remains critical for interpreting hydrogeochemical results, and several advances since 2007 are relevant to aqueous geochemical exploration. Climate-conditioned

hydrological regimes exert a strong control on the expression and detectability of hydrogeochemical anomalies. The global compilation of Kidder *et al.* (2025) includes case studies across arid, semi-arid, temperate, tropical, and Arctic settings, providing climate-specific guidance on survey timing, sample media selection, and anomaly interpretation.

Remote sensing of groundwater recharge areas, groundwater depth, and drainage patterns now assists survey design. Satellite-based estimates of evapotranspiration, precipitation, and topographically driven flow paths can support regional hydrogeochemical programmes in data-sparse areas (*e.g.*, Adams *et al.*, 2022). Airborne electromagnetic surveys commonly provide hydrogeological information (depth to water table, saline groundwater extent) directly relevant to hydrogeochemical survey planning (*e.g.*, Zhdanov *et al.*, 2026).

The distinction between gaining and losing stream reaches is critical for interpreting whether a stream samples groundwater or loses water to the subsurface and is now more readily assessed using temperature profiling, tracer tests, and hydrograph separation. Understanding groundwater residence times and flow systems is critical for interpreting hydrogeochemical anomalies (Edmunds and Smedley, 2000). Such information is particularly valuable where the objective is to detect deeply buried deposits through their groundwater signature in streams.

Data Science and Multi-Element Analysis

Advances in analytical capability have made it routine to measure 50–70 elements simultaneously in water samples by ICP-MS. The resulting multi-element datasets require sophisticated statistical and machine-learning approaches for optimal interpretation. Principal component analysis, cluster analysis, and discriminant analysis remain standard tools. More recently, random forests, gradient boosting, and neural network classifiers have been applied to distinguish mineralized from background groundwaters and to predict ore-related element concentrations from multi-element datasets (Attanasi *et al.*, 2026; Rodriguez-Galiano *et al.*, 2015; Xu *et al.*, 2025). These approaches are particularly powerful when combined with geological and mineralogical priors to constrain model training. Recent work has also shown that examining the feature importance of inputs used for prediction of element concentrations can provide insight into controlling factors driving hydrogeochemical anomalies (Podgorski *et al.*, 2022).

Compositional data analysis (CoDa), treating geochemical data as compositions that sum to a constant (the total dissolved solids), is now recognized as more appropriate than classical statistical methods for many hydrogeochemical datasets. Log-ratio transformations applied before multivariate analysis avoid the spurious correlations introduced by the constant-sum constraint (Buccianti and Pawlowsky-Glahn, 2005).

Recommendations for Sampling and Analytical Protocols

The sampling and analytical recommendations of Leybourne (2007) remain broadly valid. The following updates reflect advances since 2007.

Routine Exploration

1. Groundwaters can be sampled rapidly with a flow-through bailer or portable submersible pump. Samples should be taken from at least 5 m below the static water level. Surface waters are sampled from the actively flowing part of the stream, avoiding stagnant pools.
2. At minimum, one 250–500 mL unacidified aliquot for anion analysis and one acidified aliquot (1% v/v ultrapure HNO_3) for cation and trace element analysis should be collected. Samples should be filtered to 0.45 μm using disposable cartridge filters and plastic syringes (*i.e.*, no rubber septum). For Au-focused programmes, a separate aliquot acidified to 1% with BrCl is required to stabilise dissolved Au, Ag, and Hg.
3. Field measurements should include, at minimum: pH, electrical conductivity, dissolved oxygen, temperature, and where applicable, Eh (ORP). These should be measured in a sealed flow-through cell where possible to avoid atmospheric contamination of redox-sensitive parameters.
4. QA/QC protocols: include field duplicates (minimum 1 in 20 samples), field blanks (deionized water), and submitted standards or certified reference materials. Charge balance calculations (using measured cations and anions) should be evaluated for all samples as an internal consistency check; imbalances >10% warrant repeat analysis.
5. ICP-MS with collision/reaction cell technology (CRC-ICP-MS) is the preferred analytical method, providing multi-element capability with low detection limits and reduced polyatomic interferences for Se, As, and other problematic elements. ICP-OES supple-

ments ICP-MS for major elements (Fe, Mn, Ca, Mg, Na, K, S). Ion chromatography (IC) is required for halides (Cl, Br, F), sulphate, and nitrate.

Exploration Research

6. Groundwater samples collected for research programmes should use a double-valve pump or straddle-packer system to ensure representative sampling at depth in fracture-dominated aquifers. In-line multiparameter probes measuring pH, Eh, conductivity, dissolved oxygen, and temperature from the pump discharge are strongly recommended.
7. Additional sample aliquots should be collected for stable isotopes of water ($\delta^{2}H$, $\delta^{18}O$), dissolved sulphate ($\delta^{34}S$, $\delta^{18}O_{SO4}$), and where appropriate for non-traditional isotopes (Fe, Cu, Zn, Li, B, Se). Isotope samples require specific preservation protocols (*e.g.*, $BaCl_2$ precipitation for sulphur isotopes; refrigeration without acidification for water isotopes).
8. For Au exploration: activated carbon sachets (field preconcentration) or BrCl acidification remain the recommended preservation approaches. For dissolved ppt-Au analyses, purpose-cleaned HDPE bottles and contamination-free sampling protocols (no stainless steel, no rubber seals, no gold jewellery) are essential.
9. Where budget permits, DGT (diffusive gradients in thin films) passive samplers deployed in groundwater or surface water provide time-integrated labile metal concentrations and can enhance anomaly contrast over spot samples.
10. Geochemical speciation modelling (PHREEQC or equivalent) should be applied routinely to research-quality datasets to understand element mobility controls and guide interpretation.
11. Integration with hydrological data (groundwater levels, hydraulic head, isotopic age dates) is essential for spatial interpretation of hydrogeochemical data.

Future Directions and Knowledge Gaps

1. Dissolved gold detection at ppt levels has matured considerably. Future work should focus on extending this capability to other precious and critical metals, including Pt, Pd, and REEs at ultra-low concentrations.

2. Colloid and nanoparticle geochemistry in exploration hydrogeochemistry remains under-exploited. The distinction between dissolved and colloidal fractions remains a central challenge in aquatic geochemistry (Lead and Wilkinson, 2006). Standardized sampling and analysis protocols for the colloidal fraction are needed, and case studies linking colloidal metal anomalies to specific deposit types are required to build interpretive frameworks.
3. Non-traditional stable isotopes (Fe, Cu, Zn, Se, Li, B, Mo, Sb, Tl) are ready for broader application in mineral exploration hydrogeochemistry. Cost reductions in MC-ICP-MS analyses and the development of reference materials for aqueous samples will accelerate adoption. Systematic characterization of isotopic fractionation factors relevant to near-surface ore weathering is still ongoing.
4. Application of hydrogeochemistry to critical mineral commodities—particularly Li, Co, Mn, Sc, REEs, and Ga—is at an early stage. There is an urgent need for deposit-scale case studies, characterization of element mobility under relevant near-surface conditions, and integration with brine and regolith geochemistry.
5. Machine learning and data fusion approaches show great promise for extracting more information from multi-element hydrogeochemical datasets. Well-curated, openly accessible datasets from historic exploration programmes would greatly accelerate development of these methods.
6. The influence of climate change on near-surface hydrogeology—including changes in groundwater recharge, depth to water table, salinity, and redox conditions—will affect the expression of hydrogeochemical anomalies in many environments. Understanding these impacts is critical for designing surveys that will remain fit for purpose under changing climate conditions.
7. Improved integration of hydrogeochemical surveys with airborne geophysical data (EM, magnetics, gravity), remote sensing, and geological mapping will maximise the value of hydrogeochemical results in exploration programmes.

Conclusions

Aqueous geochemistry has established itself as a powerful and cost-effective exploration tool for a wide range of deposit types, particularly for detecting buried or deeply concealed mineralization beneath cover sequences. Since Leybourne's (2007) synthesis, the field has

advanced substantially across analytical capability, isotopic tools, conceptual understanding of metal transport and attenuation, and application to new commodity types. These advances build on a long foundation of hydrogeochemical theory and exploration geochemistry (Appelo and Postma, 2004; Rose *et al.*, 1979), while increasingly incorporating modern analytical and computational approaches. The key conclusions and recommendations are:

1. Hydrogeochemistry is uniquely suited to detecting buried mineralization through its ability to integrate chemical signals along groundwater flow paths. Case studies document anomalies detectable up to 10 km from deposit sources (Kidder *et al.*, 2025).
2. Dissolved gold at ppt levels in groundwater is now a routine and reliable exploration tool for orogenic Au deposits, enabled by rigorous field protocols and modern ICP-MS (Buskard *et al.*, 2020). Dissolved Au provides the most direct aqueous vector to Au mineralization.
3. Non-traditional metal stable isotopes (Fe, Cu, Zn, Se, Li, B, Mo) have emerged as valuable additions to the hydrogeochemical toolkit, providing source discrimination and process fingerprinting capabilities that are not available from elemental data alone (Kidder *et al.*, 2025).
4. Metal nanoparticles and colloids are significant carriers of ore-related geochemical signatures in natural waters. The 0.45 μm operational filter boundary does not separate truly dissolved from colloidal species. Research programmes should consider ultrafiltration to characterize these fractions.
5. Hydrogeochemistry is rapidly expanding into critical mineral exploration, particularly for lithium (brines and pegmatites), cobalt, and rare earth elements. Li and B isotopes are powerful tools for brine characterization and exploration.
6. Isotopic analyses—particularly Pb, S, and non-traditional metal isotopes—are becoming more accessible and cost-effective, and their routine incorporation into exploration programmes is strongly recommended.
7. Survey design must be adapted to local hydrology, climate, and cover type. Understanding groundwater flow paths, recharge areas, and gaining *vs.* losing stream reaches is essential for interpreting hydrogeochemical data.

8. Machine learning approaches offer powerful tools for interpreting multi-element hydrogeochemical datasets and should be increasingly integrated into exploration data workflows.

References

Adams, K.H., Reager, J.T., Rosen, P., Wiese, D.N., Farr, T.G., Rao, S., Haines, B.J., Argus, D.F., Liu, Z., Smith, R., Famiglietti, J.S. and Rodell, M., 2022: Remote sensing of groundwater: Current capabilities and future directions. Water Resources Research, Volume 58(10).

Allison, J.D., Brown, D.S. and Novo-Gradec, K.J., 1991: MINTEQA2/PRODEFA2, a geochemical assessment model for environmental systems. EPA/600/3-91/021, U.S. Environmental Protection Agency, Athens, GA.

Allison, M.J., 2021: Effects of preservation methods on environmental DNA detection and quantification. Environmental DNA, Volume 3, pages 815–822.

Appelo, C.A.J. and Postma, D., 2004: Geochemistry, Groundwater and Pollution (2nd ed.). CRC Press.

Attanasi, E., McDevitt, B., Freeman, P. and Coburn, T., 2026. Evaluating machine learning approaches to identify and predict oil and gas produced water lithium concentrations. Data Science in Science, Volume 5(1).

Bethke, C.M., 2008: The Geochemist's Workbench. University of Illinois.

Blowes, D.W., Ptacek, C.J., Jambor, J.L., Weisener, C.G., Paktunc, D., Gould, W.D. and Johnson, D.B., 2014: The geochemistry of acid mine drainage. *In* Treatise on Geochemistry. *Edited by* H.D. Heinrich and K.K. Turekian. Elsevier, pages 131–190.

Bowell, R.J., 1992: Supergene gold mineralogy at Ashanti, Ghana: Implications for the supergene behaviour of gold. Mineralogical Magazine, Volume 56(385), pages 545–560.

Braxton, D. and Mathur, R., 2011: Exploration applications of copper isotopes in the supergene environment; a case study of the Bayugo porphyry copper-gold deposit, southern Philippines. Economic geology and the bulletin of the Society of Economic Geologists, Volume 106(8), pages 1447–1463.

Buccianti, A. and Pawlowsky-Glahn, V., 2005: New perspectives on water chemistry and compositional data analysis. Mathematical Geology, Volume 37(7), pages 703–727.

Buskard, J., Reid, N. and Gray, D., 2019: Parts per trillion (ppt) gold in groundwater: Can we believe it, what is anomalous and how do we use it? Geochemistry: Exploration, Environment, Analysis, Volume 20(2), pages 189–198.

Cameron, E.M., Hamilton, S.M., Leybourne, M.I., Hall, G.E.M. and McClenaghan, B., 2004: Finding deeply-buried deposits using geochemistry. Geochemistry: Exploration, Environment, Analysis, Volume 4, pages 7–32.

Cameron, E.M. and Leybourne, M.I., 2005: Relationship between groundwater chemistry and soil geochemical anomalies at the Spence copper porphyry deposit, Chile. Geochemistry: Exploration, Environment, Analysis, Volume 5, pages 135–145.

Cameron, E.M., Leybourne, M.I. and Kelley, D.L., 2002: Exploring for deeply covered mineral deposits: Formation of geochemical anomalies in northern Chile by earthquake-induced surface flooding of mineralized groundwaters. Geology, Volume 30, pages 1007–1010.

Carey, M.L., McPhail, D.C. and Taufen, P.M., 2003: Groundwater flow in playa lake environments: Impact on gold and pathfinder element distributions in groundwaters surrounding mesothermal gold deposits, St. Ives area, Eastern Goldfields, Western Australia. Geochemistry: Exploration, Environment, Analysis, Volume 3, pages 57–71.

Carranza, E.J.M., 2011: Analysis and mapping of geochemical anomalies using logratio-transformed stream sediment data with censored values. Journal of Geochemical Exploration, Volume 110(2), pages 167–185.

Chi, G., Chu, H., Petts, D., Potter, E., Jackson, S. and Williams-Jones, A., 2019: Uranium-rich diagenetic fluids provide the key to unconformity-related uranium mineralization in the Athabasca Basin. Scientific Reports, Volume 9(1). https://doi.org/10.1038/s41598-019-42032-0

Cracknell, M.J. and Reading, A.M., 2014: Geological mapping using remote sensing data: A comparison of five machine learning algorithms, their response to variations in the spatial distribution of training data and the use of explicit spatial information. Computers & Geosciences, Volume 63, pages 22–33.

Dickson, B. and Giblin, A., 2006: New horizons for groundwater geochemistry in uranium exploration, AESC2006, Melbourne, Australia.

Drever, J.I., 1997: The Geochemistry of Natural Waters. Prentice-Hall, Englewood Cliffs, NJ, USA, 436 pages.

Earle, S.A.M. and Drever, G.L., 1983: Hydrogeochemical exploration for uranium within the Athabasca Basin, northern Saskatchewan. Journal of Geochemical Exploration, Volume 19, pages 57–73.

Edmunds, W.M. and Smedley, P.L., 2000: Residence time indicators in groundwater: The East Midlands Triassic sandstone aquifer. Applied Geochemistry, Volume 15, pages 737–752.

Enders, M.S., Knickerbocker, C., Titley, S.R. and Southam, G., 2006: The role of bacteria in the supergene environment of the Morenci Porphyry Copper Deposit, Greenlee County, Arizona. Economic Geology, Volume 101(1), pages 59–70.

Filella, M., 2006: Colloidal properties of submicron particles in natural waters. Environmental Colloids and Particles, pages 17–93.

Gagnevin, D., Boyce, A.J., Barrie, C.D., Menuge, J.F. and Blakeman, R.J., 2012: Zn, Fe and S isotope fractionation in a large hydrothermal system. Geochimica et Cosmochimica Acta, Volume 88, pages 183–198.

Garrels, R.M. and Christ, C.L., 1965: Solutions, Minerals, and Equilibria. Freeman, Cooper & Co., San Francisco, 450 pages.

Godfrey, L.V., Herrera, C., Gamboa, C. and Mathur, R., 2019: Chemical and isotopic evolution of groundwater through the active Andean arc of Northern Chile. Chemical Geology, Volume 518, pages 32–44.

Gray, D.J., 2001: Hydrogeochemistry in the Yilgarn Craton. Geochemistry: Exploration, Environment, Analysis, Volume 1, pages 253–264.

Gray, D.J., Noble, R.R.P., Reid, N., Sutton, G.J. and Pirlo, M.C., 2016: Regional scale hydrogeochemical mapping of the northern Yilgarn Craton, Western Australia; a new technology for exploration in arid Australia. Geochemistry: Exploration, Environment, Analysis, Volume 16(1), pages 100–115.

Hattori, K.H. and Cameron, E.M., 2004: Using the high mobility of palladium in surface media in exploration for platinum group element deposits: Evidence from the Lac des Iles region, northwestern Ontario. Economic Geology, Volume 99, pages 157–171.

Hochella, M.F., Jr., Mogk, D.W., Ranville, J., Allen, I.C., Luther, G.W., Marr, L.C., McGrail, B.P., Murayama, M., Qafoku, N.P., Rosso, K.M., Sahai, N., Schroeder, P.A., Vikesland, P., Westerhoff, P. and Yang, Y., 2019: Natural, incidental, and engineered nanomaterials and their impacts on the Earth system. Science, Volume 363(6434).

Hough, R.M., Noble, R.R.P. and Reich, M., 2011: Natural gold nanoparticles. Ore Geology Reviews, Volume 42(1), pages 55–61.

Johannesson, K.H., Stetzenbach, K.J., Hodge, V.F. and Lyons, W.B., 1996: Rare earth element complexation behavior in circumneutral pH groundwaters: Assessing the role of carbonate and phosphate ions. Earth and Planetary Science Letters, Volume 139(1-2), pages 305–319.

John, S.G., Rouxel, O.J., Craddock, P.R., Engwall, A.M. and Boyle, E.A., 2008: Zinc stable isotopes in seafloor hydrothermal vent fluids and chimneys. Earth and Planetary Science Letters, Volume 269(1-2), pages 17–28.

Johnson, C.M., Beard, B.L. and Albarède, F., 2004: Geochemistry of non-traditional stable isotopes. Reviews in Mineralogy and Geochemistry, Mineralogical Society of America, Volume 55.

Kendall, C. and McDonnell, J.J.E., 1988: Isotope tracers in catchment hydrology. Elsevier.

Kidder, J. and Jones, S., 2017: Exploration under total cover: A case study from northwest Botswana.

Kidder, J.A., Reid, N., Noble, R.R.P., Leybourne, M.I., Buskard, J., Bowell, R.J., Stoltze, A. and Garrett, R.G., 2025: A review of hydrogeochemical techniques for mineral exploration: History, present and future. Geochemistry: Exploration, Environment, Analysis, Volume 25(2).

Knaack, D., Ivey, G., MacPhee, C., Peterzon, J., Price, L., Williams, M. and Leybourne, M.I., 2021: The effect of filtration size on the geochemistry of groundwater samples from a massive sulfide deposit at the Bathurst Mining Camp, New Brunswick, Canada. Geochemistry: Exploration, Environment, Analysis, Volume 21(4).

Lead, J. and Wilkinson, K., 2006: Aquatic colloids and nanoparticles: Current knowledge and future trends. Environmental Chemistry, Volume 3, pages 159–171.

Leybourne, M.I., 2007: Aqueous geochemistry in mineral exploration. *In* Mineral Resources of Canada: A Synthesis of Major Deposit-types, District Metallogeny, the Evolution of Geological Provinces, and Exploration Methods. *Edited by* W.D. Goodfellow. Geological Association of Canada, Mineral Deposits Division, Special Publication No. 5, pages 1007–1034.

Leybourne, M.I., Boyle, D.R. and Goodfellow, W.D., 2003: Interpretation of stream water and sediment geochemistry in the Bathurst Mining Camp, New Brunswick: Applications to mineral exploration. *In* Massive Sulphide Deposits of the Bathurst Mining Camp, New Brunswick, and Northern Maine. *Edited by* W.D. Goodfellow, S.R. McCutcheon and J.M. Peter. Society of Economic Geologists, Inc., Littleton, CO, pages 741–762.

Leybourne, M.I. and Cameron, E.M., 2006: Composition of groundwaters associated with porphyry-Cu deposits, Atacama Desert, Chile: Elemental and isotopic constraints on water sources and water-rock reactions. Geochimica et Cosmochimica Acta, Volume 70, pages 1616–1635.

Leybourne, M.I. and Cameron, E.M., 2008: Source, transport, and fate of rhenium, selenium, molybdenum, arsenic, and copper in groundwater associated with porphyry-Cu deposits, Atacama Desert, Chile. Chemical Geology, Volume 247, pages 208–228.

Leybourne, M.I. and Goodfellow, W.D., 2003: Processes of metal solution and transport in ground waters interacting with undisturbed massive sulfide deposits, Bathurst Mining Camp, New Brunswick. *In* Massive Sulphide Deposits of the Bathurst Mining Camp, New Brunswick, and Northern Maine. *Edited by* W.D. Goodfellow, S.R. McCutcheon and J.M. Peter. Society of Economic Geologists, Inc., Littleton, CO, pages 723–740.

Leybourne, M.I., Goodfellow, W.D. and Boyle, D.R., 1998: Hydrogeochemical, isotopic, and rare earth element evidence for contrasting water-rock interactions at two undisturbed Zn-Pb massive sulphide deposits, Bathurst Mining Camp, N.B., Canada. Journal of Geochemical Exploration, Volume 64, pages 237–261.

Leybourne, M.I., Goodfellow, W.D. and Boyle, D.R., 2002: Sulfide oxidation and groundwater transport of base metals at the Halfmile Lake and Restigouche Zn-Pb massive sulfide deposits, Bathurst Mining Camp, New Brunswick. Geochemistry: Exploration, Environment, Analysis, Volume 2, pages 37–44.

Leybourne, M.I., Goodfellow, W.D., Boyle, D.R. and Hall, G.E.M., 2000a: Form and distribution of anthropogenic gold mobilized in surface waters and sediments from a gossan tailings pile, Murray Brook massive sulfide deposit, New Brunswick, Canada. Applied Geochemistry, Volume 15, pages 629–646.

Leybourne, M.I., Goodfellow, W.D., Boyle, D.R. and Hall, G.M., 2000b: Rapid development of negative Ce anomalies in surface waters and contrasting REE patterns in groundwaters associated with Zn-Pb massive sulphide deposits. Applied Geochemistry, Volume 15, pages 695–723.

Leybourne, M.I., Layton-Matthews, D., Peter, J.M. and Kidder, J.A., 2022: Controls on groundwater selenium, arsenic and base metals in groundwater around a selenium-bearing volcanogenic massive sulfide deposit: Constraints from stable isotopes, trace elements and redox controls. Geochemistry: Exploration, Environment, Analysis, Volume 22(2).

Majaneva, M., Diserud, O.H., Eagle, S.H.C., Boström, E., Hajibabaei, M. and Ekrem, T., 2018: Environmental DNA filtration techniques affect recovered biodiversity. Scientific Reports, Volume 8, Article 4682.

Marsh, E., Anderson, E., Gray, F., 2013: Nickel-cobalt laterites: A deposit model. 2010-5070H, Reston, VA.

Mathur, R., Titley, S., Barra, F., Brantley, S., Wilson, M., Phillips, A., Munizaga, F., Maksaev, V., Vervoort, J. and Hart, G., 2009. Exploration potential of Cu isotope fractionation in porphyry copper deposits. Journal of Geochemical Exploration, Volume 102(1), pages 1–6.

McClenaghan, M.B., 2005: Indicator mineral methods in mineral exploration. Geochemistry: Exploration, Environment, Analysis, Volume 5(3), pagesa 233–245.

Mohammadi, A., Corbett, T., French, A., Lehto, N., Hadfield, J., Jarman, P., Sandwell, D., Shokri, A., Schipper, L. and Hartland, A., 2022. Application of diffusive gradients in thin films for monitoring groundwater quality. ACS ES&T Water, 2.

Munk, L.A., Boutt, D., Butler, K., Russo, A., Jenckes, J., Moran, B. and Kirshen, A., 2025: Lithium brines: Origin, characteristics, and global distribution. Economic Geology, Volume 120(3), pages 575–597.

Newsome, L., Solano Arguedas, A., Coker, V.S., Boothman, C. and Lloyd, J.R., 2020: Manganese and cobalt redox cycling in laterites; biogeochemical and bioprocessing implications. Chemical Geology, Volume 531.

Nordstrom, D.K., 2011. Mine waters: Acidic to circumneutral. Elements, Volume 7(6), pages 393–398.

Pelchat, P., Gammon, P.R., Vaive, J.E., McCurdy, M.W., Dunbar, A., Bryson, S. and Khan, B., 2013: On-site analysis of wetland surface-water samples by total reflection x-ray fluorescence spectrometry. Natural Resources Canada.

Pinti, D.L., Larocque, M., Méjean, P., Saby, M., Hernández-Hernández, M.A., Gagné, S., Roulleau, E., Sano, Y., Castro, M.C., Matsumoto, T. and Horoi, V., 2022: Regional-scale distribution of helium isotopes in aquifers: How informative are they as groundwater tracers and chronometers? Water, Volume 14(12).

Pirlo, M.C. and Giblin, A.M., 2004: Application of groundwater-mineral equilibrium calculations to geochemical exploration for sediment-hosted uranium: Observations from the Frome Embayment, South Australia. Geochemistry: Exploration, Environment, Analysis, Volume 4, pages 113–127.

Podgorski, J., Araya, D. and Berg, M., 2022: Geogenic manganese and iron in groundwater of Southeast Asia and Bangladesh - Machine learning spatial prediction modeling and comparison with arsenic. Science of the Total Environment, Volume 833, Article 155131.

Pokrovsky, O.S., Shirokova, L.S., Zabelina, S.A., Vorobieva, T.Y., Moreva, O.Y., Klimov, S.I., Chupakov, A.V., Shorina, N.V., Kokryatskaya, N.M., Audry, S., Viers, J., Zoutien, C. and Freydier, R., 2012: Size fractionation of trace elements in a seasonally stratified boreal lake: Control of organic matter and iron colloids. Aquatic Geochemistry, Volume 18(2), pages 115–139.

Reid, N., Plet, C., Thorne, R.L., Hunt, A., Hille, J., Noble, R.R.P. and Gray, D.J., 2023: Gold exploration using groundwater in Western Australia. Geochemistry: Exploration, Environment, Analysis, Volume 23(2).

Reith, F., Stewart, L. and Wakelin, S.A., 2012: Supergene gold transformation: Secondary and nano-particulate gold from southern New Zealand. Chemical Geology, Volume 320-321, pages 32–45.

Renshaw, M.A., Olds, B.P., Jerde, C.L., McVeigh, M.M. and Lodge, D.M., 2015: The room temperature preservation of filtered environmental DNA samples and assimilation into a phenol-chloroform-isoamyl alcohol DNA extraction. Molecular Ecology Resources, Volume 15(1), pages 168–176.

Rodriguez-Galiano, V., Sanchez-Castillo, M., Chica-Olmo, M. and Chica-Rivas, M., 2015: Machine learning predictive models for mineral prospectivity: An evaluation of neural networks, random forest, regression trees and support vector machines. Ore Geology Reviews, Volume 71, pages 804–818.

Rose, A.W., Hawkes, H.E. and Webb, J.S., 1979: Geochemistry in Mineral Exploration. Academic Press, 657 pages.

Rouxel, O., Shanks, W.C., Bach, W. and Edwards, K.J., 2008: Integrated Fe- and S-isotope study of seafloor hydrothermal vents at East Pacific Rise 9–10°N. Chemical Geology, Volume 252(3), pages 214–227.

Sader, J.A., Harrison, A.L., McClenaghan, M.B., Hamilton, S.M., Clark, I.D., Sherwood Lollar, B. and Leybourne, M.I., 2021: Generation of high-pH groundwaters and H2 gas by groundwater–kimberlite interaction, northeastern Ontario, Canada. The Canadian Mineralogist, Volume 59(5), pages 1261–1276.

Sader, J.A., Leybourne, M.I., McClenaghan, M.B. and Hamilton, S.M., 2007: Low-temperature serpentinization processes and kimberlite groundwater signatures in the Kirkland Lake and Lake Timiskiming kimberlite fields, Ontario, Canada: Implications for diamond exploration. Geochemistry: Exploration, Environment, Analysis, Volume 7, pages 3–21.

Southam, G. and Saunders, J.A., 2005: The Geomicrobiology of Ore Deposits. Economic Geology, Volume 100(6), pages 1067–1084.

Sukanya, S., Noble, J. and Joseph, S., 2022: Application of radon ((222)Rn) as an environmental tracer in hydrogeological and geological investigations: An overview. Chemosphere, Volume 303(Pt 3), Article 135141.

Tang, J. and Johannesson, K.H., 2010: Ligand extraction of rare earth elements from aquifer sediments: Implications for rare earth element complexation with organic matter in natural waters. Geochimica et Cosmochimica Acta, Volume 74(23), pages 6690–6705.

Webster, J.G. and Mann, A.W., 1984: The influence of climate, geomorphology and primary geology on the supergene migration of gold and silver. Journal of Geochemical Exploration, Volume 22, pages 21–42.

Wegleitner, B.J., Jerde, C.L., Tucker, A., Chadderton, W.L. and Mahon, A.R., 2015: Long duration, room temperature preservation of filtered eDNA samples. Conservation Genetics Resources, Volume 7, pages 789–791.

Whitford, D., Andrew, A., Carr, G. and Giblin, A., 1997: Multi-isotopic studies of groundwaters: exploration for concealed mineralization. Exploration and Mining Research News, Volume 7, pages 5–7.

Xu, Y., Zuo, R., Chen, Z., Shi, Z. and Kreuzer, O.P., 2025: Recent advances and future research directions in deep learning as applied to geochemical mapping. Earth-Science Reviews, Volume 270.

Zhdanov, M.S., Jorgensen, M., Cox, L., Johnson, W.P. and Solomon, D.K., 2026: Airborne geophysical imaging of freshwater reservoir beneath the eastern margin of Great Salt Lake. Scientific Reports, Volume 16(1).

Zhu, C., Fryar, A.E. and Apps, J., 2024: Inorganic hydrogeochemistry in the 21st century. Ground Water, Volume 62(2), pages 174–183.

Ziwa, G., Crane, R. and Hudson-Edwards, K.A., 2020: Geochemistry, mineralogy and microbiology of cobalt in mining-affected environments. Minerals, Volume 11(1).

Zuo, R., Carranza, E.J. and Wang, J., 2016: Spatial analysis and visualization of exploration geochemical data. Earth-Science Reviews, Volume 158.

Isotopes in Drift Prospecting: Concepts, Case Histories, and Practical Workflows

Alexandre Voinot* and James Kidder
Geological Survey of Canada–Natural Resources Canada,
601 Booth Street, Ottawa, ON, K1A 0E8
*corresponding author: alexandre.voinot@nrcan-rncan.gc.ca

Abstract

Except for portions of Yukon territory, much of the Canadian land mass is obscured by Quaternary-aged glacial sediments of variable thickness (Bond et al.*, 2010; Hickin* et al.*, 2017). This glacial veneer presents a challenge to mineral explorers who require information on the underlying bedrock to assess the prospectivity of geological formations. Exploration in glaciated terrain is traditionally based on the study and analysis of glacial sediment, among which till is generally the preferred material. This approach inherently presents itself with challenges, as data interpretation is complicated by 1) mechanical mixing and long-range transport of debris by continental ice sheets, 2) overprinting by post-glacial weathering and 3) stratigraphic complexity in tills. Mixing of locally derived and far-travelled material can potentially weaken anomaly contrasts and mask relationships between till geochemistry and its bedrock sources. Reconstructing ice-flow history is therefore essential for accurate source attribution and vectoring. In recent years, several syntheses have been published, aiming to provide practical protocols addressing these challenges, and including aspects of survey design, sampling, quality assurance and control (QA/QC), and interpretation (McClenaghan and Paulen, 2018; McClenaghan* et al.*, 2023).*

After glacier retreat, near-surface weathering processes further remobilize metals (such as Cu, Zn or Pb) by breaking down their primary host minerals and subsequent adsorption onto secondary Fe–Mn (oxyhydr)oxides and clay-size minerals, making the use of bulk elemental abundances to track geochemical anomalies in till more complicated. These issues can be somewhat mitigated by following thorough till sampling protocols, aiming at collecting the correct till unit amid multilayered, locally reworked and exotic components. These protocols also emphasize stratigraphic logging, focus on the importance of various size fractions for different

applications and targets, as well as rigorous QA/QC to mitigate false positives or negatives (McClenaghan and Paulen, 2018; McClenaghan et al.*, 2023; Paulen, 2024).*

These issues motivate integrated workflows that couple till-matrix geochemistry, indicator-mineral methods, and glacial geomorphology. These modern approaches constitute a solid framework for drift prospecting that has been refined for decades (McClenaghan et al.*, 2023).*

*Nevertheless, challenges remain, as efforts to deconvolute the overlapping mineralogical and geochemical signals in till can oftentimes lead to ambiguous results. Integration of additional proxies is usually required to differentiate mineralization-related anomalies from background till signatures in drift-covered terrains. Radiogenic and non-traditional metal isotopes often display highly contrasting signatures in ore minerals (*e.g.*, Kyser* et al.*, 2020;Kidder* et al.*, 2021), making them potentially promising tools for identifying dispersion patterns in till material that incorporate some degree of material derived from mineralized targets. The goal of this paper is to synthesize existing case studies, develop a conceptual framework for the effective application of isotopic methods in mineral exploration within glaciated regions, and outline avenues for future research.*

The Potential of Radiogenic Isotopes

Fundamentals

Radiogenic isotopes (*e.g.*, ^{87}Sr, ^{143}Nd, ^{176}Hf, ^{206}Pb or ^{207}Pb) are isotopes produced by the natural radioactive decay of long-lived parent isotopes (half-lives in the range of 10^8 to 10^{10} years), such as ^{235}U, ^{238}U, ^{147}Sm and ^{87}Rb. Over geological timescales, these parent isotopes decay into stable daughter isotopes (for example, ^{238}U to ^{206}Pb or ^{87}Rb to ^{87}Sr), causing the isotopic composition of a closed-system rock or mineral to evolve slowly and predictably. Ratios between radiogenic daughter isotopes and their non-radiogenic counterparts (*e.g.*, ^{86}Sr or ^{204}Pb) are commonly used to compare geological materials and determine their age or provenance. The terms *more radiogenic* and *less radiogenic* refer to higher or lower values of these ratios, respectively, reflecting the relative accumulation of radiogenic daughter isotopes (Banner, 2004).

Because the rate of decay is well known, the ratios between parent and daughter isotopes preserve information about the age, origin, and evolution of geological materials. Radiogenic isotope ratios evolve predictably in various Earth reservoirs and are largely conservative during weathering and adsorption and are not fractionated by such processes, unlike elemental abundances (Frank, 2002). As a result, there is clear evidence that isotopic compositions of source material are typically preserved in the fine fraction of glacial sediments, in past and present settings (Farmer *et al.*, 2003; Maccali *et al.*, 2018). Additionally, radiogenic isotopes have been used historically for mineral exploration purposes in the early days of isotope geochemistry (Gulson, 1986), and as such, exhibited promise early on for exploration in glaciated terrains.

How They Can Help in Glaciated Terrains

Glacial comminution processes lead to the formation of very fine-grained rock flour (Haldorsen, 1981) that is highly reactive during post-glacial processes due to its small grain size and high reactive surface area (Gunnarsen *et al.*, 2023). As a result, post-glacial alteration can decouple metal concentrations from sources when minerals that are very vulnerable to physical and chemical alteration are involved (*e.g.*, sulphides, McClenaghan *et al.*, 2023). Radiogenic isotope systems have the potential to overcome these issues by recording the signature of the source material and retaining it, independently of the remaining proportion of an element after weathering. Foundational Antarctic studies show that Nd–Sr–Pb signatures in modern and Last Glacial Maximum (LGM) tills vary systematically with bedrock along flow paths and that offshore tills are mechanical mixtures of detritus eroded across outlet-glacier traverses, demonstrating robust provenance sensitivity despite reworking (Farmer *et al.*, 2006; Farmer and Licht, 2016).

Beyond polar settings, recent marine work shows that combined Nd–Sr–Hf in multiple clay-sized fractions can help resolve multiple detrital sources and quantify their relative inputs, which is directly relevant to choosing appropriate size fractions and end-member models in drift geochemistry (Lenz *et al.*, 2024).

Foundational Till Provenance Studies

Studies conducted on fine-fraction till samples from the Transantarctic Mountains and Ross embayment along the Byrd and Nimrod Glaciers indicate that the radiogenic isotope signature of local bedrock (Nd, Sr and Pb) is recorded in glacial sediments (Farmer *et al.*, 2006; Farmer and Licht, 2016). Data suggest that nunatak moraines contain exotic debris from inland sources (Farmer and Licht, 2016), further demonstrating the ability of radiogenic isotope proxies to track the source of material in glacial sediment over large distances. Tills from the Western Ross also contain material from late Cenozoic volcanic rocks (Farmer *et al.*, 2006), further highlighting the potential for radiogenic isotopes to identify more localized volcanic units that are point-source, a key trait of many ore deposits, thus highlighting potential for mineral exploration under drift cover. These studies validate radiogenic isotopes as high-fidelity trackers of various sources of material through complex ice dynamics.

Isoscape: Looking at the Bigger Picture

An isoscape is a spatial map that shows the isotopic compositions of various materials across a landscape. The term itself is a contraction of *isotope* and *landscape;* they can potentially serve as the framework for larger-scale studies (Holt *et al.*, 2021). Although still a relatively new concept in mineral exploration, they can prove to become very valuable tools for drift cover mineral exploration, as an isoscape of a given area might provide precious insight into sampling strategies as well as choice of analytical techniques. Significant research has been conducted in various parts of the world (Australia, Western Europe, Northern Africa and South America) to generate isoscapes maps for radiogenic Sr or Pb that aim to support environmental studies (*e.g.*, looking at isotopic compositions of bioavailable Sr to trace food products and migration patterns of humans and animals) and mineral exploration (Keller *et al*., 2016; Bataille *et al.*, 2018; Lugli *et al.*, 2022; Desem *et al.*, 2024; Wang *et al.*, 2024; Caritat *et al.*, 2025; Dosseto *et al.*, 2025; Pacheco-Forés *et al.*, 2025).

In Canada, the availability of such isoscapes remains limited to this day (Tarrant *et al.*, 2024; Tarrant and Richards, 2024; Le Corre *et al.*, 2025), and further research and investment are required to generate that framework for future research and exploration ventures based on isotopic

analyses. Novel data analysis techniques, such as machine learning, may provide crucial help by making full use of existing datasets and extrapolating them to larger scales to generate district or regional-scale isoscapes day (Le Corre *et al.*, 2025).

Mineral Exploration Case Histories: Successes and Limits

VMS Systems and Pb ± Sr Isotopes: Consistent Success?

To date, several studies have been published on the potential for radiogenic isotopes to track volcanic massive sulphide deposits (VMS) under cover of glacial sediment (Bell and Franklin, 1993; Sitnonetti *et al.*, 1996; Hussein *et al.*, 2003; van Geffen *et al.*, 2013; Rukhlov and Ferbey, 2015). In this context, Pb isotopes have proved very effective, as Pb in sulphides typically shows less radiogenic signatures than Pb in surrounding lithologies (Fig. 1).

Early studies, conducted in Canada in the 1990s around various VMS deposits (Chisel Lake, MB; Manitouwadge, ON; Buchans, NL), investigated the use of Pb isotopes as proxies for mineral exploration in glaciated regions, by establishing proof-of-concept for vectoring beneath drift (Bell and Franklin, 1993; Bell and Murton, 1995; Sitnonetti *et al.*, 1996).These studies show that the fine-fraction of till retains Pb-isotope compositions that converge toward VMS galena signatures, despite extensive post-depositional weathering. In contrast, whole-rock Pb-isotope ratios often obscure this signal because they integrate material from multiple mineral phases. Easily altered minerals, such as sulphides, are heavily altered during oxidative weathering, and their constituent metals are subsequently retained in fine clay minerals and secondary Fe–Mn oxides and hydroxides (Sitnonetti *et al.*, 1996). Selective leaching can thus provide better contrast by focusing on the exchangeable Pb fraction, improving the ability to distinguish mineralization-related anomalies from background till (Fig. 1).

These studies then paved the way for subsequent work that further demonstrated the potential of radiogenic isotopes to trace material from VMS deposits in drift covered regions. In the early 2000s, a study in the Halfmile Lake area, near the Bathurst mining camp in New Brunswick, once again demonstrated the ability of radiogenic Pb isotopes to identify mineralization under cover, using selective leach to access the exchangeable Pb fraction (Hussein *et al.*, 2003). However, the authors highlighted the limitations of this approach, mainly citing the long and costly analytical

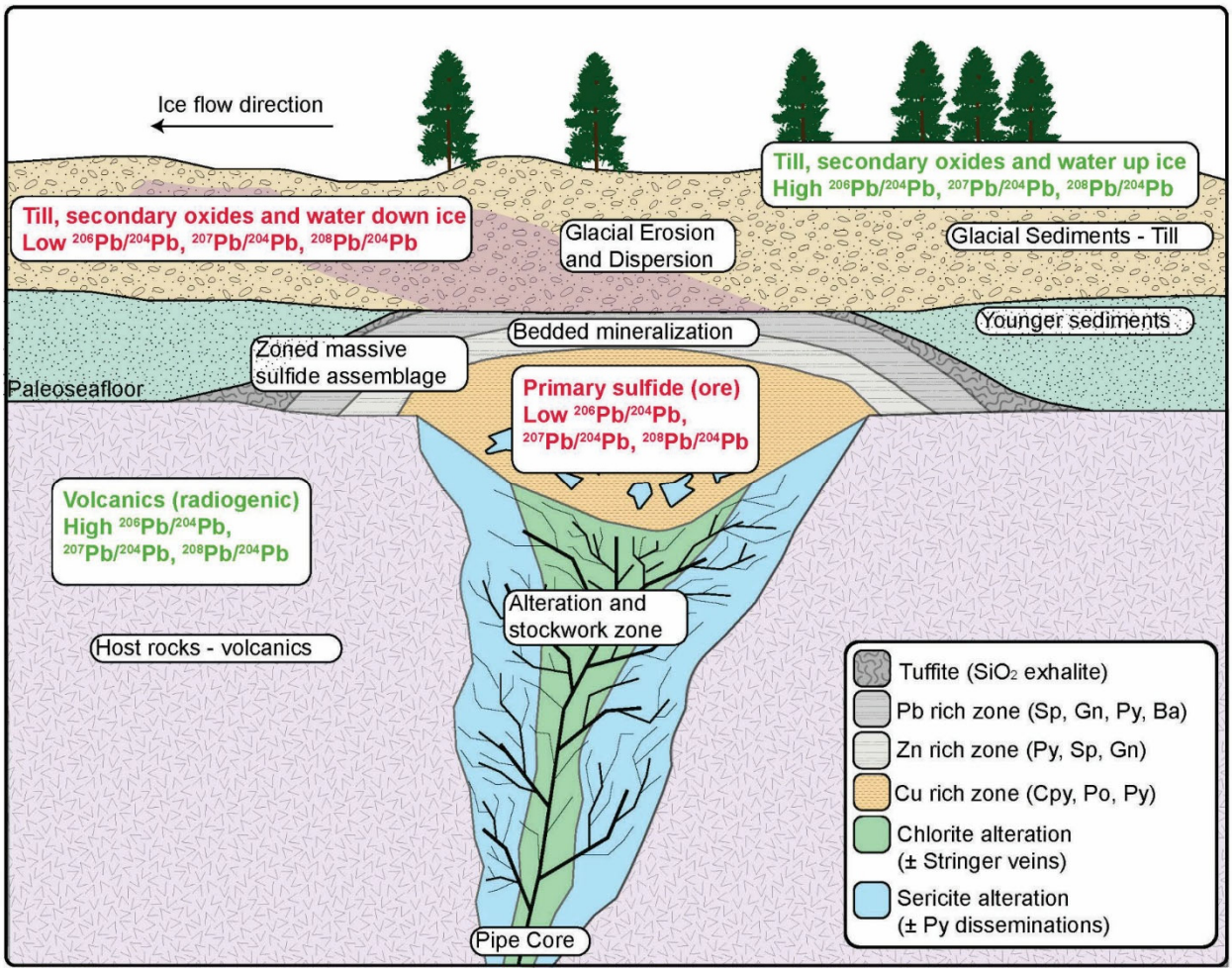


Figure 1. *Schematic representation of a VMS deposit, including the various zones of mineralization, as well as expected radiogenic Pb isotope compositions for the various parts of the system relevant to mineral exploration.*

procedures to analyze Pb isotopes at the time, which they thought would undermine the application of these techniques in a day-to-day context of greenfield exploration, which oftentimes relies on quick analysis of large numbers of samples. These limitations were mostly due to complex sample preparation procedures (ion chromatography) required prior to analysis by thermal ionization or multi-collector inductively-coupled mass spectrometry (TIMS or MC-ICP-MS, respectively) that were commonly used at the time for isotope analyses. A subsequent provincial survey led in British Columbia by Rukhlov and Ferbey published in 2015, demonstrated that cheaper and faster analyses of Pb isotopes by high resolution ICP-MS (HR-ICP-MS), while not exhibiting the same level of precision and accuracy as MC-ICP-MS, can still prove to be fit-for-purpose, and help resolve isotopic contrasts and map linear to hyperbolic mixing arrays between country rock and VMS material. These anomalies were still present about 1 km down-ice and outperformed elemental concentrations (Rukhlov and Ferbey, 2015).

A study led at Talbot Lake (Snow Lake belt, MB, Canada) looked at combining Pb and Sr isotope data in till as well as vegetation samples near a VMS deposit, and in the context of proximity to a smelter, to assess potential for anthropogenic contamination. Till data reveal less-radiogenic $^{206}Pb/^{204}Pb$ anomalies (in the <2 µm clay fraction) directly above a fault, tracking the upward migration of ore-derived Pb through >100 m of dolostone (van Geffen *et al.*, 2013). Additional radiogenic Sr ($^{87}Sr/^{86}Sr$) co-anomalies delineate zones of enhanced vertical groundwater flow. The novelty of this approach, combining both isotope systems, contributed to the deconvolution of geogenic signals from smelter aerosols retained in organic horizons and vegetation. Lead isotopes (with Sr as a hydrologic/host-rock tracer) thus provide robust vectors under transported cover and in contaminated terrains, particularly in the clay fraction and/or mild leaches targeted at labile phases.

Leybourne *et al.* (2009) took that concept even further by looking at the Pb isotopic composition of the dissolved fraction in waters proximal and distal to the Restigouche massive Zn–Pb sulphide deposit in the Bathurst Mining Camp (NB, Canada). The data reveal a clear trend towards less radiogenic values as the distance to mineralization decreases, showcasing the utility of Pb isotopes in waters as a potential vectoring tool for mineral exploration (Fig. 1).

Sr Isotopes as a Vector Towards LCT-Pegmatites

Lithium–cesium–tantalum (LCT) pegmatites carry extremely radiogenic Sr signatures and high Rb/Sr (Fig. 2) due to Rb enrichment and Sr depletion during magmatic fractionation, with subsequent decay of ^{87}Rb to ^{87}Sr (Cerny *et al.*, 1985). These distinct whole-rock values (typical pegmatites $^{87}Sr/^{86}Sr > 1.0$; Rb/Sr > 10, (Clark and Černý, 1987)) contrast sharply with common host rocks and global soils ($^{87}Sr/^{86}Sr < 0.75$-1.0; Rb/Sr < 10, (Capo *et al.*, 1998)). Surface soils can inherit these pegmatite Sr-isotope fingerprints, enabling delineation of buried dikes (Hall *et al.*, 2025). At two contrasting sites (Animikie Red Ace, Wisconsin, USA; Tin-Spodumene Belt, North Carolina, USA), soils developed directly above dikes exhibit elevated $^{87}Sr/^{86}Sr$ (to ~6.8) and Rb/Sr (to ~120) relative to background ones. These samples plot along pegmatite-host mixing trends and reliably distinguish anomalous from background areas (Fig. 2). Pairing $^{87}Sr/^{86}Sr$ with Rb/Sr provides a robust, scalable proxy for locating subsurface LCT pegmatites across varied climates,

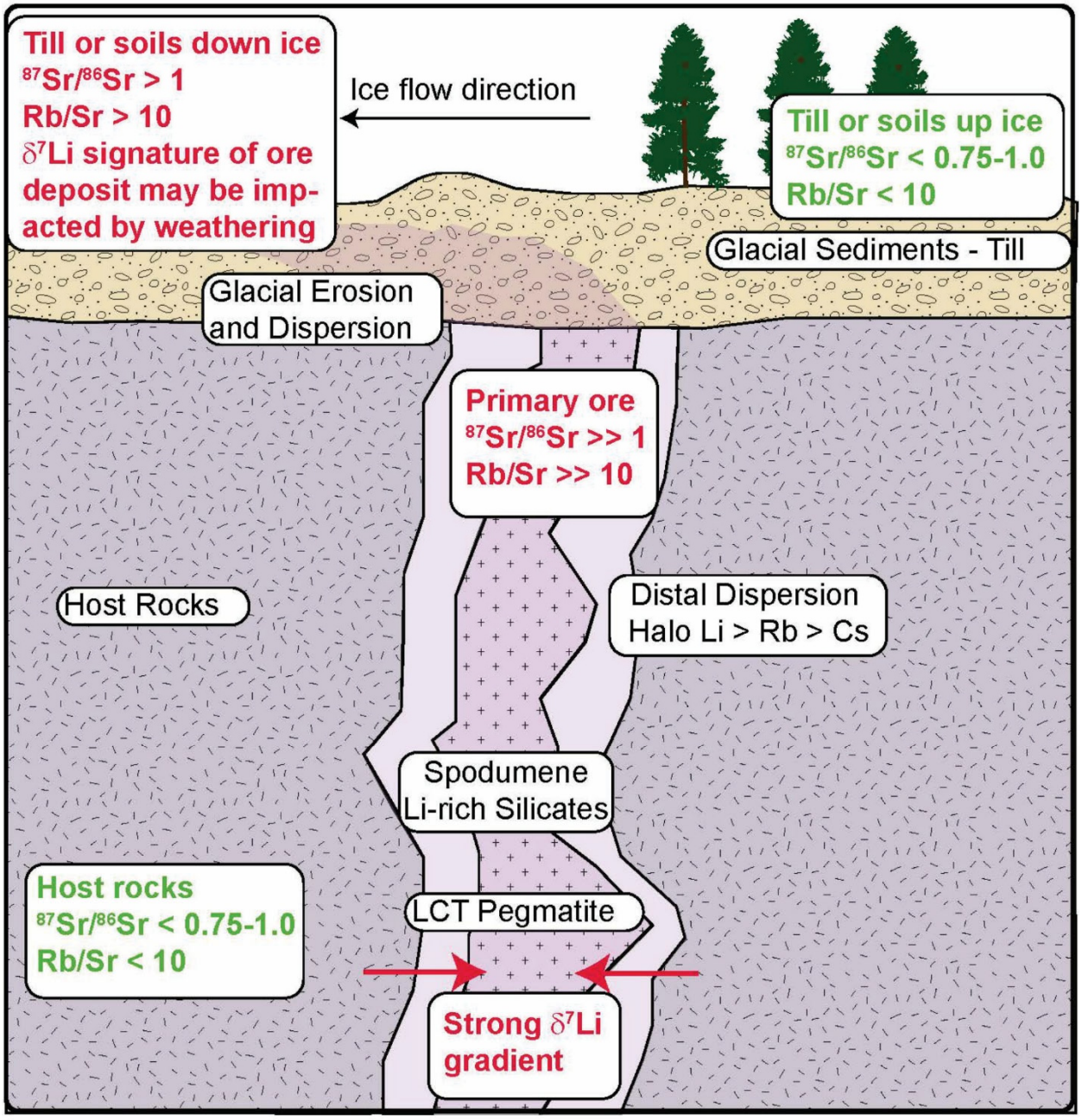


Figure 2. *Schematic representation of a LCT-pegmatite with expected radiogenic Sr, Rb/Sr and d*^{7}*Li compositions for the various parts of the system relevant to mineral exploration.*

cover types (soil, till), and depths, as Sr isotopes are expected to remain a conservative tracer even under significant weathering conditions (Capo *et al.*, 1998).

SEDEX Zn–Pb Systems (Pb–S isotopes): Source Discrimination under Till

A study led by Paulen and colleagues in NW Alberta (Canada) revealed abundant angular sphalerite and minor galena in till defining a local dispersal train (Paulen *et al.*, 2011). Although

Pb isotope analyses of galena from the till match MVT signatures of the Pine Point MVT (Mississippi Valley Type) Zn–Pb deposit located 330 km away, the morphology of the galena grains suggests the presence of more proximal basement sources along the Great Slave Lake Shear Zone. On the other hand, sulphur isotope analyses ($d^{34}S$) of sphalerite exhibit values that differ from those of known districts, suggesting a previously unrecognized sedimentary exhalative (SEDEX) Zn–Pb system in Cretaceous shales (Rukhlov, 2011). This study highlights the importance of reconciling geochemical and observational data when using isotopes to help determine the various sources of material in till. Combined Pb–S isotopes on indicator minerals have the potential to sharpen source discrimination beyond counts alone, but care must be taken to avoid misinterpretation of the data.

Radiogenic Pb Signatures as Proxies to Unconformity-related U Mineralization

As discussed earlier, Pb is the decay product of U; it is thus expected that highly radiogenic Pb signatures be observed near areas of elevated U content. Several studies have demonstrated the potential for Pb isotopes as vectoring tools towards U mineralization. Extensive work has been completed on unconformity-related deposits from the Athabasca Basin (Canada), showing that radiogenic Pb isotope signatures can be observed in various surficial media, including soil clay minerals and vegetation, at Halliday Lake (Stewart *et al.*, 2017) or Cigar West (Kyser *et al.*, 2015), for example, where U mineralization occurs at depths upwards of 700 and 400 m, respectively (Beyer *et al.*, 2021).

Sm–Nd as Vectors Towards Magmatic Ni–Cu–PGE Sulphide Mineralization

The Thompson nickel belt in Manitoba (Canada) hosts world-class high-grade Ni–Cu–PGE mineralization associated with ultramafic rocks. Radiogenic Sm–Nd isotope analyses of multiple samples from the area contributed to mapping the extent of the supracrustal rock formations hosting the mineralization (part of the Ospwagan group) in the Northeastern reaches of the district, thanks to their contrasted isotopic composition when compared to surrounding ultramafic rock units (Böhm *et al.*, 2007). Although this study made use of outcropping material for isotope analyses, it shows potential for radiogenic isotopes to distinguish sources of material in this context.

Porphyry Cu Systems (Pb–Sr–Nd): Limits Under Thick, Heterogeneous Drift

At the Pebble porphyry Cu–Au–Mo deposit (Alaska, USA), granodiorites exhibit relatively non-radiogenic Pb and Sr isotopic ratios, along with positive ε_{Nd} values, which combined are indicative of a mantle-derived magmatic source (Ayuso *et al.*, 2013). Although some soils and pond sediments exhibit isotope compositions that partially overlap those of mineralized rocks – particularly samples with the least radiogenic Pb – the majority show more radiogenic signatures influenced by heterogeneous glacial till, post-mineral volcanic rocks, and country-rock contamination. Glacial processes, a thick sediment cover, and limited age contrast between mineralized rocks and surrounding country rocks make it difficult to differentiate between the various lithologies, which significantly obscures the isotopic fingerprint of the deposit. As a result, Pb, Sr, and Nd isotopes in surficial materials do not form consistent spatial or vertical patterns and cannot reliably vector toward the orebody. Nonetheless, isotopic compositions help characterize till stratigraphy and identify mixtures of local and external sediment sources. Overall, the study concludes that although isotope data provide valuable baseline information, radiogenic isotopes alone are insufficient as exploration tools for the deeply concealed Pebble deposit.

Stable Isotopes: What Can They Teach Us?

Notation Considerations

Stable isotopes can undergo mass-dependent as well as mass-independent fractionation during geological processes (Schauble, 2004). Unlike previously discussed radiogenic isotope systems, these processes lead to minute changes in isotope ratios. As a result, isotopic compositions of stable isotopes are typically expressed as parts per thousand, or per mil (‰), variations relative to an internationally recognized reference material. The following is an example of this equation for Li, which can be extrapolated to any other stable isotope system:

$$\delta\,{}^{7}Li_{sample} = \left(\frac{\frac{{}^{7}Li}{{}^{6}Li}_{sample}}{\frac{{}^{7}Li}{{}^{6}Li}_{LSVEC}} - 1 \right) \times 1000 \qquad \text{(Eq. 1)}$$

where $\delta\ ^{7}Li_{sample}$ represents the isotopic composition of the sample; $\frac{^{7}Li}{^{6}Li}_{sample}$ is the measured isotopic ratio in the sample, and $\frac{^{7}Li}{^{6}Li}_{LSVEC}$ the measured isotopic ratio in the isotopic reference material (here LSVEC, Penniston-Dorland *et al.*, 2017).

The relative change in isotope ratios decreases with increasing atomic number (Young *et al.*, 2015); as a result, heavier elements, such as Tl, exhibit much smaller ranges of isotopic fractionation. In this case, the epsilon notation is commonly used, with one epsilon unit (e-unit) expressing changes in parts per ten thousand rather than parts per thousand, as with the delta notation. Using Tl as an example, equation 1 for such elements becomes:

$$\varepsilon^{205}Tl_{sample} = \left(\frac{\frac{^{205}Tl}{^{203}Tl}_{sample}}{\frac{^{205}Tl}{^{203}Tl}_{NIST997}} - 1 \right) \times 10{,}000 \qquad \text{(Eq. 2)}$$

where $\varepsilon^{205}Tl_{sample}$ represents the isotopic composition of the sample; $\frac{^{205}Tl}{^{203}Tl}_{sample}$ is the measured isotopic ratio in the sample, and $\frac{^{205}Tl}{^{203}Tl}_{NIST997}$ the measured isotopic ratio in the isotopic reference material (here NIST997, Nielsen *et al.*, 2017).

Traditional Stable Isotopes

Traditional stable isotopes (H, C, O, N, and S) have been widely studied in the context of mineral exploration, as they uniquely provide insight into the origin and evolution of fluids involved in ore-forming processes and later alteration, potentially expanding the footprint of a mineralized system (Kyser *et al.*, 2020). They can help identify false positives in elemental data, track element migration pathways, constrain metal sources, and assist environmental compliance by contrasting natural fluids from anthropogenic ones. Additionally, $\delta^{18}O$ and $\delta^{13}C$ in carbonate rocks can fingerprint alteration around hydrothermal ore systems. Stable isotope analyses revealed that alteration halos around the Screamer Carlin-type gold deposit (Nevada, USA) extend at least

3 to 4 km from the main mineralization, much farther than traditional geochemical and mineralogical proxies exhibit (Barker *et al.*, 2013).

Non-traditional Stable Isotopes

Non-traditional metal stable isotopes differ from traditional stable and radiogenic isotope systems in that they can potentially fractionate during geological processes such as water/rock interaction (adsorption, desorption, weathering), partial crystallization or melting. As a result, stable isotope data in the context of mineral exploration and ore deposit geology might be more indicative of primary ore-forming processes and secondary remobilization. To date, no studies have examined the potential for non-traditional isotopes to be used as vectors for mineralization under drift. However, we can gain some insight from other studies conducted in glaciated terrains.

Li Isotopes and LCT Pegmatites

Lithium isotopes can exhibit very strong gradients around LCT pegmatites (Fig. 2). For example, a significant decrease in δ^7Li values (+7.6 to -19.9‰) has been observed with concentration decreasing from 471 to 68 ppm over a short distance of less than 10 m at the Tin Mountain pegmatite (South Dakota, USA; Teng *et al.*, 2006). These strong gradients in Li isotopic compositions are potentially attributed to diffusion processes during emplacement of these intrusions and have been observed in other LCT pegmatites (Liu *et al.*, 2010; Marks *et al.*, 2007).

However, Li undergoes significant isotopic fractionation during surficial weathering and water/rock interaction processes (Penniston-Dorland *et al.*, 2017). For example, samples of West Greenland rivers show high d^{7}Li values in dissolved loads, with glacial rivers exhibiting slightly lower Li isotopic compositions compared to non-glacial ones (+26‰ *vs.* +30‰, respectively, Wimpenny *et al.*, 2010). Both river types show high δ^7Li relative to bedrock (around +8‰); this isotopic fractionation largely reflects the preferential adsorption of ^{6}Li to Fe-oxyhydroxides that form subglacially.

These observations suggest that, although Li isotopes may have the potential to be used as vector towards LCT pegmatite mineralization at the very small scale, these contrasted signatures

may quickly be obscured in a context of larger-scale mineral exploration in drift covered regions (Fig. 2). At these scales, Li isotope compositions of the bulk till are likely to provide insight into weathering processes. However, spodumene, the main host mineral for Li in LCT pegmatites, is very resistant to glacial erosion processes and as such, has been used successfully to identify mineralized pegmatites under till cover (*e.g.*, Brazil Lake pegmatite, NS, Canada, McClenaghan *et al.*, 2025). In this context, analyses of Li isotopes in spodumene grains separated from the till matrix could provide insight into the potential grade and size of the deposit.

Ca and Fe Isotopes, Potential for IOA Exploration?

In the Damma Glacier forefield in Switzerland, Ca isotopes ($\delta^{44/42}Ca$) exhibit near-zero fractionation during early silicate weathering (Hindshaw *et al.*, 2011). As a result, young soils and stream waters are isotopically indistinguishable from bedrock, and vegetation appears to be the dominant driver of Ca isotopic fractionation. Conversely, significantly lower $d^{56}Fe$ values are observed in secondary weathering products (such as Fe(III)-(hydr)oxides and clays (up to ~0.6‰ lighter than parent minerals) during weathering of Fe(II)-bearing silicates in the area *(Kiczka et al.*, 2011). The dominant fractionation mechanism appears to be a kinetic effect during the release of Fe from biotite and chlorite, and this signal persists throughout 150 years of pedogenesis. Secondary Fe(III) phases become increasingly abundant yet maintain light signatures, while residual phyllosilicates become heavier.

Although exploration value seems limited at first glance, these studies show that Ca isotopes could potentially be used to track the source of mineralization under cover (for example when targeting iron oxide apatite mineralization, Miloski *et al.*, 2023; Potter *et al.*, 2019), provided little to no remobilization in vegetation occurs (*e.g.*, in tundra or Arctic environments). On the contrary, mineral-weathering processes strongly impact Fe isotopic patterns, making them potential tracers of early weathering dynamics, but less effective for direct vectoring towards mineralization.

Isotopes as Proxies for U, Zn, Cu (and Au?) Mineralization

Uranium, Mo, and Tl isotopes offer varying degrees of promise for tracing U ore-forming processes. Uranium isotopes can reflect the grade of various types of U-ore deposits *(Uvarova et*

al., 2014), but, as is the case with Mo isotopes, are highly susceptible to overprinting by secondary processes such as alteration, fluid-rock interaction, and precipitation, which can rapidly obscure the primary isotopic signal of mineralization, even before taking surficial weathering processes into consideration (Voinot *et al.*, 2024). In contrast, Tl isotopes appear to be more robust, retaining signatures of primary U-ore-forming processes in secondary clay minerals distal to the orebody (Voinot *et al.*, 2025). Because of this resilience, Tl isotopes show strong potential as tracers across multiple ore systems, including U ore deposits as previously discussed, but also sediment-hosted massive sulphide (Knaack *et al.*, 2023).

Thallium is also a common pathfinder element for Au mineralization, alongside Te, Sb, Hg or Bi (Goldfarb *et al.*, 2016; Ikramuddin *et al.*, 1983). A preliminary study of samples from the world-class Carlin trend (Nevada, USA) shows that, although not conclusive on their own, Tl isotopes are bringing insights on the potential sources of Au in the system (Wickham, 2014). In Cu–Mo–Au porphyry deposits like the Bingham Canyon (Utah, USA), Tl isotopes appear to exhibit very contrasted isotopic values with very positive and negative signatures associated with elevated Tl, Sb or As concentrations (Fitzpayne *et al.*, 2018). Overall, these studies highlight that additional research is required to better understand the mechanisms driving Tl isotopic fractionations in some of these mineralized systems, but that the potential for use as vectoring tools exists.

Isotopes for Exploration in Glaciated Terrains: A Practical Workflow

Based on the present review of the various radiogenic and stable isotope systems applied to mineral exploration of several types of mineralization (*e.g.*, VMS, U-ore deposits or LCT-pegmatites) in drift covered areas, we can define a practical workflow, with associated guidelines and recommendations, for optimal use of isotopes in such a context.

1. Define questions and end-members

The key to success for exploration in glaciated areas is to establish geological and geochemical contrasts between ore, country rock, and potential exotic sources. As a result, compile radiogenic isotope data targeting ore-Pb (*e.g.*, galena) and wall-rock Sr or Nd (*e.g.*, silicates) data to define the endmembers in the study area. A strong knowledge of the till (texture, structure) and ice-flow history in the area of interest, as well as in nearby districts, is primordial for delineating the context

for proper interpretation of the radiogenic isotope data (McClenaghan *et al.*, 2023). Access to preliminary data from regional surveys and isoscapes might help determine sampling and analytical strategies (*see* point #3 below).

2. Sampling design and stratigraphy

As with any geochemical or mineralogical analysis of glacial material, target the correct till unit(s) (basal *vs.* ablation; avoid reworked veneers). The till sections should be logged carefully to determine till characteristics, as well as the number, direction and intensity of ice-flows. Lastly, if the mineralized target is composed of easily altered phases (*e.g.*, sulphides), prioritize the <63 µm and <2 µm fractions. Use field duplicates, blanks, and reference materials per GSC protocols (McClenaghan *et al.*, 2023).

3. Size-fraction and leach strategy

Target the fine fraction (<63 µm) for maximum isotopic homogeneity and sensitivity to labile Pb, especially when targeting mass sulphide deposits like VMS (Sitnonetti *et al.*, 1996; Hussein *et al.*, 2003). In this scenario, mild acid leaches (*e.g.*, 1 to 2.5 N HCl) are preferrable to liberate labile Pb to maximize contrast between background and mineralized area. In addition, while offering lower precision, analytical techniques like HR-ICP-MS or triple quadrupole ICP-MS (ICP-MS/MS) might be fit-for-purpose (Rukhlov and Ferbey, 2015; Chanakya *et al.*, 2025), due to their lower cost and faster turnaround time.

4. Pair isotopes systems to gain more insight

Combine Pb (ore fingerprint) with Sr (tracer of carbonate *vs.* silicate mixing and groundwater flow) and, where needed, Nd (crustal age/lithology) to separate geogenic sources from anthropogenic inputs and to map hydrologic pathways (van Geffen *et al.*, 2013). Stable isotopes might provide additional insight into the origin and evolution of fluids (*e.g.*, H or O isotopes) or the mineralization itself in the case of non-traditional stable isotopes relevant to the study area (*e.g.*, Li for LCT-pegmatites, U or Tl for U-ore deposits).

5. Interpretation via mixing models

Use two- and three-component mixing in Pb–Pb, $^{87}Sr/^{86}Sr$-1/Sr, or ε_{Nd}-1/Nd space to quantify contributions from ore *vs.* background *vs.* exotic inputs. The results should then be compared with

indicator-mineral counts, and grain morphology, and placed in a broader geomorphological context (*e.g.*, mega-scale glacial lineation corridors, dispersal fans) (McClenaghan *et al.*, 2023).

6. The added value of non-traditional stable isotopes

Some non-traditional stable isotopes (*e.g.*, Li, Ca, Tl, U) appear to have potential value in the context of mineral exploration. Although some of these elements undergo significant isotopic fractionation during surficial weathering processes, they might bring insights into some key processes (weathering, adsorption, redox or even provide information on key aspects of the deposit, such as grade. However, at this stage, their use might be restricted to be generally supporting tools rather than first-pass vectors under drift cover.

7. Contextualize with regional compilations

Cross-check anomalies against provincial and federal till geochemistry/indicator-mineral databases and glacial-history layers to validate vectors and plan up-ice step-outs *(McClenaghan et al.*, 2023).

Acknowledgments

We would like to thank Steve Beyer for reviewing the present manuscript. His comments and suggestions greatly helped improve the quality and readability of the present work. We also would like to thank the organizers of the 2026 GAC–MAC conference and associated short course (surficial geochemistry and indicator minerals methods in mineral exploration) for allowing us to contribute to the present volume.

References

Ayuso, R.A., Kelley, K.D., Eppinger, R.G. and Forni, F., 2013: Pb-Sr-Nd isotopes in surficial materials at the Pebble Porphyry Cu-Au-Mo Deposit, southwestern Alaska: Can the mineralizing fingerprint be detected through cover? Economic Geology, Volume 108(3), pages 543–562.

Banner, J.L., 2004: Radiogenic isotopes: Systematics and applications to earth surface processes and chemical stratigraphy. Earth-Science Reviews, Volume 65(3), pages 141–194.

Barker, S.L.L., Dipple, G.M., Hickey, K.A., Lepore, W.A. and Vaughan, J.R., 2013: Applying stable isotopes to mineral exploration: Teaching an old dog new tricks. Economic Geology, Volume 108(1), pages 1–9.

Bataille, C.P., *et al.*, 2018: A bioavailable strontium isoscape for Western Europe: A machine learning approach. PLOS ONE, Volume 13(5), Article e0197386.

Bell, K. and Franklin, J.M., 1993: Application of lead isotopes to mineral exploration in glaciated terrains. Geology, Volume 21(12), pages 1143–1146.

Bell, K. and Murton, J.B., 1995: A new indicator of glacial dispersal: Lead isotopes. Quaternary Science Reviews, Volume 14(3), pages 275–287.

Beyer, S.R., Stewart, P., Lahusen, L., Kyser, K. and Bzdel, L., 2021: Exploration advancement of the Stewardson Lake uranium project (Athabasca Basin, Canada) using an integrated geological and geochemical methodology and academic–industry collaboration. The Canadian Mineralogist, Volume 59(5), pages 885–912.

Böhm, C.O., Zwanzig, H.V. and Creaser, R.A., 2007: Sm-Nd isotope technique as an exploration tool: Delineating the northern extension of the Thompson Nickel Belt, Manitoba, Canada. Economic Geology, Volume 102(7), pages 1217–1231.

Bond, J.D., Lipovsky, P.S., MacFarlane, K., Weston, L. and Relf, C., 2010: Surficial geology, soils and permafrost of the northern Dawson Range. Yukon Exploration and Geology, pages 19–32.

Capo, R.C., Stewart, B.W. and Chadwick, O.A., 1998: Strontium isotopes as tracers of ecosystem processes: Theory and methods. Geoderma, Volume 82(1), pages 197–225.

Caritat, P., Dosseto, A. and Dux, F., 2025: A strontium isoscape of southwestern Australia and progress toward a national strontium isoscape. Earth System Science Data, Volume 17(1), pages 79–93.

Černý, P., Meintzer, R.E. and Anderson, A.J., 1985: Extreme fractionation in rare-element granitic pegmatites; selected examples of data and mechanisms. The Canadian Mineralogist, Volume 23(3), pages 381–421.

Chanakya, I.V.S., Misra, S. and Rahaman, W., 2025: Accurate and precise determination of Pb/Ca and lead isotopes ($^{20X}Pb/^{207}Pb$) from mass-limited coral samples by ICP-QQQ-MS. Journal of Analytical Atomic Spectrometry, Volume 40(7), pages 1776–1787.

Clark, G.S. and Černý, P., 1987: Radiogenic ^{87}Sr, its mobility, and the interpretation of Rb□Sr fractionation trends in rare-element granitic pegmatites. Geochimica et Cosmochimica Acta, Volume 51(4), pages 1011–1018.

Desem, C.U., de Caritat, P., Woodhead, J., Maas, R. and Carr, G., 2024: A regolith lead isoscape of Australia. Earth System Science Data, Volume 16(3), pages 1383–1393.

Dosseto, A., Dux, F., Bataille, C. and de Caritat, P., 2025: A bioavailable strontium isoscape of Australia. Earth System Science Data, Volume 17(9), pages 4865–4880.

Farmer, G.L., Barber, D. and Andrews, J., 2003: Provenance of Late Quaternary ice-proximal sediments in the North Atlantic: Nd, Sr and Pb isotopic evidence. Earth and Planetary Science Letters, Volume 209(1), pages 227–243.

Farmer, G.L. and Licht, K.J., 2016: Generation and fate of glacial sediments in the central Transantarctic Mountains based on radiogenic isotopes and implications for reconstructing past ice dynamics. Quaternary Science Reviews, Volume 150, pages 98–109.

Farmer, G.L., Licht, K., Swope, R.J. and Andrews, J., 2006: Isotopic constraints on the provenance of fine-grained sediment in LGM tills from the Ross Embayment, Antarctica. Earth and Planetary Science Letters, Volume 249(1), pages 90–107.

Fitzpayne, A., *et al.*, 2018: Assessing thallium elemental systematics and isotope ratio variations in porphyry ore systems: A case study of the Bingham Canyon District. Minerals, Volume 8(12), pages 548.

Frank, M., 2002: Radiogenic isotopes: Tracers of past ocean circulation and erosional input. Reviews of Geophysics, Volume 40(1), pages 1-1–1-38.

Goldfarb, R.J., Hofstra, A.H.and Simmons, S.F., 2016: Critical elements in carlin, epithermal, and orogenic gold deposits. *In* Rare Earth and Critical Elements in Ore Deposits. *Edited by* P.L. Verplanck and M.W. Hitzman. Society of Economic Geologists, Volume 18. https://doi.org/10.5382/Rev.18.10

Gulson, B.L., 1986: Lead isotope in mineral exploration. Elsevier, Amsterdam, Netherlands.

Gunnarsen, K.C., Jensen, L.S., Rosing, M.T. and Dietzen, C., 2023: Greenlandic glacial rock flour improves crop yield in organic agricultural production. Nutrient Cycling in Agroecosystems, Volume 126(1), pages 51–66.

Haldorsen, S., 1981: Grain-size distribution of subglacial till and its realtion to glacial scrushing and abrasion. Boreas, Volume 10(1), pages 91–105.

Hall, G.A., *et al.*, 2025: Strontium isotopes and Rb/Sr tracers in surface soils for locating subsurface lithium pegmatites. Applied Geochemistry, Volume 195, Article 106631.

Hickin, A., Ward, B., Plouffe, A. and Nelson, J., 2017: Introduction to the geology, physiography, and glacial history of the Canadian Cordillera in British Columbia and Yukon, pages 1–25.

Hindshaw, R.S., Reynolds, B.C., Wiederhold, J.G., Kretzschmar, R. and Bourdon, B., 2011: Calcium isotopes in a proglacial weathering environment: Damma glacier, Switzerland. Geochimica et Cosmochimica Acta, Volume 75(1), pages 106–118.

Holt, E., Evans, J.A. and Madgwick, R., 2021: Strontium ($^{87}Sr/^{86}Sr$) mapping: A critical review of methods and approaches. Earth-Science Reviews, Volume 216, Article 103593.

Hussein, A.A., Lochner, C. and Bell, K., 2003: Application of Pb Isotopes to Mineral Exploration in the Halfmile Lake Area, Bathurst, New Brunswick. *In* Massive Sulfide Deposits of the Bathurst Mining Camp, New Brunswick, and Northern Maine. Society of Economic Geologists.

Ikramuddin, M. *et al.*, 1983: Thallium: A potential guide to mineral deposits. Journal of Geochemical Exploration, Volume 19(1), pages 465–490.

Keller, A.T., Regan, L.A., Lundstrom, C.C. and Bower, N.W., 2016: Evaluation of the efficacy of spatiotemporal Pb isoscapes for provenancing of human remains. Forensic Science International, Volume 261, pages 83–92.

Kiczka, M., *et al.*, 2011: Iron speciation and isotope fractionation during silicate weathering and soil formation in an alpine glacier forefield chronosequence. Geochimica et Cosmochimica Acta, Volume 75(19), pages 5559–5573.

Kidder, J.A., Voinot, A., Leybourne, M.I., Layton-Matthews, D. and Bowell, R.J., 2021: Using stable isotopes of Cu, Mo, S, and $^{87}Sr/^{86}Sr$ in hydrogeochemical mineral exploration as tracers of porphyry and exotic copper deposits. Applied Geochemistry, Volume 128, Article 104935.

Knaack, D.R., Sullivan, K.V., Leybourne, M.I., Dunn, C.E. and Layton-Matthews, D., 2023: Thallium isotopes as indicators of ore mineralization at the Zn-rich sediment-hosted massive sulfide TL Deposit, British Columbia, Canada. Geochemistry: Exploration, Environment, Analysis, Volume 23(1) Article geochem2022–042.

Kyser, T.K., *et al.*, 2015: Using Pb isotopes in surface media to distinguish anthropogenic sources from undercover uranium sources. Comptes Rendus. Géoscience, Volume 347(5-6), pages 215–226.

Kyser, T.K., Leybourne, M.I. and Layton-Matthews, D., 2020: Advances in the use of isotopes in geochemical exploration: Instrumentation and applications in understanding geochemical processes. Geochemistry: Exploration, Environment, Analysis, Volume 20(2), pages 199–204.

Le Corre, M., *et al.*, 2025: An ensemble machine learning bioavailable strontium isoscape for Eastern Canada. FACETS, Volume 10, pages 1–17.

Lenz, N., *et al.*, 2024: Provenance of clay-sized detrital sediments in the North Sea and the Skagerrak region based on radiogenic Nd-Sr-Hf isotopes and clay mineral compositions: assessing the impact of coastal and seabed erosion. Frontiers in Marine Science, Volume 11.

Leybourne, M.I., Cousens, B.L. and Goodfellow, W.D., 2009: Lead isotopes in ground and surface waters: fingerprinting heavy metal sources in mineral exploration. Geochemistry: Exploration, Environment, Analysis, Volume 9(2), pages 115–123.

Liu, X.-M., Rudnick, R.L., Hier-Majumder, S. and Sirbescu, M.-L.C., 2010: Processes controlling lithium isotopic distribution in contact aureoles: A case study of the Florence County pegmatites, Wisconsin. Geochemistry, Geophysics, Geosystems, Volume 11(8).

Lugli, F., *et al.*, 2022: A strontium isoscape of Italy for provenance studies. Chemical Geology, Volume 587, Article 120624.

Maccali, J., Hillaire-Marcel, C. and Not, C., 2018: Radiogenic isotope (Nd, Pb, Sr) signatures of surface and sea ice-transported sediments from the Arctic Ocean under the present interglacial conditions. Polar Research, Volume 37(0).

Marks, M.A.W., Rudnick, R.L., McCammon, C., Vennemann, T. and Markl, G., 2007: Arrested kinetic Li isotope fractionation at the margin of the Ilímaussaq complex, South Greenland: Evidence for open-system processes during final cooling of peralkaline igneous rocks. Chemical Geology, Volume 246(3), pages 207–230.

McClenaghan, M.B., Brushett, D.M., Paulen, R.C., Beckett-Brown, C.E. and Rice, J.M., 2025: Glacial dispersal of indicator minerals from the Brazil Lake lithium–caesium–tantalum pegmatites, SW Nova Scotia, Canada. Geochemistry: Exploration, Environment, Analysis, Volume 25(1), Article geochem2024–047.

McClenaghan, M.B., *et al.,* 2023: Review of till geochemistry and indicator mineral methods for mineral exploration in glaciated terrain. Geochemistry: Exploration, Environment, Analysis, Volume 23(4), Article geochem2023–013.

McClenaghan, M.B. and Paulen, R.C., 2018: Chapter 20 - Application of till mineralogy and geochemistry to mineral exploration. *In* Past Glacial Environments (second edition). *Edited by* J. Menzies and J.J.M. van der Meer.ition). Elsevier, pages 689–751.

Miloski, P., Dare, S., Morisset, C.-E., Perrot, M.G. and Davies, J.H.F.L., 2023: Petrogenesis of oxide-apatite mineralization associated with proterozoic anorthosite massifs at Lac Mirepoix, Québec, Canada: A multi-injection model for Fe-Ti-P mineralization in the Central Grenville Province. Ore Geology Reviews, Volume 163, Article 105734.

Nielsen, S.G., Rehkämper, M. and Prytulak, J., 2017: Investigation and application of thalliumisotope fractionation. Reviews in Mineralogy and Geochemistry, Volume 82(1), pages 759–798.

Pacheco-Forés, S.I., Gauthier, N., Carpenter, L.B., Gordon, G. and Knudson, K.J., 2025: Radiogenic strontium isotope variability in the Valley of Oaxaca: A predictive isoscape for Mesoamerican paleomobility studies. PLOS ONE, Volume 20(12), pages e0338628.

Paulen, R.C. and McClenaghan, M.B., 2024: Till geochemistry and indicator-mineral methods for exploration in glaciated terrains, Natural Resources Canada.

Paulen, R.C., Paradis, S., Plouffe, A. and Smith, I.R., 2011: Pb and S isotopic composition of indicator minerals in glacial sediments from NW Alberta, Canada: Implications for Zn-Pb base metal exploration. Geochemistry: Exploration, Environment, Analysis, Volume 11(4), pages 309–320.

Penniston-Dorland, S., Liu, X.-M. and Rudnick, R.L., 2017: Lithium isotope heochemistry. Reviews in Mineralogy and Geochemistry, Volume 82(1), pages 165–217.

Potter, E.G., Corriveau, L. and Kjarsgaard, B.A., 2019: Paleoproterozoic iron oxide spatite (IOA) and iron oxide-copper-gold (IOCG) mineralization in the East Arm Basin, Northwest Territories, Canada. Canadian Journal of Earth Sciences, Volume 57(1), pages 167–183.

Rukhlov, A., 2011: Review of metallic mineralization in Alberta with emphasis on gold potential. Government of Alberta.

Rukhlov, A. and Ferbey, T., 2015: Application of lead isotopes in till for mineral exploration: A simplified method using ICP-MS: 93.

Schauble, E.A., 2004: Applying stable isotope fractionation theory to new systems. Reviews in Mineralogy and Geochemistry, Volume 55(1), pages 65–111.

Sitnonetti, A., Bell, K. and Hall, G.E.M., 1996: Pb isotopic ratios and elemental abundances for selective leachates from near-surface till: implications for mineral exploration. Applied Geochemistry, Volume 11(5), pages 721–734.

Stewart, P., Kyser, T.K., Griffiths, D. and Lahusen, L., 2017: Dendrochemistry and soil clay geochemistry applied to exploration for deep U mineralization at the Halliday Lake Prospect, Athabasca Basin, Canada. Geochemistry: Exploration, Environment, Analysis, Volume 17(2), pages 164–181.

Tarrant, D., Hepburn, J., Renson, V. and Richards, M., 2024: A pilot bioavailable strontium isotope baseline map of Southern British Columbia, Canada. FACETS, Volume 9, pages 1–11.

Tarrant, D. and Richards, M.P., 2024: Modern plants and sulfur isoscapes — A review, discussion, and construction of a pilot δ34S isoscape for mobility and provenance studies. Rapid Communications in Mass Spectrometry, Volume 38(21), Article e9908.

Teng, F.-Z., McDonough, W.F., Rudnick, R.L. and Walker, R.J., 2006: Diffusion-driven extreme lithium isotopic fractionation in country rocks of the Tin Mountain pegmatite. Earth and Planetary Science Letters, Volume 243(3), pages 701–710.

Uvarova, Y.A., Kyser, T.K., Geagea, M.L. and Chipley, D., 2014: Variations in the uranium isotopic compositions of uranium ores from different types of uranium deposits. Geochimica et Cosmochimica Acta, Volume 146, pages 1–17.

van Geffen, P.W.G., Kyser, T.K., Oates Christopher, J. and Ihlenfeld, C., 2013: Lead isotope ratios in till and vegetation over a VMS occurrence under significant allochthonous cover. Geochemistry: Exploration, Environment, Analysis, Volume 13(1), pages 53–61.

Voinot, A., Beyer, S., Layton-Matthews, D. and Kyser, K., 2025: Uranium, molybdenum and thallium isotopes in clay-sized material (< 2 μm size fraction) from the McArthur River uranium deposit (Saskatchewan, Canada): A moving story. EXPLORE, Volume 207.

Voinot, A., *et al.*, 2024: Tl, Mo and U isotopes in U-ore deposits record Earth's fundamental redox processes. Chemical Geology, Volume 661, Article 122154.

Wang, X., Bocksberger, G. and Oelze, V., 2024: Modeling documents for manuscipt Wang *et al.* “Strontium isoscape of sub-Saharan Africa allows tracing origins of victims of the transatlantic slave trade”. figshare.

Wickham, K.M., 2014: Thallium isotope implications for the metalliferous source of Carlin-type deposits in northern Nevada.

Wimpenny, J., *et al.*, 2010: Glacial effects on weathering processes: New insights from the elemental and lithium isotopic composition of West Greenland rivers. Earth and Planetary Science Letters, Volume 290(3), pages 427–437.

Young, E.D., *et al.*, 2015: High-temperature equilibrium isotope fractionation of non-traditional stable isotopes: Experiments, theory, and applications. Chemical Geology, Volume 395, pages 176–195.

Overview of the Latest Advances in Automated Mineralogy Using a Scanning Electron Microscope (SEM)

Jonathan Tremblay* and Réjean Girard
IOS Geosciences Inc., 1319 St-Paul Boulevard, Saguenay, QC, G7J 3Y2
**Corresponding author's email: jtremblay@iosgeo.com*

Introduction

Automated mineralogy based on scanning electron microscopy (SEM) has undergone significant development over the past two decades and is now an established tool in mineral exploration, ore deposit studies, and geometallurgy. Since their widespread adoption in the early 2000s, Mineral Liberation Analysis (MLA) and QEMSCAN (Quantitative Evaluation of Minerals by SCANning electron microscopy) have enabled rapid, repeatable, and statistically robust characterization of mineral assemblages, grain size distributions, mineral associations, and liberation characteristics (Gottlieb *et al.*, 2000; Gu, 2003; Fandrich *et al.*, 2007). By integrating high-resolution backscattered electron (BSE) imaging with automated energy-dispersive X-ray spectroscopy (EDS), SEM-based automated mineralogy overcomes many limitations of traditional optical petrography and manual geochemical analysis, particularly for fine-grained and compositionally complex materials.

In mineral exploration, these techniques have proven especially valuable for indicator mineral studies, till and sediment characterization, and source discrimination in glaciated and covered terrains, where large populations of minerals must be analyzed consistently and objectively (Pirrie *et al.*, 2013; Layton-Matthews and McClenaghan, 2022). However, these methods had significant limitations, particularly regarding the need to use pre-established mineral libraries and the lack of true grain-by-grain analysis, notwithstanding cost and throughput issues. Recent advances in electron microscopy, detector design, data acquisition speed, mineral classification algorithms, and data integration workflows have further expanded the scope of automated SEM-based mineralogy. This paper provides an overview of the latest advances in automated mineralogy using a SEM, with an emphasis on developments relevant to mineral exploration and geometallurgy.

Recent Advancements in Electron Microscopy

Recent years have seen significant technological advances in scanning electron microscopy and the emergence of new analytical platforms, enhancing the efficiency, robustness, and scope of previously established methods. SEM-based methods continue to evolve and can be tailored to the specific needs of geoscientists across disciplines, including fundamental research, mineral exploration, and optimization of mineral recovery in mining operations. The following are a list of some of the recent advancements in electron microscopy, automated mineralogy and correlative microscopy.

Versatility of a SEM

Advances in scanning electron microscope design over the past two decades have significantly expanded the capabilities of automated mineralogy. The widespread adoption of field-emission gun SEMs (FEG-SEMs) represents a major technological step over conventional thermionic sources (tungsten and LaB_6), providing improved spatial resolution and current stability over a very long period of time. FEG sources generate a smaller probe size at a given beam current, enabling higher-resolution imaging and more precise EDS analyses, particularly for fine-grained assemblages.

Modern SEMs also commonly feature large specimen chambers, accommodating multiple polished thin sections, grain mounts, polished drill cores or any other sample holders (Fig. 1). When combined with high-precision motorized stages, these chambers enable fully automated sequences on multiple samples for high-throughput characterization projects (Schulz *et al.*, 2020). The integration of turbomolecular pumping systems has improved vacuum performance and pumping times, allowing rapid switching between operating modes and samples. Many modern instruments support variable-pressure (VP) or low-vacuum operation, facilitating the analysis of weakly conductive or uncoated samples, but with some analytical drawbacks, such as beam diffusion and lower spatial resolution.



Figure 1. *Compucentric five-axis stage (X-Y-Z-R-T) with a 10 x 10 cm sample holder, enabling the analysis of multiple samples. Note the absence of an interlock chamber. The pumping time is only a few minutes.*

Latest Generation of EDS

The most significant development in EDS detectors was the introduction of silicon drift detectors (SDDs) around the turn of the 21st century. Since then, technology has continued to evolve and significant progress in energy-dispersive X-ray spectroscopy over the past five years has substantially improved their performance. These advances are driven primarily by developments in large-area SDD sensor sizes up to 170 mm^2, low-noise electronics, and high-speed pulse-processing computers. They enhance sensitivity, spectral resolution, and analytical throughput. A spectral resolution of 125-130 eV at Mn Kα with an input count rates per second (cps) approaching or exceeding 200 000 cps is now achievable (Newbury and Ritchie, 2015; Goldstein *et al.*, 2018). This enables precise mineral characterization while minimizing analysis time. When general characterization is required and speed is more important than spectral resolution, next-generation detectors can achieve an input count rate of over 600,000 cps per detector, more than 25x higher than conventional Si–Li EDS detectors and almost 5x of the previous SDD generation.

Improvements in low-energy X-ray detection have also been critical for mineralogical applications, particularly for accurate identification of light elements and improved peak separation at low accelerating voltages. Recent studies report sub 50 eV resolution at C Kα under moderate count-rate conditions, representing a major enhancement in low-energy performance compared to earlier EDS generations (Goldstein *et al.*, 2018; Castellano *et al.*, 2020). These gains are enabled by optimized detector entrance windows, improved charge-collection efficiency, and more stable thermal and electronic regulation (Peltier cooling). Quantitative analysis of carbon and oxygen is now possible with proper calibration.

Equally important are advances in pulse-processing algorithms and pile-up correction, which now allow accurate spectral deconvolution and quantitative analysis at high count rates that support rapid X-ray mapping and large-area automated acquisition (Newbury, 2017). When coupled with improved SEM beam stability and stage reproducibility, the latest EDS detectors reduce the traditional trade-off between resolution and speed. A fully quantitative micro-analysis, of similar or better the quality of electron microprobe analysis, can now be performed in seconds.

Parallel and Multi-channel EDS

The emergence of parallel and multi-channel detector architectures, such as Bruker's QUANTAX FlatQUAD and Oxford Instruments' Unity (Fig. 2) significantly enhance X-ray collection efficiency and analytical throughput relative to conventional single-detector systems. They use multiple independent SDD channels operating simultaneously close to the sample. The resulting increase in effective solid angle enables order-of-magnitude gains in count rates, while preserving energy resolution and minimizing pulse pile-up effects. Some manufacturers obtained up to 3,200,000 cps in optimal conditions (bruker.com), while the authors achieve above 1,000,000 cps on routine mineralogical studies.

By distributing X-ray processing across parallel channels, spectral degradation at high count rates is reduced, allowing rapid mapping. For automated mineralogy, these parallel EDS detectors provide several critical advantages, including faster large-area mapping, improved detection of low-abundance and fine-grained phases, and reduced sensitivity to sample topography (Schulz *et al.*, 2020; Han *et al.*, 2022). Shadowing due to the position of conventional EDS is significantly

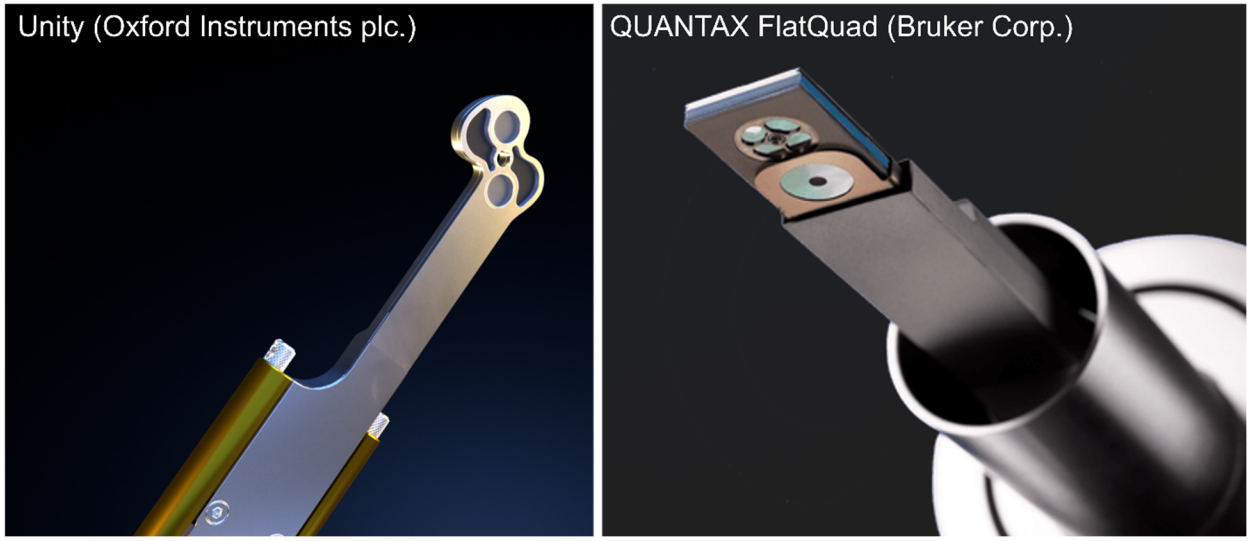


Figure 2. *Renderings of parallel and multi-channel detectors from Oxford Instruments plc (left) and Bruker Corp. (right), two manufacturers of EDS detectors. Images taken from their respective websites.*

reduced with the addition of a parallel detector. Those detectors must however be coupled with a conventional EDS detector due to their incapacity of detecting low energy elements (Na and below).

Specific manufacturers now combine BSE and X-Ray on a single parallel detector, allowing the acquisition of BSE images simultaneously of the X-Ray map, accelerating again the throughput of samples acquired daily.

Next Generation Mineralogical Platforms

Alongside hardware improvements in SEM and EDS, the past decade has seen major advances in automated mineralogy software, notably with the development of newer platforms such as TESCAN Integrated Mineral Analyzer (TIMA), Zeiss Mineralogic and many others, which are built upon, but differ fundamentally from earlier systems such as MLA and QEMSCAN. Traditional MLA and QEMSCAN workflows rely primarily on rule-based mineral libraries and pre-defined spectral matching routines combined with BSE segmentation, that has enabled decades of successful application in mineral exploration and process mineralogy (Gottlieb *et al.*, 2000; Gu, 2003). However, their reliance on mineral libraries and BSE images and their software rigidity limit the performance of those popular, although now-discontinued software suites.

Newer generation platforms introduce more flexible workflows, including mineral classification based on deconvoluted spectra, adaptive decision trees, and even machine-learning routines that improve phase discrimination in complex mineral systems (Schulz *et al.*, 2020; Juránek *et al.*, 2022). These platforms are designed to work natively with large-area EDS mapping and high count-rate acquisition. Each grain can be scanned pixel per pixel rather than relying solely on limited spot analyses. As a result, subtle compositional differences, zoning patterns, and fine intergrowths can be resolved more reliably, particularly in fine-grained. High-resolution EDS maps can be acquired to characterize specific grains, while low-resolution and fast analysis can be performed on mounts with thousands of grains, making these systems well suited for exploration applications such as indicator mineral studies, till surveys, and regional metallogenic screening (Schulz *et al.*, 2020; Han *et al.*, 2022). Table 1 summarizes the differences between the older methods (MLA and QEMSCAN) and newer automated mineralogy platforms, highlighting advances in classification flexibility, spatial resolution, and throughput.

Table 1. Comparison between legacy and latest SEM-based automated mineralogy platforms

Aspect	**Legacy platforms (MLA/QEMSCAN)**	**Latest platforms (*e.g.*, TIMA, Mineralogic)**
Primary development period	1990s–2010s	Mid-2010s to present
Core classification approach	Mineral libraries; spectrum-matching	Full-spectrum–based classification; decision trees customizable workflows
EDS acquisition strategy	Point analyses based on BSE segmentation or fixed grids	Large-area, high-count-rate EDS spots, grain scanning, or pixel per pixel
Handling of compositional variability	Limited flexibility for solid solutions and zoning	Improved discrimination of solid solutions, zoning, and subtle compositional shifts
Throughput vs. resolution trade-off	High throughput achieved at reduced spatial resolution only	High spatial resolution and high throughput by faster detectors
Correlative microscopy support	Limited. Rigid softwares	Versatile, manufacturers are more user-driven; correlative microscopy easier with basic programmation skills

At present, these advances make it feasible to routinely generate quantitative mineralogical datasets at higher spatial resolution, over larger areas, and with improved compositional confidence than what was previously achievable. Looking forward, continued development is expected to focus on deeper machine-learning integration, real-time classification during acquisition, and interpretation. As of now, new platforms have shown to be increasingly adaptive, predictive, and capable of supporting data-intensive exploration and ore deposit research.

Electron Backscatter Diffraction (EBSD)

Electron backscatter diffraction (EBSD) has become an increasingly valuable complement to SEM-EDS automated mineralogy for indicator mineral studies and deformation-controlled ore systems, where crystallographic information is essential. EBSD enables determination of grain orientation, grain boundaries, lattice misorientation, and polymorph identity, allowing discrimination of minerals with identical chemistry (*e.g.*, pyrite and marcasite, rutile and anatase, *etc.*) and recognition of deformation, recrystallization, or overgrowth textures that cannot be resolved chemically (Prior *et al.*, 1999; Halfpenny and Prior, 2009). Concepts are similar to X-Ray diffraction (XRD), but at the pixel scale.

This technology is not new, but its applications to geosciences are slowly being worked on. Over the past decade, EBSD technology has evolved rapidly with the introduction of high-sensitivity CMOS cameras and faster indexing algorithms, transforming EBSD from a niche method into a high-throughput technique. Modern EBSD systems now routinely achieve hundreds of indexed patterns per second, while maintaining high angular precision and pattern quality, even at low beam currents (Nowell *et al.*, 2020; Wright *et al.*, 2020). These improvements enable large-area orientation mapping of specific textures or crystal lattices of certain grains to resolve zoning, overprinting deformation, and crystallographic fabrics (*e.g.*, Henriksson, 2022).

In exploration contexts, EBSD is used to fingerprint ore-related deformation, distinguish primary and remobilized sulphfides, and define structural controls on mineralization (Halfpenny and Prior, 2009). It can be used to detect presence of strained minerals, polymorphs, or light elements (lithium, boron)-bearing minerals based on their crystal structure.

EBSD can be acquired on the same samples as BSE and EDS in automated routines to get the maximum correlative information.

Correlative Microscopy

Recent developments in correlative microscopy have further expanded the analytical outcomes of automated mineralogy by integrating optical microscopy, SEM and other analytical approaches.

High-resolution optical scanners, such as the Zeiss AxioScan, can automate up to 100 polished thin sections from rocks or mineral concentrates and acquire various optical images at very high resolution (*e.g.*, transmitted light, crossed-plane polarization at various angles, reflected light, *etc.*). Optical microscopes equipped with motorized stages is also capable of rapid imaging of polished thin sections, providing high-resolution images of mineralogy and textural relationships that are not accessible in electron images alone (Holding *et al.*, 2013). When registered to SEM coordinate systems, optical images can be directly correlated with BSE and EDS datasets, allowing the detection, quantification, and characterization of mineral phases across entire sections (Fig. 3).

A key advantage of this approach is the ability to identify minerals of interest optically, extract their precise X-Y coordinates, and relocate them reproducibly within the SEM chamber through automated stage navigation and triangulation. This enables to easily trace back minerals of interest for further characterization, either by point analysis or EDS mapping. Other analytical methods can also be used in addition to SEM-EDS, such as laser ablation (LA-ICP-MS) for trace-element characterization (Sylvester *et al.*, 2008; George *et al.*, 2018). By linking optical images to BSE images and EDS maps through shared coordinates, correlative microscopy represents a powerful tool to detect rare mineral phases and assemblages. Petrographic image analysis through AI is currently an active field of research (Basso *et al.*, 2025; Morales *et al.*, 2025).

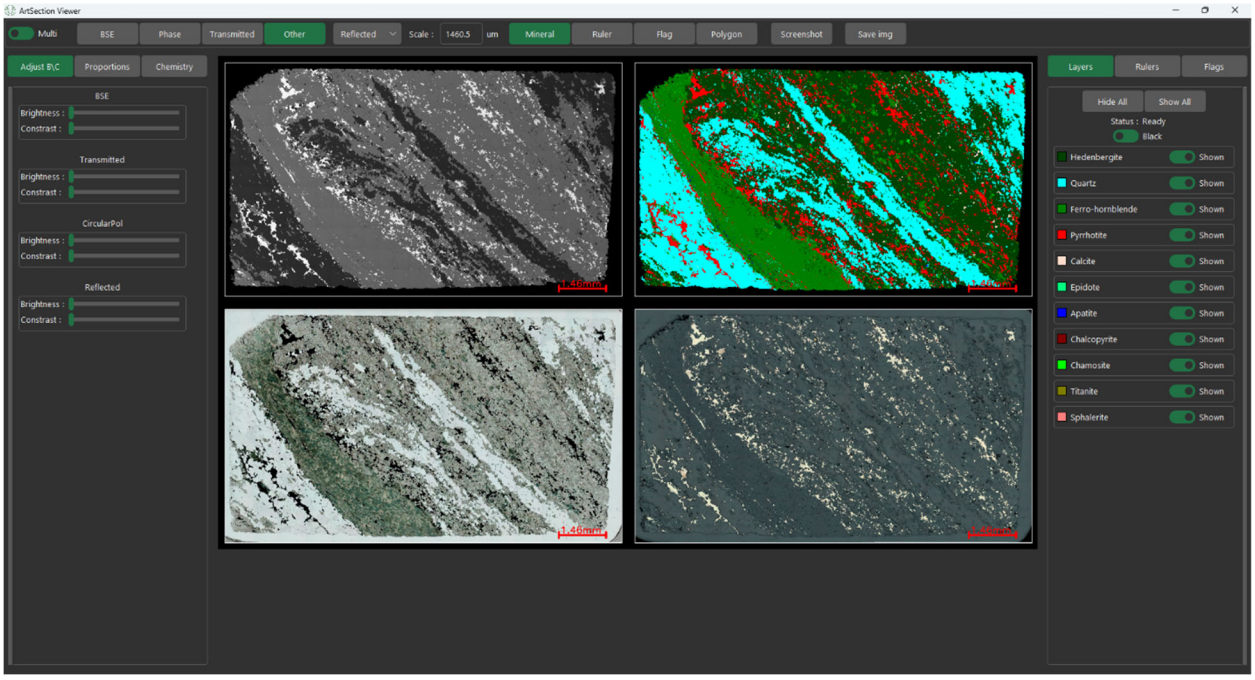


Figure 3. *Screenshot of in-house software showing a polished thin section under various imaging modes (transmitted light, reflected light, BSE, and false-colour mineral map). This demonstrates what can be achieved through correlative microscopy and programming.*

Another benefit of this approach is that the images and analytical datasets are archived digitally and can be shared globally, enabling collaborative interpretation without physical sample transfer. Unlike conventional petrography where observations rely on individual expertise, automated petrography provides quantitative results. Automated routines can extract physical parameters, such as modal proportions, grain sizes, and phase relationships. Samples can therefore be compared and interpreted as a whole for a better understanding of the deposits. Correlative microscopy also overcomes a fundamental limitation of optical petrography that is the difficulty of distinguishing minerals with similar optical properties or identifying rare and compositionally complex phases. As a result, effort is less on mineral identification, and more on data interpretation and geological synthesis, where the scientific value is meaningful.

An Example from Detrital Zircon Geochronology

Correlative microscopy is easing zirconology workflows by eliminating the need for manual sorting of detrital zircon grains from heavy mineral concentrates (HMC). HMC epoxide mounts can be analyzed using integrated SEM-BSE, EDS, and cathodoluminescence (CL) imaging to rapidly identify zircon grains based on the Zr signal (Fig. 4). Cathodoluminescence imaging is particularly important, as it reveals growth zoning, inherited cores, and metamorphic overgrowths essential for interpreting zircon histories (Hanchar and Miller, 1993; Corfu *et al.*, 2003).

Automated routines allow zircon grains to be detected, imaged, and catalogued directly within the mount, after which correlative microscopy enables precise relocation of selected grains or

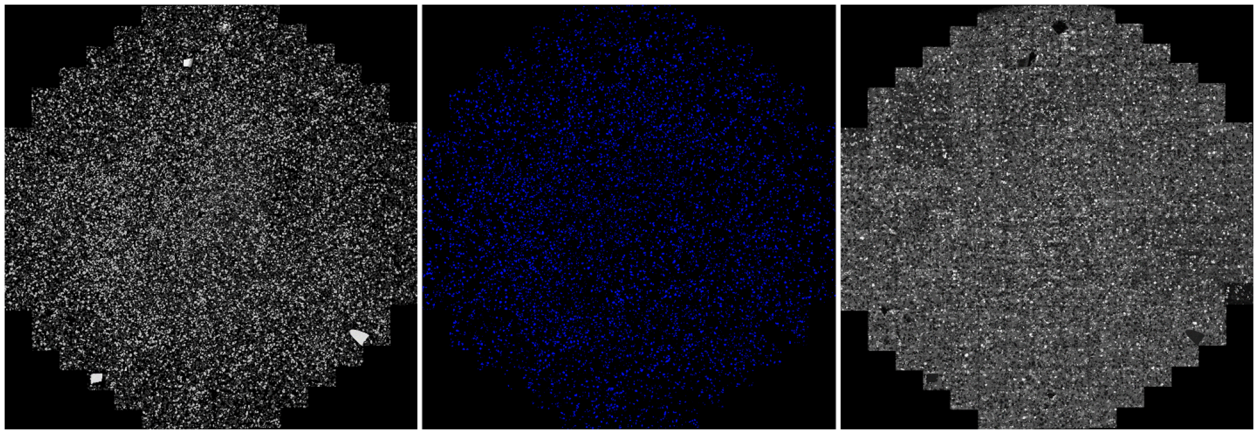


Figure 4. *Mosaics of BSE images (left), zirconium X-ray maps (center), and cathodoluminescence images (right) of a 30 mm diameter polished epoxy mount. Zircon grains can be easily detected by the EDS map, and grains extracted from the BSE and CL images.*

specific domains for complementary microanalytical techniques. BSE and CL images of grains can be extracted, then compared to determine which grains are prospects and critical for U–Pb geochronology by LA-ICP-MS, which method is known as an exploration vectoring tool (Jackson *et al.*, 2004; Gehrels *et al.*, 2008). Compared with traditional methods, this integrated approach improves throughput and reproducibility.

Modern SEM-based Techniques in Applied Mineral Exploration

Recent advances in SEM-based automated mineralogy platforms (*e.g.*, TESCAN TIMA, Zeiss Mineralogic, AztecMineral) have significantly expanded the range of mineral systems that can be characterized quantitatively, particularly those with complex and variable mineralogies. Porphyry copper deposits in the Andes are a meaningful example, where alteration assemblages include diverse aluminum phosphate and sulphate (APS) minerals (*e.g.*, svanbergite, woodhouseite, and crandallite group minerals). These minerals are critical indicators of advanced argillic alteration associated to this type of deposit but are difficult to distinguish using optical methods due to similar optical properties and fine grain size (Deyell *et al.*, 2004; Sillitoe, 2010). High-skilled personnel are also mandatory for this type of work where specific mineralogical assemblages are required, and often from various types of deposits.

Current SEM-based capabilities enable the quantification of APS minerals to pinpoint porphyry systems as an exploration vectoring tool. Similar benefits apply to other complex deposits, including epithermal Au–Ag, IOCG, and VMS systems, where fine-grained alteration minerals and polymorphs challenge traditional methods (Cook *et al.*, 2017).

Another example is for gold grain counting in glaciated terrain. Gold grains are notoriously small, and consequently hard to reliably recover and visually identify. Automated routines can be tailored to detect grains down to a few micrometers in diameter, and automatically acquire a spot chemical analysis along a high-resolution BSE image for shape analysis (Averill, 1988; Girard *et al.*, 2021).

These are two examples among many of how modern automated SEM-based routines can be used in mineral exploration. Many other applications are to be considered, from environmental studies to geometallurgical assessments.

Conclusions

The complementarity of new detector technologies, advances in SEM configuration, increased computational power, and modern automated mineralogy software has fundamentally reshaped exploration workflows based on mineralogy. Traditional trade-offs between analytical resolution, speed, and statistical robustness have largely been decreased. FEG-SEM with improved beam stability now supports very long automated analyses, while large-area and parallel EDS detectors enable very high-count rates and improve signals on material with topographic features. Processing cost and throughout of these automated methods now surpass visual mineral sorting, providing a reliable and quantitative datasets in regards of any mineral species of interest.

These advances are particularly impactful for exploration in geologically complex deposits (*e.g.*, porphyry copper systems), as well as regional till sampling surveys across Canada for lithium, gold, copper-nickel-PGE, *etc.* Latest automated mineralogy platforms can reliably discriminate solid solution minerals or chemical subtilties, and rare phases that were historically difficult to resolve using optical petrography or legacy MLA/QEMSCAN workflows. Quantitative mineralogical datasets generated at project scale improve exploration vectoring.

The improvement of EBSD technology with the latest CMOS sensors and real time indexing has added crystallographic importance to exploration. EBSD now operates at acquisition speeds compatible with automated workflows, enabling routine characterization of deformation, recrystallization, and structural controls on mineralization.

Correlative microscopy integrating optical imaging, SEM (BSE, EDS, EBSD CL) within a digital software is reshaping petrography. Automated petrography yields reproducible, shareable, and precise calculations of phase relationships.

Looking ahead, continued integration of high-speed detectors and correlative workflows will further enhance rock characterization and mineral classification. The use of machine-learning will surely be used to better detect and label spectra peaks, decrease pile-up effects and remove automatically interferences by selecting the right elements, as well as classify chemical compositions into minerals in an unprecedent speed. Modern SEM has yet to show what's coming.

References

Averill, S.A., 1988: Regional gold grain studies in till as an exploration tool. *In* Drift Prospecting. Geological Survey of Canada, Paper 88-19, pages 263–270.

Basso, M., da Ponte Souza, J.P., Chinelatto, G.F., Mansini, L.A.A. and Vidal, A.C., 2025: Petrographic image classification of complex carbonate rocks from the Brazilian pre-salt using convolutional neural networks. Scientific Reports, Volume 15, Article 30700.

Castellano, A., Rinaldi, R. and Altamura, D., 2020: Recent advances in silicon drift detectors for X-ray microanalysis. Microscopy Research and Technique, Volume 83, pages 1225–1236.

Cook, N.J., Ciobanu, C.L. and Spry, P.G., 2017: Trace minerals and textures in complex ore systems. Mineralogical Magazine, Volume 81, pages 1–24.

Corfu, F., Hanchar, J.M., Hoskin, P.W.O. and Kinny, P., 2003: Atlas of zircon textures. Reviews in Mineralogy and Geochemistry, Volume 53, pages 469–500.

Deyell, C.L., Cooke, D.R., Walshe, J.L. and Fanning, M., 2004: Chemical characteristics of APS minerals in porphyry systems. Canadian Mineralogist, Volume 42, pages 933–951.

Fandrich, R., Gu, Y., Burrows, D. and Moeller, K., 2007: Modern SEM-based mineral liberation analysis. International Journal of Mineral Processing, Volume 84, pages 310–320.

Gehrels, G.E., Valencia, V. and Pullen, A., 2008: Detrital zircon geochronology by LA-ICP-MS. Reviews in Mineralogy and Geochemistry, Volume 69, pages 1–20.

George, L.L., Cook, N.J., Ciobanu, C.L., Wade, B.P. and Griffin, W.L., 2018: Trace element mapping and quantitative mineral chemistry using LA-ICP-MS. Chemical Geology, Volume 490, pages 15–32.

Girard, R., Tremblay, J., Néron, A., Longuépée, H. and Makvandi, S., 2021: Automated gold grain counting. Part 2: What a gold grain size and shape can tell. Minerals, Volume 11, 379 pages.

Goldstein, J.I., Newbury, D.E., Michael, J.R., Ritchie, N.W.M., Scott, J.H.J. and Joy, D.C., 2018: Scanning Electron Microscopy and X-Ray Microanalysis. Fourth edition. Springer.

Gottlieb, P., Wilkie, G., Sutherland, D., Ho-Tun, E., Suthers, S., Perera, K., Jenkins, B., Spencer, S., Butcher, A. and Rayner, J., 2000: Using quantitative electron microscopy for process mineralogy applications. Journal of Minerals and Materials Characterization and Engineering, Volume 1, pages 41–58.

Gu, Y., 2003: Automated scanning electron microscope based mineral liberation analysis. Journal of Minerals and Materials Characterization and Engineering, Volume 2, pages 33–41.

Halfpenny, A. and Prior, D.J., 2009: Crystallographic controls on mineralization revealed by EBSD. Geology, Volume 37, pages 951–954.

Han, S., Löhr, S.C., Abbott, A.N., Baldermann, A., Farkas, J., McMahon, W., Milliken, K.L., Rafiei, M., Wheeler, C. and Owen, M., 2022: Earth system science applications of next-generation SEM-EDS automated mineral mapping. Frontiers in Earth Science, Volume 10, Article 956912.

Hanchar, J.M. and Miller, C.F., 1993: Zircon zonation patterns revealed by CL and BSE. American Mineralogist, Volume 78, pages 129–139.

Henriksson, J., 2022: EBSD investigation of high-temperature magnetite from apatite-iron-oxide deposits: Implications for the formation of giant Kiruna-type deposits. Issue 574, Uppsala University.

Holding, A.J., Tripp, A.S. and Searle, M.P., 2013: Automated optical–SEM correlation for quantitative petrography. Journal of Microscopy, Volume 249, pages 1–14.

Jackson, S.E., Pearson, N.J., Griffin, W.L. and Belousova, E.A., 2004: *In-situ* U-Pb zircon geochronology by LA-ICP-MS. Chemical Geology, Volume 211, pages 47–69.

Juránek, R., Výravský, J., Kolář, M., Motl, D. and Zemčík, P., 2022: Graph-based deep learning segmentation of EDS spectral images for automated mineral phase analysis. Computers and Geosciences, Volume 165.

Layton-Matthews, D. and McClenaghan, M.B., 2022: Current techniques and applications of mineral chemistry to mineral exploration: Examples from glaciated terrain. Minerals, Volume 12, 59 pages.

Morales, J., Saldivia, C., Lobo, R., del Pino, M., Muñoz, M., Caniggia, G., Catalán, J., Hayde, R. and Poblete, V., 2025: Visual analysis of deep learning semantic segmentation applied to petrographic thin sections. Scientific Reports, Volume 15, Article 14612.

Newbury, D.E., 2017: Deadtime, pile-up, and accurate quantitative EDS analysis at high count rates. Microscopy and Microanalysis, Volume 23, pages 399–410.

Newbury, D.E. and Ritchie, N.W.M., 2015: Performing elemental microanalysis with high accuracy and precision by SEM/EDS. Journal of Materials Science, Volume 50, pages 493–518.

Nowell, M.M., Wright, S.I., Biermann, H. and Crimp, M.A., 2020: Evolution of EBSD camera technology and impacts on speed and data quality. Microscopy and Microanalysis, Volume 26, pages 3–17.

Pirrie, D., Butcher, A.R., Power, M.R., Gottlieb, P. and Miller, G.L., 2004: Rapid quantitative mineral and phase analysis using automated scanning electron microscopy (QEMSCAN); potential applications in forensic geoscience. Geological Society Special Publication, Volume 232, pages 123-136.

Prior, D.J., Boyle, A.P., Brenker, F., Cheadle, M.C., Day, A., Lopez, G., Peruzzi, L., Potts, G., Reddy, S., Spiess, R., Timms, N.E., Trimby, P., Wheeler, J. and Zetterstrom, L., 1999: EBSD application to textural problems in rocks. American Mineralogist, Volume 84, pages 1741–1759.

Schulz, B., Sandmann, D. and Gilbricht, S., 2020: Automated mineralogy and its contribution to ore characterization. Minerals, Volume 10, Article 1007.

Sillitoe, R.H., 2010: Porphyry copper systems. Economic Geology, Volume 105, pages 3–41.

Sylvester, P.J., 2008: Laser ablation ICP-MS in the Earth Sciences: Current practices and outstanding issues. Mineralogical Association of Canada, Short Course Series 40.

Wright, S.I., Nowell, M.M. and Field, D.P., 2020: Advances in EBSD: Faster and more reliable mapping. Microscopy Today, Volume 28, pages 22–27.

QA/QC Concepts for Mineral Exploration in Glaciated Terranes

Cliff Stanley, Ph.D., P.Geo., Professor of Applied Geochemistry
Dept. of Earth & Environmental Science, Acadia University, Wolfville, NS, B4P 2R6

Introduction

Quality Assurance/Quality Control (QA/QC) measures are essential to implement when collecting data for scientific purposes. This is true for geochemical or mineralogical exploration methods in glacial terranes, and includes the tasks of: ***sample collection***, ***sample preparation***, and ***sample analysis***. Additionally, three basic aspects of data quality exist, and the three quality aspects generally align with these three measurement steps. The aspects of data quality include: ***representativity*** (during sampling), ***accuracy*** and ***precision*** (during sample preparation and analysis). The QA/QC process involves periodically assessing these three measures of data quality, judging whether the measurements produced are ***fit for purpose*** (Bettaney and Stanley, 2001), and fixing the data (either discarding or replacing it), if not.

Types of Errors

Geochemical or mineralogical data used in mineral exploration and mining may not be acceptable because they contain errors. In general, there are three types of errors: ***systematic errors***, ***random errors***, and ***blunders***. Systematic errors are generally not acceptable, but fortunately can often be corrected mathematically, as the effect of this error is predictable in each sample. In contrast, random errors take place from time to time and can frequently be described by statistical distributions. Normal, binomial, and Poisson distributions commonly explain the frequency of errors in geochemical and mineralogical data. Unfortunately, because these errors are statistically predictable, they aren't really errors, and so geoscientists mostly have to live with them, as they are part of an expected statistical distribution. Lastly, blunders are errors created by the misapplication of procedure (either during sample collection, preparation, or analysis). These errors need to be avoided because they are measuring something different from the other samples. Thus, if they occur, they should be corrected or even discarded, but they should only be discarded if a reason can be surmised to ensure the error is caused by a procedural goof (*via* Chauvenet's

Principle; Barnett, 1983). This distinguishes a blunder from a random error producing a measurement on the tail of the data distribution.

Recommended Types and Number of QA/QC Samples

To detect errors in geological measurements, geoscientists commonly include ***site replicates*** (replicates from different locations in the same sample cell) and/or ***sample replicates*** (replicates from the same location in the same sample cell; Fig. 1), ***blanks***, and ***reference materials*** in their sample batches. These samples complement the QA/QC samples commonly used by the laboratory to detect errors during sample preparation and analysis, which include crushed and powder duplicates, analytical duplicates, method blanks, and reference materials. Geoscientists commonly submit QA/QC samples at a rate of approximately 15% (5% duplicates, 5% blanks, and 5% reference materials, plus one blank to start off the batch and to detect any cross-over contamination. These allow the geoscientist to detect (and quantify) measurement errors. Several different reference materials are commonly employed to ensure that measurements are accurate and precise near:

1. the lowest and highest expected concentrations for the ore and pathfinder elements,
2. near the critical measurement (either the expected geochemical threshold or the mining cut-off grade),
3. at a zero concentration, and
4. at measurement values in between.

Note that blanks can typically serve as a reference material at or near the zero concentration.

Importantly, different levels of data quality are necessary for different survey purposes. In resource estimation, 5% relative error is commonly the maximum error threshold necessary for

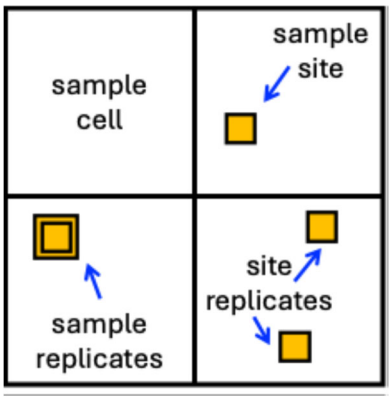


Figure 1. *Illustration of sample cells representing a small portion of a square geochemical grid. Samples (orange squares) are collected from each sample cell (white squares). Sample replicates are collected from the same sample site, whereas site replicates are collected from two locations within a single sample cell.*

stock exchange reports and other official documents, but in exploration geochemistry or indicator mineral exploration in glacial terranes, lower levels of data quality (say 10% relative error) may be acceptable. This is because during exploration, data patterns involving several samples are typically more important than the absolute magnitude of any one measurement. As a result, a higher magnitude of error is acceptable because several samples comprise the pattern, instead of one sample, and more confidence can be placed in several samples with larger error than in one sample with smaller error.

Sampling Representativity

Representativity is a measure of how similar samples are, in terms of their petrological, mineralogical, geochemical, geophysical, textural, and other relevant characteristics, to the geological material the samples are meant to represent (the sample cell). This important measurement feature can be validated using duplicate measurements, because if multiple samples from a sample cell are the same, then it is likely that they mimic the characteristics of the cell. Geoscientists can undertake a variety of statistical tests: Fisher's F-test, Levine's W-tests, Bartlett's X tests, Permutation tests, and Semivariogram Analysis, depending on the nature of the data and character of the data distribution (Yonar *et al*., 2024) to determine whether the average within-site variance (calculated from replicate samples) is different from the between-site variance (calculated from the regular samples in a survey). If the between site variance is greater than the within-site variance, then it is likely that the samples are representative, and will be effective in achieving the goals of the survey.

Variations Within Sample Sites

Two types of variation commonly exist in most geochemical or mineralogical exploration survey sites: ***constitutional heterogeneity*** and ***distributional heterogeneity*** (Pitard, 1989). Constitutional heterogeneity occurs in virtually all geological materials that are composed of different types of particles (e.g., ore and gangue mineral grains). Constitutional heterogeneity occurs because samples of a geological material are likely not going to have the exact same proportions of gangue grains and mineral grains every time they are sampled. This form of variation can be described statistically, and if it involves samples with large concentrations, its

variations are described by the binomial distribution, which has the following relationship between the binomial concentration and its error:

$$\sigma_B^2 = \frac{c(1-c)}{n}, \quad (1)$$

where σ_B^2 is the binomial variance, $\boldsymbol{c}$ is the element concentration (expressed as a proportion), and $\boldsymbol{n}$ is the effective number of mineral grains in the samples (essentially a fitting parameter). In contrast, if it involves samples with small concentrations, its variations are described by the Poisson distribution, which has the following relationship between the concentration and its error:

$$\sigma_P^2 = kc, \quad (2)$$

where σ_P^2 is the Poisson variance, $\boldsymbol{c}$ is an element concentration (in this case, not necessarily expressed as a proportion), and $\boldsymbol{k}$ is the concentration contributed by one grain (again, essentially a fitting parameter). In the extreme, constitutional heterogeneity is called the 'nugget effect' and creates an important challenge when sampling for mineral grains that have low concentrations.

In contrast, distributional heterogeneity involves samples that exhibit systematic variations (zoning) across the sample cell. This variation can be produced by geological processes (*e.g.*, Fe-oxide mottled soil horizons, melanosomes and leucosomes in migmatites, heavy mineral-rich sediment horizons, or fracture-controlled chalcopyrite mineralization in porphyry Cu deposits), or by inadvertent sample treatment procedures (*e.g.*, the accumulation of Au nuggets or other high-density grains at the bottom of the sample because of shaking during transport). Statistical distributions describing these variations are typically not available, except perhaps the multi-modal mixtures of normal distributions that reflect different geological populations with different means and standard deviations (Sinclair, 1991; Stanley, 1988).

Analytical Precision

Precision is the second type of data quality assessed in most QA/QC programs and is a measure of how close sample measurements are to each other. Precision can be measured using replicates (site, sample, sub-sample, analytical, and analyte replicates) so some of these replicates will be inserted into a batch by the laboratory (particularly, the last three), and some will be inserted into the batch by the geoscientist (notably, the first two). Precision is typically characterized by the absolute or relative error of measurements and is calculated by the average standard deviation of replicates, or the relative standard deviation of replicates:

$$\sigma_e = \sqrt{\frac{1}{n}\sum_{i=1}^{n}\sigma_i^2} \quad \text{or:} \quad \gamma_e = \sqrt{\frac{1}{n}\sum_{i=1}^{n}\frac{\sigma_i^2}{\mu_i^2}} = \sqrt{\frac{1}{n}\sum_{i=1}^{n}\gamma_i^2}, \tag{3}$$

respectively, and σ_e equals the absolute error, γ_e, equals the relative error (σ/μ). In both cases, precision is calculated using a root-mean square procedure and can be characterized as a straight line on a Thompson-Howarth scatterplot with replicate means plotted against replicate standard deviations (either as a horizontal line with intercept equal to the absolute error, or a sloping line through the origin with slope equal to the relative error, respectively; Fig. 2; Stanley and Lawie, 2008). Again, in exploration applications, 10% relative error is probably an adequate 'fit for purpose' precision (Bettaney and Stanley 2001) in mineral exploration in glaciated terrane.

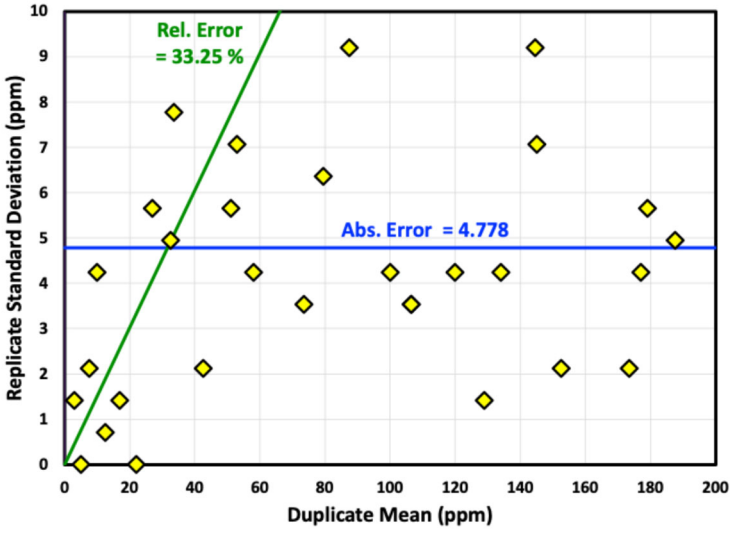


Figure 2. *Modified Thompson-Howarth scatterplot (Stanley and Lawie, 2008) depicting 30 duplicate means and standard deviations, and the* ***descriptive*** *absolute error line (blue) and* ***descriptive*** *relative error line (green) for these data.*

Errors measured using a Thompson-Howarth scatterplot in the above manner are *descriptive* measures of precision and are commonly used in statistical comparisons of error magnitude and in the decomposition of total error into its component parts (*e.g.*, $\sigma_T^2 = \sigma_S^2 + \sigma_P^2 + \sigma_A^2$; where σ_T^2 is the total error, σ_S^2 is the sampling error, σ_P^2 is the preparation error, and σ_A^2 is the analytical error) and the measurement of those parts.

However, error models on a Thompson-Howarth scatterplot can also provide *predictive* measures of error if calculated using regressions. Several regression models have been employed in this regard, including linear, Poisson, and binomial models (Fig. 3), and these produce best-fit estimates of error as a function of concentration (Stanley 2007). Although linear models are most often used, Poisson and binomial models are consistent with sampling theory and thus may be appropriate in many applications (*e.g.*, Poisson models for Au, Pt, Pd, or diamond concentrations

in associated mineral deposits; binomial models for Fe and Al concentrations in banded iron formations and bauxites; Stanley and Smee, 2007; Stanley, 2006). This regression-based application of error analysis thus provides a prediction of the magnitude of error for every measurement (as it is a function of the measurement), and so can be used to estimate measurement error when error propagation through important calculations is necessary (aspirationally, in resource estimation).

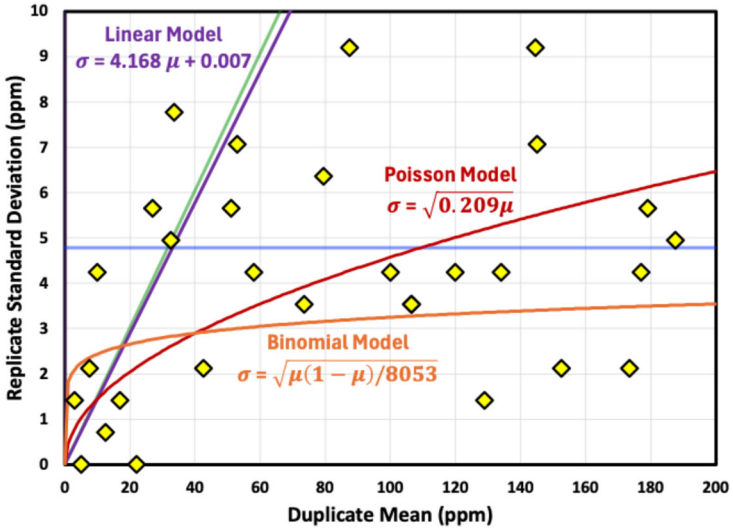


Figure 3. *Modified Thompson-Howarth scatterplot (Stanley and Lawie, 2008) depicting 30 duplicate means and standard deviations, and the predictive linear error model (purple), the predictive Poisson error model (red), and the predictive binomial model (purple) for these data (the absolute and relative error models are in blue and green, respectively).*

Several challenges exist when assessing the precision of measurements in geological applications. First, many geoscientists plot duplicate measurements against each other on a scatterplot, thinking this is an appropriate way to depict and describe measurement error. Unfortunately, this commonly results in high data correlations (say, R > 0.80) even though the magnitude of relative error is likewise rather high (say, > 15 %). This apparent contradiction results from the fact that the range of measurements in most geological applications is commonly very much larger than the magnitude of error, making such plots mistakenly appear to reflect 'high-quality data'. As a result, duplicate scatterplots are not recommended for precision assessment.

Another problem that affects QA/QC programs is the misuse of historical statistics (*e.g.*, precision measurements such as the average relative difference [ARD] and the half the average relative difference [HARD]). These statistics were devised in the 1960's when calculators didn't even have square root functions, and so statisticians at the time devised these measurements to cleverly avoid complicated calculations involving square roots:

$$ARD = \frac{|x_1 - x_2|}{\mu} \quad \text{or:} \quad HARD = \frac{|x_1 - x_2|}{2\mu}. \tag{4}$$

Unfortunately, these statistics are only proportional to relative error (***they are not equal to relative error***) as ARD = $\gamma_e \times \sqrt{2}$ and HARD = $\gamma_e \times \sqrt{2}/2$. Both statistics have been improperly used numerous times in the literature, as noted by Stanley and Lawie (2007) and probably countless times in QA/QC reports. This is because geoscientists are generally not aware of the proportionality (not equality) of these statistics with relative error. As a result, geoscientists should use appropriate statistics to measure precision, such as the absolute *standard* deviation (absolute error) or the relative *standard* deviation (relative error). After all, they are the 'standard'.

The last problem involving precision in QA/QC involves the Thompson-Howarth scatterplots themselves. Commonly, these plots exhibit very poor correlations between measurements and their errors (means *versus* standard deviations; *e.g.*, Figs. 2 and 3), and this poor correlation undermines the geoscientist's perception of the quality of the error model used to describe or predict the magnitude of error as a function of concentration. Importantly, it should be noted that the low correlation is not generally a reflection of a poor error model but rather is a consequence of trying to estimate a mean and standard deviation using only two measurements. Understandably, this results in large errors in the estimates of these statistics and so result in large error ellipses about data points on Thompson-Howarth scatterplots (which unfortunately are usually not presented).

To ensure the calculation of a stable error model (which is all one needs for a reliable estimate of precision), whether it be absolute, relative, linear, Poisson, or binomial, one needs a large number of degrees of freedom in the scatterplot. This can be obtained by measuring the means and standard deviations of an adequately large number of duplicates (n), or by using a larger number of replicates (m) to increase the number of degrees of freedom ($df = n*m$) and reduce the error in the estimates of each mean and standard deviation. Both strategies are effective in ensuring that the descriptive or predictive precision model is satisfactory.

Analytical Aaccuracy

Accuracy in QA/QC is commonly measured using reference materials (RMs). Reference materials that are '*certified*' (CRMs) have been analyzed by 10 or more laboratories and exhibit

average measurements that are less than 5% different from the accepted value. In contrast, reference materials with differences between 5 and 15% of the accepted value and that have been analyzed by 10 or more laboratories are commonly referred to as '*indicated*' (IRMs), whereas those analyzed by less than 10 laboratories are referred to as '*provisional*' (PRMs).

Accuracy is commonly evaluated using a Shewharts Control Chart (Fig. 4), which plots the measurements of a reference material against batch, date, or measurement order. On this chart, measurements are compared with the accepted value (the mean; μ) and the $\mu \pm$ 1, 2, and 3 σ tolerances determined using a laboratory round-robin of the reference materials by the CRM manufacturer.

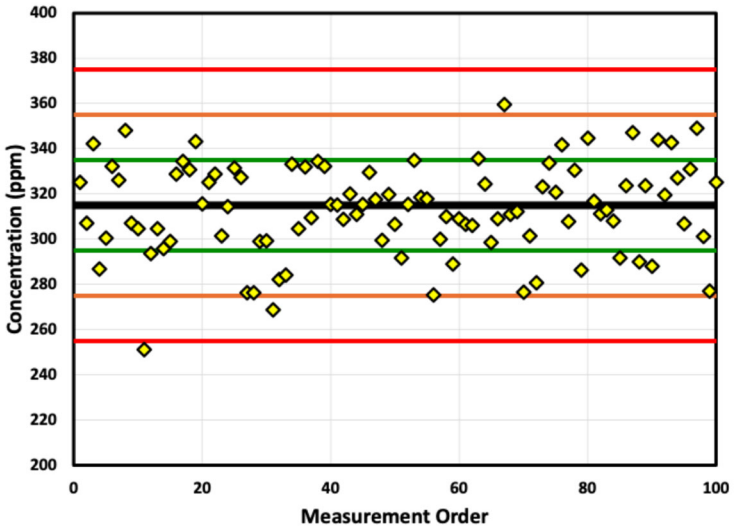


Figure 4. *A Shewharts Control Chart assessing the accuracy of a CRM. Only a small number of measurements fall outside the $\mu \pm 3\sigma$ lines (red; 1) and the $\mu \pm 2\sigma$ lines (orange; 2). If the #'s of measurements plotting outside these tolerances exceeds those expected at random (with n = 100, ~5 measurements should plot outside the $\mu \pm 2\sigma$ lines, and ~1 measurement should plot outside the $\mu \pm 2\sigma$ lines), then measurement accuracy is suspect.*

Outliers on such control charts can be detected using measurements and measurement patterns that are not likely to occur at random. If an unexpected number of such patterns is present on a Shewharts Control Chart, there is cause for concern regarding the quality of the measurements.

Alternatively, if measurement patterns appear to be distributed as expected (based on the CRM means and standard deviations), one can statistically test the distribution of the reference material results in one's batch of samples by comparing it with the distribution of the round-robin data used to obtain an accepted value (mean) and tolerances (mean $\pm$ 1, 2, or 3 standard deviation) for the reference material. This can most appropriately be undertaken using a Mann-Whitney U test (Asare 2026), which determines whether the two data distributions are derived from the same distribution.

If so, then the measurements analyzed with the reference material are not only considered accurate but also precise.

Indicator Minerals

Most of the QA/QC concepts presented above involve geochemical analyses of particulate materials such as glacial till in the search for mineral deposits. An alternative method used to undertake mineral exploration in glacial terranes involves measuring the number of specific indicator minerals from these same glacial tills. This procedure is commonly undertaken by collecting large till samples (say 12 kg), preparing them by sieving them to -8 mm, separating the clay and light minerals from them on a shaking table, and then sieving them again into sizes where the grains are predominantly liberated (0.25 to 2 mm). These samples are then treated with a reducing acid to remove weathering crusts and stains and typically undergo density separation using heavy liquids and magnetic separation using plunge magnets to further concentrate the indicator minerals in these materials. In each step, the resulting sample fraction is retained. As a result, although these sample preparation procedures are enacted to isolate specific mineralogical fractions of the samples, no significant sub-sampling error is introduced into the various fractions of the sample. This is because no formal sub-sampling is undertaken, except for the collection of any archival sub-sample. Fortunately, such archival sub-samples are generally small and so represent a very small proportion of the original sample (0.25%). As a result, this sub-sampling activity does not impose any significant sub-sampling error.

These sample preparation practices result in sub-samples with indicator minerals with different grain sizes (usually 0.25 to 0.5 mm, 0.5 to 1 mm, and 1 to 2 mm), different densities (>3.20 gm/cc and <3.20 gm/cc), and either strongly magnetic, weakly magnetic, or non-magnetic characteristics. Then, depending on the target mineral deposit type and its indicator mineralogy, one or several of these twelve sub-sample fractions are then commonly examined visually to identify and count the number of different ‘indicator minerals’ present in the glacial material. Finally, the indicator mineral counts are standardized through division by the original sample mass or the mass of the indicator mineral sub-sample, producing a standardized metric that can be used in mineral exploration.

A major advantage of this mineralogical form of mineral exploration is that no geochemical analysis is undertaken. As a result, no calibration or other geochemical procedures are necessary. Although sampling is identical, sample preparation becomes complicated, but analysis is significantly simplified. In fact, provided that accurate recognition of the indicator minerals is achieved, the only significant errors introduced into these samples are: (i) the original sampling error that takes place in the field (and cannot be avoided but can be reduced by selecting a larger sample), and (ii) the counting errors associated with the measurement of how many indicator minerals are present. Consequently, counting statistics, governed by the Poisson distribution, can be used to estimate these counting errors, providing an ideal, but realistic, measure of data quality.

The advantage of using Poisson counting statistics is that a relationship exists between the mean and variance:

$$\sigma_P^2 = \mu, \quad \text{so:} \quad \sigma_P = \sqrt{\mu_P}\,. \tag{5}$$

As a result, for any indicator mineral counting measurement, the error on that measurement can immediately be determined. Dividing both sides of the above equation by the Poisson mean produces the relative error:

$$\frac{\sigma_P}{\mu_P} = \phi_P = \frac{1}{\sqrt{\mu_P}}, \tag{6}$$

allowing the geoscientist to also immediately determine whether their measurements are 'fit for purpose' (Bettaney and Stanley, 2001; Fig. 5).

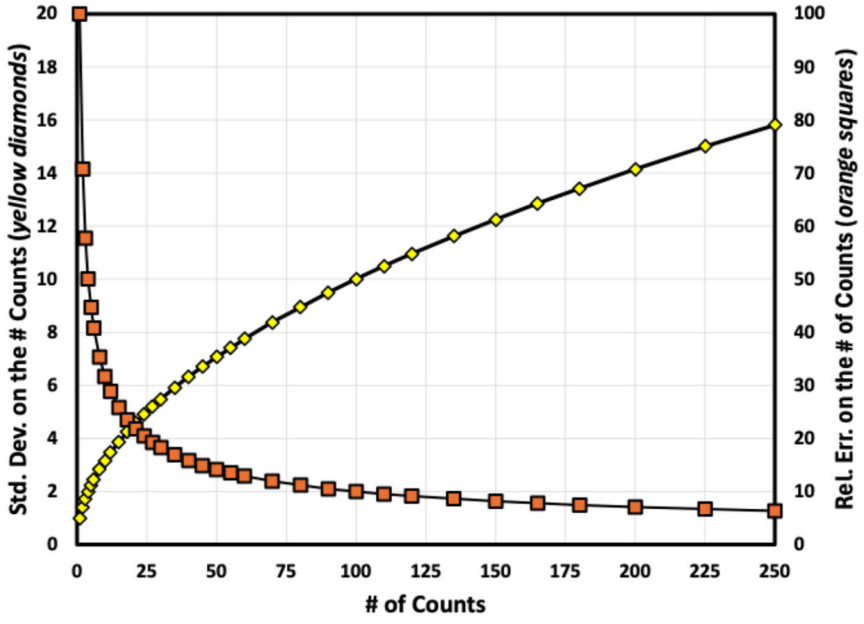


Figure 5. *A scatterplot showing the relationship between grain counts (means) and the Poisson counting errors in those grain counts (standard deviations; yellow), and between grain counts and the relative errors in those grain counts (orange), based on a Poisson distribution.*

Conclusions

So, the three aspects of data quality that one needs to monitor in any measurement survey are: representativity, accuracy, and precision. The former aspect is generally restricted to sample collection, whereas the two latter aspects are predominant in sample preparation and analysis. QA/QC samples consisting of replicates, blanks, and reference materials are used to assess these aspects of data quality and help the geoscientist to determine whether their data are 'fit for purpose' (Bettaney and Stanley, 2001). It is important to recall that data quality in mineral exploration surveys does not have to be as high as that required in resource estimation.

Lastly, in general, it is highly recommended to undertake a QA/QC assessment of data collected in any survey of glacial materials before evaluating the data for the purposes of your mineral exploration survey. This is because the conclusions identified by geoscientists in their data analysis are generally far more interesting (and hopefully more exciting) than the relatively 'dry' QA/QC results. Consequently, many geoscientists have spent significant time evaluating data from an exploration survey they just undertook only to conclude, when they have subsequently evaluated the associated QA/QC data, that their survey data were not 'fit for purpose' and do not support the initial conclusions that they hypothesized. This is primarily because the QA/QC results provide the scientific foundation necessary to have confidence in the exploration survey results.

References

Asare, B., Arthur, Y.D., Obeng, B.A. and Alija, S., 2026: Mann-Whitney U Test for two independent groups. Journal of Research in Didactical Sciences, Volume 5(1), pages 13–30.

Barnett, V., 1983: Principles and methods for handling outliers in data sets. *In* Statistical Methods and the Improvement of Data Quality: Proceedings of a Small Conference on the Improvement of the Quality of Data Collected by Data Collection Systems, Oak Ridge, TN, Academic Press, pages 131–166.

Bettaney, L. and Stanley, C.R., 2001: Geochemical data quality: The "fit-for-purpose" approach. EXPLORE: Newsletter of the Association of Exploration Geochemists, Volume 111, pages 21–22.

Pitard, F.F., 1989: Pierre Gy's Sampling Theory and Sampling Practice. CRC Press, Baton Rouge, LA.

Sinclair, A.J., 1991: A fundamental approach to threshold estimation in exploration geochemistry: Probability plots revisited. Journal of Geochemical Exploration, Volume 41(1-2), pages 1–22.

Stanley, C.R.. 1988: Comparison of data classification procedures in applied geochemistry using Monte Carlo simulation. The University of British Columbia, Unpublished Ph.D. Dissertation, 289 pages.

Stanley, C.R.. 2006: On the special application of Thompson-Howarth error analysis to geochemical variables exhibiting a nugget effect. Geochemistry: Exploration, Environment, Analysis, Volume 6, pages 357–368.

Stanley, C.R., 2007: The fundamental relationship between sample mass and sampling variance in real geological samples and corresponding ideal statistical models. Exploration and Mining Geology, Volume 16(1-2), pages 111–125.

Stanley, C.R. and Lawie, D., 2007: Average relative error in geochemical determinations: Clarification, calculation and a plea for consistency. Exploration and Mining Geology, Volume 16(3-4), pages 267–275.

Stanley, C.R. and Lawie, D., 2008: Thompson–Howarth error analysis: Unbiased alternatives to the large-sample method for assessing non-normally distributed measurement error in geochemical samples. Geochemistry: Exploration, Environment, Analysis, Volume 8(2), pages 173–182.

Stanley, C.R. and Smee, B.W., 2007: Strategies for reducing sampling errors in exploration and resource definition drilling programs for gold deposits. Geochemistry: Exploration, Environment, Analysis, Volume 7(4), pages 329–340.

Yonar, A., Yonar, H., Demirsoz, M. and Tekindal, M.A., 2024: A comparative analysis for homogeneity of variance tests. Journal of Science and Arts, Volume 12(2), pages 305–328.

Gold Grain Analysis in Tills: Examples from Newfoundland

Peter Dimmell
Krinor Resources, 56 Carpasian Road, St. John's, NL, A1B 2R2

Abstract

Till analysis for number and size of gold grains, and their morphology (shape), is utilized in exploration in Newfoundland to determine distance and direction of transport and the possible source area for the gold grains. Overburden Drilling management of Ottawa, has found that all tills deposited by the Laurentide and Newfoundland ice sheets, contain gold grains with the gold grain background of an area depending mainly on the number of kilometres of gold fertile rock units that the ice crossed. Gold grains in till analysis in exploration is compared to geochemical till analyses as utilized by the Newfoundland and Labrador (NL) government. It is described using case studies from 2 areas, with four Au gold grain in till anomalies, the Joe Batts Pond (JBP) area, to the west of Gander, owned by New Found Gold and the Rambler South area on the Baie Verte Peninsula owned mostly by Firefly Metals with claims over the South Brook (SB) gold zone and the Brass Buckle Trend (BBT) owned by Krinor Resources Inc. Results are also shown for the Krissy Trend (K) area (Figs. 1 and 2).

Newfoundland and Labrador Provincial Till Database

At present the provincial government till sample database consists of 26,286 samples, 20,015 on the island and 6,271 in Labrador, with 20,846 regional samples taken at approximately 1 sample per km^2 along roads and 1 sample per 4 km^2 in areas where helicopter access is required (GSNL, 2024). Fractions sampled include: <63 microns - 15,933 and <180 microns - 10,351. Analyses are primarily by INAA (instrument neutron activation analysis) and ICP-OES (4 acid) with 55 elements reported in the database. On the island sampling covers central Newfoundland and much of the Avalon Zone. Background for Au is 5 to 9 ppb, considered a high background by exploration geologists, but reflective of the gold mineralization discovered mainly in the central area (pers. comm., Sarah Hashmi, GSNL). The JBP area is covered by this sampling however the Rambler South area has not yet been covered.

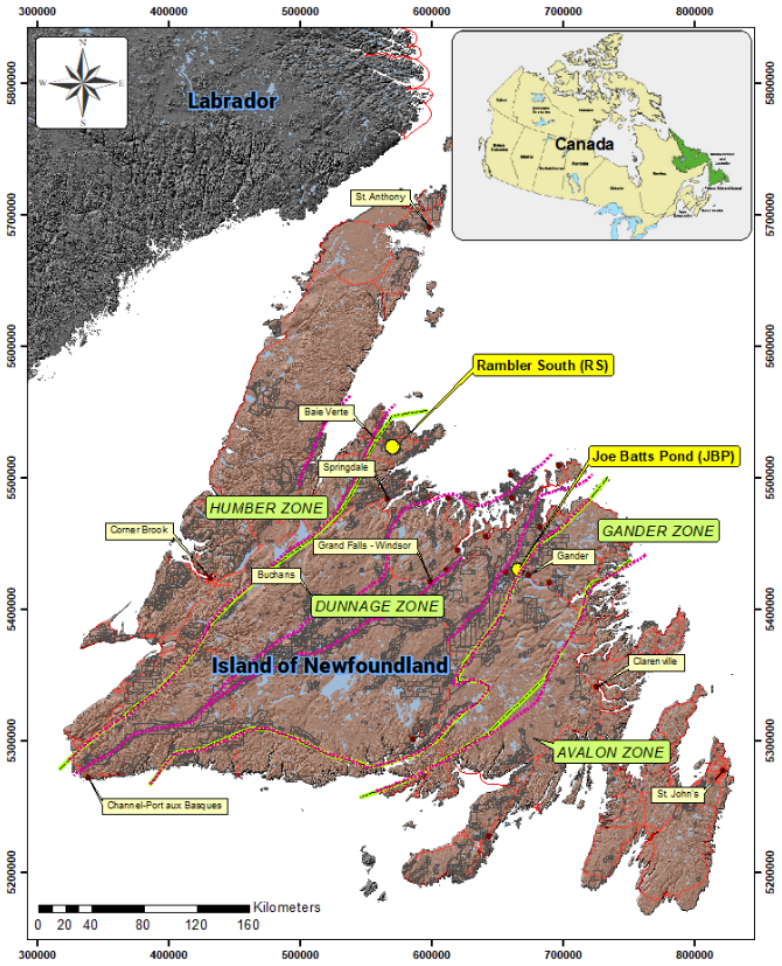


Figure 1. *Tectonostratigraphic subdivisions of Newfoundland with project locations.*

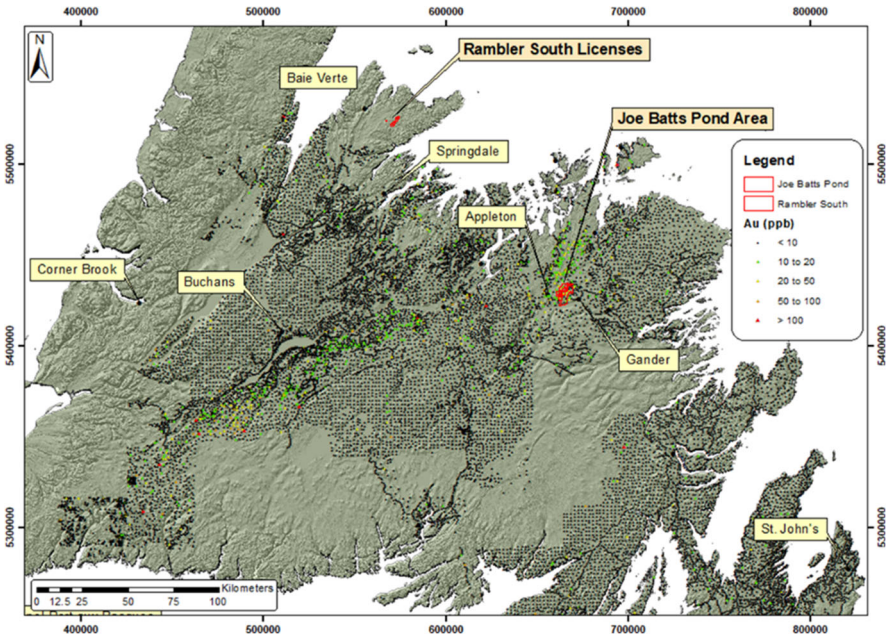


Figure 2. *Newfoundland – GSNL till sample locations with project areas highlighted.*

Rationale for Gold in Till Grain Analysis

Most geochemical surveys give some analyses that are statistically anomalous, however gold grain anomalies are found only in areas that are fertile for gold. ODM measurements of the gold grain content of tens of thousands of till samples from many regions of Canada has found that all till deposited by the Laurentide and Newfoundland ice sheets contains gold grains with the gold grain background of an area depending mainly on the number of kilometres of gold fertile rock units that the ice crossed (Averill, 1988). Also, whether occurring at background or anomalous levels, and whether pristine or significantly modified by glacial transport, ~95% of gold grains in till are silt sized – *i.e.*, <0.063 mm or 63 μm in width – because (a) this is the natural grain size at which gold tends to crystallize in bedrock; and (b) gold grains are malleable and do not break down into smaller particles during transport.

Their conclusion is: A till sample is considered to be anomalous in gold grains when: (1) the sample contains at least two to three times more gold grains than the average background level; (2) the grains show no evidence of hydraulic sorting; (3) their morphologies are dominantly pristine + modified; and (4) neighboring till samples are similarly anomalous.

Why Use Gold Grain Analysis?

The government till analyses excellent regional data but generally no idea of distance of transport, number of gold grains, or size of the grains. Possible general directions to source for anomalous Au values are sometimes shown by a decrease in gold values away from the source although no discoveries are yet known using this technique. Gold grain analysis for morphology, number of grains, and size of grains, with calculated Au values using the gold grain sizes, by ODM can be used to show the strength of an anomaly (*i.e.*, # of grains), the size of the grains (*i.e.*, is there free / visible Au in the bedrock source), a calculated Au value of the source based on the size of the grains, and the probable distance of transport as shown on Figs. 3 and 4.

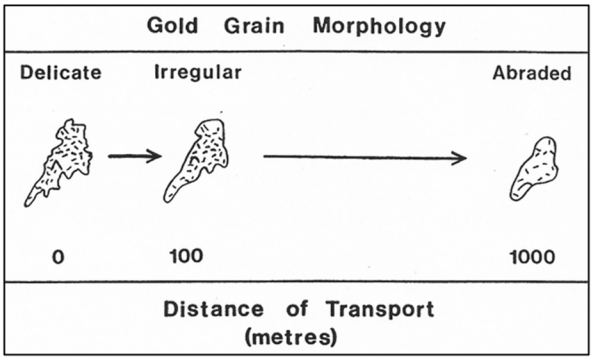


Figure 3. *ODM cartoon illustrating distance of transport for gold grains.*

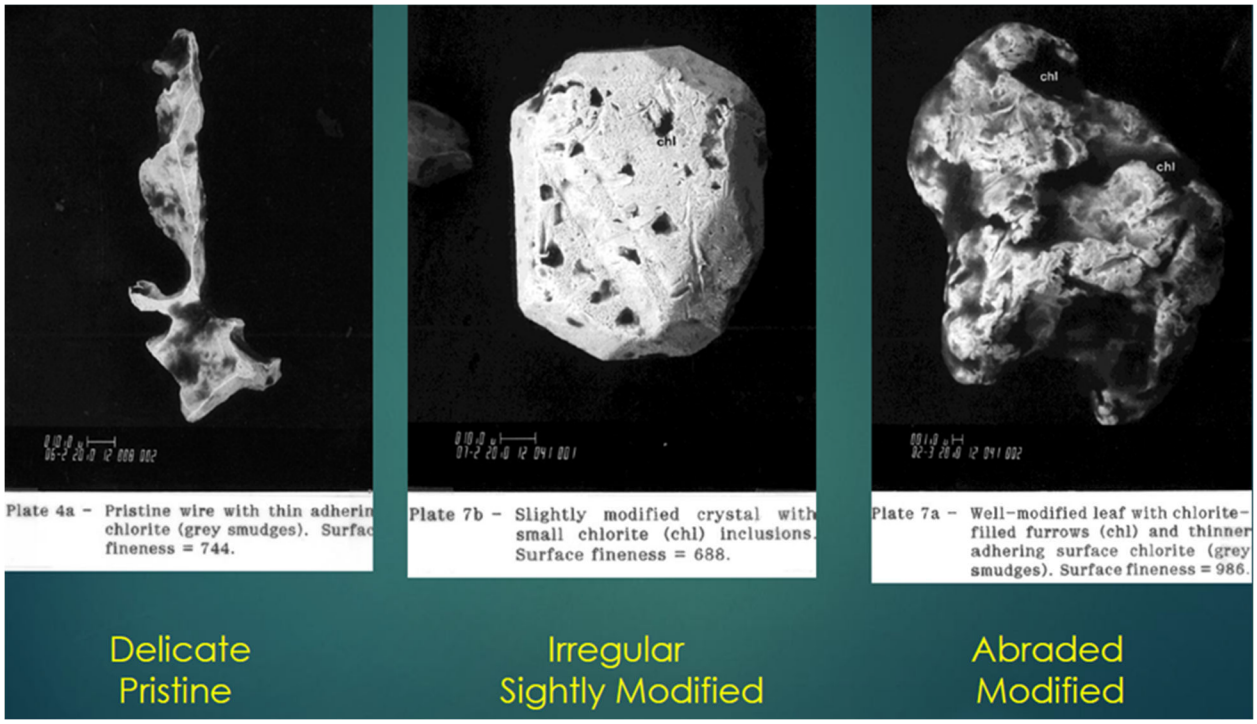


Figure 4. *Photomicrographs from RS tills – ODM 1989 test survey.*

An example of the data provided by ODM from the Brass Buckle Trend (BBT) area and how I use this data is shown in Figs. 5 and 6. My interest is in 3 aspects of the data – 1) the pristineness of the grains (*i.e.*, an idea of distance from source), 2) the number and 3) the size of the gold grains. I usually plot the till values using the number of grains and the percent pristine using the calculated value, which ODM indicates can mimic the Au values in the source area, as a secondary aspect. The size of the gold grains is also important as very fine grains, <50 microns, are not visible in source hand samples or drill core making it difficult to identify the gold mineralization without analysis.

Gold Grain Summary

Client: Krinor Resources
File Name: 20198206 - Krinor - Dimmell - (Gold, HMC) - December 2019
Total Number of Samples in this Report: 6
ODM Batch Number(s): 8206

	Number of Visible Gold Grains					Calculated PPB Visible Gold in HMC			
Sample Number	Total	Reshaped	Modified	Pristine	Nonmag HMC Weight (g)	Total	Reshaped	Modified	Pristine
RSBB-19-T-01	37	8	9	20	13.7	202	67	70	66
RSBB-19-T-02	107	42	25	40	19.9	456	211	182	64
RSBB-19-T-03	20	15	0	5	3.4	1735	1690	0	44
RSBB-19-T-04	20	8	3	9	4.0	1304	92	1054	158
RSBB-19-T-05	179	75	43	61	2.2	36019	24302	3984	7733
RSBB-19-T-06	141	24	24	93	9.4	1424	320	145	959

Figure 5. *ODM data – BBT area 2019.*

BBT Till Samples				2019		
Number	Gold	Pristine	%	Calc Au	Horizon	Notes
	Grains		pristine	ppb		
RSBB-19-T-01	37	20	54	202	C	BBT; grn sericite
RSBB-19-T-02	107	40	37	456	C	BBT - mv
RSBB-19-T-03	20	5	25	1735	B	BBT; grn sericite
RSBB-19-T-04	20	9	45	1304	C	BBT
RSBB-19-T-05	179	61	34	36019	B/C	BBT
RSBB-19-T-06	141	93	66	1424	C	BBT

Figure 6. *My interpretation (use) of the 2019 BBT ODM data and unpublished data.*

Area 1 – JBP Fault Zone

Location

The JBP Fault / fracture zone lies approximately 10 km to the west of Gander in central NL. It is part of New Found Gold's Queensway project which at present is focused on the Appleton Fault Zone (AFZ), located 5 km further west.

Geology

Dunnage Zone of the Newfoundland Appalachians just to the west of the Gander River Complex which lies along the contact of the Gander Zone. The JBP area, like the AFZ to the west is underlain by argillic sedimentary units of the Davidsville Group which are cut by mafic intrusives, mainly dikes. The JBP fault system, an anastomosing area of shears / faults with associated quartz veining carrying visible gold mineralization, trends north-northeasterly generally parallel to the stratigraphy. Two areas of gold mineralization, the Pocket Pond and H Pond areas, discovered by Paragon Minerals, lie along the JBP fault system. Paragon drilling has given Au intersections such as: Pocket Ponds – HP-08-48 - 11.1 g/t / 11.9 m and H Pond – HP-04-03 11.7 g/t / 3.4 m (Fig. 7) New Found Gold exploration drill tested the zones plus areas between and to the north and south along strike from 2020 to 2022 with variable success but has been focused on the Appleton Fault Zone (AFZ) and the gold showings found along it such as the Keats, Iceberg, K2, Keats West and others.

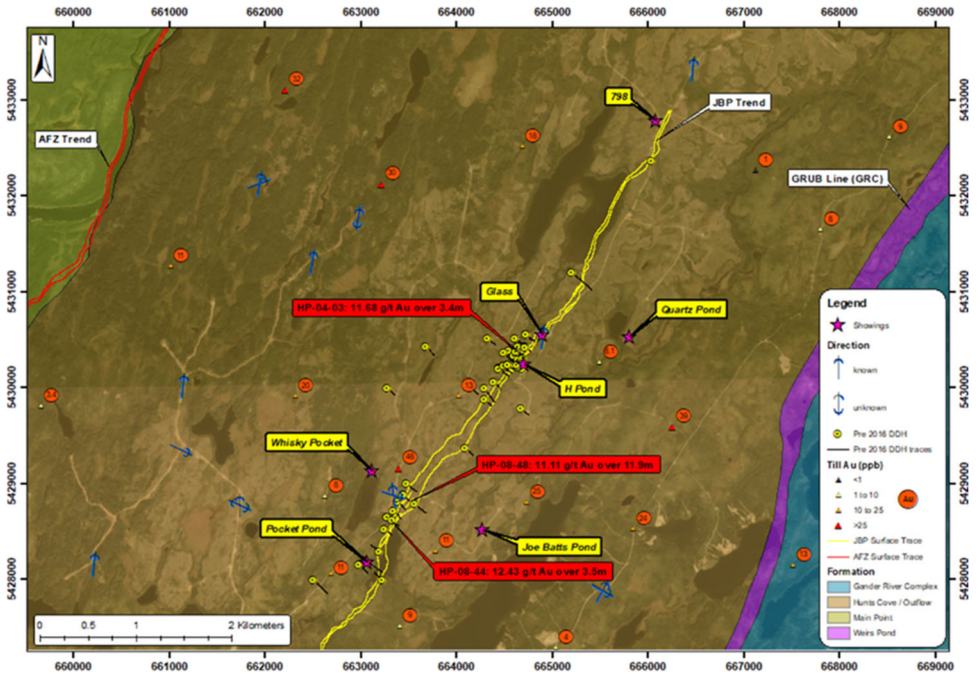


Figure 7. *Geology (Blackwood, 1983) with ice flow directions, GSNL tills and Au showings.*

Surficial Geology

A regional study which includes the area from the east coast to west of the Gander River, found three ice-flow directions affecting the western area including the JBP, with sediment deposited by an early eastward ice flow, reworked by later northward-flowing ice, both to the NNE and NW (*e.g.,* St, Croix and Taylor, 1991; Brushett, 2012; Organ, 2022). The dispersal pattern of ultramafic clasts associated with the Gander River Complex suggest that the dominant ice flow was north westward in the eastern area (Carmanville to east of Island Pond), with granitic clasts derived from Gander Lake Granite found in areas underlain by the Gander Group (Barry's Brook and Island Pond areas) suggest glacial transport northward (Brushett, 2012). Glacial directions noted in the JBP are mainly NNE, considered to be the last glaciation, but also include eastward ice flow directions.

Ice flow patterns in the Mount Peyton region in central NL sometimes diverge from regional models as till from older and younger flow events are variably preserved, and sediments are reworked through ice marginal, ice streaming and other processes (Campbell and Lachance, 2026). The earliest flow orientations are to the east-southeast, noted in striations to the south of H Pond, with southeast flow fabrics also preserved to the northwest of the Gander River (Scott, 1994). This pattern decreases in the same orientation as the early striations in the area (~108°), suggesting a

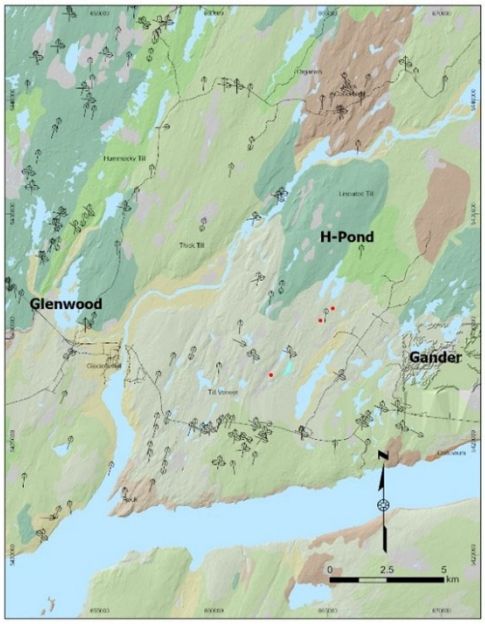


Figure 8. *Ice flow direction – Glenwood to Gander area (Campbell, 2026).*

preserved early dispersal train, not reworked by later glacial dispersal. Isolated mineral trains from early ice flow events appear to be untouched by later events (*e.g.,* NNW flow at 352°). The lack of offset by later northward flow could be attributed to less erosive, colder based conditions, postulated to have affected the transport distances of boulders in the same region (Campbell and Lachance, 2026) and correlate with local studies indicating dispersal distances of <2 km (Batterson and Liverman, 2000). Later northward flow generally follows the bedrock linears and the many gold showings along the Appleton and JBP Faults, makes it difficult to distinguish between regional anomalies from northward dispersal from those indicating underlying showings. The till in the H-Pond area is very shallow, silt poor and sandy, (Holmes, 2016; Organ, 2022) and has possibly been reworked by meltwater, making heavy mineral samples/gold grain morphology important in targeting source areas as they can "see" through the aggregated glacial dispersal directions represented in multiple tills, and in tills of different textures and origins in this region (Campbell *et al.*, 2024; Holmes, 2016).

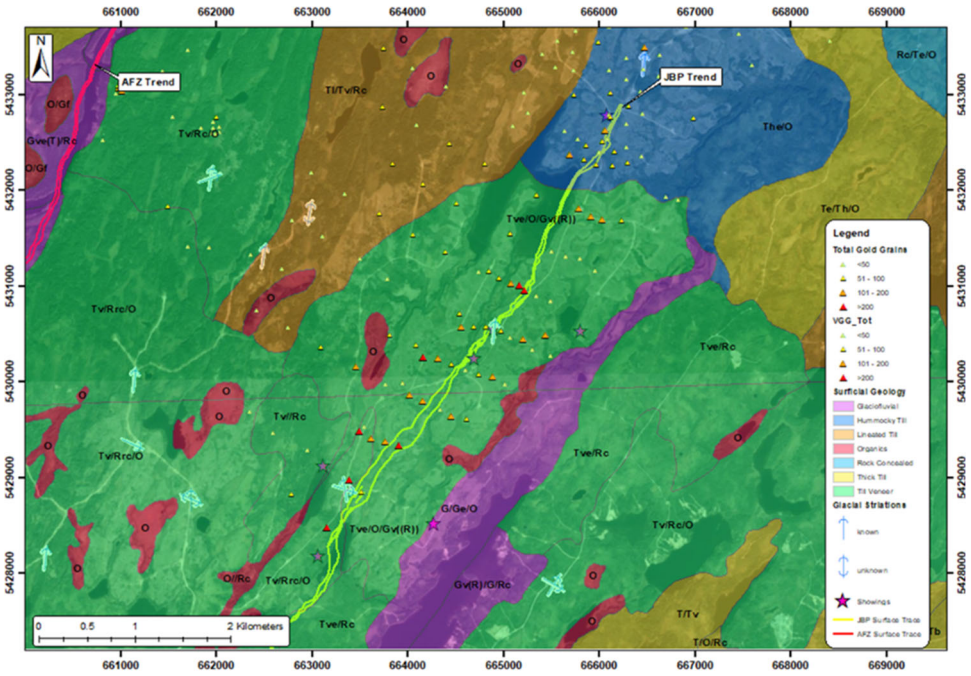


Figure 9. *Surficial geology – JBP area (Scott, 1994) with ODM till grid.*

Exploration

A 2016 till survey by ODM for Palisade (now NFG) focused on the area of the Pocket Ponds and H Pond showings. Fifty nine till samples were taken at approximately 150 m intervals on lines 500 m apart oriented WNW / ESE, roughly orthogonal to the general NNE ice-flow direction. No such survey has evaluated the AFZ, the main area of gold mineralization on the Queensway property, located 5 km to the west. ODM summarizes their procedure as follows (Holmes, 2017). Pits were hand dug to approximately 1 m to the minimally oxidized C-horizon with each sample hand screened to -8 mm, into a pail, to remove the large clasts. Approximately 13 kg of the -8 mm fraction, along with a representative sample of the +8 mm pebbles, was packed in a heavy-duty 30 x 50 cm plastic rock bag sealed with a cable tie (Holmes, 2017). At the laboratory a representative ~500 g split is removed from the sample and reserved for geochemical analysis. The remaining bulk sample material is wet screened at 2.0 mm with a -2.0 mm table concentrate prepared. Geological observations on the character of the sample are made during both the screening and tabling operations. The table concentrate is purposely large (typically 300–400 g) and of low grade (10–25% heavy minerals) in order to achieve a high, 80 to 90% recovery rate for all desired heavy minerals irrespective of their grain size or relative specific gravity. The gold grains, which by nature are mostly silt-sized, are observed at this stage with the aid of micropanning and are counted, measured and classified as to degree of wear (*i.e.*, distance of glacial transport). The relative abundances of any sulphides or similar indicator minerals or metallic contaminants are also estimated and the expected gold assay value of the contained gold grains is calculated based on the gold grain sizes. The results are summarized in Excel spreadsheets and a pdf version and sent to the Company. *Note: The same technique is used for all the till surveys described in this paper so it is not repeated.*

Results

An extensive area of high gold grain counts were found, which ODM indicated was one of the most anomalous areas they had ever sampled (pers. comm., Don Holmes, 2017). Gold grain size was generally 50 microns or less. The lowest number of gold grains was 11 with background values in the 20 to 40 range, with 75% >50 grains, 39% >100 grains and a high value of 1744 grains. Unfortunately while the data was impressive due to the high background level and many gold

grains it was difficult to use the morphology of the samples to give a distance to source or to identify possible source areas since most samples were "far travelled". Two areas show higher pristineness – the first line north of the Pocket Ponds deposit, 4 samples from 122 to 378 grains with 64 to 83% pristine, probably reflecting the NNE ice flow from the showing and three / four samples, with lower grain counts on the east side 68 to 80% pristine, reflecting either unknown mineralization along strike to the south or the eastward ice direction from the main mineralized areas.

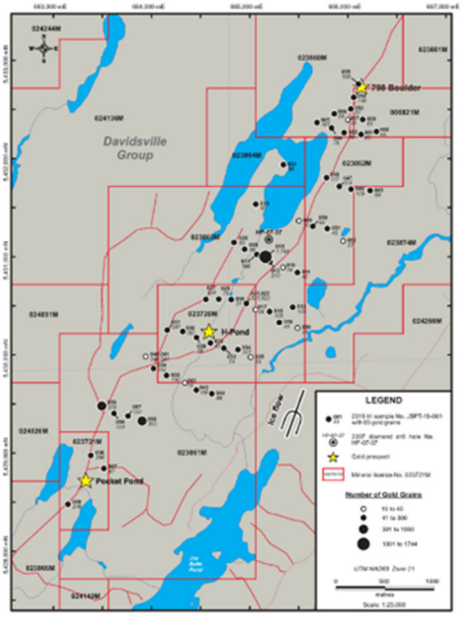


Figure 10. *2016 ODM /Palisade (NFG) till survey results.*

Follow Up Exploration

Included prospecting, geology, trenching and later diamond drilling resulting in the discovery of quartz vein float with visible gold in the mostly cut over areas, which became areas for trenching (1744, Glass, Quartz Pond). Quartz veins with visible gold in trenches (*i.e.*, the Glass showing) was found however most trenches did not expose significant gold mineralization and all were reclaimed. In the 1744 trench, so named as it tested the area of the 1744 gold grain in till value, two tills were located, the upper a yellow brown till full of white quartz vein float, 1.5–2 m thick, and a lower, darker grey brown till carrying no quartz veins. Bedrock was not found at 5–6 m down, at the bottom of the trench. Only limited diamond drilling has been carried out in the area by NFG since emphasis is being placed on the Appleton Fault Zone (AFZ) showings.

Area 2 – Rambler South

Location

On the Baie Verte peninsula in northwestern Newfoundland, approximately 5 to 8 km to the south of the LaScie highway, Route 414 and the old Rambler Mines area (Main, East and Big Rambler Pond deposits). Access is *via* the Gull Pond resource road, 15 km along the poorly maintained road which takes an hour to drive.

Geology

Primarily underlain by Pacquet Harbour Group (PHG) mafic volcanics and intrusives which are cut by quartz feldspar porphyry (QFP) dikes, related either to the Cape Brule Porphyry (CBP), which intrudes the PHG to the east or the Burlington Granodiorite (BG) to the west. The CBP is overlain by the Cape St. John Group (CSJ), an overlying remnant of felsic crystal lithic tuffs that die out to the east over the CBP and do not occur again until the Tilt Cove area, 30 km to the east. In the west the BG intrudes the PHG hornfelsing the PHG contact and continuing the hornfelsing along the QFP dike that extends from the BG to the CBP. Structures are mainly northeasterly to east-northeasterly trending and are either dike related (QFP dikes) or are shears (Krissy trend - K) or faults (Brass Buckle Trend - BBT). A QFP dike extends along the BBT structure from the CBP, southwesterly, for at least 5 km.

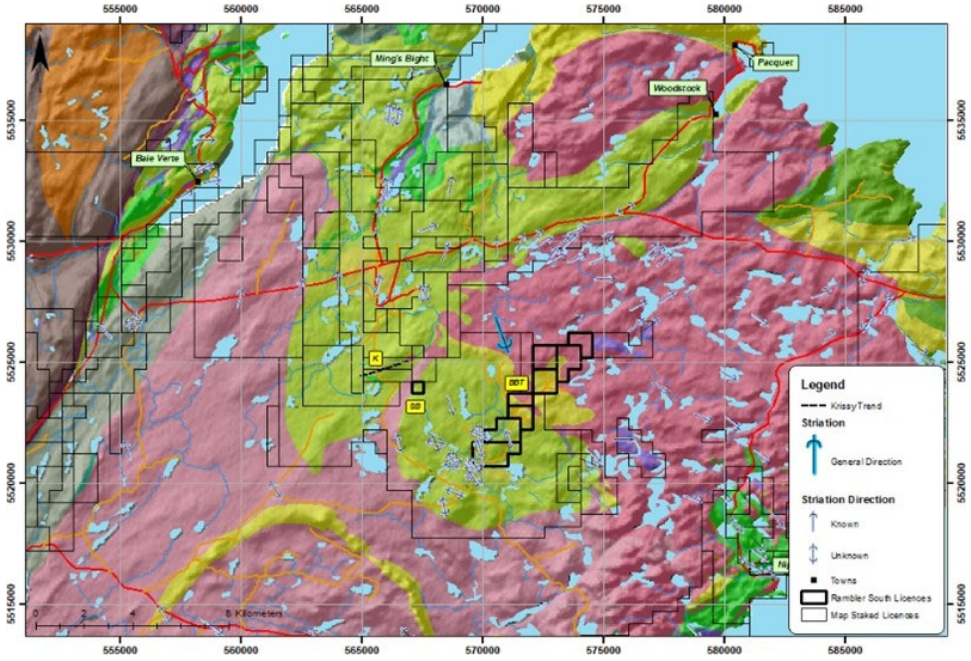


Figure 11. *Baie Verte area geology (Hibbard, 1983) with project locations and ice flow direction.*

Surficial Geology

Ice directions are mainly northeast (045) in the northern part of the southern PHG but become primarily 160° to the south of the main QFP dike, with the northeast trend becoming less prominent. The first ice movement was 160, with the 045 direction the second based on the till results that led to the discovery of the SB gold zone.

Exploration

Lacana Corp / Corona Corporation staked the southern Pacquet Harbour Group (PHG), the host unit for the Rambler VMS deposits, to the south of the Consolidated Rambler properties, in 1986. The exploration was targeted at VMS deposits. An airborne electromagnetic (EM) / VLF-EM / magnetic survey flown in 1986/87 led to a grid along the contact with the CBP/CSJ over a magnetic anomaly now known to have reflected the magnetite rich, basal portion, of the CSJ. Ground follow up started in 1987 and continued until 1992 when Corona exited Newfoundland. This exploration, gridding, soil geochemistry, geology and prospecting, resulted in the discovery of two significant gold showings, the Brass Buckle, and 660 and a few others, either related to, or to the south of, a regional structure (now termed the BBT), which was defined by a VLF-EM Fraser Filter conductor even though the survey, which was flown perpendicular to the PHG / CSJ/CBP boundary was almost parallel to the structure. The EM didn't locate any conductive VMS style anomalies so emphasis was placed on gold exploration and ODM were contracted for a test till program in the southern part of the claimed area in 1989. The survey showed that gold grains were present in the tested area and a regional till survey was laid out to cover the northern portion of the Corona claim block, to the north of the BBT. Three hundred and ten samples were taken by Corona personnel at approximately 300 m intervals. Samples were acquired per ODM instructions from the C horizon, as generally unoxidized, grey white till with many pebbles. Samples were field sieved to remove larger pebbles to give an approximate 10 kg sample. Samples were shipped to ODM in Ottawa for gold grain analysis.

Results

Background for the survey is considered to be <5 grains / sample. Two areas, the Krissy Trend (K) and South Brook (SB) Au gold grain in till anomalies were located and are described following.

Krissy Trend: At the northern extent of the survey, follow up of weak, anomalous, samples - 12 to 15 grains, resulted in the discovery of an altered / sericitized / quartz veined boulder carrying extensive visible gold on an old cut line (West Coast Ventures (WCV), 1988). Subsequently, using their gold in soils data, a shear zone, the KT trend, with similar boudinaged alteration, quartz veining and gold mineralization, including visible gold, was found extending over a 500 m strike

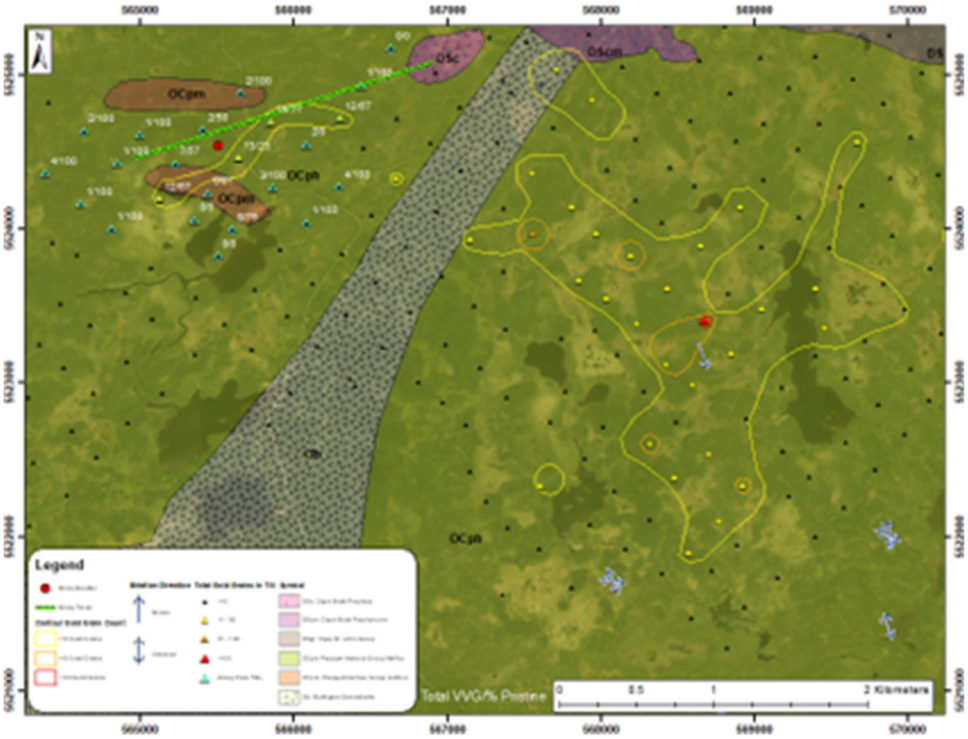


Figure 12. *1989/90 Corona / ODM regional till survey results.*

length both to the east and west of the road. Soils gave gold values up to 700 ppb (background <5 ppb) over a conductive, VLF-EM Fraser Filter anomaly, the KT shear structure, consisting of altered / mineralized mafic and felsic units. Follow up exploration by **Connecticut Development** (1996-98) and **Silver Spruce** (SSE – 2009/10) defined 2, approximately 80 m long by up to 5 m wide, east-west trending, altered, mineralized, quartz veined and sheared boudins approximately 100 m apart to the east of the Gull Pond access road. SSE drilling gave values up to 4.2 g/t Au over 1.43 m including 9.96 g/t over 0.51m. No resource has been defined.

South Brook: Till data contouring in the central part of the survey area, using gold grain counts and calculated values, showed a gold grain in till anomaly up to 500 m wide extending 3 km to the SSE, from the southern contact of the NE trending QFP dike. Three ENE trending apophyses of anomalous values, generally parallel to the 045° ice direction, extended 500 m from the main anomaly which had a sharp, but curvilinear, western boundary. The anomaly shape suggested that it represented three separate source areas along the western edge with the apophyses representing the down-ice flow to the ENE.

Follow up exploration, by ODM for Krinor and optionors, was carried out four different times over 20 years, in 1996 by **Connecticut Development**, in 2005 by **Krinor Resources**, from 2006

to 2007 by **Springbok / Ranger Ridge** and in 2009/10 by **Silver Spruce**. The 1995/96 exploration infilled parts of the anomalous till area but didn't help to define the source area with **Connecticut** subsequently dropping the option. The 2005 exploration by **Krinor** consisted of trenching in seven of the higher Au in grains areas on the presumed ENE ice direction in the possible source areas. It again added little to help define the source area. In 2006 three trenches tested the SW ends of the presumed ENE ice flow direction for **Ranger Ridge**. No gold mineralization was found however striations trending 340/160 degrees were located in outcrop in Trench 10, and given this ice direction, the first noted in the area, the Au source was presumed to be up-ice at the northern end of the anomaly, on the south side of the QFP dike. Follow up in 2007 consisted of excavator basal till sampling at 50 m centres which defined a strong Au in gold grain anomaly, with very high pristine gold grain counts, along the contact of the QFP dike in altered (chloritized) PHG mafic volcanics. Selected gold grain counts were up to 1360 with 1330 pristine (98%) giving a calculated value of 5546 ppb (RST-07-23) and 203, with 127 pristine (63%), with a calculated value of 10,364 ppb (RST-07-11). The host unit for the gold mineralization is a chlorite schist / altered mafic volcanic along the sheared contact with the QFP dike. **Ranger Ridge** dropped the option in 2008 without any follow up and **Silver Spruce** optioned the property in 2008/09 and drilled the assumed source area of the Au in tills in 2009/10 discovering and partially defining the South Brook (SB)

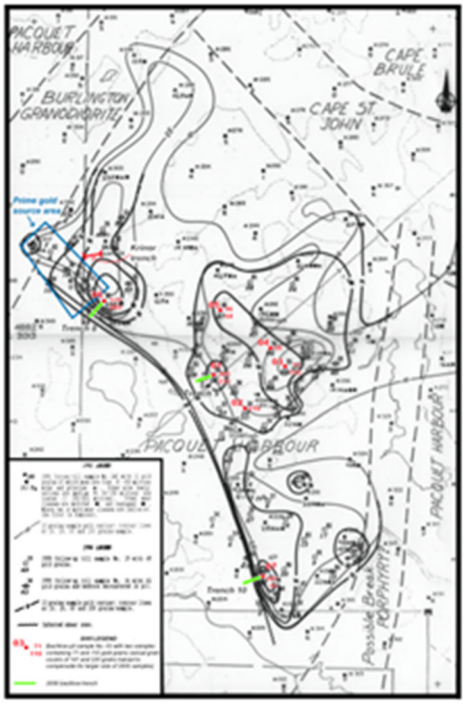


Figure 13. *RS regional till follow-up – 1996 to 2007.*

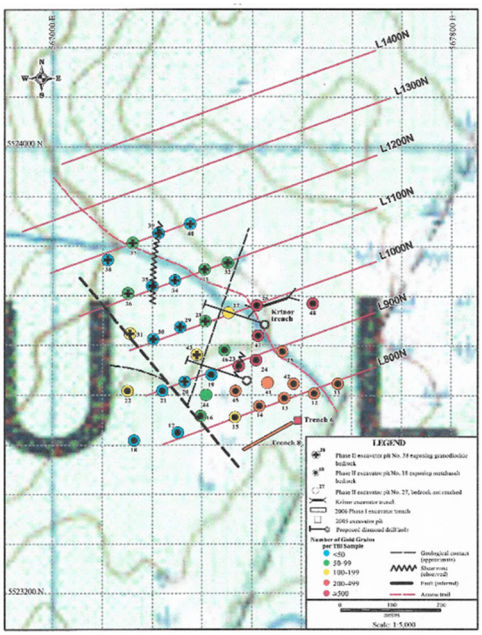


Figure 14. *SB area – 2007 detailed till survey.*

Au zone. Au intersections include: 1.4 g/t / 17.5 m including 10 g/t over 0.7 m and 3.5 g/t / 3 m incl 6.2 g/t / 1.5 m. No resource has been defined. **Silver Spruce** dropped the option in 2012 and today **Krinor** retains a single claim over the main portion of the Au mineralization.

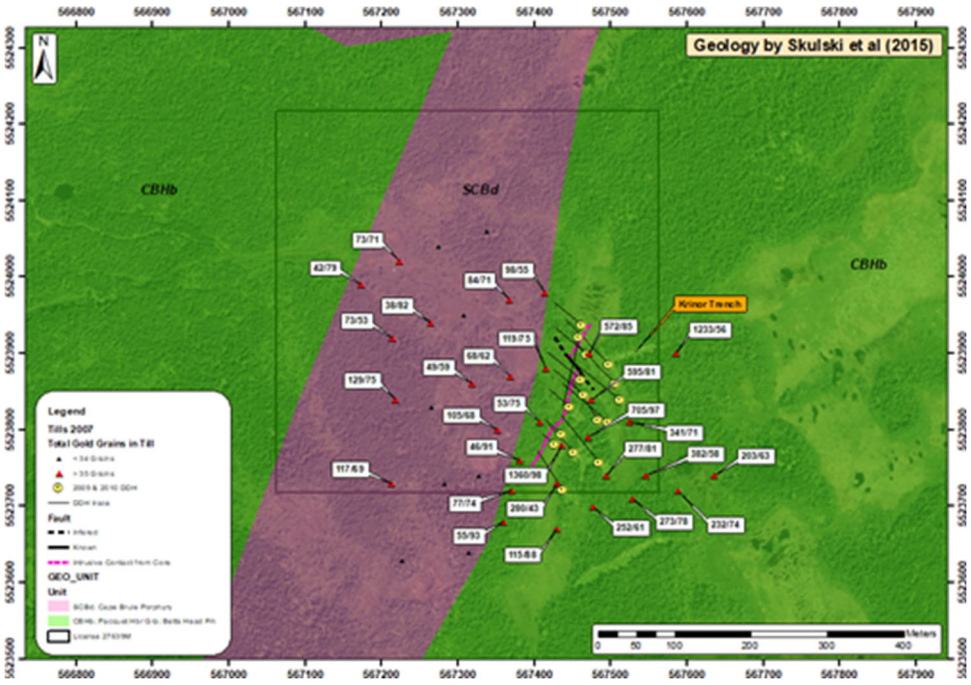


Figure 15. *SB Compilation – detailed tills / DDH.*

Area 3 – Brass Buckle Trend (BBT) Structure

Location

The Krinor BBT property consists of 34 claims extending in a NE direction covering the BBT fault structure. The claims are surrounded to the NW, SE and SW by Firefly Metals claims.

Geology

Mafic volcanics and intrusives of the PHG are in contact in the NE with the CBP QFP intrusive and the overlying CSG crystal lithic tuffs. The PHG is cut by a 20–25 m + QFP dike which extends along the BBT from the CBP and other, parallel to subparallel, felsic dikes? field termed quartz porphyries (QP) which are fine grained and variably altered by white micas (phengite to muscovite).

Ice Direction

Glacial straie are lacking however it appears that ice directions are: 1st SSE at 160°, 2nd a weaker NE trend.

Mineralization

Gold mineralization is found in all units on the property (Fig. 17) The main showings, all discovered by geochemistry (soils) and prospecting follow up (from North to South along the BBT trend) are:

660 – a sulphidized (py) zone in the basal, magnetite rich portion, of the CSJ, with a 4 m channel at 1 g/t Au. It lies on the NE extension of the BBT;

263 – Au associated with pyrite as euhedral crystals in altered (green) CBP along the strike of the BBT structure

Brass Buckle – a 25m long, 20–30 cm wide, quartz/pyrite vein at the contact between QP and mafic volcanics to the south of the BBT. Au values are in the 200–300 g/t range w/ anomalous Te.

BBT – Au in a brecciated / silicified mafic volcanic in contact with QP with values to ??

Erratic – narrow (few cms) quartz/pyrite veins with grab sample values up to 4 g/t in a QP outcrop intruding PHG to the south of the BBT;

BP – altered PHG mv o/c w/ diss / ff magnetite – 2 g/t Au, 22 g/t Ag, 0.4% Cu lying in, or near, the south side of the BBT;

Corona – a 5 cm quartz/pyrite vein in QP to the south of the BBT. Grabs to 15 g/t Au

Skidder Pond – diss. py / mt in the QFP dike to the SW of Skidder pond. Grabs to 1.5 g/t.

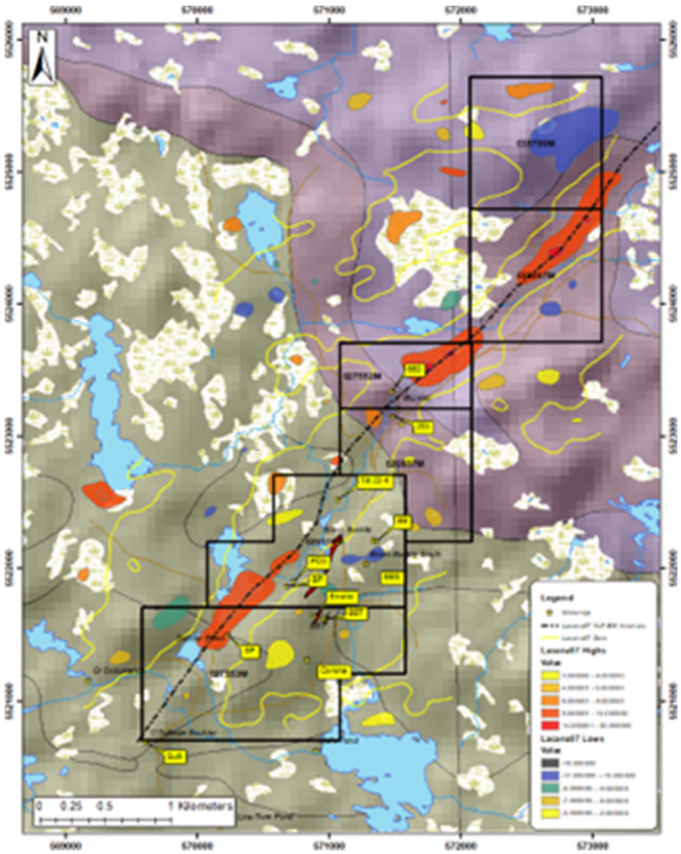


Figure 16. *BBT area geology / structure / Au showing.*

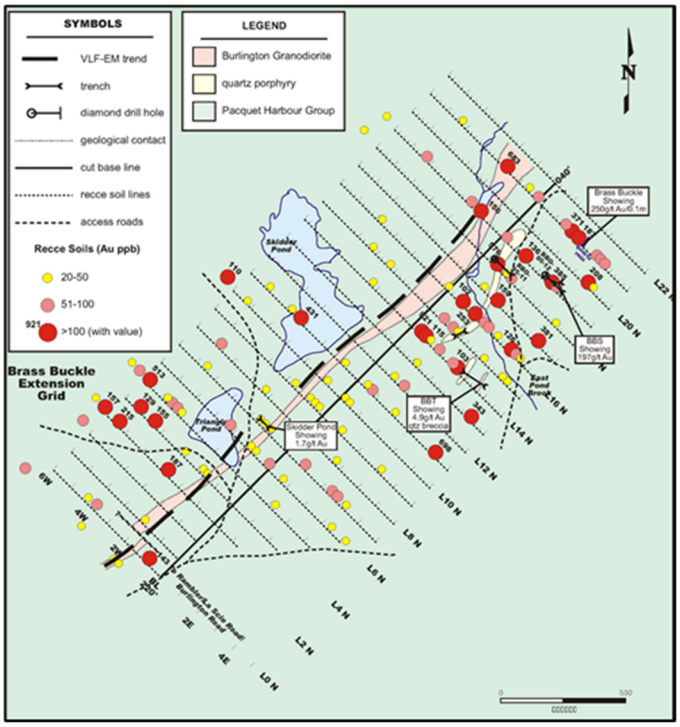


Figure 17. *BBT grid – historical Au soil results.*

Exploration

Companies including: **Lacana / Corona** 1987-1992; **Major General** 1995; **Connecticut Development** 1996-98; **Ranger Ridge** 2003-2006, **Silver Spruce** 2009-2012; Prospectors and associated companies such as Krinor Resources.

Exploration has been generally continuous since 1986 and has included: prospecting, gridding (cut lines), geological mapping, geochemistry (soils, tills), trenching and diamond drilling (13 ddh). Drilling / trenching has not tested any targets along the BBT except for the trench that exposed the 660 showing in the CSJ. Geochemistry has defined significant grid soil anomalies in, and to the south of, the BBT with trenching exposing the Erratic and Corona showings and grid prospecting resulting in the discovery of the 660 in CSJ, 263 in CBP, Brass Buckle in PHG, BBS in PHG, BBT in PHG/QP, BP in PHG and Skidder Pond in QFP. The first till sampling was carried out by ODM for Corona as a test for the RS area in 1989 (Fig. 19). It was both a regional and detailed survey taking widely spaced samples to the northwest of Skidder Pond and tightly spaced samples up ice in a NE direction of the BB and 660 showings. The BB sampling gave two anomalous samples of 15 grains, 15 pristine (100%), 104 grains, 86 pristine (83%) whereas the 660 samples were all non anomalous.

The regional sampling gave 3 anomalous values (# grns/# pristine grains (% pristine) of 17/11 (65%),18/9 (50%) and 25/6 (24%) grains on the road extending towards the major till anomaly

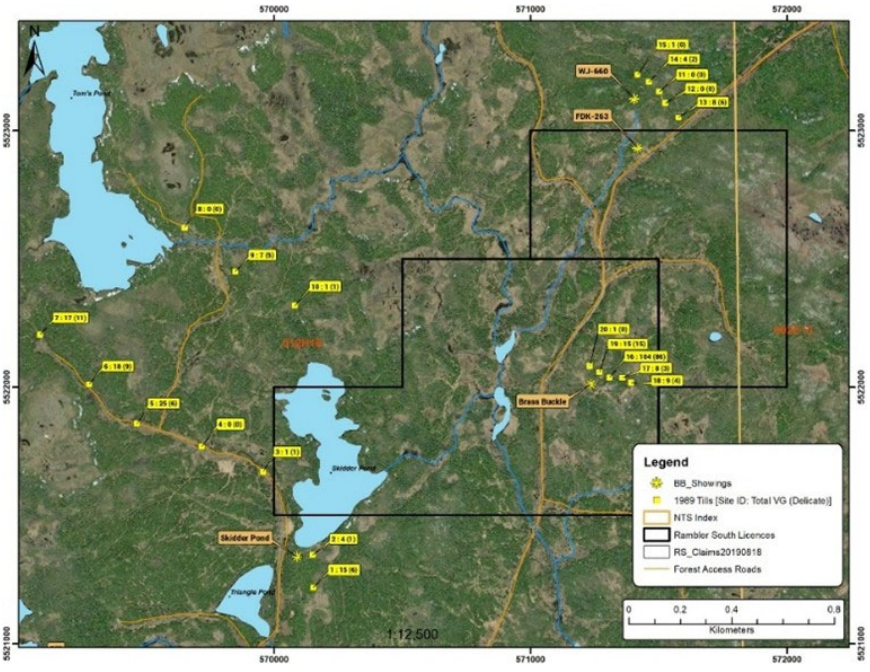


Figure 18. *ODM 1989 – Brass Buckle area test till survey.*

sourced at the SB gold zone with the # of pristine grains declining towards the SSE along the 160° ice direction trend.

In 2019 after much exploration, most to the south of the BBT structure, with money tight and no new targets, although the high Au soil geochemistry had not been explained, further exploration/evaluation was becoming difficult to promote. Till sampling, not done in the area since 1989, started in 2019 with 6 samples along / near the road. Results showed significant gold grain values with good pristineness in 3 areas (Fig. 20): T19-1 (37) and T19-2 (107) to the west of the

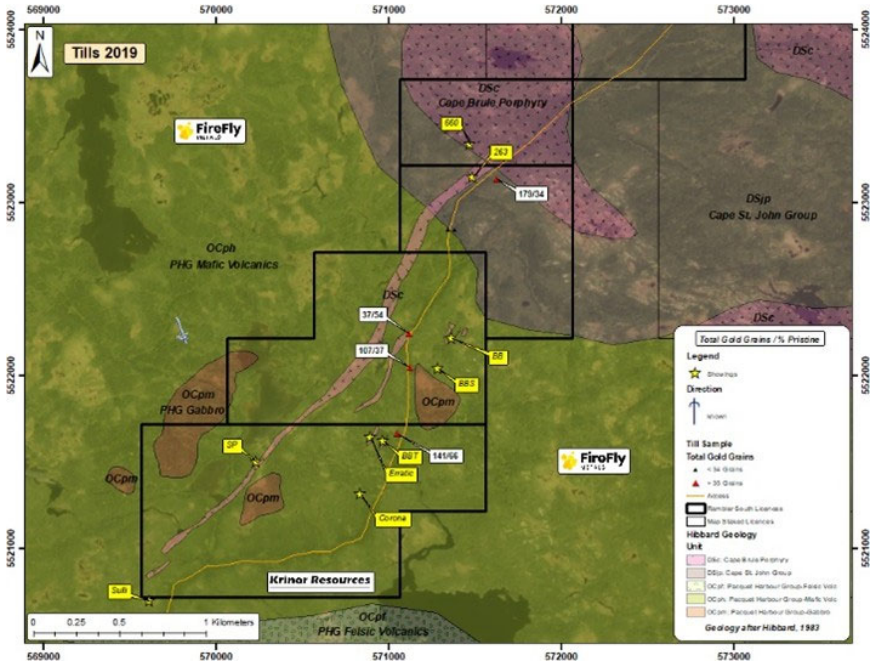


Figure 19. *Till sample results – 2019.*

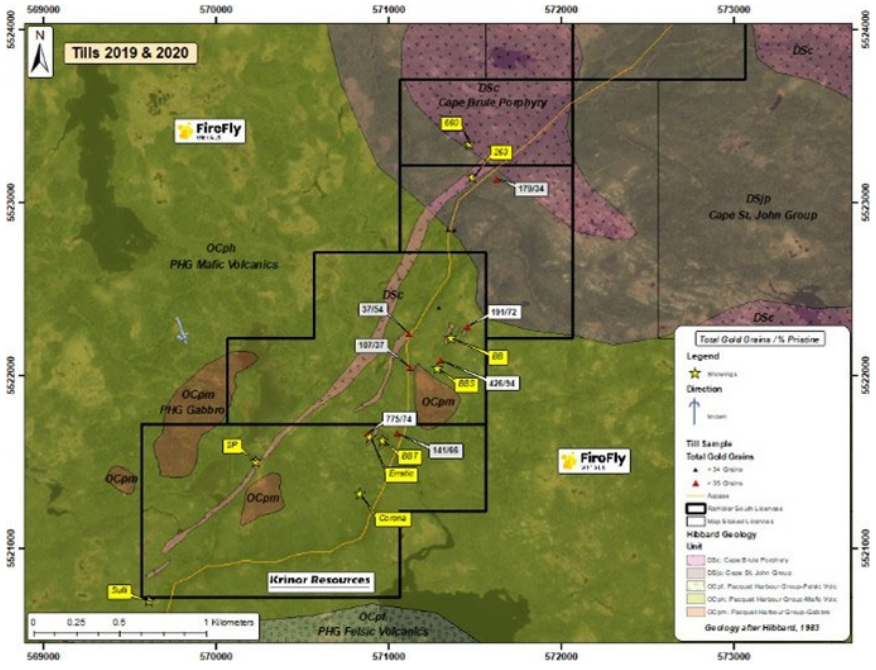


Figure 20. *Till sample results – 2019–2020.*

BB and BBS showings; T19-5 (179 grains, 34% pristine) to the east of the road and the 263 showing, to the south of the 660 showing; and T19-6 (141 grains, 66% pristine), to the west of the road, to the east of the BBT and Erratic showings.

Four follow up tills in 2020 gave 3 highly anomalous gold grain samples: 2 in the BB / BBS area to the south of the road T20-1 (426, 94% pristine), T20-2 (191, 72% pristine) and T20-4 (775, 74% pristine) to the west of the road in the Erratic showing area but up ice of it at the 160° ice direction. The two samples to the southeast of the road are most likely related to the NE ice direction and the BB/BBS showings however the one to the west indicates a source area to the NNW, along the BBT structure.

Sixteen tills were taken in 2021 to better define the source area for the Au grains to the northwest of the road. Four significant gold in grain values were located: T21-6 – 83, 80% pristine; T21-7 – 502, 91% pristine; T21-12 – 176, 64% pristine; and T21-16 – 88, 59% pristine. Tills 21-6 and 7 with very strong pristineness (at 80 and 91%) were up ice of the 775 grains Till 20-4. Noting these results Stu Averill of ODM said to go 50 m up ice at 340°, dig down and we would get gold. We did and we did – the BP showing outcrop was located. It is a narrow 15-20 cm vein that grades up to 2 g/t Au, 22 g/t Ag and 0.4% Cu, the only Au showing in this part of the BBT. Till 21-12 with 64% pristine also indicates a source along the BBT, along strike to the NE from the BP mineralization.

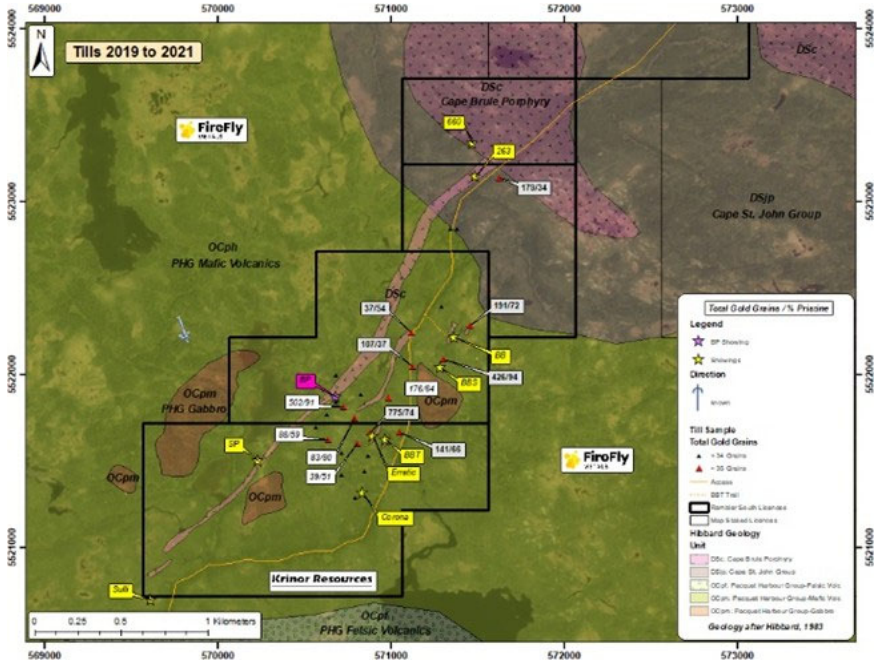


Figure 21. *Till sample results – 2019–2021.*

Till sampling in 2022 was targeted at the BBT to the NE testing down ice (at 160°) of the presumed location of the structure. One significant value T22-4 (302 grains, 80% pristine) was located just to the south of the BBT. The QFP dike is 20 m to the north of the sample, approximately 700 m to the NE of the BP showing. Strong, soft, alteration was noted in the sample pit at depth – it was not identified.

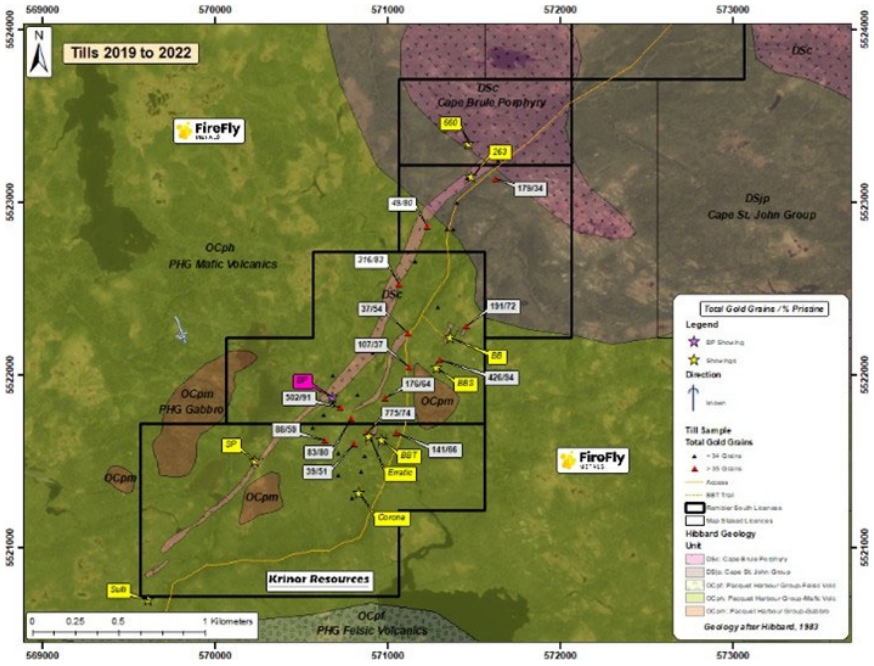


Figure 22. *Till sample results – 2019–2022.*

No trenching or diamond drilling has tested the BBT with only 1 DDH, by Major General in 1995 on the south margin, drilling away from the structure, on the bog just west of the road and to the north of the BB showing. This hole collared in, and intersected, 9.9 m of a phengitic / muscovitic altered QP, with no gold values, that can be traced to the north to the CBP/CSJ contact. Similar incipient to intense alteration, demonstrating very strong fluid flow probably related to the BBT structure, is noted in other areas of the BBT property.

The Au geochemistry of the area, both in soils and tills, indicates that the BBT structure and associated splays are the probable source area of the gold grains in the tills. The BP showing, the only gold mineralization (2 g/t) found to date is associated with minor copper (0.4%) and gives anomalous Ag values (22 g/t). It is in an altered / chloritized mafic volcanic with fine disseminated and fracture filling magnetite, pyrite, tourmaline and tungsten (scheelite).

An IP geophysical survey by **Major General** in 1993 (Fig. 23), which covered part of the same area, shows a chargeability anomaly extending from the BBT structure generally along a QP unit over the Erratic and Corona showings – both quartz/pyrite veining with associated Au values. Airborne EM / magnetic geophysical surveys by **Firefly Metals** in 2024 and 2025 (Fig. 24), over both Rambler South properties, show strong linear magnetic anomalies along the BBT structure from the area of the BP showing to the CBP/CSJ contact.

None of the geophysical targets have been tested by either trenching or drilling.

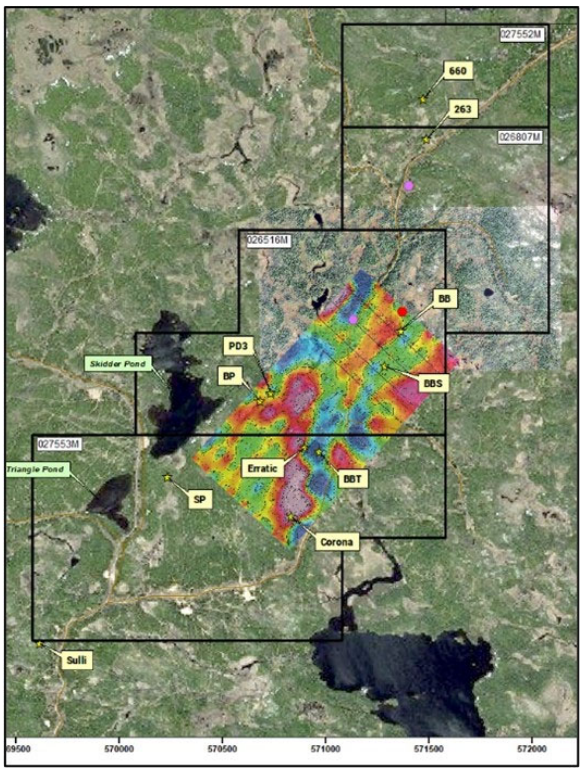


Figure 23. *Major General Resources IP chargeability – 1993.*

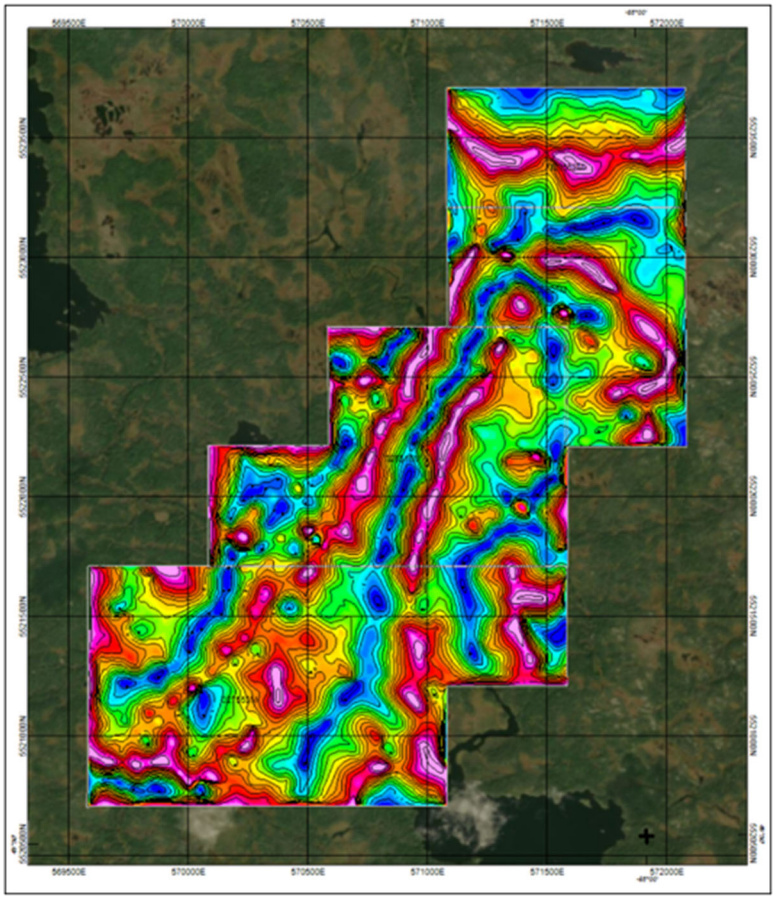


Figure 24. *Firefly / Novatem magnetic survey – 2025. (TMI-TDR – Contours0.2 radians, 1.0 radians).*

Acknowledgments

Mike Regular, Dylan Abbott, Ean Finch, Robert Hearst, **GSNL personnel** – Nicolas Gomez; Heather Campbell, Sarah Hashmi, Greg Sparkes; **ODM personnel** – Don Holmes, Stu Averill, Mike Crawford, Mike Michaud, Dave Hozjan.

References

Averill, S.A., 1992: "Rambler South till samples". Unpublished letter report prepared by ODM for Corona Corporation.

Averill, S.A., 1996: Follow-up heavy mineral till geochemistry survey for gold on Corona Anomalies 1 and 2, Rambler South Property, Baie Verte Peninsula, Newfoundland. Unpublished report by ODM for Connecticut Development Corporation, March 1996.

Averill, S.A., 2005: Significance of gold grain counts in June 2005 backhoe trenches, Rambler South property, Baie Verte, Newfoundland". Unpublished report by ODM prepared for Krinor Resources Inc.

Averill, S.A. and Holmes, D.R.S., 2006: Till sampling for gold grains by excavator trenching – procedures and results, Rambler South Property, Baie Verte Peninsula, NL. Unpublished report by Overburden Drilling Management for Springbok Resources Inc., January 11, 2007.

Averill, S.A. and Holmes, D.R.S., 2007: Till sampling for gold grains in excavator pits – Phase II: procedures and results, Rambler South Property, Baie Verte Peninsula, Newfoundland. Unpublished report by Overburden Drilling Management (ODM) for Ranger Ridge Resources, Sept. 28, 2007.

Brushett, D., 2012: Till geochemistry of northeast Newfoundland (NTS map areas 2C/13, 2D/15, 2D/16, 2E/01, 2E/08, 2F/04 and 2F/05). Government of Newfoundland and Labrador, Department of Natural Resources, Geological Survey, Open File NFLD/3174, 161 pages.

Campbell, H. and Lachance, N., 2026: Boulder tracing and terrestrial cosmogenic sampling in north-central Newfoundland. *In* Current Research. Government of Newfoundland and Labrador, Department of Energy and Mines, Geological Survey, Report 26-1, pages 139-164.

Campbell, H.E., Organ, J.S. and Conliffe, J., 2025: Fine-fraction indicator mineralogy in tills overlying mineralization from northeastern and southwestern Newfoundland: Implications for gold and critical-mineral exploration. *In* Current Research. Government of Newfoundland and Labrador, Department of Industry, Energy and Technology Geological Survey, Report 25-1, pages 223-247.

Delazzer, A., Dimmell, P.M. and Averill, S., 2010: First, fourth, fifth, sixth, eighth, ninth, tenth, eleventh, seventeenth and eighteenth year assessment report on prospecting and geochemical, trenching and diamond drilling exploration for licences 6979M, 10101M, 10186M, 10235M-10237M, 10266M, 12150M-12151M, 16624M and 16626M-16627M on claims in the South Brook area, on the Baie Verte Peninsula, NL; 12 H/16; for Krinor Resources Inc., Silver Spruce Resources Inc., Dimmell, P., Hillier, L. Newfoundland and Labrador Geological Survey, Assessment File 12H/16/2130, 219 pages.

Dimmell, P.M., 1998: First, second, third and fourth year assessment report on geological, geochemical and geophysical exploration for licence 4335 on claim block 8066, licence 4342 on claim block 8064, licence 4562 on claim block 8068 and licence 4723 on claim 16335 in the Big Rambler Pond area, on the Baie Verte Peninsula, NL.; Connecticut Development Corp., Krinor Resources Inc. Newfoundland and Labrador Geological Survey, Assessment File 012H/16/1533, 68 pages.

Dimmell, P.M., 1998: Third, fourth and fifth year assessment report on geochemical and geophysical exploration for licence 4335 on claim block 8066, licence 4342 on claim block 8064 and licence 4562 on claim block 8068 in the Big Rambler Pond area, on the Baie Verte Peninsula, NL.; Connecticut Development Corp., Krinor Resources Inc. Newfoundland and Labrador Geological Survey, Assessment File 012H/16/1425, 80 pages.

Dimmell, P.M., 2009: First, third, fourth, fifth, sixth, eighth, ninth, tenth, sixteenth and seventeenth year assessment report on prospecting and geochemical and diamond drilling exploration for licences 6979M, 10101M, 10186M, 10235M-10237M, 10266M, 12150M-12151M, 16624M and 16626M-16627M on claims in the South Brook area, on the Baie Verte Peninsula, NL.; 12 H/16, for Silver Spruce Resources Inc., Dimmell, P.M, Northeast Exploration Services, Krinor Resources Inc. Newfoundland and Labrador Geological Survey, Assessment File 12H/16/2026, 129 pages.

Dimmell, P.M. and Averill, S.A., 1996: Second year assessment report on geochemical exploration for licence 4335 on claim block 8066, licence 4341 on claim block 8065 and licence 4342 on claim block 8064 in the Gull Pond area, on the Baie Verte Peninsula; Krinor Resources Inc., Connecticut Development Corp. Newfoundland and Labrador Geological Survey, Assessment File 012H/16/1544.

Dimmell, P.M. and Mersereau, T.G., 1998: First year assessment report on geochemical and geophysical exploration for licence 4562 on claim block 8068 in the Rambler Brook area, on the Baie Verte Peninsula, NL.; 12 H/16, for Connecticut Development Corp., Krinor Resources Inc. Newfoundland and Labrador Geological Survey, Assessment File 012H/16/1537, 34 pages.

Dimmell, P.M. and Regular, M., 2025: 2025 assessment / junior exploration assistance (JEA) report, Rambler South (RS) Properties, Licences 26516M, 27369M, 26807M, 27552M, 27553M, 38287M 38706M, 38857M, 38943M, Baie Verte Peninsula, NL., NTS 12 H/16/2 E/3 for Krinor Resources Inc., December 21, 2025.

Dimmell, P.M. and Scott, W.J., 1998: Second year supplementary, third and fourth year assessment report on geophysical and diamond drilling exploration licence 4249 on claim block 7856, licence 4335 on claim block 8066 and licence 4372 on claim block 7857 in the Big Rambler Pond area, on the Baie Verte Peninsula, NL. Newfoundland and Labrador Geological Survey, Assessment File 012H/16/1530, 100 pages.

Geological Survey of Newfoundland and Labrador (GSNL), 2024: "Till Geochemistry" Newfoundland and Labrador GeoScience Atlas OnLine. Government of Newfoundland and Labrador, Department of Energy and Mines, Geological Survey, last update: March 2024; https://geoatlas.gov.nl.ca/

Hibbard, J., 1983: Geology of the Baie Verte Peninsula, NF. Government of Newfoundland and Labrador, Department of Mines and Energy, Mineral Development Division, Memoir 2.

Hinchey, J.P., 1987: First year assessment report on geological, geochemical and geophysical exploration for licence 2877 on claim block 4669 in the Big Rambler Pond area on the Baie Verte Peninsula, NL; West Coast Ventures Ltd., Newfoundland and Labrador Geological Survey, Assessment File 012H/16/0989, 96 pages.

Hinchey, J.P., 1988: Second year assessment report on geochemical exploration for licence 2877 on claim block 4669 in the Big Rambler Pond area on the Baie Verte Peninsula; West Coast Ventures Ltd.; Newfoundland and Labrador Geological Survey, Assessment File 012H/16/1034, 30 pages.

Holmes, D.R.S. and Michaud, M.D.J., 2017: Report on November 2016 till sampling for gold, JBP Property, Newfoundland, for Palisade Resource Corp., Overburden Drilling Management Ltd. Ottawa, Ontario, Canada, January 16, 2017.

Liverman, D. and St. Croix, L., 1989: Quaternary geology of the Baie Verte Peninsula. *In* Current Research. Government of Newfoundland and Labrador, Department of Mines, Geological Survey, Report 89-1, pages 237-247.

Organ, J.S., 2022: Northwest Gander surficial mapping project: Preliminary investigations. *In* Current Research. Government of Newfoundland Labrador, Department of Industry, Energy and Technology Geological Survey, Report 22-1, pages 211-235.

Scott, S., 1994: Surficial geology and drift exploration of Comfort Cove-Newstead and Gander River map areas (NTS 2E/7 and 2E/2). *In* Current Research. Government of Newfoundland and Labrador, Department of Mines and Energy, Geological Survey Branch, Report 94-1, pages 29-42.

Reverse Engineering Indicator Mineral Surveys

Derek Wilton[1, 2] and Carol Seymour[3]
[1]College of the North Atlantic, 1 Prince Phillip Drive, St. John's, NL, A1C 5P7
[2]Dept. of Earth Sciences, Memorial University, 9 Arctic Avenue, St. John's, NL, A1B 3X5
[3]Altius Minerals Corporation, Suite 300, 53 Bond Street, St. John's, NL, A1B 3V7

Introduction

As well described in this short course, indicator mineral surveys have become a common exploration tool in Canadian till-covered regions (*cf.* Averill, 2011; McClenaghan *et al.*, 2000, 2017; McClenaghan, 2005, 2007, 2011). Standard procedures involve collection of 10–20 kg till samples, sieving into a range of grain sizes, preparation of a heavy mineral concentrate (HMC) from the 0.25–2.0 mm size fraction through gravity techniques ultimately involving heavy liquids (McClenaghan, 2011). The 0.25–2.0 mm grain size samples are optically examined with a binocular microscope and grains of specific "indicator" minerals are identified; so-called "traditional visual analysis" or TVA (Averill and Huneault, 2016). Positive identification of each mineral phase picked typically requires subsequent micro-analyses (*e.g.*, McClenaghan, 2011).

Since 2010, MUN–Altius have been developing analytical procedures that use automated scanning electron microscopy (MLA-SEM) to identify indicator minerals in till. The first use of the technique examined till and stream sediments for awaruite associated with ophiolitic rocks on the island of Newfoundland (Wilton and Winter, 2012). The survey led to the identification of awaruite in bedrock at Pipestone Pond (Piller, 2011, 2012) which is now a key component of First Atlantic Nickel's Pipestone exploration project in central Newfoundland.

In contrast to traditional grain-picking methodologies, the MLA technique allows the Energy Dispersive X-ray (EDX) component of the SEM to accurately identify and quantitatively define the abundance, association, and size of all minerals from a sample in an automated, systematic fashion (*cf.* Wilton and Winter, 2012; Wilton *et al.*, 2015, 2017a, b, 2021; McNeil *et al.*, 2020). Because sample material for the MLA analysis is mounted in polished epoxy pucks, grain interiors are essentially exposed and minute mineral phases are preserved for observation that might otherwise breakdown in normal weathering processes, thus providing a novel way to identify

important indicator minerals. Our preparation technique is not as complex, nor rigorous, as standard HMC techniques which involve heavy liquid and even magnetic susceptibility separations. Hence, some of the lighter minerals will be present in the HMC produced for our analytical technique; most likely as intergrowths with HMC minerals. Furthermore, we also analyse some of the non-HMC (*i.e.*, light mineral concentrate) mineral separates to make sure that any light indicator minerals were not missed.

The Project

This project had two main objectives, the first of which was the identification of mineralogical fingerprints for each of four different types of mineralization including (a) the Buchans volcanogenic massive sulphide mineralization in central Newfoundland, (b) the Moosehead orogenic lode gold prospect, also in central Newfoundland, (c) komatiite-hosted Ni–Cu–PGE mineralization in the Florence Lake Group of central Labrador, and (d) the Strange Lake REE deposit in northern Labrador (Fig. 1). For each deposit, samples of mineralized host rock and barren material was crushed to create "anthropogenic" till (AT), which in each case was evaluated using the MLA analytical techniques that had been successfully applied to regional till surveys. In the case of Strange Lake, the AT comprised coarse rejects from the crushing of deposit drill core for assay. Minerals that were robust enough to survive the initial crushing of the AT sample material were deemed to be potential "indicator minerals" for each deposit (*i.e.*, the crushing was somewhat analogous to natural erosion). Therefore, these minerals might provide a mineralogical fingerprint for each deposit type and could then be used to vector towards similar styles of mineralization buried beneath glacial overburden elsewhere.

Anthropogenically crushed whole rock material (bedrock and drill core) cannot duplicate thousands of years of weathering and km's of transport. But the act of disaggregating whole rock materiel can demonstrate how the rock might break, along which mineral faces, and which minerals would be destroyed in the crushing (and conversely which minerals would survive breakage). Physical disaggregation will also reveal what mineral intergrowths might survive breakdown into transport. The MLA technique essentially involves cutting cross-sections through minerals (*i.e.*, polishing the epoxy puck sample surface) and hence can reveal minute mineral inclusions that might be present within larger, more robust, host minerals. Though typical

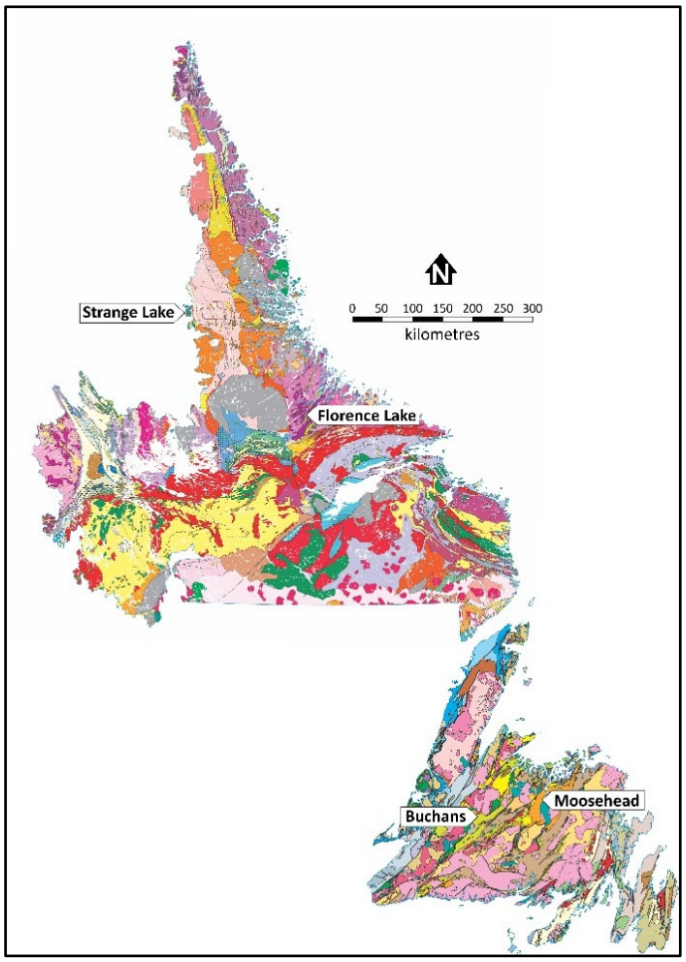


Figure 1. *Location of the mineral occurrences examined in this study; the Newfoundland geology base map is from Colman-Sadd* et al. *(2000) and the Labrador base map is from Wardle* et al. *(1997).*

petrographic analysis might reveal the nature and form of inclusions in larger minerals, some of the host minerals might actually break along crystallographic planes defined by the inclusions and thus not survive weathering. The crushing of whole rock material illustrates which inclusions might be observed in host minerals within a surficial sediment.

The study examined four completely different classes of mineral deposits. Based on standard indicator mineral surveys, certain minerals have been defined as being associated with particular mineral deposits (*e.g.*, Cr-diopside with kimberlite, gahnite with VMS deposits, and scheelite with skarns, *etc.*). This work attempted to define a greater range of indicator minerals for each deposit type, along with mineral intergrowth textures. The program was designed to define a matrix of indicator minerals that might be specific to each deposit type; standard indicator mineral surveys typically look for three to five indicator minerals in a given sample. The ultimate aim was to use the automated quantitative mineralogy capabilities of the MLA to parse through an AT sample and define whether, and what, indicator minerals of any mineral deposit type are present. To accomplish this, candidates for the indicator mineral fingerprints were identified as the most abundant minerals in the samples in addition to the known ore and associated minerals for each deposit type. The minerals identified for each of the mineralized samples were ranked in order of abundance. Using the list of minerals for each anthropogenic till sample enabled the identification of the most abundant minerals in each deposit type. A similar list of minerals from a barren rock from each deposit type was subtracted

from the list of mineralized samples to eliminate common minerals not associated with the mineralization.

The second objective was to determine whether the assemblage of indicator minerals from the crushed whole rock material (AT) at each prosect was detectable in till surrounding the four prospects. To achieve this, till samples were collected down-ice from each of the mineralization centers and analysed using the same MLA techniques to evaluate which indicator minerals in the AT were detectable outwards from each of the known mineral occurrences. For the Buchans-Moosehead-Florence Lake (BMFL) portions of the study, till sampling was restricted to areas within mineral claims that surrounded each deposit as held by Altius in 2016.

Samples

Six rock samples for AT processing were collected from Buchans consisting of massive lead-zinc-rich ore, massive copper-rich ore with lesser zinc and lead, stockwork mineralization consisting of chalcopyrite with quartz and chlorite, massive barite, quartz–sericite–pyrite altered host rock, and pyrite-quartz altered host rock. Four rock samples for AT were collected from near the Baikie prospect at Florence Lake and included two ultramafic rocks representing mineralization and alteration, an unmineralized granodiorite sample spatially associated with the Baikie prospect, and a mafic volcanic (country rock) sample with 5–10% sulphides. Two rock samples were collected in 2015 during mechanical trenching operations at Moosehead that consisted of heavily mineralized, auriferous quartz vein boulders (assay values of 328 g/t Au and 411 g/t Au, respectively). The Strange Lake coarse reject samples were collected in 2016 at the NL Energy and Mines core storage facility from plastic containers that contained material from hole SL-147.

Till sample collection for three of the project areas was completed in 2015. At Buchans, 180 till samples were collected by truck or ATV with an additional 33 samples collected using a helicopter in areas with poor access. A total of 94 till samples were collected from the Florence Lake project area *via* helicopter. In general, till was obtained from hand-dug, 0.25 to 1.0 m deep, pits. From the Moosehead property, a total of 102 till samples were collected, at a nominal spacing of 250 m, centered on the known gold showing; most samples were from hand-dug pits, but 25

were collected using an excavator during trenching operations at several sites on the property. The Strange Lake till samples were collected in 2016 from till exposed on the ground surface. Except for 25 samples at Moosehead, the till samples were collected using a steel shovel which was cleaned with water and allowed to dry between samples. The Strange Lake till samples were garnered with a steel trowel that was cleaned with paper towels between samples; there was insufficient water for washing.

Processing

All till and AT rock samples, except those from Strange Lake, were shipped from the project areas to the Altius processing facility in Mount Pearl, NL, where they were processed for analysis by MLA. The whole rocks were crushed and pulverized and then sieved into fractions. The till samples were dried and sieved into fractions as well. Partial Heavy Mineral Concentrate (HMC) separation for both the till and AT sieved fractions were conducted using a Wilfley Table. The desired HMC's were further subdivided by an eight-test tube riffler such that a final sample aliquot of *ca.* 0.3g was derived. For each sample, an aliquot was mounted in a plastic epoxy-filled puck which was polished (Fig. 2). The Strange Lake AT samples did not have an HMC derived and the Strange Lake till samples were sieved by hand without a mechanical sieve and were not separated on a Wifley table; preparation for both Strange Lake sets was completed at the CREAIT labs, Memorial University.

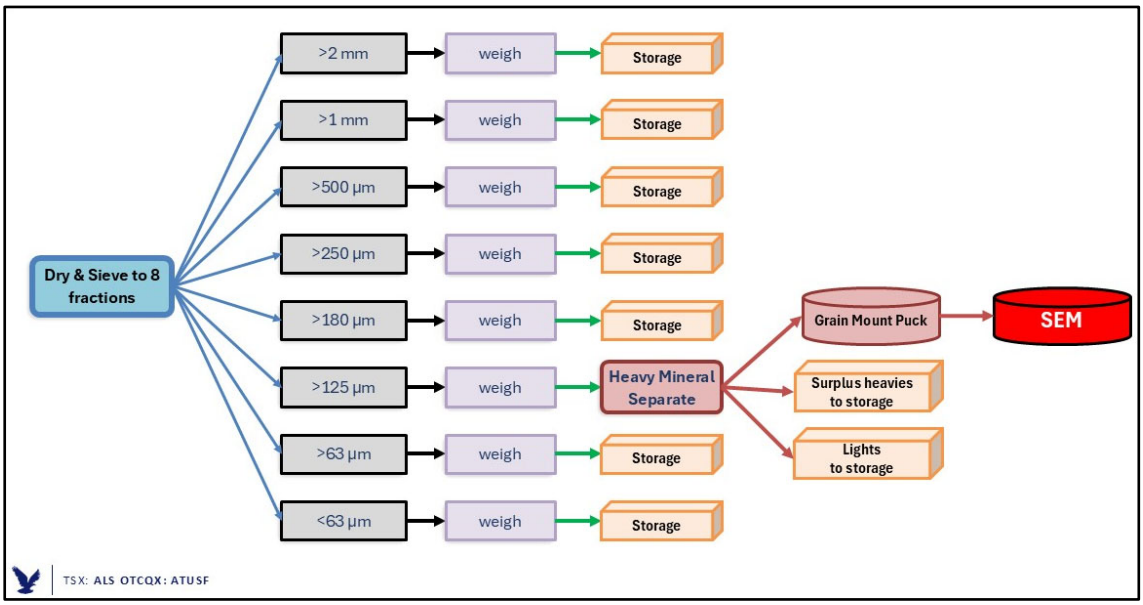


Figure 2. *Flowchart of the Altius–MUN till processing procedure.*

Wilton and Winter (2012) had determined that the 125–180 µm separate size was optimal for MLA analysis. If the grain size was smaller than 0.125 mm, the analyses took longer (30–50%) and the minerals were more difficult to definitively identify as the X-ray beam would be statistically more likely to miss a grain centroid and instead land on a grain boundary or crack/pit producing an unwanted result. If the grain size was larger than 180 µm, the number of particles that could be analyzed in a given grain mount decreased by 25 to 75% and the range of observable intergrowth textures decreased. All size fractions from each BMFL AT sample were analysed as were 10% of till samples for 250–500 µm, 180–250 µm, 125–180 µm and 63–125 µm size fractions. In both cases, the results confirmed that 125–180 µm was the ideal sample size for MLA work.

MLA-SEM Analysis

The pucks were transported to the CREAIT MLA-SEM laboratories, Memorial University, where they were graphite-coated and then analyzed using an FEI 400 MLA-SEM (*see* Wilton and Winter, 2012 and Wilton *et al.*, 2017a).

In experiments analyzing different mounts of a 125–180 µm fraction from a single till sample, the CREAIT MLA-SEM routinely identified 7000 to 20 000 particles in an individual grain mount; "particles" include larger mineral grains as well as inclusions within a larger grain. With standardization of the material amount mounted in a puck and analytical parameters, the range of particles typically identified in a grain mount for this study was 10 000 to 17 000. The analytical area was set as close to 25 mm in diameter as the grain mount allowed.

Detailed descriptions of the FEI 400 MLA instrument parameters are provided by Wilton *et al.* (2017b). The MLA software requires that the SEM be configured in back-scatter electron (BSE) image mode wherein minerals that contain denser elements produce brighter images. Essentially the MLA detects mineral particles in the grain mount based on variations in BSE grey scale and then analyses each particle. The particles can be inclusions, in many cases several inclusions, within a larger grain.

The SEM maps each polished grain mount in 'frames' per mount, typically 100–120, and the frame is the fundamental organizational template for the MLA technology. The software can produce a BSE map of all particles in a frame and a false-colour map of particles based on an assigned colour legend for each particle. The frames can be stitched together to provide a map of the entire grain mount analyzed. When queried the MLA can provide statistics for each sample puck including the number of grains of each mineral, the number of particles containing each mineral (a particle can contain more than one grain), the size of each mineral, and the weight and area %'s of each mineral compared to the whole. The particle counts were used to identify the most abundant phases in the BFML AT and till samples; area % was used for the Strange Lake samples.

In the BMFL AT samples no minerals were identified as being so highly unique or rare that they could serve as a definitive indicator mineral. In the Strange Lake AT and till samples, gittinsite ($CaZrSi_2O_7$) proved to be a unique diagnostic indicator mineral for the associated REE mineralization.

Error measurements for MLA analysis have been derived by Wilton (unpublished data) for six replicate samples of crushed drill core from the Strange Lake REE deposit. The six separates from hole SL-147 (135.64–145.42 m) were sieved and prepared in exactly the same manner as the till and AT samples from this study. Errors varied with respect to the different relative contents. Orthoclase, the most abundant mineral had a mean content of 27.52% with a Standard Deviation of 0.44 reflecting an error of ± 1.6% at 95%. Gittinsite, a mineral with intermediate concentration, had a mean of 1.39% with a Standard Deviation of 0.14 reflecting an error of ± 10.2% at 95%. Finally, apatite, a mineral with low concentrations, had a mean of 0.028% with a Standard Deviation of 0.0079 reflecting an error of ± 28.19% at 95%.

Indicator Mineral Fingerprints in AT samples and Till Samples

As the Buchans AT control samples were predominantly sulphide-bearing, the most common (and potentially best) indicator minerals were predominantly sulphide phases. Other diagnostic minerals were barite and some silicates. The simplest way of evaluating the MLA-SEM mineral data for the tills was to produce maps of 'key' indicator mineral abundances in the samples. The indicator minerals sphalerite, chalcopyrite, galena, and barite were selected for initial

interpretation of the mineral data because of their predominance in the Buchans deposits and their definition as part of the indicator mineral fingerprint. The MLA mineral abundances of these phases in till correspond to areas of known mineralization with a general dispersion in the down-ice direction indicating that the past-producing Buchans deposits, as well as other well documented occurrences, are detectable in the till profile (Figs. 3 and 4).

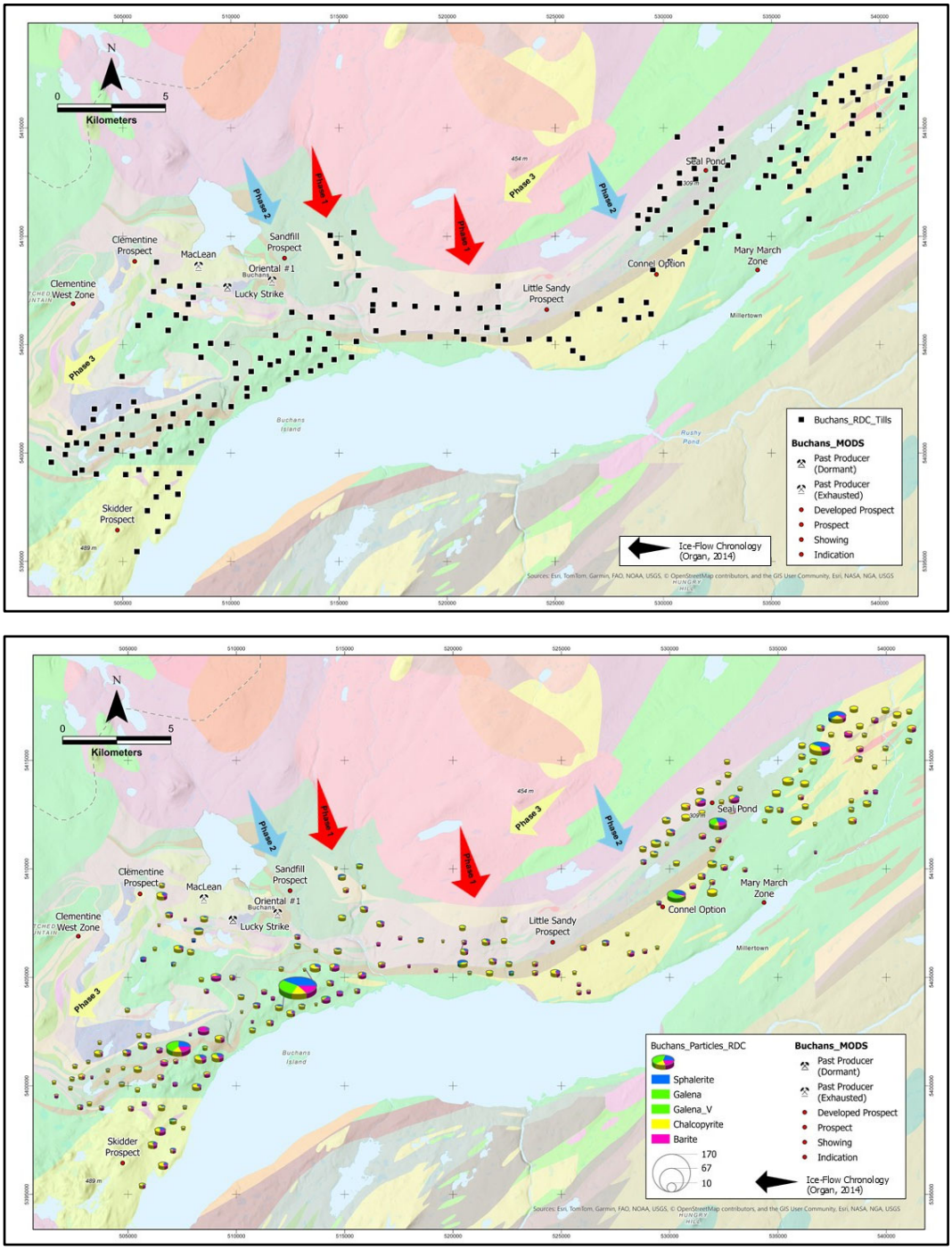


Figure 3. *A) Till sample locations in the Buchans region; B) Sulphide particle contents in the till samples as mapped by the MLA.*

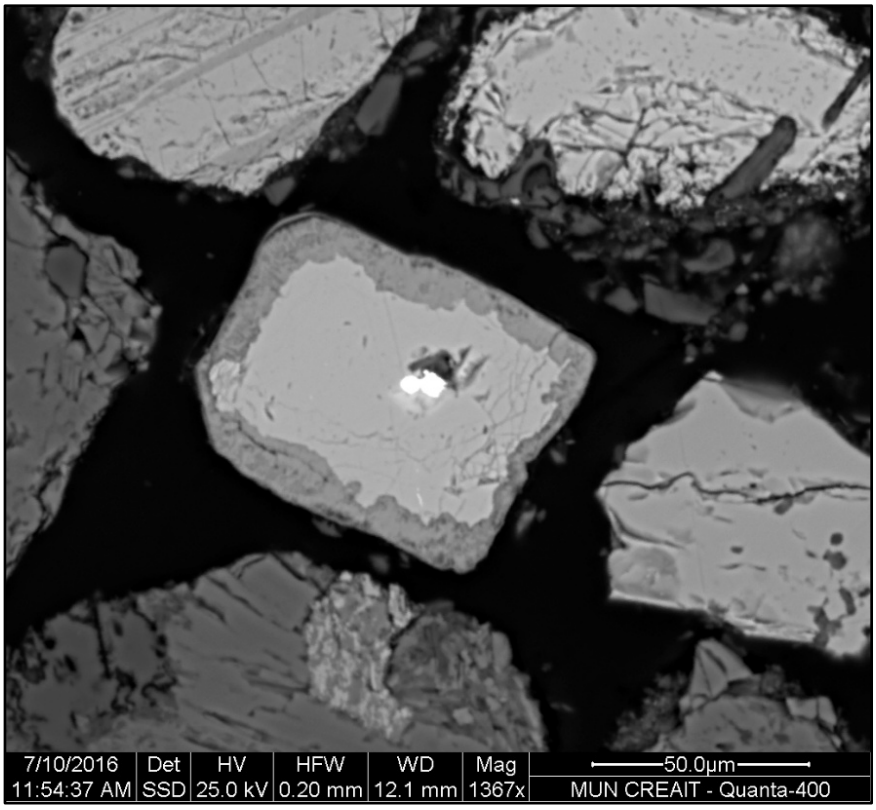


Figure 4. *Buchans till sample 7114 – BSE SEM of image galena (white) inclusion in pyrite grain with oxidized rim; note scale bar on lower right.*

In the Moosehead AT samples a variety of sulphide minerals, including Sb-bearing ones, along with some diagnostic non-sulphide phases, such as gold, fuchsite, and jarosite constituted key indicator minerals; non-diagnostic silicates and carbonates were also part of the assemblage. The abundance of AT indicator mineral fingerprints identified from the Moosehead occurrence in the till samples was likewise plotted on simple abundance maps. The abundance maps showed the distribution of each indicator mineral throughout the project area in relation to the known mineral occurrences. The absence of many of these minerals suggests that they did not survive in the till. For example, pyrite was not identified in the till samples, however, arsenian pyrite and oxidized pyrite were identified and form a well-defined northeast-trending anomaly along the area of known mineralization which seems to follow glacial dispersal trends (Figs. 5 and 6). Gold was notably absent from the minerals mapped by the MLA in the Moosehead till samples, but presents well in the anthropogenic samples. The reason for the absence of gold grains in the till is unknown and requires further research.

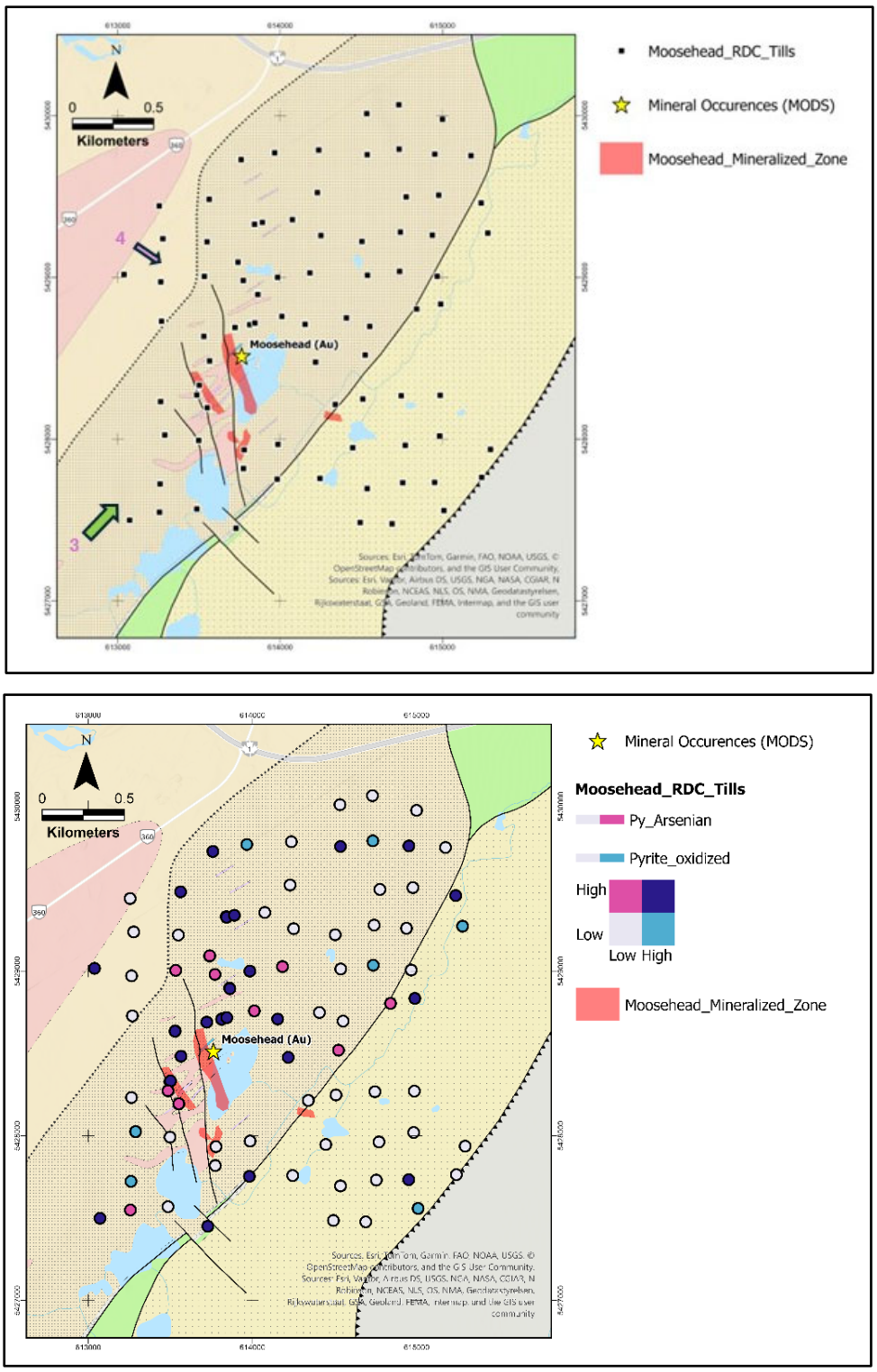


Figure 5. *A) Till sample locations in the Moosehead region; glacial directions from Campbell and Lachance (2026); B) Sulphide particle contents in the till samples as mapped by the MLA.*

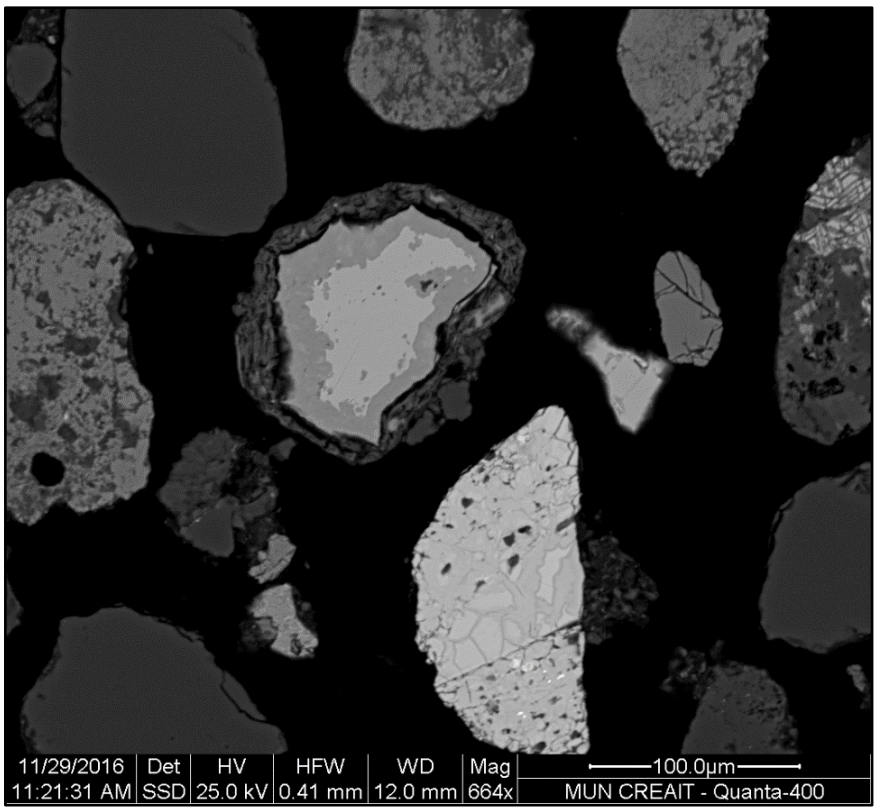


Figure 6. *Moosehead till sample 6702 – BSE SEM of image of oxidized pyrite grain with rim (upper) and altered zircon (lower); note scale bar on lower right.*

For the Florence Lake AT samples, the sulphide minerals pentlandite, pyrrhotite, pyrite, and chalcopyrite, all diagnostic of komatiitic nickel sulphide mineralization, were identified as key indicator minerals. Sulphide grain counts amongst the four main indicator minerals are generally dominated by pyrite, followed by pyrrhotite, chalcopyrite and pentlandite. When grain counts for chalcopyrite, pyrrhotite, and pentlandite are plotted together there is an anomaly in the northeastern part of the property, down-ice from the Boomerang, Baikie, DCP, and DCP Northeast showings (Fig. 7). When these sulphide grains were examined in detail, several of the samples contained sulphide grains with mineral associations and textures that are possibly indicative of a nickel sulphide-bearing system, for instance some pyrrhotite grains contained exsolved pentlandite (Fig. 8).

In 2008, during the MLA-SEM examination (Wilton and Thompson, unpub. data) of till and stream sediment samples from Vosiey's Bay on the Labrador coast, grains of feathery gittinsite intergrown with quartz were observed (Fig. 9). The only known location of gittinsite in Labrador is at the Strange Lake REE deposit, *ca.* 110 km to the southwest. Batterson and Taylor (2009) mapped a well-defined geochemical dispersion halo of anomalous Be, La, Pb, Nb, and Y contents down-ice from the Strange Lake deposit (SL) for up to 55 km. Altius personnel were interested in both the gittinsite discovery within surficial sediments and the MLA-SEM technology. From *ca.*

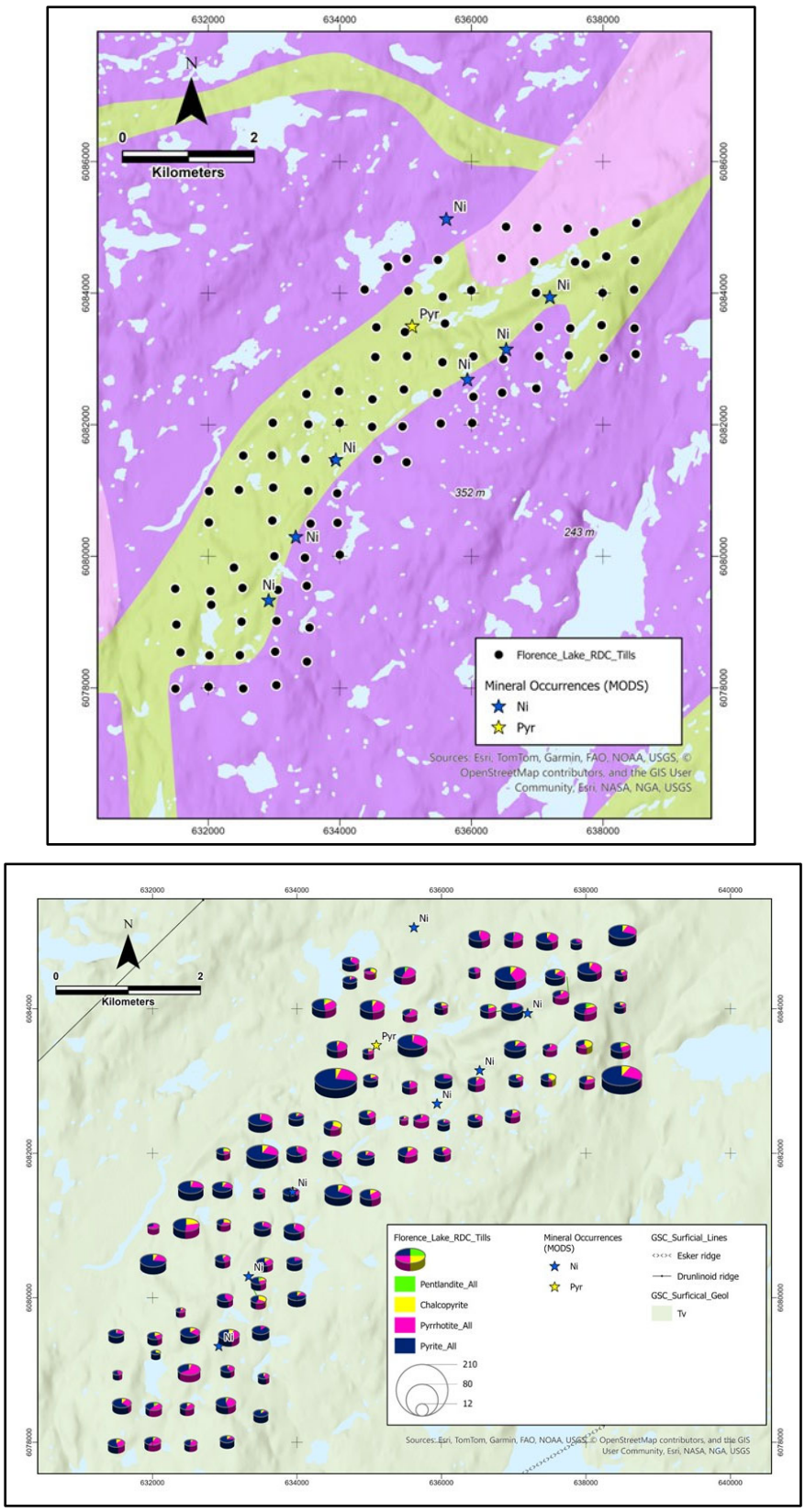


Figure 7. *A) Till sample locations in the Florence Lake (Baikie) region; B) Sulphide particle contents in the till samples as mapped by the MLA.*

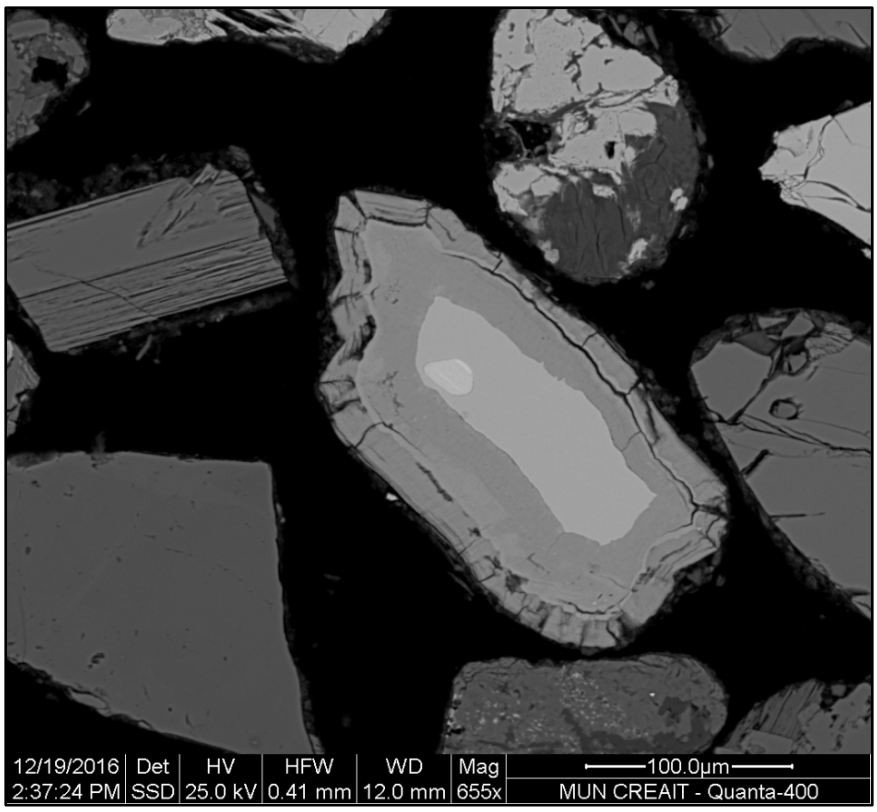


Figure 8. *Florence Lake till sample 6186 – BSE SEM of image of oxidized pyrite grain with pyrrhotite inclusion and exsolved pentlandite; note scale bar on lower right.*

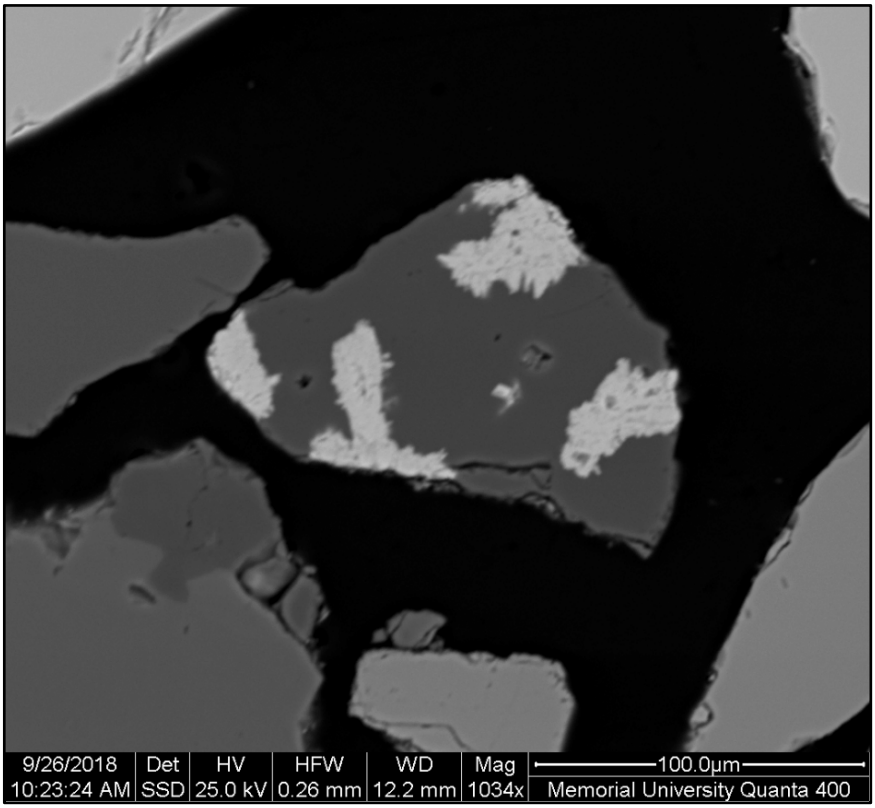


Figure 9. *Till sample VBT-007 from Voisey's Bay – BSE SEM of image of feathery gittinsite (white) intergrown with quartz (grey); note scale bar on lower right.*

2010–2014 Altius conducted regional till surveys across the regional trend as far Strange Lake (Fig. 10), encountering a band of tills with similar gittinsite–quartz grains in a single 100-km and up to 10-km wide corridor. Margol *et al.* (2015) identified the outflow from the SL deposit area as an ice-stream which corresponded with Batterson and Taylor's (2009) dispersal halo. McClenaghan *et al.* (2019) subsequently reported gittinsite from till samples down-ice in the ice-stream glacial dispersion train from SL.

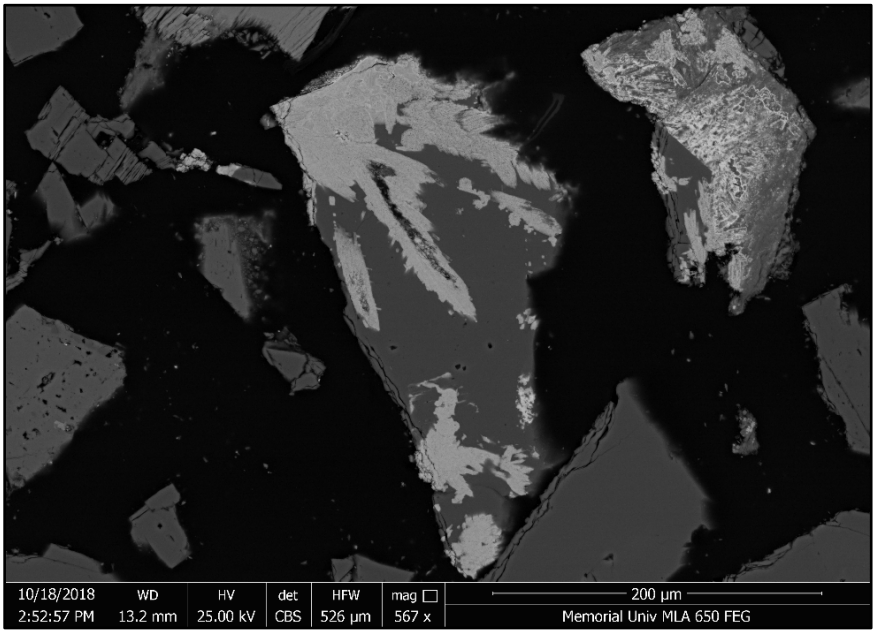


Figure 10. *Coarse reject (AT) sample from drill hole SL-147, 46.64 m – BSE SEM of image of feathery gittinsite (white) intergrown with quartz (grey); note scale bar on lower right.*

Baird (2018), Currie (2019), and Wilton (unpub. data) examined AT coarse rejects of SL core and found that gittinsite was present with the same feathery textures intergrown with quartz as observed in the Vosiey's Bay region and the Altius LIMS tills (Fig. 11). Currie (2019) completed LA ICP-MS analyses of REE contents in gittinsite grains from SL AT samples and the till near Voisey's Bay and found that the gittinsites from both areas had the same composition, suggesting a common source.

MLA analysis of exposed till samples down ice from SL were completed in 2022 to evaluate whether gittinsite grains were detectable between the LIMS sample grid lines. The analyses demonstrated that texturally similar gittinsite was present over the ice stream train and confirmed the elevated contents in the LIMS samples. Four esker samples paralleling the dispersal train from SL, however, were found to contain relatively much lower gittinsite contents.

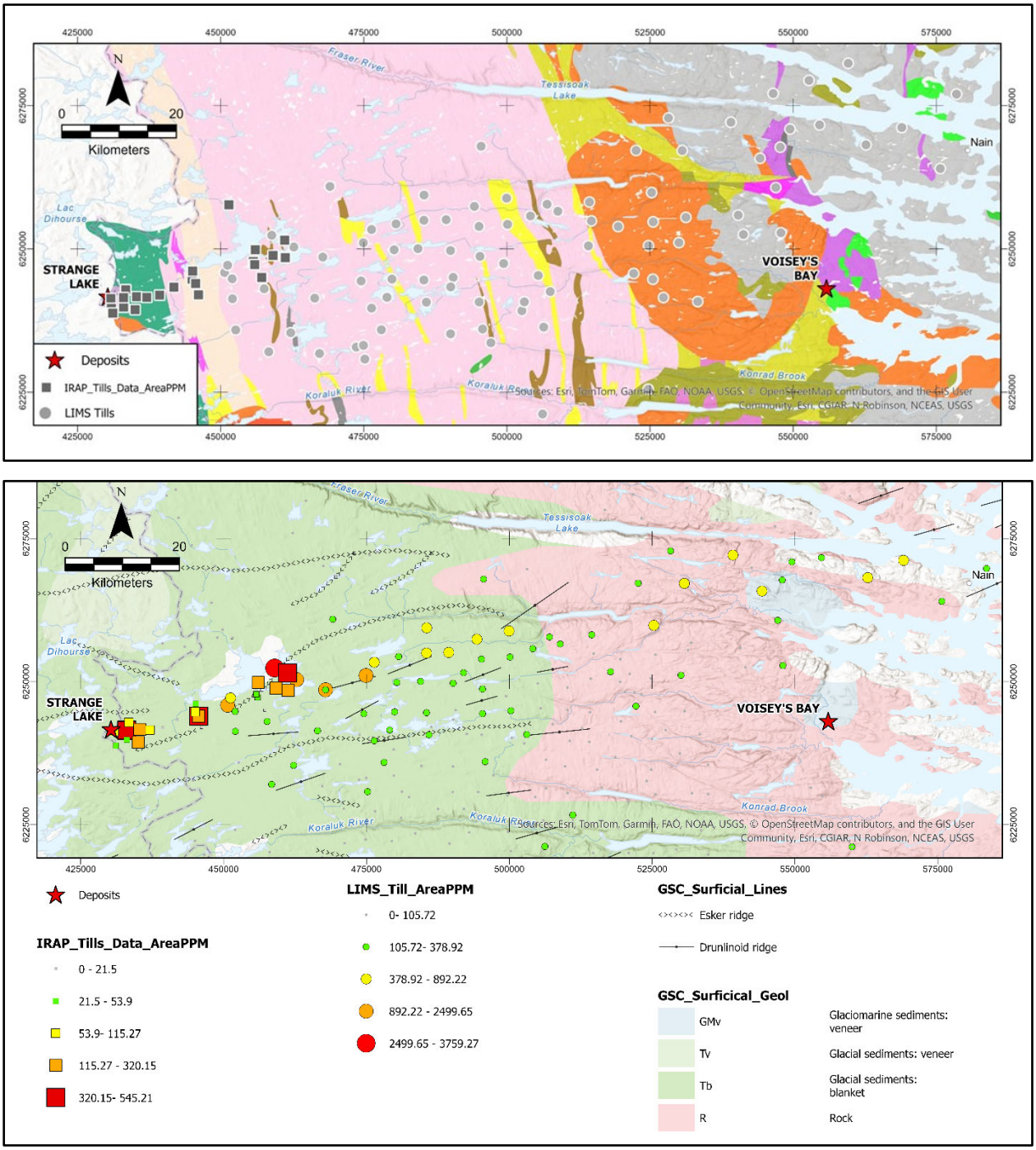


Figure 11. *A) Till sample locations from SL to Voisey's Bay; B) Gittinsite area % in till samples as mapped by MLA; note LIMS regional survey samples are round and the IRAP samples are square.*

Conclusions

The main objective of this study was to characterize an indicator mineral fingerprint for each of the four deposit types studied. The second objective was to determine whether the mineralogical fingerprint for each deposit type could be detected in till surrounding the relevant deposit and

whether till analysis by MLA-SEM techniques could provide advantages over conventional TVA and/or geochemical analyses of till samples.

Overall, the project produced results as originally planned. An indicator mineral fingerprint could be determined for each deposit based on the mineralization and altered host rocks associated with each deposit type. This mineralogical fingerprint consisted of the most abundant minerals that comprise the rock samples which survived crushing and generally excludes non-distinctive common rock-forming minerals (*e.g.*, quartz, feldspar, *etc.*). Many of the indicator minerals making up the mineralogical fingerprints were detected in the till and some even defined distinct anomalies down-ice from the known mineral occurrences. Some minerals, however, were not detected in the till samples, possibly due to many factors, in particular, the mineral was not sufficiently robust to survive in a dynamic till environment. One of the key indicator minerals for the Moosehead project, gold, was not detected in the till and the reason is at present unknown.

A significant advantage of the MLA-SEM technique is the capacity to observe relationships between key indicator minerals at a fine scale. For example, at Florence Lake it was possible to identify a single grain of pyrrhotite with exsolved pentlandite, a key indicator of a fertile nickel sulphide system. Such mineralogical relationships and textures would not normally be observed using conventional techniques. In other cases, indicator minerals could be observed as inclusions within more robust minerals, particularly in the case of sulphide phases; standard techniques can’t “see” inside grains.

Another advantage of this technique is the ability to customize the mineral library and filter the dataset to essentially "remove" minerals that might be "diluting" the indicator mineral(s) that are of interest. Sample preparation techniques are also simpler than other procedures and don’t involve labor-intensive steps such as heavy liquid separation.

Of the four deposits, only the Strange Lake example contained a unique indicator mineral phase, in this case gittinsite. This unique phase could be tracked in till over a transport distance of at least 110 km. Gittinsite itself is not a particularly robust mineral able to survive glacial transport, it is the intergrowth with quartz that allows the mineral to travel and be an indicator mineral.

Funding

The Buchans-Moosehead-Florence Lake (BMFL) portions of the study were funded by a research grant from the NL Research & Development Corporation (RDC) to Altius Minerals entitled "Developing Micro-Analytical Till Indicator Mineral Exploration Techniques for the Discovery of Hidden Ore Deposits in Glaciated Terrains". Field work and analyses for the BMFL project were completed in 2015–2017. The Strange Lake portion was funded by an RDC grant to the Nunatsiavut Government, Memorial University and Wilton entitled "A potential regional mineral exploration tool for Labrador: Correlating mineralogical and geochemical signatures of indicator minerals of the Strange Lake REE deposit". Field work was conducted in 2016, and MLA-SEM analyses were completed in 2022 through the assistance of an NRCan IRAP grant to Altius Minerals through CNA. Regional till surveys (LIMS) in the Strange Lake area had been conducted by Altius Minerals 2010–2015.

References

Averill, S.A., 2011: Viable indicator minerals in surficial sediments for two major base metal deposit types: Ni-Cu-PGE and porphyry Cu. Geochemistry: Exploration, Environment, Analysis, Volume 11, pages 279–291.

Averill, S.A. and Huneault, R.G., 2016: Basic indicator mineral math: Why visual analysis of the entire heavy mineral fraction of large sediment samples is required on indicator mineral exploration programs in glaciated terrains. Explore Number 172 – September.

Batterson, M.J. and Taylor, D., 2009: Geochemical re-analysis of till samples from the Strange Lake area, Labrador (NTS map sheets 14D/5 and 24A/8). Government of Newfoundland and Labrador, Department of Natural Resources, Geological Survey, Open File LAB/1479, 116 pages.

Colman-Sadd, S. P., Hayes, J. P. and Knight, I., 2000: Geology of the Island of Newfoundland (digital version of Map 90-01 with minor revisions). Government of Newfoundland and Labrador, Department of Mines and Energy, Geological Survey, Map 2000-30, scale 1:1 000 000.

Baird, E., 2018: Mineralogy of the Main Zone, Strange Lake REE deposit as determined from SEM-MLA analysis, Unpublished B.Sc. (Hons.) thesis, Memorial University, 101 pages.

Campbell, H. and Lachance, N., 2026: Boulder tracing and terrestrial cosmogenic sampling in north-central Newfoundland. Government of Newfoundland and Labrador, Department of Energy and Mines, Report 26-1, pages 139–164.

Currie, V., 2019: Evaluation of hercynite and gittinsite as indicator minerals, Voisey's Bay area, Labrador. Unpublished B.Sc. (Hons.) thesis, Memorial University of Newfoundland, 80 pages.

Margold, M., Stokes, C.R. and Clark, C.D., 2015: Ice streams in the Laurentide Ice Sheet: Identification, characteristics and comparison to modern ice sheets: Earth-Science Reviews, Volume 143, pages 117–146.

McClenaghan, M.B., 2005: Indicator mineral methods in mineral exploration. Geochemistry: Exploration, Environment, Analysis, Volume 5, pages 233–245.

McClenaghan, M.B., 2007: Till geochemistry and indicator mineral methods for exploration in glaciated terrain. Exploration 07 Workshop 2 Exploration Geochemistry: Basic Principles and Concepts.

McClenaghan, M.B, 2011: Overview of common processing methods for recovery of indicator minerals from sediment and bedrock in mineral exploration. Geochemistry: Exploration, Environment, Analysis, Volume 11, pages 265–278.

McClenaghan, M.B. and Paulen, R., 2017: Application of till mineralogy and geochemistry to mineral exploration. *In* Past Glacial Environments, 2nd Edition. *Edited by* J. Menzies and J.J.M. van der Meer. Elsevier, pages 685–791.

McClenaghan, M.B., Paulen, R.C. and Kjarsgaard, I.M., 2019: Rare metal indicator minerals in bedrock and till at the Strange Lake peralkaline complex, Québec and Labrador, Canada. Canadian Journal of Earth Sciences, Volume 56, pages 857–869.

McClenaghan, M.B., Paulen, R.C., Kjarsgaard, I.M. and Fortin, R., 2017: Rare earth element indicator minerals: An example from the Strange Lake deposit, Québec and Labrador, eastern Canada. Geological Survey of Canada, Open File 8345.

McClenaghan, M.B., Thorleifson, L.S. and Dilabio, R.N.W., 2000: Till geochemical and indicator mineral methods in mineral exploration. Ore Geology Reviews, Volume 16, pages 145–166.

McNeil, R.J., Williamson, M.-C. and Wilton, D.H.C., 2020: Geochemical, mineralogical, and indicator-mineral data for stream silt sediment, water, and heavy-mineral concentrates, Axel Heiberg Island, Nunavut (NTS 49-G, 59-H and 560-A). Geological Survey of Canada, Open File 8719, 29 pages.

Organ, J.S., 2014: Till geochemistry of the Red Indian Lake Basin (NTS map areas 12A/04, 5, 6, 7, 9, 10, 11, 15 and 16). Government of Newfoundland and Labrador, Department of Natural Resources, Geological Survey, Open File 012A/1572, 175 pages.

Paulen, R.C., Stokes, C.R., Fortin, R., Rice, J.M., Dube-Loubert, H. and McClenaghan, M.B., 2017: Dispersal trains produced by ice streams: An example from Strange Lake, Labrador, Canada. *In:* Exploration 17 - Proceedings of the Sixth Decennial International Conference on Mineral Exploration, Toronto, Canada, pages 871–875.

Piller, M., 2011: An examination of awaruite (Ni_3Fe) formation during serpentinization of the Pipestone Pond Ophiolitic Complex in the Atlantic Lake area, central Newfoundland. Unpublished B.Sc. (Hons.) thesis, Memorial University of Newfoundland, 72 pages.

Piller, M.P., Wilton, D.H.C. and Winter, L., 2012: An examination of awaruite (Ni_3Fe) formation during serpentinization of the Pipestone Pond Complex in the Atlantic Lake area, central Newfoundland. St. John's 2012 GAC/MAC program with abstracts.

Wardle, R.J., Gower, C.F., Ryan, B., Nunn, G.A.G., James, D.T. and Kerr, A., 1997: Geological map of Labrador; 1:1 million scale. Government of Newfoundland and Labrador, Department of Mines and Energy, Geological Survey, Map 97-07.

Wilton, D.H.C., Thompson, G.M. and Evans-Lamswood, D., 2015: MLA-SEM examination of sulphide mineral breakdown and preservation in till, Voisey's Bay Ni-Cu-Co deposit, Labrador - The distribution and quantitative mineralogy of weathered sulphide phases in a transect from massive sulphide through gossanous regolith to till cover. *In* Environmental and Economic Significance of Gossans. *Edited by* M.-C. Williamson. Geological Survey of Canada, Open File 7718, pages 31–41.

Wilton, D.H.C., Thompson, G.M. and Evans-Lamswood, D., 2021: MLA-SEM characterization of sulphide weathering, erosion, and transport at the Voisey's Bay orthomagmatic Ni-Cu-Co sulphide mineralization, Labrador, Canada. Minerals, Volume 11, Special Issue on Automated SEM.

Wilton, D.H.C., Thompson, G.M. and Grant, D.C., 2017a: The use of automated indicator mineral analysis in the search for mineralization – A next generation drift prospecting tool. Explore, Volume 174, March.

Wilton, D.H.C., Williamson, M.-C., McNeil, R.J., 2017b: Quantitative MLA-SEM mineralogy of gossans and stream sediments in the HALIP: Implications for economic potential. *In:* GEM 2 High Arctic Large Igneous Province (HALIP) Activity: Workshop Report. *Edited by* M.-C. Williamson. Geological Survey of Canada, Open File 8151, pages 45–50.

Wilton, D.H.C. and Winter, L.S., 2012: SEM-MLA (Scanning Electron Microprobe – Mineral Liberation Analyser) research on indicator minerals in glacial till and stream sediments – An example from the exploration for awaruite in Newfoundland and Labrador. *In* Quantitative Mineralogy and Microanalysis of Sediments and Sedimentary Rocks. *Edited by* P.J. Sylvester. Mineralogical Association of Canada, Short Course 42, St. John's, pages 265–283.

Glacial Dispersal from Rare Earth Element and Critical Mineral Deposits

Roger C. Paulen and Beth M. McClenaghan
Geological Survey of Canada, 601 Booth Street, Ottawa, ON, K1A 0E8

Abstract

Rare and critical metals are used in a variety of applications including consumer electronics, green technology, and defense systems. Interest in rare metal exploration in Canada has increased in recent years because of these technologies and domestic supply challenges. Two examples are presented in this case study, 1) glacial dispersal of indicator minerals at the Strange Lake Zr–Y–heavy rare earth element (REE) deposit in northern Québec and Labrador, and 2) glacial dispersal of indicator minerals at the Brazil Lake lithium–caesium–tantalum (LCT)-type pegmatites (North, South, and Army Road pegmatites) in Nova Scotia.

These two deposits occur in contrasting subglacial environments. The Strange Lake deposit was strongly impacted by a large palaeo-ice stream in which a large volume of REE-rich debris was glacially eroded from the deposit and glacially transported a long distance (>50 km). The net result is a long ribbon-shaped dispersal train formed by strong unidirectional flow. The Brazil Lake LCT-type pegmatites were subjected to glacial dispersal through several documented phases of glaciation. The net result was that spodumene dispersal was the product of multiple ice-flow events with varying trajectories, and formed a broad, fan-shaped footprint extending at least 12 km down ice that is considerably larger than the pegmatite subcrop areas.

Introduction

The aim of this paper is to demonstrate that rare and critical metal indicator minerals can be recovered from till and applied to mineral exploration, specifically using two examples from eastern Canada. The purpose of those two studies was to optimize the collection of till down ice from the selected mineral deposits, identify the indicator minerals, and determine how they were glacially transported and deposited down ice. This paper summarizes detailed previous research

conducted by the Geological Survey of Canada, Geological Survey of Newfoundland and Labrador, and the Nova Scotia Department of Energy and Mines, and all the information from that research is available in government publications and journal papers that are cited in the following two paragraphs.

The first case study summarizes the extensive research conducted at Strange Lake over the past 40 years of boulder mapping (Batterson *et al.*, 1985; Batterson, 1989) and matrix till geochemistry, most notably Be, Ce, La, Nb, Pb, Rb, Th, U, Y, and Zr (McConnell and Batterson, 1987; Batterson, 1989; Batterson and Taylor, 2009). Airborne gamma-ray spectrometry data revealed that the dispersal train can be detected in excess of 50 km down ice to the northeast, well beyond the original till survey (Geological Survey of Canada, 1980; Zajac, 2015) and more recent research on glacial dispersal (Paulen *et al.*, 2017, 2024a) and indicator minerals (McClenaghan *et al.*, 2017a, b, 2019).

The second case study conducted at Brazil Lake, draws information from historical till geochemical investigations by the Nova Scotia Department of Natural Resources (MacDonald *et al.*, 1992), a university M.Sc thesis by Lundrigan (2008), and exploration company assessment reports (*e.g.*, Black, 2012). Recent systematic indicator mineral studies were part of a multi-faceted collaborative Federal–Provincial study that included regional-scale surficial geological mapping, sediment-thickness modelling, till fabric measurements, clast lithology analyses, till matrix geochemical analysis, indicator mineral analysis, and studies of glacial stratigraphy (Brushett and Tupper, 2021; McClenaghan *et al.*, 2023a, b, 2025; Brushett *et al.*, 2022, 2023a, b, c, 2024a, b; Grondin, 2025).

Strange Lake

A study of rare metal indicator minerals and glacial dispersal was carried out at the Strange Lake Canada. The heavy mineral (>3.2 specific gravity) and mid-density (3.0–3.2 specific gravity) nonferromagnetic fractions of mineralized bedrock from the deposit and till up to 50 km down ice of the deposit were examined to determine the potential of using rare earth element indicator minerals for exploration. The Strange Lake intrusive complex occurs on the border between the provinces of Québec and Newfoundland and Labrador (Fig. 1) and is currently accessible only by

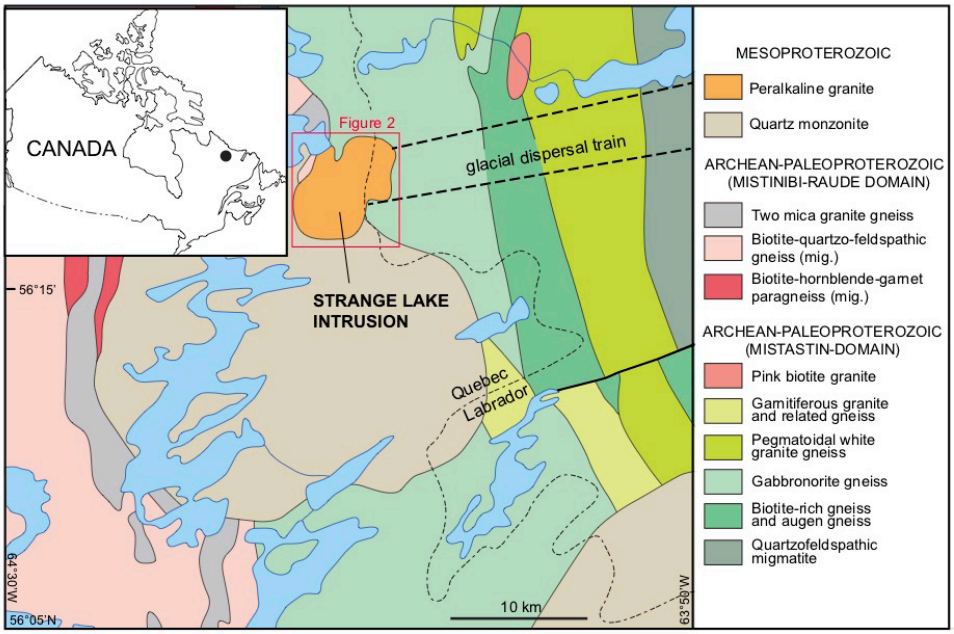


Figure 1. *Location of the study area in eastern Canada (inset) and regional bedrock geology map of the Strange Lake area (geology summarized from Miller* et al.*, 1997; from McClenaghan* et al.*, 2019).*

air. The deposit is just southeast of Lac Brisson approximately 240 km northeast of Schefferville, Québec, and 125 km west of the world class Voisey's Bay Ni–Cu–Co mine in Labrador.

The Strange Lake intrusion is a peralkaline granite within the Paleoproterozoic Churchill Structural Province in the northeastern part of the Canadian Shield. The granite, dated at 1240 ± 2 Ma (Miller, 1990), intrudes along the contact between Late Archean to Early Proterozoic metasedimentary and metagabbroic rocks to the north and Middle Proterozoic quartz monzonite to the south (Fig. 1). The highest-grade mineralization is in the pegmatitic exotic-rich granites in the upper parts of the peralkaline intrusion, particularly in the Main Zone (also known as the A Zone) and the B Zone. The deposit is relatively enriched in HREE (Eu to Lu) and Y as compared to light rare earth elements (LREE) (Zajac *et al.*, 1984).

Eastern Québec and western Labrador were strongly scoured by the Laurentide Ice Sheet throughout the Wisconsin glaciation by ice that flowed outward from a large ice dome over central Québec (Dyke and Prest, 1987; Vincent, 1989), with the Ancestral Labrador ice divide situated some 60 km to the west in the George River region (Dubé-Loubert *et al.*, 2021; Rice *et al.*, 2019). Bedrock outcrops in the region are uncommon and most of the landscape is covered by till of variable thickness, from veneers (<2 m) to several metres (Batterson *et al.*, 1985). The landscape is characterized by streamlined glacial landforms consisting of megaflutings and megalineations

that were formed by fast flow of the Kogaluk River ice stream (IS No. 187) (Margold *et al.*, 2015; Paulen *et al.*, 2017). Measurements of striations and landforms indicate that the ice stream flowed east-northeast towards the Labrador coast (Fig. 2). The till (Fig. 3) in the region is very sandy (average 58% sand, 37% silt, and 5% clay; McClenaghan *et al.*, 2017a) having been derived mainly from local rapakivi granite and the Strange Lake intrusive complex.

The Strange Lake intrusive complex has a strong gamma-ray signature that was identified in the 1980s (Geological Survey of Canada, 1980). Cumulative values for eTh (Fig. 4) and eU reflect the presence of the intrusion as well as the presence of radioactive boulders and minerals in till that have been glacially dispersed down ice to the northeast (Miller, 1985; Batterson, 1989; Zajac, 2015). The upper part of the Main Zone was removed by erosion, which Zajac (2015) attributed

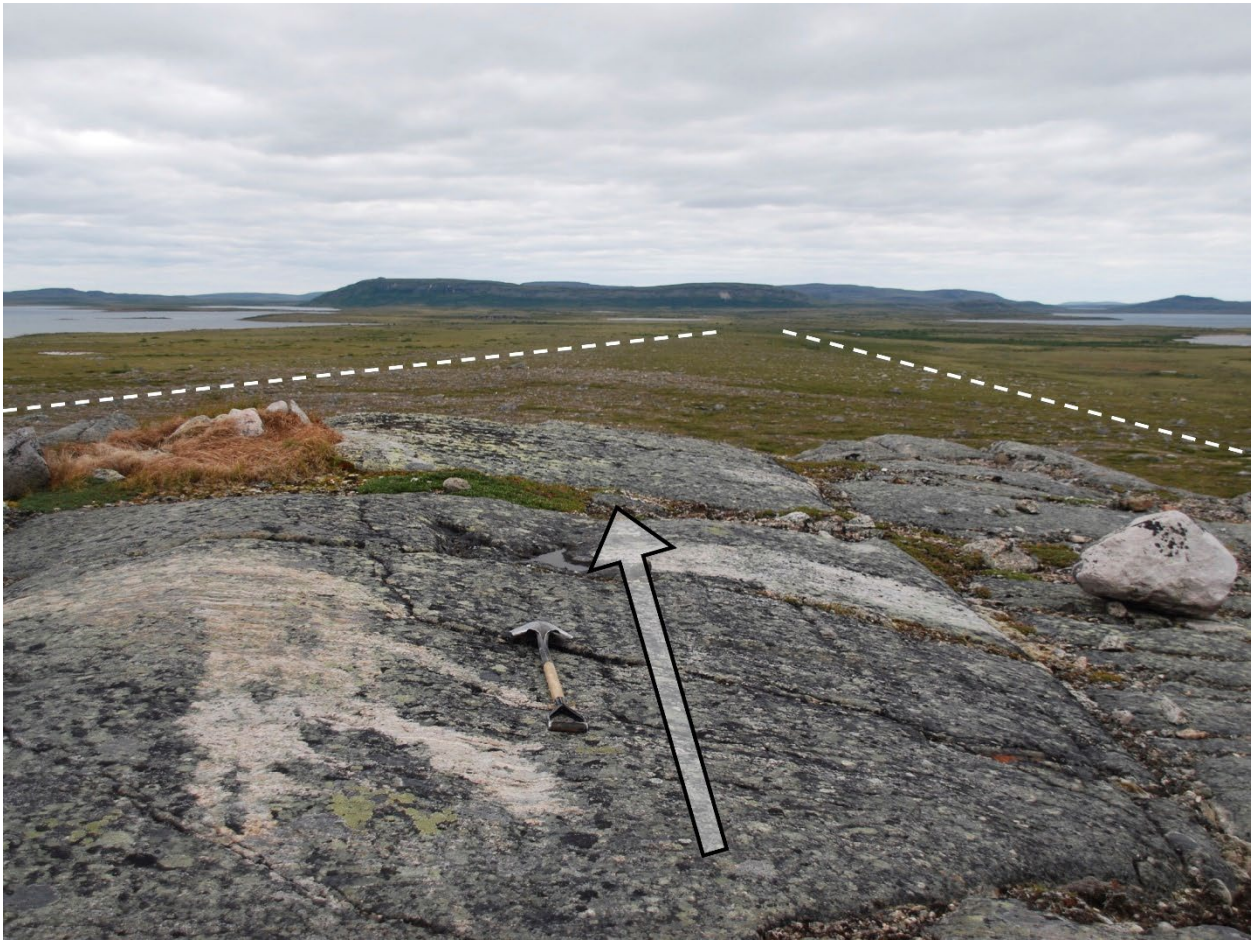


Figure 2. *Glacially sculpted outcrop south of Strange Lake (at left). The dominant outcrop shape and large glacial landforms (outlined by the dashed line) were formed by ice streaming directly away from the viewer, toward the Labrador Sea. A later ice flow occurred during deglaciation (shovel with arrow), likely coinciding with the formation of the esker network in Strange Lake sculpting only the bedrock on the crag-and-tail landforms, and almost no reworking of the glacial sediments, preserving the megascale glacial lineation landforms.*



Figure 3. *Grey stony, sandy C-Horizon till sampled at site 15-MPB-008, 16 km down ice of the Strange Lake intrusion. Refer to McClenaghan* et al. *(2017a) for till sample location.*

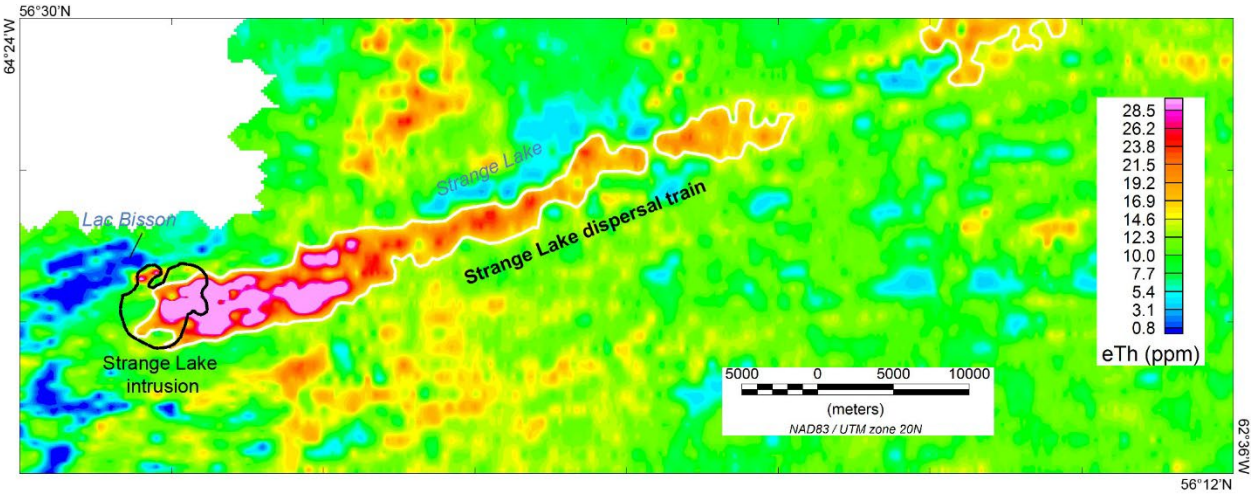


Figure 4. *Equivalent Th from airborne gamma-ray spectrometry data for the Strange Lake area. The area with similar Th values outlined in white and trending northeast is the signature of the Strange Lake glacial dispersal train. The Strange Lake intrusion is outlined with a black line. Modified from McClenaghan* et al. *(2017b); from McClenaghan* et al. *(2019) and radiometric data from Geological Survey of Canada (1980).*

largely to glacial erosion. It is likely that preglacial erosion also removed some of the Main Zone prior to glaciation. Because of the highly-altered nature of the minerals in the Strange Lake intrusion (Fig. 5), it is likely that preglacial weathering formed a regolith in the upper part of the intrusion that was the source of a significant volume of REE-rich debris that was glacially eroded and dispersed down ice. In contrast, the B Zone is largely intact because it suffered only minimal glacial erosion (Zajac, 2015).



Figure 5. *A large erratic of rapikivi granite from the Strange Lake intrusive complex. The degree of post-glacial weathering that has occurred over a relatively short time since deglaciation (*ca. *8.5 ka; Dalton* et al. *(2023)), in a subarctic climate, highlights the potential high degree of erodibility of the bedrock prior to glaciation.*

The indicator mineral suite at Strange Lake was studied from ten bedrock samples, one cobble (*i.e.*, mineralized float), five composite till samples, amalgamated from previous till surveys and six bulk till samples. Additional information regarding the composite and bulk till samples are presented in detail in McClenaghan *et al.* (2017a, 2019).

The deposit contains oxide, silicate, phosphate, and carbonate indicator minerals, some of which (*i.e.*, cerianite, uraninite, fluorapatite, rhabdophane, thorianite, danburite, and aeschynite) have not been reported in previous bedrock studies of Strange Lake (McClenaghan *et al.*, 2019). Indicator minerals that were observed in bedrock and till heavy mineral concentrates in this study are listed in Appendix 1. Some indicator minerals in bedrock were difficult to visually differentiate because of their (i) small size, (ii) tendency to be intergrown with other minerals, and (iii) discoloration from hematite staining. The following minerals were particularly difficult to differentiate: (1) thorite and thorianite, (2) rhabdophane and monazite, and (3) zircon and gittinsite.

Indicator minerals that could be useful in the exploration for similar deposits include Zr silicates (zircon, secondary gittinsite, pyrochlore, and thorite as well as rare earth element minerals monazite, chevkinite, parisite, bastnaesite, kainosite, and allanite). Some of the minerals recovered from the bedrock and till samples are shown in Fig. 6. Minerals that were recovered from bedrock and (or) in till down ice from the deposit and that are indicative of rare metal mineralization and could be considered as potential indicator minerals for this deposit include thorite/thorianite, pyrochlore, monazite/ rhabdophane, chevkinite, parisite, gittinsite, zircon, allanite, bastnaesite, kainosite, and komarovite (*see* Appendix 1). This list of indicator minerals identified for the



Figure 6. *Colour photographs of selected indicator minerals from bedrock or from till samples overlying and down ice of the Strange Lake deposit: a) Reddish brown to black fibrous arfvedsonite grains from till; b) Dark green acicular aegirine from till; C) Dark purple fluorite grains from bedrock; d) Orange–brown octahedral pyrochlore grains from bedrock; e) Orange monazite grains from till; f) White bastnaesite grains from till; g) Black chevkinite from till; h) Dark brown allanite intergrown with white gittinsite from till. Digital photography by Michael J. Bainbridge Photography. Details about picked indicator grains and their respective sample numbers are available from McClenaghan* et al. *(2019).*

Strange Lake deposit reflects the ability of indicator mineral methods to recover and recognize a broad range of minerals in the >0.25 mm nonferromagnetic heavy mineral concentrate from till samples.

The glacial dispersal train trending east-northeast from the Strange Lake deposit for at least 50 km had been previously defined using airborne gamma-ray spectrometry data, radioactive boulders, lake and stream sediment geochemistry, and till geochemistry. This study has shown that indicator mineral methods can also detect the distal parts of the dispersal train. Pyrochlore, gittinsite, bastnaesite, and chevkinite were recovered from till up to 35 km down ice, and rhabdophane, parisite, and allanite were recovered from till 50 km down ice (refer to Appendix 2 in McClenaghan *et al.*, 2019).

The Strange Lake deposit sits right in the trunk of a large palaeo-ice stream with its onset zone approximately 20 km to the west, and extended out to the Labrador Sea (Paulen *et al.*, 2017; 2024a). The Strange Lake dispersal train most likely extends more than 50 km down ice, due to the erosive nature and subglacial rheology of the former ice stream. Wilton *et al.* (2017) recovered gittinsite in till collected 100 km down ice (east-northeast) of the deposit, which may have been eroded from the Strange Lake pluton. Distribution patterns for elevated Be, Nb, Pb, Y, and Zr contents in organic lake sediments (McCurdy *et al.*, 2018) and other minerals associated with the larger peralkaline granite host, such as Sn (McCurdy *et al.*, 2018; Amor *et al.*, 2018), suggest that glacial dispersal from Strange Lake by streaming ice may have extended up to 150 km down ice (Paulen *et al.*, 2024b).

Brazil Lake

The Brazil Lake lithium–caesium–tantalum (LCT)-type pegmatites (North, South, and Army Road pegmatites) in eastern Canada, were the focus of a detailed till study to document glacial dispersal of LCT pegmatite indicator minerals from bedrock. These types of deposits are important sources of Li, Sn, and Rb and the primary source of Ta. This research was undertaken as part of the GSC's Targeted Geoscience Initiative Program and has been carried out in partnership with the Nova Scotia Department of Natural Resources. The aim of this study was to 1) investigate how spodumene (the key Li ore mineral in the Brazil Lake pegmatites) and associated minerals are

glacially dispersed in a region that is extensively covered by unconsolidated glacial sediments; 2) determine the till matrix geochemical dispersal from this style of mineralization; 3) define net glacial dispersal patterns of the Brazil Lake pegmatites in an area affected by multiple phases of ice flow; and 4) test analytical methods for Li in till that can be used for the exploration of Li and associated critical minerals in southwest Nova Scotia, and glaciated terrain in general.

The pegmatites are northeast of the town of Yarmouth and 200 km southwest of the city of Halifax in the province of Nova Scotia (Fig. 7). The glaciated landscape consists of gently rolling hills consisting of drumlin fields with a near-continuous cover of glacial sediments of varying thickness. The region is accessed by truck along numerous local primary and secondary roads.

The Brazil Lake area is underlain by rocks of the Meguma terrane and is characterized by a thick sequence of Early Cambrian to Early Ordovician metasedimentary rocks, comprising the

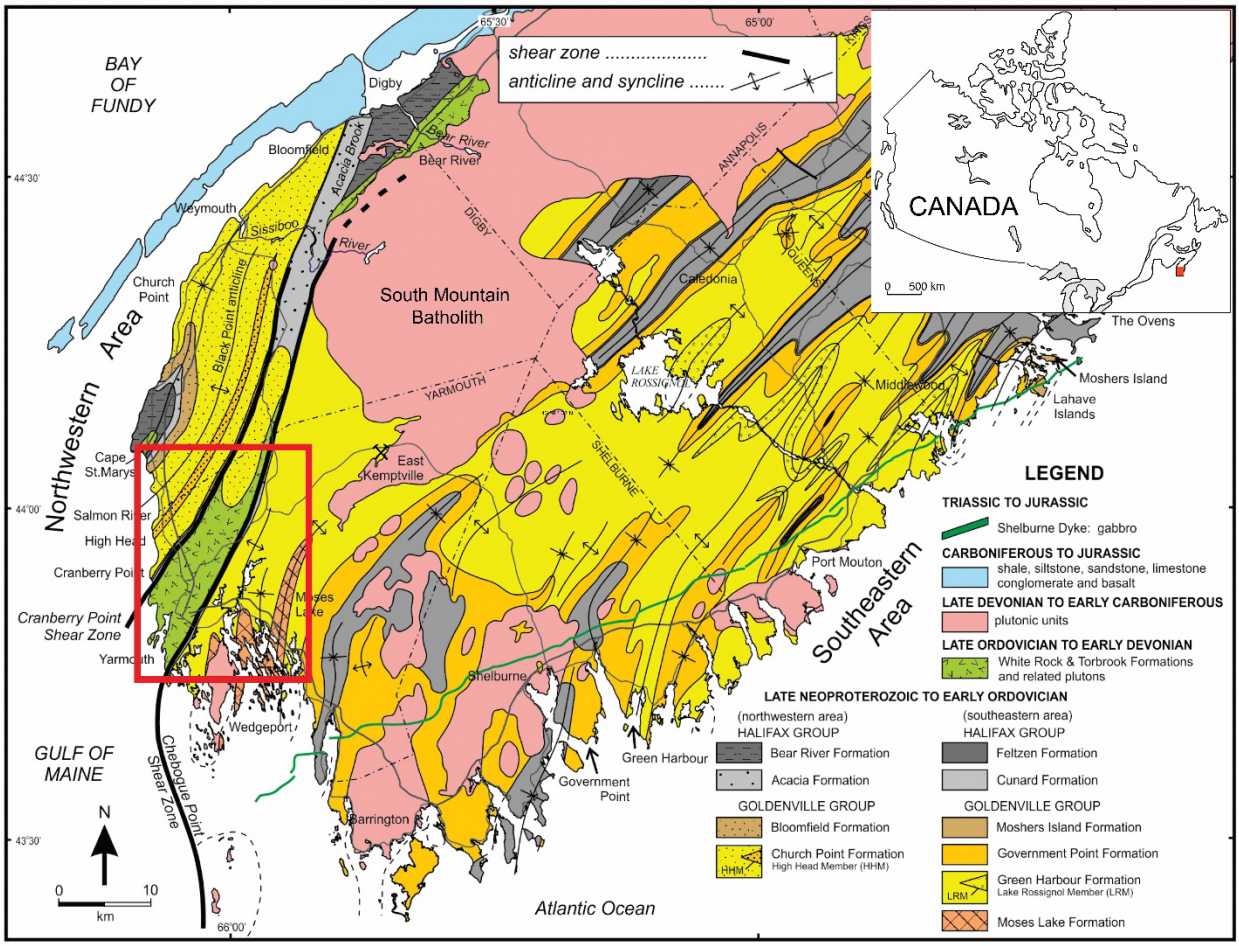


Figure 7. *Bedrock geology of southwestern Nova Scotia. The location of the till sampling survey area is indicated by the red-outlined box and the location of Brazil Lake pegmatites is indicated by the white star. Bedrock geology modified from White (2010) and White* et al. *(2018); from McClenaghan* et al. *(2025).*

metasandstone-dominated Goldenville Group and the overlying siltstone- and slate-dominated Halifax Group (White, 2010). Locally, the Meguma Group is unconformably overlain by a thin sequence of Silurian to Early Devonian slate, quartzite, and volcanic rocks of the Rockville Notch Group (White and Barr, 2017; White *et al.*, 2018). The majority of these rocks were intruded by the *ca.* 373 Ma peraluminous South Mountain Batholith and related granitoid rocks (White and Barr, 2017). The western edge of the batholith is ~20 km east of the Brazil Lake area and the South Mountain Batholith is host to the East Kemptville Sn deposit and numerous critical mineral occurrences that form the Nova Scotia Tin Domain (Chatterjee, 1983).

Three northeast-trending, steeply-dipping pegmatite dykes (referred to as Brazil Lake South, Brazil Lake North, and Army Road pegmatites) are hosted by the Silurian White Rock Formation (Rockville Notch Group), comprising shallow marine metasedimentary rocks (quartzite, amphibolite, and pelitic schist) interbedded with minor mafic metavolcanic units (White, 2010; White and Barr, 2017). Northeast-southwest trending shear zones crosscut the area and the metamorphic grade of the White Rock Formation and Halifax Group increases from greenschist to amphibolite facies localized to the contact between the White Rock Formation and Goldenville Group on the south side of the Yarmouth Syncline – this coincides with the Chebogue Shear zone (Culshaw and Liesa, 1997; MacDonald *et al.*, 2003). Field mapping by Kontak (2006) suggests that the two Brazil Lake pegmatites (North and South) were emplaced in an active shear zone where high-temperature ductile deformation occurred during consolidation of the pegmatite. Tantalite U–Pb geochronology from the South pegmatite indicates that pegmatite crystallization occurred at *ca.* 395 Ma (Kontak *et al.*, 2005; Kontak and Keyser, 2009).

The pegmatites are of the albite–spodumene type and are characterized by coarse crystals of spodumene (maximum size 1.5–2.0 m; Fig. 8a, b) and K-feldspar, with intergranular spodumene, muscovite, albite and quartz (Fig. 8b). Accessory phases include columbite–tantalite (Fig. 8c), black tourmaline (Fig. 8d), apatite, beryl, sphalerite, and cassiterite. Spodumene, the most abundant Li-bearing mineral in the pegmatites, is a light-coloured silicate (hardness 6.5–7) with two perfect cleavages, a vitreous lustre that is pearly on its cleavage surface and a moderate density of 3.18 g cm^{-3}. Minerals reported to be present in the North and South pegmatites which could be useful indicators for drift prospecting include spodumene, black tourmaline, black columbite–



Figure 8. *a) Coarse-grained (≤0.5 m in length) elongate white spodumene crystals exposed on the weathered subcropping surface of the South dyke; b) Fresh unweathered spodumene boulder (1.5 m in length and 1.0 m in height) extracted from the South dyke; c) Black columbite–tantalite crystals in quartz at the North dyke, with pen nib for scale; d) Cross-section of the South dyke in contact with the metavolcanic country rocks. At the outer contact of the pegmatite, abundant black tourmaline is observed, which formed as a result of the exsolution of B-rich fluids from the pegmatite. Source photographs: a) M.B. McClenaghan, NRCan photo 2022-571; b) D. Brushett, Nova Scotia Department of Natural Resources; c) D. Archibald, St Francis Xavier University; d) C. Beckett-Brown, NRCan photo 2023-484.*

tantalite, red garnet, blue apatite and other phosphate minerals, green beryl, cassiterite, wolframite, sphalerite, zircon, epidote, topaz, and titanite (Appendix 2).

The surficial geology of southwestern Nova Scotia is described as the product of multiple glacial advances and retreats throughout several glacial events (Stea, 2004; Stea *et al.*, 2011) during the Quaternary. Multiple till units, identified in coastal sections in southwest Nova Scotia, and mapped striations are interpreted as a product of several phases of glacial advances and shifting

ice-flow directions (Grant, 1980; Stea and Grant, 1982). These ice-flow phases were largely controlled by local topography during ice advances and retreats, and were likely influenced by thinner marine ice margins at lower sea-levels and ice streams (*cf.* Shaw *et al.*, 2006). Three main phases are described below from oldest to youngest (Fig. 9):

Regional eastward to southeastward ice flow emanating from New Brunswick during the Caledonia phase (marine isotope stage (MIS) 4; ~75–50? ka) was responsible for the early formation of drumlins in southwest Nova Scotia. The tills that comprise drumlins are silt-rich (as well as shell-rich in coastal sections) and contain a high percentage of exotic bedrock components with transport distances of >80 km from New Brunswick (Stea and Finck, 2001; ice-flow phase 1 red arrows in Fig. 9).

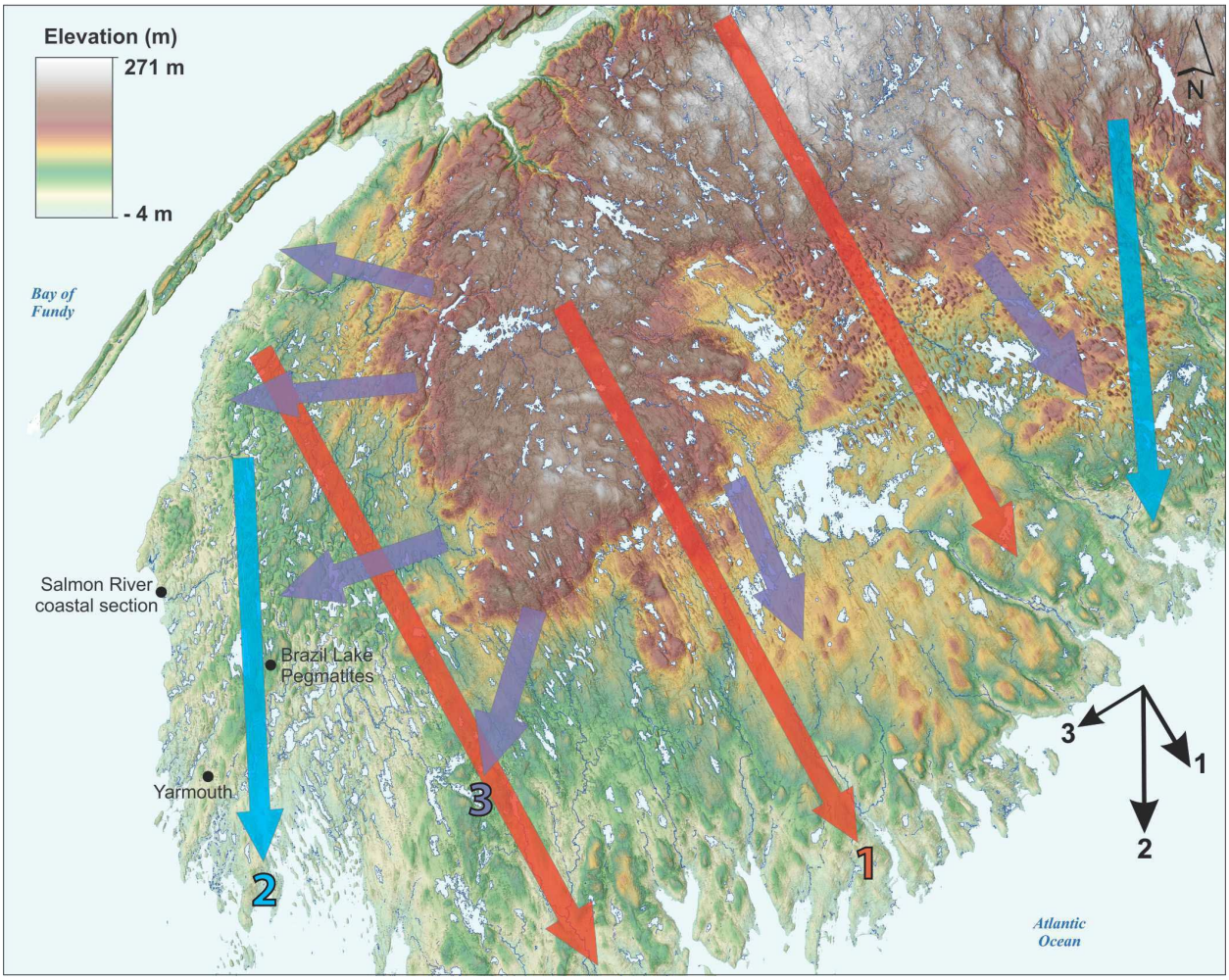


Figure 9. *Generalized ice-flow chronology of southern Nova Scotia summarized from Stea and Grant (1982), Finck and Stea (1995) and Stea* et al. *(2011). The oldest documented ice-flow phase, prior to the last interglacial, is not shown here. Generalized ice-flow phases are indicated by the red, blue and purple arrows with '1' being the oldest flow. Black arrows in bottom right corner indicate regional ice-flow phases; 1 is the oldest. Source: Hillshade LiDAR image compiled from data published by the Government of Nova Scotia (from McClenaghan* et al.*, 2025).*

Subsequent southward regional ice flow during the Escuminac phase (MIS 2; 22–18 ka; Stea *et al.*, 2011) modified older drumlins and formed new ones that reflect a more southward flow (ice-flow phase 2 blue arrows in Fig. 9). Ice streaming in the Gulf of Maine towards the marine glacial margins also strongly influenced the strong southward ice flow in western Nova Scotia (Shaw *et al.*, 2006). During the subsequent Scotian phase (~20–17 ka), regional ice centres shifted and Nova Scotia was cut off from the larger continental ice centres (*i.e.*, the Appalachian Glacier Complex) mainly due to drawdown of the ice profile from a major ice stream in the Bay of Fundy (Shaw *et al.*, 2006; Stea *et al.*, 2011). The resultant Scotian Ice Divide formed lengthwise down the centre of the province such that ice-flow direction varied from west-NW to SW to SE in southwestern Nova Scotia (Grant, 1980; Stea and Grant, 1982; ice-flow phase 3 purple arrows in Fig. 9).

As a result of this complex glacial evolution, there is extensive till cover over much of southwestern Nova Scotia that has made bedrock mapping and mineral exploration challenging. The study area is no exception, where extensive glacial modification through the last glacial cycle resulted in highly variable glacial sediment thicknesses and complex landforms. Till thickness in the area is variable, ranging from thin veneers (<2 m) to thick drumlin ridges composed of over 40 m of till (Brushett *et al.*, 2023b, c).

In 2020, 2021, and 2022, a total of 84 bulk (7–20 kg) till samples were collected from 77 sites around and down-ice of the three pegmatites. A total of 184 till samples were collected for till geochemistry and include widely spaced regional samples collected across southwest Nova Scotia and proximal samples collected up-ice and down-ice of the Brazil Lake pegmatites (Fig. 10). The widely spaced till samples provide the regional context for the interpretation of the closely-spaced samples and assess the potential for additional pegmatites buried by extensive till cover. Analyses over the three years (2020-2021-2022) include various combinations of different digestions or fusions to test and compare their efficacy for the various pathfinder elements for LCT pegmatites: 1) *aqua regia* (partial) digestion, 2) Na peroxide fusion (total), 3) 4-acid (near total) digestion, 4) Li-meta/tetraborate fusion, 5) loss on ignition, and 6) portable X-ray fluorescence (XRF).

Glacial dispersal from the pegmatites is best defined by spodumene (the primary ore mineral) which can be found proximal to the pegmatites as spodumene-bearing clasts ranging from pebbles to boulders (Fig. 11). In the heavy mineral concentrate of till samples, spodumene occurs in the

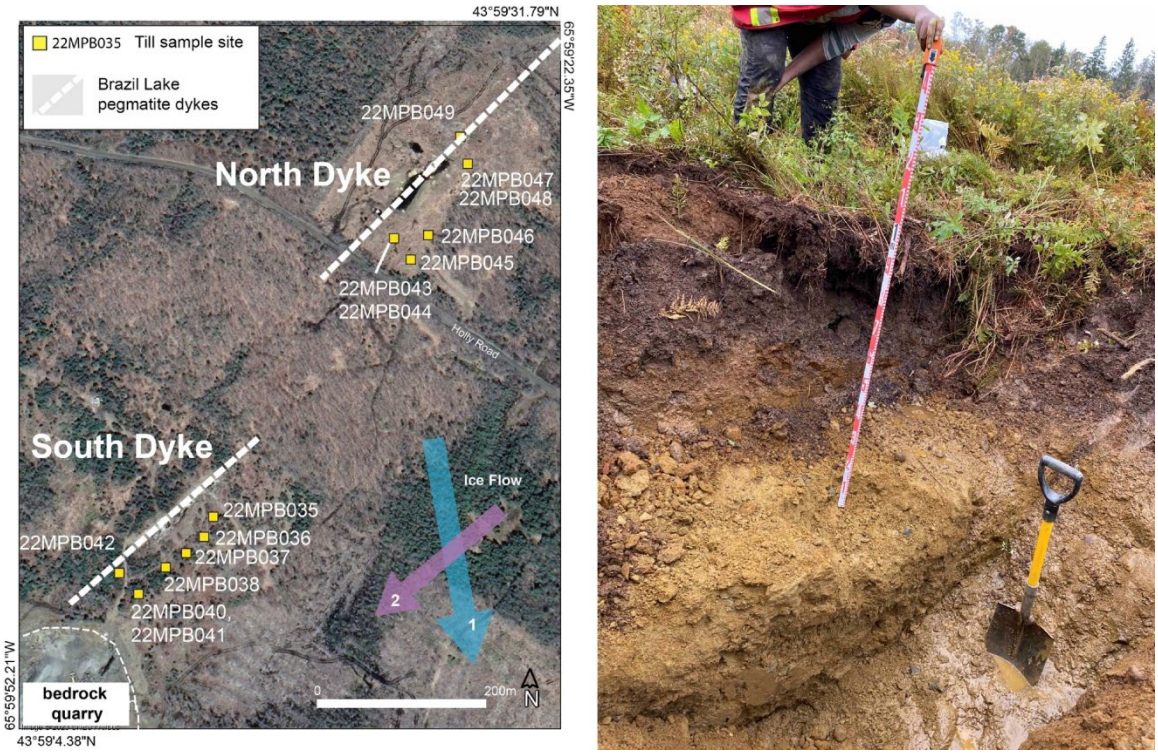


Figure 10. *Detailed portion of the till sampling program conducted around the Brazil Lake LCT pegmatites, and a field photograph of one of the backhoe pits proximal to the North pegmatite. All sample site details and heavy mineral concentrate results are reported in McClenaghan* et al. *(2023a), and till matrix geochemistry reported in Brushett* et al. *(2024a).*

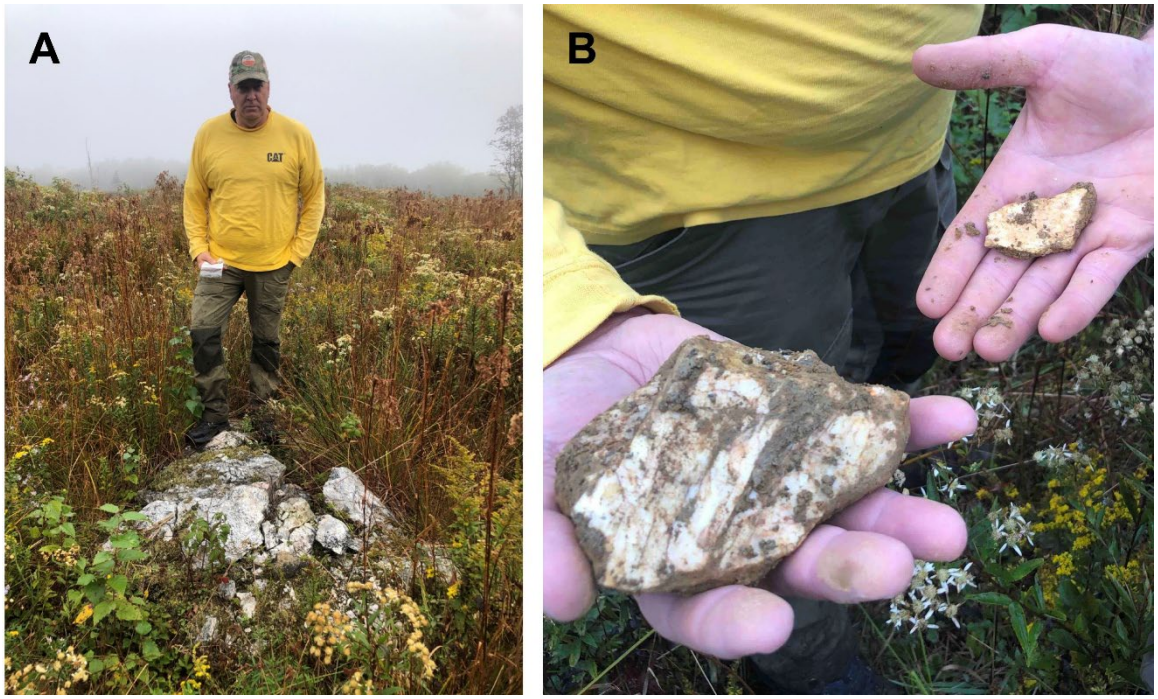


Figure 11. *a) A large spodumene pegmatitic boulder occurring at the ground surface in a recent forestry clearcut a few tens of metres down-ice of the North pegmatite; b) A cobble and pebble glacially eroded from spodumene crystals, recovered from a backhoe till pit down-ice of the North pegmatite.*

0.25–0.5 mm fraction of the 2.8–3.2 SG concentrates, and its presence in the till (hundreds to thousands of grains per sample) is visual confirmation of the existence of nearby LCT pegmatites. If both density fractions of the 0.25–0.5 mm size fraction are compared side by side (Fig. 12a, b), it is readily apparent that the spodumene dispersal patterns are similar but most distinct and well-developed for the 2.8–3.2 SG fraction. Glacial dispersal of spodumene in the 2.8–3.2 SG fraction forms a fan-shaped exploration target 12 km down-ice that is considerably larger than the pegmatite subcrop areas. The 0.25–0.5 mm picked fraction dispersal footprint is much larger than both the coarse 2–4 mm (granule) fraction (Fig. 12c) and the till matrix geochemistry with the best response (Fig. 12d; *see* Brushett *et al.*, 2024a).

Other useful LCT pegmatite indicator minerals in the local till include apatite and tourmaline (tens to hundreds of grains) and lesser amounts of columbite–tantalite, cassiterite, and scheelite (single units to tens of grains), however, their abundances and spatial distributions are much less/smaller than that for spodumene (Fig. 13). Figure 14 shows grain photographs of some of the visually distinctive indicator minerals that could potentially be applied to lithium exploration.

These results clearly demonstrate that indicator mineral methods are the most useful for lithium exploration in the glaciated terrains of eastern Canada, other glaciated terrain across Canada, and other prospective glaciated terrains globally, where Li exploration is currently ongoing (Romppanen *et al.*, 2026). The research conducted at Brazil Lake and summarized by McClenaghan *et al.* (2023a, 2025) and Brushett *et al.* (2024a) demonstrates the ideal sampling and mineral lab methods to be used, ideal analytical methods for till geochemistry, types of indicator minerals which can be expected proximal to an LCT pegmatite, and the importance of understanding glacial flow paths and glacial transport for interpreting glacial dispersal patterns.

Summary

Rare and critical metal indicator minerals can be added to the expanding list of indicator minerals that can be recovered from surficial sediments and used to explore for a broad range of deposit types and commodities that already include diamonds and precious, base, and strategic metals. The style of mineral dispersal will depend on many factors, which includes the size of the buried mineral deposit, or its alteration halo, as well its outcropping or subcropping shape and

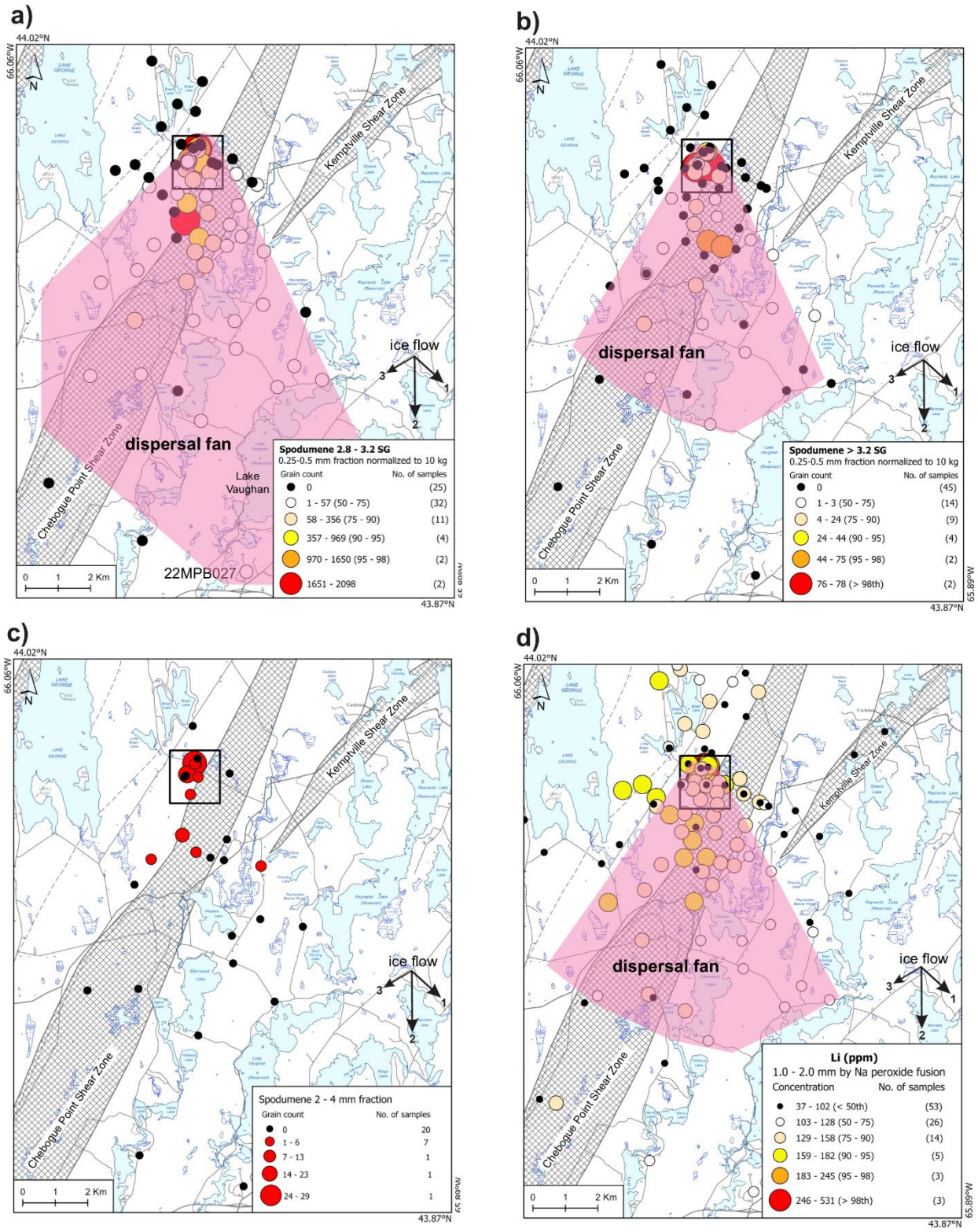


Figure 12. *Comparison of proportional dot maps of spodumene grain abundance (*see *McClenaghan* et al.*, 2023a, 2025) normalized to 10 kg (table feed) in the 0.25–0.5 mm fraction of till: a) 2.8– 3.2 SG fraction; b) >3.2 SG fraction; c) Spodumene clast abundance in the 2–4 mm granule fraction of selected till samples; d) Li concentration (ppm) determined by Na-peroxide fusion for the 1–2 mm fraction. Interpreted dispersal fans are highlighted by pink polygons. Location of pegmatites is inside the black box. Black arrows in bottom right corner indicate regional ice-flow phases; 1 is the oldest. Specific Gravity (SG).*

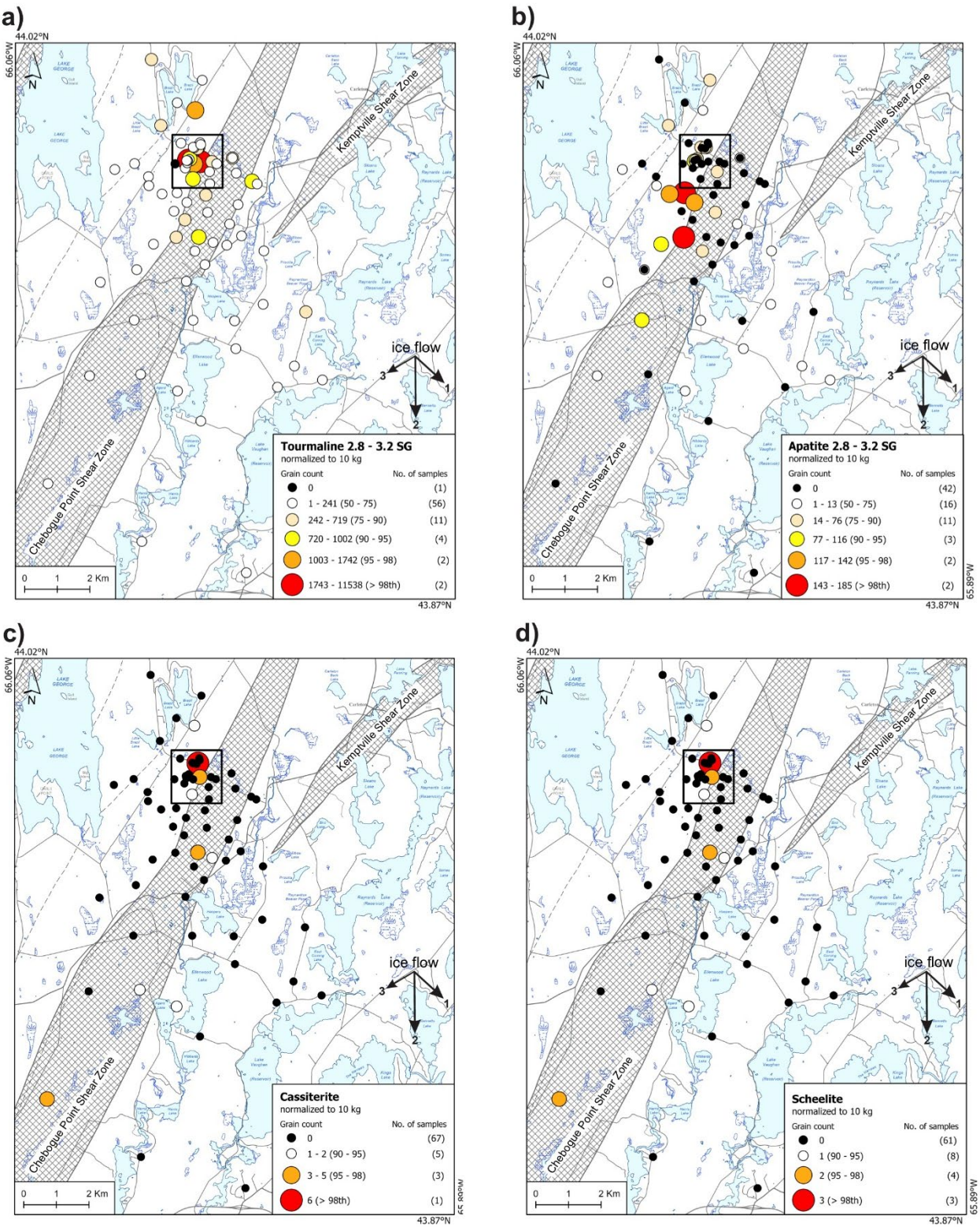


Figure 13. *Proportional dot maps of indicator mineral abundance (*see *McClenaghan* et al.*, 2023a, 2025) in the 0.25–0.5 mm fraction of till normalized to 10 kg of <2 mm material (table feed): a) Tourmaline in the 2.8–3.2 SG fraction; b) Apatite in the 2.8–3.2 SG fraction; c) Cassiterite in the >3.2 SG fraction; d) Scheelite in the >3.2 SG fraction. Location of pegmatites is inside the black box. Black arrows in bottom right corner indicate regional ice-flow phases; 1 is the oldest. Specific Gravity (SG).*

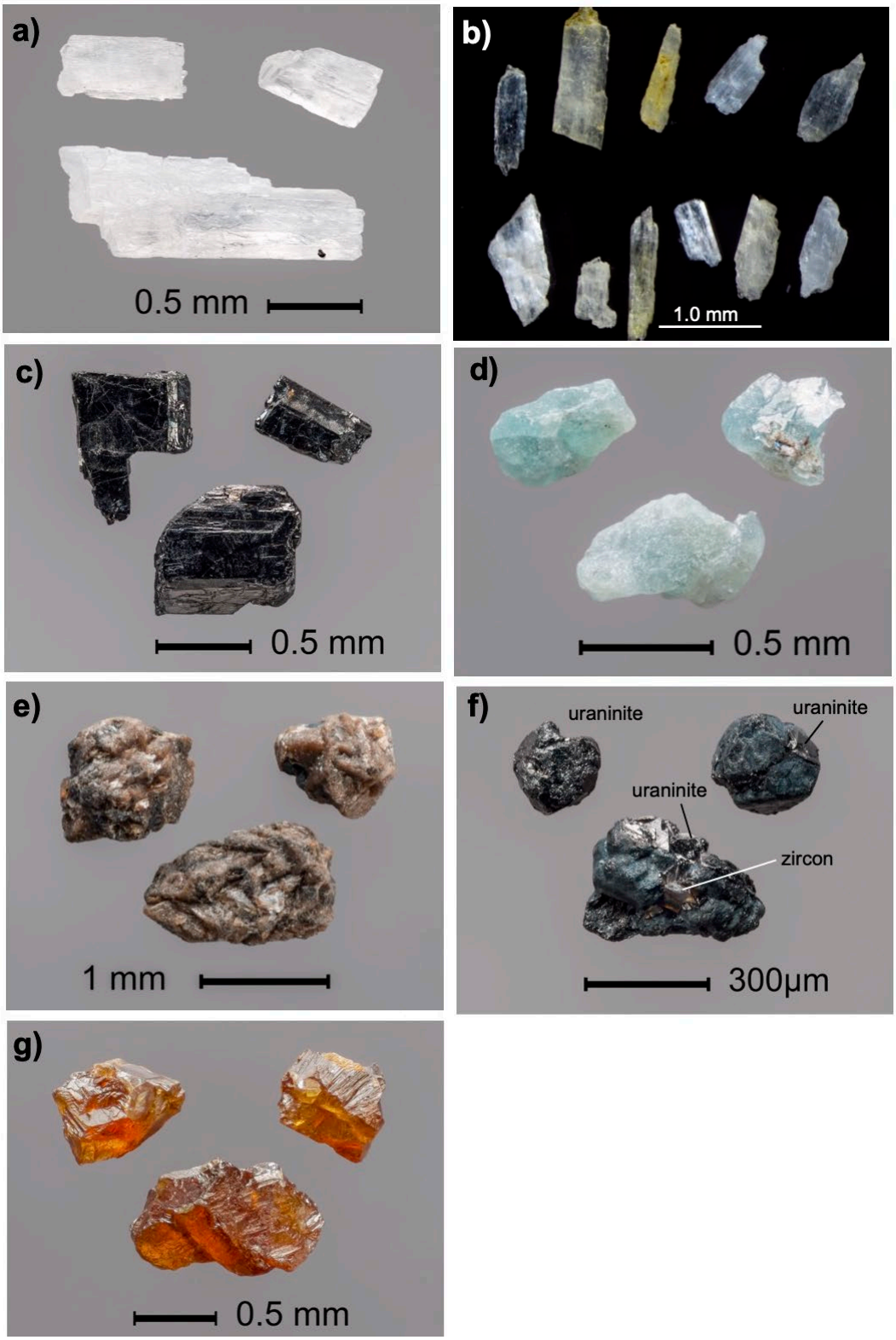


Figure 14. *Photographs of Li–Cs–Ta pegmatite indicator minerals recovered from bedrock sample 20DB-031 BDK (refer to McClenaghan* et al.*, 2023a); a) Spodumene; b) Spodumene on black background; c) Black columbite–tantalite; d) Blue apatite; e) Zircon; f) Uraninite with minor zircon;g) Orange (iron-poor) sphalerite. Source: a, c–g) photographs provided by Michael J. Bainbridge Photography; b) Photograph provided by Overburden Drilling Management Limited.*

orientation relative to direction of glacial flow. A mineralized pegmatite dyke transverse to the dominant ice flow versus a bedrock structure parallel to former ice flow will result in very different dispersal patterns at the surface (*see* Strand *et al.*, 2009, for an example of glacial dispersal with kimberlite pipes *versus* dykes). Mineralized bedrock subjected to highly erosive ice streams, such as the example from Strange Lake, will create longer dispersal trains with linear dispersal concentrations down-ice (Paulen *et al.*, 2024a, b).

Greenfield explorers likely have little/if any information as to the size, shape, and orientation of the pegmatites they are exploring for, especially if they are under glacial sediments. For the Brazil Lake example presented, close (500 m) offset sample spacing along parallel lines (1–2 km apart) perpendicular to ice flow would be recommended. Additional considerations could include budgetary restrictions, property size, access, and existing datasets. There is no one option suitable to all situations.

Acknowledgments

Contributions to this short course volume were made possible under the Geological Survey of Canada's (GSC) Critical Minerals Geoscience and Data Program under the 'Ice stream paradigm and search for critical minerals in Canada: exploiting the power of automated geospatial mapping techniques' research activity (2023–2027). This paper summarizes research conducted under the GSC's Targeted Geoscience Initiative (TGI-3, 2005–2010) and Geo-mapping for Energy and Minerals (GEM-2) Program (2014–2018) at Strange Lake, Labrador. The research at Brazil Lake was funded by the Geological Survey of Canada through TGI-6 and by the Nova Scotia Department of Natural Resources – Geoscience and Mines Branch (2021–2024).

Finally, this short paper acknowledges the years of scientific interactions and partnerships with Canadian scientists in government and academia. In particular, we would like to thank Rob DiLabio (GSC Ottawa, retired), Martin Batterson (Geological Survey of Newfoundland and Labrador, retired), and Ralph Stea (Nova Scotia Department of Energy and Mines, retired) for many fruitful discussions and providing historical perspectives from their previous Quaternary research at these sites.

References

Amor, S., McCurdy, M. and Garrett, R., 2018: Creation of an atlas of lake-sediment geochemistry of western Labrador and northeastern Québec. Geochemistry: Exploration, Environment, Analysis, Volume 19, pages 369–393. https://doi.org/10.1144/geochem2018-061

Batterson, M.J., 1989: Glacial dispersal from the Strange Lake alkalic complex, northern Labrador. *In* Drift Prospecting. *Edited by* R.N.W. DiLabio and W.B. Coker. Geological Survey of Canada, Paper 89-20, pages 31–40. https://doi.org/10.4095/127362

Batterson, M.J. and Taylor, D.M., 2009: Geochemical re-analysis of till samples from the Strange Lake area, Labrador (NTS map sheets 14D/5 and 24A/8). Government of Newfoundland and Labrador, Department of Natural Resources, Geological Survey, Open File LAB/1479.

Batterson, M.J., Taylor, D.M. and Vatcher, S.V., 1985: Quaternary mapping and drift exploration in the Strange Lake areas, Labrador. *In* Current Research. Government of Newfoundland and Labrador, Department of Mines and Energy, Mineral Development Division, Report 85-1, pages 4–10.

Birkett, T.C., Miller, R.R., Roberts, A.C. and Mariano, A.N., 1992: Zirconium-bearing minerals of the Strange Lake intrusive complex, Québec–Labrador. The Canadian Mineralogist, Volume 30, pages 191–205.

Birkett, T.C., Trzcienski, W.E., Jr. and Stirling, J.A.R., 1996: Occurrence and compositions of some Ti-bearing minerals in the Strange Lake intrusive complex, Québec–Labrador boundary. The Canadian Mineralogist, Volume 34, pages 779–801.

Black, D.L., 2012: Report on prospecting, Brazil Lake property, EL 09083, EL09084, EL 09085. Champlain Mineral Ventures Ltd, Assessment Report AR 2012-048. https://novascotia.ca/natr/meb/data/ar/2012/AR_ME_2012- 048.pdf

Brushett, D.M., Beckett-Brown, C.E., McClenaghan, M.B., Paulen, R.C. and Rice, J.M., 2024b: Lithium signatures in till at the Brazil Lake lithium-cesium-tantalum pegmatites, Nova Scotia. *In* Till Geochemistry and Indicator Mineral Methods for Exploration in Glaciated Terrains. *Edited by* R.C. Paulen and M.B. McClenaghan. Geological Survey of Canada, Open File 9210, pages 99–109. https://doi.org/10.4095/pbmy2d03m0

Brushett, D.M., Beckett-Brown, C.E., McClenaghan, M.B., Paulen, R.C., Rice, J.M., Haji Egeh, A. and Pelchat, P., 2024a: Till geochemical data for the Brazil Lake pegmatite area, southwest Nova Scotia, Canada (NTS 21A/04, 20O/16 and 20P/13): Samples Collected in 2020, 2021, and 2022. Geological Survey of Canada, Open File 9148. https://doi.org/10.4095/332384

Brushett, D.M., Kennedy, G.W. and MacMullen, C.C., 2023b: Sediment thickness and bedrock topography maps of southwest Nova Scotia. Nova Scotia Department of Natural Resources and Renewables, Open File Map ME 2023-2, scale 1:215 000. https://novascotia.ca/natr/meb/download/mg/ofm/htm/ofm_2023-002.asp

Brushett, D.M., Kennedy, G.W. and MacMullen, C.C., 2023c: Data generated by sediment thickness and bedrock topography model of southwest Nova Scotia. Nova Scotia Department of Natural Resources and Renewables, Geoscience and Mines Branch, Digital Product ME 546. https://novascotia.ca/natr/meb/download/dp546.asp

Brushett, D.M., McClenaghan, M.B. and Paulen, R.C., 2022: Till geochemical data for till samples collected in 2020 in the Brazil Lake pegmatite area, southwest Nova Scotia, Canada (NTS 21A/04, 20O/16 and 20P/13). Nova Scotia, Department of Natural Resources and Renewables, Open File Report ME 2022-002. https://novascotia.ca/natr/meb/data/ofr/OFR_ME_2022-002.zip

Brushett, D.M., McClenaghan, M.B., Paulen, R.C., Beckett-Brown, C., Rice, J.M., Haji Egeh, A. and Nissen, A., 2023a: Using till matrix geochemistry and LiDAR-based surficial geological mapping to understand glacial dispersal patterns associated with the Brazil Lake LCT pegmatites, southwest Nova Scotia, Canada. Poster session presented at the 49th Colloquium and Annual General Meeting of the Atlantic Geoscience Society, February 2023, Truro, Nova Scotia. Nova Scotia Department of Natural Resources and Renewables, Open File Poster ME 2023-001. https://novascotia.ca/natr/meb/data/pubs/cs/cs_me_2023-001.pdf

Brushett, D.M. and Tupper, J., 2021: Till geochemistry, indicator mineralogy, and surficial geology of the Brazil Lake pegmatite area, southwest Nova Scotia, Canada. Geoscience and Mines Branch, Report of Activities 2020–2021, Nova Scotia Department of Natural Resources and Renewables, Report ME 2021-002, pages 1–9. https://novascotia.ca/natr/meb/DATA/pubs/21re02/01ROA_2021_Brushett&Tupper.pdf

Chatterjee, A.K., 1983: Metallogenic map of Nova Scotia. Nova Scotia Department of Mines and Energy, scale 1:500 000.

Corey, M., 1995: Diamond drilling of rare element pegmatites in southwestern Nova Scotia. Nova Scotia Mines and Energy Branches, Open File Report 95- 001. https://novascotia.ca/natr/meb/data/pubs/ofr_me_1995-001.pdf

Culshaw, N. and Liesa, M., 1997: Alleghanian reactivation of the Acadian fold belt, Meguma Zone, southwest Nova Scotia. Canadian Journal of Earth Sciences, Volume 34, pages 833–847. https://doi.org/10.1139/e17-068

Dalton, A.S., Dulfer, H.E., Margold, M., Heyman, J., Clague, J.J., Froese, D.G., Gauthier, M.S., Hughes, A.L.C., Jennings, C.E., Norris, S.L. and Stoker, B.J., 2023: Deglaciation of the north American ice sheet complex in

calendar years based on a comprehensive database of chronological data: NADI-1. Quaternary Science Reviews, Volume 321. https://doi.org/10.1016/j.quascirev.2023.108345

Dubé-Loubert, H., Roy, M., Veillette, J.J., Brouard, E., Schaefer, J.M. and Wittmann, H., 2021: The role of glacial dynamics in the development of ice divides and the Horseshoe Intersection Zone of the northeastern Labrador Sector of the Laurentide Ice Sheet. Geomorphology, Volume 387. https://doi.org/10.1016/j.geomorph.2021.107777

Dyke, A.S. and Prest, V.K., 1987: Late Wisconsinan and Holocene history of the Laurentide Ice Sheet. Géographie Physique et Quaternaire, Volume 41, pages 237–263. https://doi.org/10.7202/032681ar

Finck, P.W. and Stea, R.R., 1995: The compositional development of tills overlying the South Mountain Batholith. Nova Scotia Department of Natural Resources, Mines and Minerals Branch, Paper 95-1, 52 pages.

Geological Survey of Canada, 1980: Airborne gamma ray spectrometric map, Dihourse Lake Québec–Newfoundland. Geological Survey of Canada, Geophysical Series, Map 35124(08)G. https://doi.org/10.4095/124881

Gowans, R.M., Lewis, W.J., Shoemaker, S., Spooner, J. and Zalnieriunas, R.V., 2014: Quest Rare Minerals Limited NI-43-101 technical report on the preliminary economic assessment (PEA) for the Strange Lake Property, Québec, Canada. Micon International Limited (www.sedar.com).

Grant, D.R., 1980: Quaternary stratigraphy of southwestern Nova Scotia: Glacial events and sea level changes. Geological Association of Canada, Mineralogical Association of Canada Field Trip Guidebook, Trip 9, 63 pages.

Grondin, B.R., 2025: Using short-transported tills as a method of increasing mineral exploration efficiency in southwestern Nova Scotia. B.Sc (Hons) Thesis, Dalhousie University, Halifax, Nova Scotia. https://hdl.handle.net/10222/85102

Hughes, S.G., 1995: Internal zonation and mineralogy of the Brazil Lake pegmatite. B.Sc thesis, St. Mary's University, Halifax, Nova Scotia.

Hutchinson, H.E., 1982: Geology, geochemistry, and genesis of the Brazil Lake pegmatites, Yarmouth County, Nova Scotia. B.Sc thesis, Dalhousie University, Halifax, Nova Scotia. http://hdl.handle.net/10222/82231

Jambor, J.L., Roberts, A.C., Grice, J.D., Birkett, T.C., Groat, L. and Zajac, S., 1998: Gerenite–(Y), $(CaNa)_2(Y, REE)_3Si_6O_{18}\cdot 2H_2O$, a new mineral species and an associated Y-bearing gadolinite-group mineral, from the Strange Lake peralkaline complex, Québec–Labrador. The Canadian Mineralogist, Volume 36, pages 793–800.

Kontak, D.J., 2004: Geology of the southern lobe of the Brazil Lake LCT-type pegmatite (NTS 21A/04), Yarmouth County, Nova Scotia. Nova Scotia Department of Natural Resources, Mineral Resources Branch Report of Activities 2003, Report 2004-1, pages 41–68.

Kontak, D.J., 2006: Nature and origin of an LCT-suite pegmatite with late-stage sodium enrichment, Brazil Lake, Yarmouth County, Nova Scotia: I. Geological setting and petrology. The Canadian Mineralogist, Volume 44, pages 563–598. https://doi.org/10.2113/gscanmin.44.3.563

Kontak, D.J., Creaser, R.A., Heaman, L.M. and Archibald, D.A., 2005: U-Pb tantalite, Re-Os molybdenite, and $^{40}Ar/^{39}Ar$ muscovite dating of the Brazil Lake pegmatite, Nova Scotia: A possible shear-zone related origin for an LCT- type pegmatite. Atlantic Geology, Volume 41, pages 17–29. https://doi.org/10.4138/655

Kontak, D.J. and Kyser, T.K., 2009: Nature and origin of an LCT-suite pegmatite with late-stage sodium enrichment, Brazil Lake, Yarmouth County, Nova Scotia: II. Implications of stable isotopes (δ18O, δD) for magma source, internal crystallization and nature of sodium metasomatism. The Canadian Mineralogist, Volume 47, pages 745–764. https://doi.org/10.3749/canmin.47.4.745

Lundrigan, A., 2008: Glacial stratigraphy and till geochemical dispersion controls associated with the Brazil Lake pegmatite, southwestern Nova Scotia. M.Sc thesis MT109, Acadia University, Wolfville, Nova Scotia.

MacDonald, L.A., Barr, S.M., White, C.E. and Ketchum, J.W.F., 2003: Petrology, age, and tectonic setting of the White Rock Formation, Meguma Terrane, Nova Scotia: Evidence for Silurian continental rifting. Canadian Journal of Earth Sciences, Volume 39, pages 259-277.

MacDonald, M.A., Boner, F.J. and Lombard, P.A., 1992: Multi-media detailed geochemical study of the Brazil Lake pegmatites (NTS 20P/13), Yarmouth County, Nova Scotia. Nova Scotia Department of Natural Resources, Open File Report 92-016.

Margold, M., Stokes, C.R., Clark, C.D. and Kleman, J., 2015: Ice streams in the Laurentide Ice Sheet: A new mapping inventory. Journal of Maps, Volume 11, pages 380–395. https://doi.org/10.1080/17445647.2014.912036

McClenaghan, M.B., Brushett, D.M., Beckett-Brown, C.E., Paulen, R.C., Rice, J.M., Haji Egeh, A. and Nissen, A., 2023b: Indicator mineral studies at the Brazil Lake LCT pegmatites, southwest Nova Scotia. Geological Survey of Canada, Scientific Presentation, Volume 157. https://doi.org/10.4095/331686

McClenaghan, M.B., Brushett, D.M., Paulen, R.C., Beckett-Brown, C.E. and Rice, J.M., 2025: Glacial dispersal of indicator minerals from the Brazil Lake lithium–caesium–tantalum pegmatites, SW Nova Scotia, Canada. Geochemistry: Exploration, Environment, Analysis, Volume 25. https://doi.org/10.1144/geochem2024-047

McClenaghan, M.B., Brushett, D.M., Paulen, R.C., Beckett-Brown, C.E., Rice, J.M., Haji Egeh, A. and Nissen, A., 2023a: Critical metal indicator mineral studies of till samples collected around the Brazil Lake LCT pegmatite, southwest Nova Scotia. Geological Survey of Canada, Open File 8960. https://doi.org/10.4095/331537

McClenaghan, M.B., Paulen, R.C. and Kjarsgaard, I.M., 2019: Rare metal indicator minerals in bedrock and till at the Strange Lake peralkaline complex, Québec and Labrador, Canada. Canadian Journal of Earth Sciences, Volume 56, pages 857–869. https://doi.org/10.1139/cjes-2018-0299

McClenaghan, M.B., Paulen, R.C., Kjarsgaard, I.M., Averill, S.A. and Fortin, R., 2017a: Indicator mineral signatures of the Strange Lake rare earth element deposit, Québec and Newfoundland and Labrador. Geological Survey of Canada, Open File 8240. https://doi.org/10.4095/306239

McClenaghan, M.B., Paulen, R.C., Kjarsgaard, I.M., Averill, S.A. and Fortin, R., 2017b: Indicator minerals in bedrock and till at the Strange Lake REE deposit, Québec and Labrador, eastern Canada. *In* Application of Indicator Mineral Methods to Bedrock and Sediments. *Edited by* M.B. McClenaghan and D. Layton-Matthews. Geological Survey of Canada Open File 8345, pages 78–86. https://doi.org/10.4095/306305

McConnell, J.W. and Batterson, M.J., 1987: The Strange Lake Zr–Y–Nb–Be–REE deposit, Labrador: A geochemical profile in till, lake and stream sediment, and water. Journal of Geochemical Exploration, Volume 29, pages 105–127. https://doi.org/10.1016/0375-6742(87)90073-2

McCurdy, M.W., Amor, S., Corrigan, S.D., Garrett, R.G. and Solgadi, F. 2018. Geochemical atlas of northeastern Québec and mainland Newfoundland and Labrador. Geological Survey of Canada, Open File 8348. https://doi.org/10.4095/306596

Miller, R.R., 1985: Geology of the Strange Lake alkalic complex and the associated Zr–Y–Nb–Be–REE mineralization. *In* Granite-related Mineral Deposits. *Edited by* R.P. Taylor and D.F. Strong. Canadian Institute of Mining and Metallurgy, pages 193–196.

Miller, R.R., 1990: The Strange Lake pegmatite–aplite-hosted rare-metal deposit, Labrador. *In* Current Research. Government of Newfoundland and Labrador, Department of Mines and Energy, Report 90-1, pages 171–182.

Miller, R.R., 1996: Structural and textural evolution of the Strange Lake peralkaline rare-element (NYF) granite pegmatite, Québec–Labrador. The Canadian Mineralogist, Volume 34, pages 349–371.

Miller, R.R., Heaman, L.M. and Birkett, T.C., 1997: U–Pb zircon age of the Strange Lake peralkaline complex: Implications for Mesoproterozoic peralkaline magmatism in north central Labrador. Precambrian Research, Volume 81, pages 67–82. https://doi.org/10.1016/S0301-9268(96)00024-1

Oyediran, Y.O., Robart, M.C., Horsh, H. and Zajac, I.S., 2014: Historical and present day metallurgical development of the Strange Lake Alkalic Complex. *In* Proceedings of the 53rd Conference of Metallurgist – Rare Elements. Canadian Institute of Mining, Metallurgy, and Petroleum, Montreal, Que., Canada. [ISBN: 978-1-926872-24-7]

Paulen, R.C., Eyles, N. and Ross, M., 2024b: Glacial dispersal trains and ice streams on the Canadian Shield. *In* Till Geochemistry and Indicator Mineral Methods for Exploration in Glaciated Terrains. *Edited by* R.C. Paulen and M.B. McClenaghan. Geological Survey of Canada, Open File 9210, pages 140–147. https://doi.org/10.4095/pbmy2d03m0

Paulen, R.C., McClenaghan, M.B. and Evans, D.J.A., 2024a: Glacial erratics and till dispersal indicators. *In* Encyclopaedia of Quaternary Science, 3rd Edition, Reference Module in Earth Systems and Environmental Sciences. *Edited by* S.A. Elias. Elsevier. https://doi.org/10.1016/B978-0-323-99931-1.00277-4

Paulen, R.C., Stokes, C.R., Fortin, R., Rice, J.M., Dubé-Loubert, H. and McClenaghan, M.B., 2017: Dispersal trains produced by ice streams: an example from Strange Lake, Labrador, Canada. *In* Proceedings of Exploration 17. *Edited by* V. Tschirhart and M.D. Thomas. Sixth Decennial International Conference on Mineral Exploration, pages 871–875. https://geochem.nrcan.gc.ca/cdogs/content/pub/pub03698_e.htm

Rice, J.M., Ross, M., Paulen, R.C., Kelley, S.E., Briner, J.P., Neudorf, C.M. and Lian, O.B., 2019: Refining the ice flow chronology and subglacial dynamics across the migrating Labrador Divide of the Laurentide Ice Sheet with age constraints on deglaciation. Journal of Quaternary Science, Volume 34, pages 519–535. https://doi.org/10.1002/jqs.3138

Romppanen, S., Eyles, N., Putkinen, N. and Nygård, H., 2026: Fate of lithium and strategic metals under Pleistocene ice streams. Quaternary Science Reviews, Volume 377. https://doi.org/10.1016/j.quascirev.2026.109853

Shaw, J., Piper, D.J.W., Fader, G.B.J., King, E.L., Todd, B.J., Bell, T., Batterson, M.J. and Liverman, D.G.E., 2006: A conceptual model of the deglaciation of Atlantic Canada. Quaternary Science Reviews, Volume 25, pages 2059–2081. https://doi.org/10.1016/j.quascirev.2006.03.002

Shaw, J., Todd, B.J. and Li, M.Z., 2014: Geologic insights from multibeam bathymetry and seascape maps of the Bay of Fundy, Canada. Continental Shelf Research, Volume 83, pages 55–63. https://doi.org/10.1016/j.csr.2013.12.015

Stea, R.R., 2004: The Appalachian Glacier Complex in Maritime Canada. Developments in Quaternary Sciences, Volume 2, pages 213–232. https://doi.org/10.1016/S1571-0866(04)80199-4

Stea, R.R. and Finck, P.W., 2001: An evolutionary model of glacial dispersal and till genesis in Maritime Canada. *In* Drift Exploration in Glaciated Terrain. Edited by M.B. McClenaghan, P.T. Bobrowsky, G.E.M. Hall and S.J. Cook. Geological Society, London, Special Publication No. 185, pages 237–265. https://doi.org/10.1144/GSL.SP.2001.185.01.11

Stea, R.R. and Grant, D.R., 1982: Pleistocene geology and till geochemistry of southwestern Nova Scotia (sheets 7 and 8). Nova Scotia Department of Mines and Energy, Map 82–10, scale 1:100 000.

Stea, R.R., Seaman, A.A., Pronk, T., Parkhill, M.A., Allard, S. and Utting, D., 2011: Chapter 48 – The Appalachian Glacier Complex in Maritime Canada. Developments in Quaternary Sciences, Volume 15, pages 631–659. https://www.sciencedirect.com/science/article/abs/pii/B9780444534477000489

Strand, P., Banas, A., Baumgartner, M. and Burgess, J., 2009: Tracing kimberlite indicator mineral dispersal trains: an example from the Churchill Diamond Project, Kivalliq region, Nunavut. *In* Application of Till and Stream Sediment Heavy Mineral and Geochemical Methods to Mineral Exploration in Western and Northern Canada. Edited by R.C. Paulen and I. McMartin. Geological Association of Canada, Short Course Notes 18, pages 167–175. https://gac.ca/product/application-of-till-and-stream-sediment-heavy-mineral-and-geochemical-methods/

Taylor, F.C., 1967: Reconnaissance geology of the Shelburne map-area, Queen's, Shelburne, and Yarmouth counties, Nova Scotia. Geological Survey of Canada, Memoir 349, pages 73–75.

Vincent, J., 1989: Quaternary geology of the southeastern Canadian Shield. *In* Quaternary Geology of Canada and Greenland. *Edited by* R.J. Fulton. Geology of Canada. No. 1. Geological Survey of Canada. pages 249–275. https://doi.org/10.4095/127971

White, C.E., 2010: Stratigraphy of the lower Paleozoic Goldenville and Halifax groups in southwestern Nova Scotia. Atlantic Geology, Volume 46, pages 136–154. https://doi.org/10.4138/atlgeol.2010.008

White, C.E. and Barr, S.M., 2017: Stratigraphy and depositional setting of the Silurian–Devonian Rockville Notch Group, Meguma terrane, Nova Scotia, Canada. Atlantic Geology, Volume 53, pages 337–365. https://doi.org/10.4138/atlgeol.2017.015

White, C.E., Barr, S.M. and Linnemann, U., 2018: U–Pb (zircon) ages and provenance of the White Rock Formation of the Rockville Notch Group, Meguma terrane, Nova Scotia, Canada: Evidence for the 'Sardian gap' and West African origin. Canadian Journal of Earth Sciences, Volume 55, pages 589–603. https://doi.org/10.1139/cjes-2017-0196

Wilton, H.C., Thompson, G.M. and Grant, D.C., 2017: The use of automated indicator mineral analysis in the search for mineralization – A next generation drift prospecting tool. *In* EXPLORE. Association of Applied Geochemists, No. 174. pages 1–18. https://doi.org/10.70499/ROVT2038

Zajac, I.S., 2015: John Jambor's contributions to the mineralogy of the Strange Lake peralkaline complex, Québec–Labrador, Canada. The Canadian Mineralogist, Volume 53, pages 885–894. https://doi.org/10.3749/canmin.1400051

Zajac, I.S., Miller, R., Birkett, T. and Nantel, S., 1984: Le gite de Zr, Y, Nb et Be du complex alkaline de Strange Lake, Québec–Labrador. *In* Géologie et métallogénie de la Gaspésie et de la région de la Fosse du Labrador. Québec Ministère de l'Energie et des Ressources Seminaire d'Information DV 84-18. pages 127–142.

Appendix 1

List of potential indicator minerals (>2.8 SG) in the Strange Lake deposit compiled from Birkett *et al.* (1992), Miller (1996), Jambor *et al.* (1998), Gowans *et al.* (2014), Oyediran *et al.* (2014), and Zajac (2015) as well as indicator minerals that were recovered from the >3.0 SG nonferromagnetic fractions of bedrock and till samples in the Strange Lake study (modified from McClenaghan *et al.* , 2019). The yellow highlights minerals not previously known to the Strange Lake deposit, green highlights the new minerals occurring in bedrock, and orange highlights the new minerals found in till heavy mineral concentrates.

Mineral	Formula	Hardness*	Density*	Reported by others	Seen in bedrock PTS in this study	Seen in bedrock HMC in this study	Seen in Till HMC in this study	Element source in glacial dispersal train
U, Th minerals								
cerianite	$(Ce,Th)O_2$	not reported	7.2	no	no	yes	no	Ce, Th
thorite	$Th(SiO_4)$	5.0	4–6.7	Miller (1996)	no	yes	yes	Th
thorianite	ThO_2	6.0	10.0	no	yes	yes	yes	Th
uraninite	UO_2	5–6	6.5–10.95	no	yes	yes	no	U
Zr minerals								
elpidite	$Na_2ZrSi_6O_{15}•3(H_2O)$	7	2.54	Birkett et al. (1992)	yes	no	yes	Zr
hilairite	$Na_2ZrSiO_3O_9•3H_2O$	4.5	2.72	Roelofson & Veblen (1999)	no	no	no	Zr
dalyite	$K_2ZrSi_6O_{15}$	7.5	2.84	Birkett et al. (1992)	no	no	no	Zr
vlasovite	$Na_2ZrSi_4O_{11}$	6	2.97	Birkett et al. (1992)	no	no	no	Zr
zircon	$ZrSiO_4$	7.5	4.6–4.7	Birkett et al. (1992)	yes	yes	yes	Zr
armstrongite	$CaZrSi_6O_{15}•3(H_2O)$	4.5	2.7	Birkett et al. (1992)	no	no	no	Zr
catapleiite	$NaZrSi_3O_9•2(H_2O)$	4.5–5	2.8	Birkett et al. (1992)	yes	yes	no	Zr
Ca-catapleiite	$CaZrSi_3O_9•2(H_2O)$	4.5–5	2.8	Birkett et al. (1992)	yes	yes	no	Zr
calciohilairite	$CaZrSi_3O_9•3(H_2O)$	4	2.68	Birkett et al. (1992)	no	no	no	Zr
gittinsite	$CaZrSi_2O_7$	3.5–4	3.6	Birkett et al. (1992)	yes	yes	yes	Zr
Ti minerals								
aeschynite	$(Y,Ca,Fe)(Ti,Nb)_2(O,OH)_6$	5–6	4.9–9.1	no	yes	no	no	Y
ilmenite	$FeTiO_3$	5–5.5	4.7	Birkett et al. (1996)	no	yes	no	
narsarsukite	$Na_2(Ti,Fe)Si_4(O,F)_{11}$	7	2.7	Miller (1996)	no	no	no	
bafertisite	$Ba(Fe,Mn)_2TiSi_2O_7(O,OH)_2$	5	3.96–4.25	Birkett et al. (1996)	no	no	no	
neptunite	$KNa_2Li(Fe,Mn)_2Ti_2Si_8O_{24}$	5–6	3.23	Birkett et al. (1996)	no	no	no	
aenigmatite	$(Na,Ca)_4(Fe,Ti,Mg)_{12}Si_{12}O_{40}$	5–6	3.7–3.9	Birkett et al. (1996)	no	yes	yes	
astrophyllite	$K_2Na(Fe,Mn)_7Ti_2Si_8O_{26}(OH)_4$	3–3.5	3.3–3.4	Birkett et al. (1996)	yes	no	no	
titanite	$CaTiSiO_5$	5–5.5	3.4–3.56	Miller (1996)	yes	yes	yes	
komarovite	$(Ca,Mn)_2(Nb,Ti)_2Si_2O_7(O,F)_2•3.5(H_2O)$	4	3.61–3.76	no	no	no	yes	Nb
chevkinite	$(Ce,La,Ca,Th)_4(Fe,Mg)_2(Ti,Fe)_3Si_4O_{22}$	5–5.5	4.5	no	no	no	yes	Ce, La, Th

Appendix 1

Phosphate minerals								
xenotime	YPO_4	4–5	4.4–5.1	no	no	no	yes	Y
monazite	$(La,Ce,Y,Th)PO_4$	5–5.5	4.8–5.5	Miller (1996)	yes	yes	yes	Ce, La, Y, Th
fluorapatite	$Ca_5(PO_4)_3F$	5.0	3.1–3.2	no	no	yes	no	
apatite	$Ca_5(PO_4)_3(OH,F,Cl)$	5.0	3.2	Gowans et al. (2014)	yes	yes	yes	
britholite	$(Ce,Ca,Th,La,Nd)_5(SiO_4,PO_4)_3(OH,F)$		4.2–4.7	no	yes	no	no	Ce, La, Th
rhabdophane	$(Ce,La)PO_4•(H2O)$	3.5	4.0	no	no	yes	yes	Ce, La
Other minerals								
gadolinite group	$Be_2(Ca,REE, Fe)_3Si_2O_{10}$	6.5–7	4.2	Miller (1996)	no	no	no	Be, Ce, La, Y
arfvedsonite	$Na_3Fe_4Fe(Si_8O_{22})(OH)_2$	5.5–6	3.44–3.45	Miller (1996)	yes	yes	yes	
aegerine	$NaFe(Si_2O_6)$	6.0	3.5–3.6	Miller (1996)	yes	yes	yes	
pyrochlore	$(Na,Ca)_2Nb_2O_6(OH,F)$	5–5.5	4.2–6.4	Miller (1996)	yes	yes	yes	Nb
bastnaesite	$Ce(CO_3)F$	4–5	4.95–5	Miller (1996)	no	no	yes	Ce
parisite	$Ca(Ce,La)_2(CO_3)_3F_2$	4.5	4.4	Gowans et al. (2014)	no	yes	yes	Ce, La
kainosite	$Ca_2(Y,Ce)_2Si_4O_{12}(CO_3)•H_2Oleif$	5–6	3.4–3.6	Miller (1996)	no	no	yes	Ce, Y
anthophyllite	$Mg_7(Si_8O_{22})(OH)_2$	5–6	2.9–3.6	no	no	no	yes	
allanite	$(Ce,Ca,Y)_2(Al,Fe)_3(SiO_4)_3(OH)$	5.5	3.3–4.2	Birkett et al. (1992)	yes	no	yes	Ce, Y
milarite	$K_2Ca_4Al_2Be_4Si_{24}O_{60}•(H_2O)$	6	2.52	Gowans et al. (2014)	no	no	no	Be
gerenite	$(Ca,Na)_2(Y,REE)_3Si_6O_{18}•2(H_2O)$	5	3.3–3.52	Jambor et al. (1998)	no	no	no	Ce, La, Nd, Y
leifite	$Na_2(Si,Al,Be)_7(O,OH,F)_{14}$	6	2.57	Sinclair et al. (1992)	no	no	no	Be
danburite	$CaB_2Si_2O_8$	7.0	3.0	no	no	yes	no	
zajacite-(Ce)	$Na(REE_xCa_{1-x})(REE_yCa_{1-y})F_6$ where (x ne y)	3.5	4.4–4.6	Jambor et al. (1996)	no	no	no	Ce, La, Nd
gagarinite-(Y)	$NaCaY(F,Cl)_6$	4.5	4.2	Jambor et al. (1996)	yes	no	no	Y
sphalerlite	(Zn,Fe)S	3.5–4	3.9–4.2	Miller (1996)	no	no	no	
molybdenite	MoS_2	1.0	5.5	no	no	yes	no	
galena	PbS	2.5	7.2–7.6	Miller (1996)	no	no	no	
fluorite	CaF_2	4.0	3.0–3.3	Miller (1996)	yes	yes	yes	

* source of information www.webmineral.com

Appendix 2

List of potential indicator minerals of the North and South pegmatites at Brazil Lake summarized from bedrock descriptions by Taylor (1967), Hutchinson (1982), Corey (1995), Hughes (1995) and Kontak (2004, 2006), and a listing of indicator minerals found in till samples in the Brazil Lake survey (McClenaghan *et al.,* 2025). The yellow highlights minerals not previously known to the Brazil Lake pegmatites, green highlights the new minerals occurring in bedrock, and orange highlights the new minerals found in till heavy mineral concentrates

Mineral	Formula	Specific gravity (SG)	Hardness (H)	In bedrock HMC in this study?	In till HMC in this study?	First reported presence in deposit	Fractions that indicator minerals were recovered from in this study
spodumene	$LiAlSi_2O_6$	3.1–3.2	6.5–7	yes	yes	Taylor (1967); Kontak (2004)	2.8–3.2 SG 0.25–
tourmaline–schorl/dravite	$Na(Fe,Mg)_3Al_6Si_6O_{18}(BO_3)_3(OH)_2$	3.03–3.22	7	yes	yes	Taylor (1967); Kontak (2004)	2.8–3.2 SG 0.25–0.5 mm
green beryl	$Be_3Al_2Si_6O_{18}$	2.63–2.9	7.5–8	no	no	Taylor (1967); Kontak (2004)	NA
columbite	$(Mn,Fe)(Nb,Ta)_2O_6$	5.3–7.3	6	yes	yes	Taylor (1967); Kontak (2004)	>3.2 SG 0.25–0.5 HMC
tantalite	$(Fe,Mn)Ta_2O_6$	8.1-–8.2	6–6.5	yes	yes	Taylor (1967); Kontak (2004)	>3.2 SG 0.25–0.5 HMC
blue apatite	$Ca_5(PO_4)_3(OH,F,Cl)$	3.16–3.22	5	yes	yes	Taylor (1967); Kontak (2004)	2.8–3.2 SG 0.25–0.5 mm
triplite	$(Mn,Fe)_2(PO_4)(F,OH)$	3.5–3.9	5–5.5	no	no	Kontak (2004)	NA
montebrasite	$LiAlPO_4(OH)$	5.5–6	2.98–3.04	no	no	Kontak (2006)	NA
crandallite	$CaAl_3(PO_4)_2(OH)_5•(H_2O)$	2.78–2.92	4	no	no	Kontak (2006)	NA
goyazite	$SrAl_3(PO_4)_2(OH)_5•(H_2O)$	3.16–3.28	4–5	no	no	Kontak (2006)	NA
lithiophilite	$LiMnPO_4$	3.29–3.50	4	no	no	Corey (1995); Kontak (2004)	NA
fillowite	$Na_3CaMn_{11}(PO_4)_9$	3.43	4.5	no	no	Kontak (2006)	NA
variscite	$Al(PO_4)•2(H_2O)$	2.5–2.52	4–5	no	no	Corey (1995)	NA
florencite	$(La,Ce)Al_3(PO_4)_2(OH)_6$	3.46–3.71	5–6	no	yes	this study (in till only)	>3.2 SG 0.25–0.5 HMC
heterosite	$(Fe,Mn)PO_4$	4–4.5	3.4	yes	no	this study	>3.2 SG 0.25–0.5 HMC
uraninite	UO_2	6.5–10.95	5–6	yes	no	this study	pan conc, >3.2 SG 0.25–0.5 HMC
zircon	$Zr(SiO_4)$	4.6–4.7	7.5	yes	yes	Corey (1995); Kontak (2004)	>3.2 SG 0.25–0.5 HMC
cassiterite	SnO_2	6.8–7	6–7	yes	yes	Corey (1995); Kontak (2004)	pan concentrate
wolframite	$(Fe, Mn)WO_4$	7–7.5	4–4.5	no	no	Kontak (2004)	NA
scheelite	$CaWO_4$	5.9–6.1	4.5–5	no	yes	this study (in till only)	>3.2 SG 0.25–0.5 HMC
sphalerite	(Zn,Fe)S	3.9–4.2	3.5–4	yes	yes	Kontak (2004)	>3.2 SG 0.25–0.5 HMC
pyrite	FeS_2	4.8–5	6–6.5	yes	yes	this study	pan conc, >3.2 SG 0.25–0.5 HMC
arsenopyrite	FeAsS	6	5.5–6	yes	no	this study	pan concentrate
loellingite	$FeAs_2$	7.43	5–5.5	yes	no	this study	pan concentrate
pyrolusite	MnO_2	5	2–6.5	yes	no	this study	>3.2 SG 0.25–0.5 HMC

HMC = heavy mineral concentrate; NA = not applicable, SG = specific gravity

Exploration Geochemistry: From Noise to Anomaly!

Réjean Girard, P.Geo
IOS Géosciences Inc, 1319 St-Paul Boulevard, Saguenay, QC, G7J 3Y2
(email: rejeang@iosgeo.com)

Introducion

Since only 2% of the Canadian Shield is outcropping, exploration has to rely upon indirect methods, either by geophysics or by geochemistry. While geophysics is efficient at accurately pinpointing the anomalies, it usually does not provide insight on cause or significance of the anomaly. Inversely, geochemistry is perceived as providing insights on metal endowment but failing to locate the source of these metals. In fact, mines discovered with the use of geochemistry are seldom, although well-documented in literature about case studies. This issue originates from the inability to discriminate true from false anomalies typically caused by feeble signal-to-noise ratios (Fig. 1). There cannot be an anomaly related to a mineral deposit in every survey! and most statistical data processing used by geochemist ineluctably generate intrinsic "hot spots". Anomalous samples should not be limited to those that are more enriched than the others; rather, a true outlier value should be calculated based on the survey results.

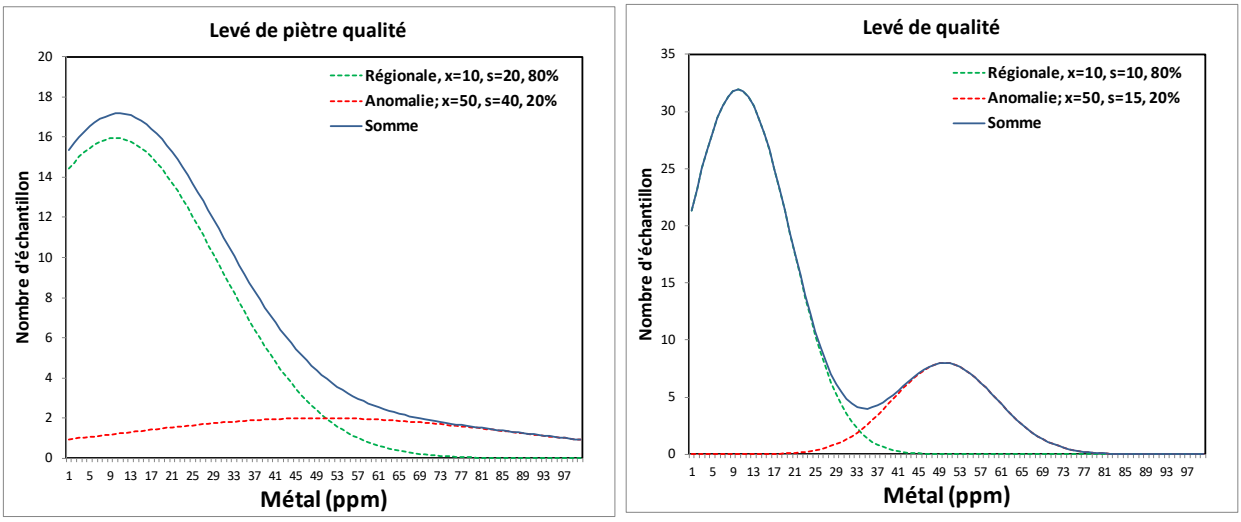


Figure 1. *Modelled density function ("histogram of grades") of a background plus anomalous populations with high variance (left) and low variance (right). Notice how the bimodality induced by the anomalous population is not discernible in a noisy survey.*

Metal enrichments in various media of the secondary environment (glacial sediments, lake bottom sediments, soils, humus, tree bark, *etc.*) relate not only to metal abundance in the source bedrock (mineralization or barren rocks), but also, and dominantly, to the capacity of the material to accumulate these metals in favorable chemical or physical conditions (*e.g.*, Eh, pH, grain size, porosity, *etc.*). Metals accumulate either in detrital minerals, or in cationic (or hydromorphic) forms adsorbed to organic matter and clays or precipitated as colloids or authigenic minerals. Metal behaviours under these two forms are fundamentally different and requires different interpretation approaches. Furthermore, different metals are expected to show different behaviours, especially in cationic form, causing differential enrichments that disrupt typical metallogenic associations.

Regardless of the care deployed by the samplers, collected material will be heterogeneous, with diverse proportions of its various constituents. Glacial till will be more or less clayey, heavy mineral rich, oxidized or reworked. Gyttja will be organic rich or terrigenous-dominated, potentially containing authigenic iron hydroxides, sulphides or carbonates, *etc*. Soils can be acidic or neutral, oxidizing or reducing, lixiviated through illuviation, enriched by evaporation, containing deflation lags (wind erosion), *etc.* Each of these parameters, randomly distributed, acts independently on the overall metal content and with a compound effect on metal availability from the source rock. Metal deportment among the diverse constituents, and in different proportions, will cause fluctuations in the overall metal content, including significant local enrichments that can be confused with an anomaly derived from local mineralized occurrences. Hence the likelihood of false anomalies induced by stochastic fluctuations of the background.

Improving Signal to Noise Ratios: Continuous Variables

In anomalous samples, chemical signal derived from local sources that is meaningful regarding exploration, adds to the meaningless, but ubiquitous regional signal. Unless the anomalous component is very intense, it will be difficult to discriminate it from the intrinsic fluctuations of the background signal. Signal-to-noise ratio is typically low and must be discriminated in most surveys, especially regional ones where sampling sites can be distant from mineral occurrences. Improving the signal-to-noise ratio requires to denoise the surveys. First steps involve high-quality sampling, and accurate quality control of the analyses. However, intrinsic noise induced by the variability of the sample material cannot be removed through analysis procedures.

Sample material, mostly sediments, are mixture of different materials, each with its own metal contrasting content. For example, copper in soil is not expected to be contained in feldspars or quartz, but rather in in ferromagnesian minerals (up to tens of ppm), adsorbed on organic matter or iron oxy-hydroxides, or in detrital chalcopyrite and other copper minerals. Since copper minerals can account for a few gains in a digested aliquot (1 gram of -100 um is expected to contain about 300,000 grains, so one chalcopyrite grain accounts for 1 ppm Cu), the presence of chalcopyrite is overshadowed by the signal induced by ferromagnesian minerals. A similar issue affects lithium, as it can become incorporated into feldspars and micas, masking the signal from rare spodumene grains.

Metal contribution of a certain material type is a linear function of the abundance of this material. Doubling the abundance of ferromagnesian minerals will double their copper contribution. Regressing (normalizing or standardizing) the metal against iron is a common practice. However, metal abundance will also be affected by the variation of abundances of oxy-hydroxide or organic matter. Minimizing the effect of these fluctuations can be achieved using multiple regressions based on chemical proxies of these various material types, labelled as “Xs” variables. For example, magnesium can be used to assess the abundance of ferromagnesian minerals, while potassium is used for feldspars and phyllosilicates, manganese or iron for oxy-hydroxides precipitates, and loss on ignition (LOI) as a proxy for organic matter. Such multiple regressions, not to be confused with cascading regressions on the various parameters, can be computed in a simple Excel spreadsheet and does not require high-end software.

Regressions are based on a few premises:

- The influenced variable (“Y” or metal content) is linearly correlated to the controlling variables (“Xs” or proxies of material types);
- The variables follow a normal distribution;
- The “Xs” are quasi-independent;
- There is no severe outliers that can leverage the regression line.

If the variables are not linear or following a normal distribution, they would require to be transformed into such distributions. Trace elements are typically log-normally distributed, meaning the regression needs to be performed on the logarithms of metal abundances. Although

the metal abundance can imperfectly correlate to numerous other metals, the regression shall be performed only on controlling variables. Using a multitude of non-influential variables induces biases on the regressions. For example, zinc is generally correlating to cadmium, adding cadmium to the multiple regression is likely to induce spurious trends. Another point of concern is in regard of digestion methods. Most geochemical surveys use partial leaching methods, and selected proxies must be properly analyzed. Common example is for sodium or potassium in felspars, which is not digested in *aqua regia*.

Regression analysis will yield a best fit brane (line, surface, *etc.*), from which a predicted metal content can be computed. The difference between the real and the predicted metal content is referred as the residual and it shall be used for survey interpretation, since it represents the metal in excess to what the sample shall contain. The variability of the background component is significantly reduced, improving the contrast between anomalous and background signal.

Improving Signal to Noise Ratios: Quantified Variables

Chemical analyses are continuous variables, down to the detection limit. However, not all data are continuous, but may group into subpopulations based on data that are:

- Tagged or labeled such as sediment type (lodgement or ablation tills), pedofacies (podzols, gleysols, brunisols), stratigraphy (quaternary or subjacent bedrock), the color of the sample, *etc.*;
- Discreet values represented by positive integers, such as the number of gold grains or indicator minerals;
- Affected by discontinuous distributions or functions, such as normative calculations or acidity that is controlled by buffer reversible reactions;
- Quantized where ranges of continuous values are binned, such as in classification diagrams based on chemical composition (*e.g.*, alkali-silica LeMaître diagram or Piper diagram for groundwater) (Fig. 2).

Subpopulations in a sample set may have distinctive chemical signatures, where anomalous values in depleted subset is comparable to the background in the other subsets. Hence, compiling all the data into a single population requires standardization of each of them to uniformize the

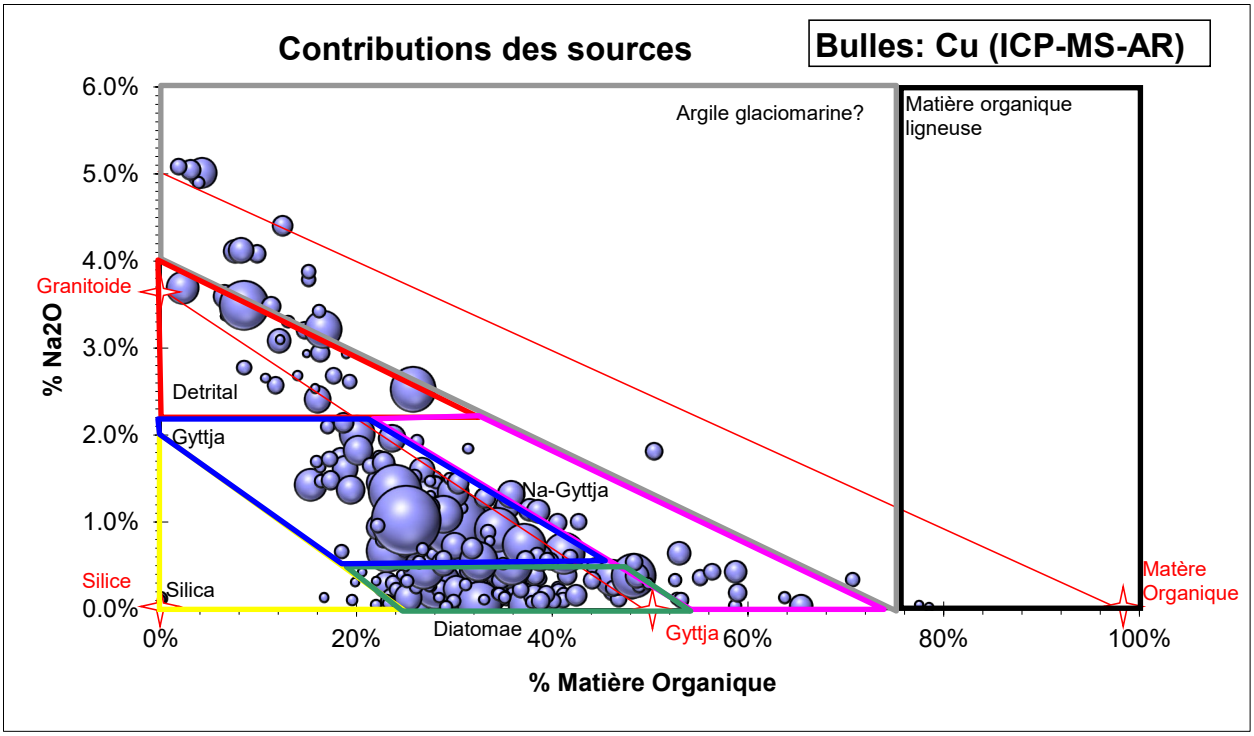


Figure 2. *Classification diagram of lake bottom sediments, opposing a proxy for organic matter against proxy for detrital matter, providing an example of quantized data. Each group of samples have different metal abundances and shall be interpreted independently.*

distribution of values. This standardization can be achieved by calculating the standard scores (Z-scores) of samples within each subpopulation, or by normalizing the data to a constant value for a specific percentile, usually the 80th. By doing such, the cumulative distribution curves of the different subpopulations are coincident, and the subgroups can be compared. Using the 80th centile enables the convergence to be close to most anomaly thresholds. Using Z-scores enable convergence of both averages and standard deviations, enabling a better fitting, although more sensitive to outliers.

A common example of this issue is in regard of metal content of various glacial sediment types. Lodgement or basal tills are typically rich in clay minerals and are impermeable, preserving the sulphides from oxidizing by the groundwater. Inversely, ablation or melt-out tills are heavily exposed to water and their sulphides are readily oxidized. Chalcophile metals, such as copper and arsenic, were leached from ablation tills and are present in quantities an order of magnitude lower than those in the lodgement tills. Another example is for soils (B horizon or humus) that are sensitive to drainage and hence support different types of vegetation. Samples collected in spruce forest, pine forest or alder strands have therefore different metallic signatures.

Cation Exchange Capacity

In most material, metals in cationic states are present in two reservoirs which are in equilibrium. First are the metals in solution in the interstitial pore water (or soil solution). The bulk of this water is usually drained during sample preparation, and typically 0–10% moisture is preserved when samples are considered dried. Metal abundance from the soil-solution can be estimated from salinity, which relates to electrolytic conductivity of the drained water or on saturated paste. Electrolytic conductivity (or total dissolved solids, TDS) is usually measured along with acidity and oxidation-reduction potential (ORP). The bulk of this salinity is induced by sodium and potassium, and variably from magnesium, calcium and ferrous iron (Fe^{2+}). Metal concentrations in the interstitial solution are expected to be more-or-less in equilibrium with the metals in adsorbed state. However, the main reservoir of metals in cationic state is the adsorption on organic matter or clays and is usually referred as the cationic exchange capacity (CEC).The CEC is usually expressed as millimole (centimole in agricultural science) of charges per kilogram of material, assuming total ionisation of the metal, such as for Na^+ ($Na^+_{equivalent}$). It represents the maximal amount of metals that can be adsorbed in the soil, whilst the excess remains in solution. Concentration of the interstitial solution is itself constantly fluctuating depending on water influx (ground water, precipitation, etc.) and outflux (evaporation, drainage, *etc.*). CEC of fatty humic soil is about 3000 mmol/kg, while clays are 300 mmol/kg. Therefore, organic matter is 10x more effective than clays at adsorbing metals. CEC of sands or fibrous undecomposed organic matter is non-existent. Inversely, anionic exchange capacity, which bound anions to positively charged particles, is dominated by iron and aluminum oxi-hydroxides and is far less prevalent than CEC. For specific metal, contribution to charge molarity in mmol/kg can be calculated as the content (ppm) multiplied by its valency, divided by its atomic weight.

Metals in solution compete to access negatively-charged sites. The strength of the bonds is related to the charge density times the ionisation rate. Charge density is dictated by ionic potential, or the ratio of charges over ionic radius. Small heavily charged atoms, such as Al^{3+} (ionic potential or ø=6) is more tightly bound than Fe^{2+} (ø=4), which is weaker than Na^{1+} (ø=1). This factor is counterbalanced by the ionization constant (K_D), where cations with high ionic potential are harder to dissociated in the soil solution, forming insoluble minerals or precipitates. The ionization constant is related to ionization potential (E_i) and electronegativity, which is the amount of energy

required to strip an electron from an atom. Inversely to ionic potential, ionization potential decreases with ionic radius, and hence with atomic weight.

Since the abundance of organic matter (abundance of clays can be ignored in most non-tropical soils) varies from sample to sample, the CEC of the sample varies accordingly, and so is its adsorbed metal content. Measured metal abundance must be standardized accordingly. However, accurate measurement of CEC is complex and costly, so very seldomly available. Proxies can be used for standardization, although not thoroughly reliable:

- Total molarity of charge, which is the sum of the molarity of each cation multiplied by its charge. Acidity (H^{+} molarity) needs to be included. Metals in very low concentrations (ppb range) are of limited effects;
- Dominant base (Na^{1+}, K^{1+}, Mg^{2+}, Ca^{2+}) molarity of charge. Commercial ionic leaching methods do not provide sodium, and most methods do not provide potassium, leaving an uncertainty to the proxy;
- Enhanced dominant base (K^{1+}, Mg^{2+}, Ca^{2+}, Fe^{2+}, Mn^{2+}), the most accurate method to the author's knowledge;
- Rb^{1+} molarity. Since rubidium is ubiquitous, uniformly distributed in most instances, thoroughly ionized, insensitive to acidity and ORP, and with a very small ionic potential, its adsorption is not controlled by the relative abundances of other cations and only by CEC;
- Electrolytic conductivity, assuming the soil-solution concentration is in equilibrium with the adsorbed metal, is a dubious assumption.

Acidity

Ambient acidity has very limited effect on metal content of the detrital minerals, but drastic effect on metals in cationic (hydromorphic) or authigenic states. Consequently, it's measurement is not useful for till geochemistry, but essential for soils, lake bottom sediments or water chemistry. It can be measured directly during fieldwork or at base camp with simple equipment. It is however plagued with imprecision and quality issue, and proper routine calibration and QAQC protocols are mandatory. Acidity measurements are usually coupled with ORP and salinity (either conductivity or TDS) measurements. However, as soon as the samples are removed from their

natural environment, they interact with ambient conditions (air), which is oxidizing, and measurements begin drifting. Acidity, and covariant ORP affects metal abundance in three ways:

1. Acidity related to H^+ concentration in the solution: H^+ cations compete with other cations to access negatively-charged adsorption sites, differentially displacing adsorbed metals. For reference purposes, a pH of 6 is equivalent to about 1 mmol/kg, or 1 ppm H^+. Under acidic conditions, hydrogen ions are significant competitors to other cations on accessing adsorption sites, but are replaced by Ca^{2+} and Mg^{2+} under more alkaline conditions.

2. Acidity and ORP affect the speciation of the metals: It is specific to each metal, according to their Pourbaix diagrams. Metals can be variably maintained in their ionic state, either in solution or adsorbed, under specific acidity or ORP ranges or precipitated into insoluble phases under other ranges. If precipitated, the metal is depleted in its cationic state but accumulates in precipitates. Some metals are insensitive and remains in ionic state in the whole eH-Ph ranges, such as alkali metals (Li^{1+}, Rb^{1+}, Cs^{1+}) that does not accumulate in soils. Some have constant valency and are consequently not affected by ORP, but only by acidity. Examples are divalent cations, such as Ca^{2+} or Mg^{2+}, which remain in cationic state except in alkaline conditions where they hydrolyse into hydroxides. Some trivalent cations (Al^{3+}) or most lanthanides or tetravalent cations, such as Zr^{4+} or Si^{4+}, undergo various states of hydrolysis depending of acidity. Finaly, most transition metals and metalloids are polyvalent, and sensitive to both acidity and ORP. They can form various species, such as positively charges cations (ex: V^{3+}) or oxycations (VOH^{++}), negatively charged oxyanions (ex: $VO_2(OH)_2^-$ or $H_2AsO_4^-$), neutral molecules (ex: $HAsO_2$) or precipitate (ex: As_{metal} or V_2O_3). These different species will exhibit different behaviour, where cations or oxycations adsorb on clays and organic matter until all negative charges are balanced, while neutral molecules and oxyanions will remain in solution, and precipitates will accumulate. Abundance of metals in solution, either in adsorption state or in the authigenic phases will change accordingly.

3. Acidity and ORP will affect the speciation of dominant cations: These are abundant enough to buffer acidity or ORP fluctuations through precipitation or dissolution of the precipitates. Precipitation of such authigenic minerals is reputed to co-precipitate a variety of other metals and hence controlling their abundances in the solution. Furthermore, dissolution or precipitation of these dominant bases (cations) change their concentrations in the solution, affecting their

availability to occupy negatively charged sites, and thus enabling higher concentration of other metals to be adsorbed. In sediments, important reversible reactions are $Fe^{2+} \leftrightarrow Fe_2O_3$ (iron oxi-hydroxides) and $H_2S \leftrightarrow SO_4^{--}$(sulphide-sulphate), which are the main pH- and Eh-dependant reactions plus $Al^{3+} \leftrightarrow AlOH^{2+} \leftrightarrow Al_2O_3 \leftrightarrow AlO_2^{-}$ and $CO_2 \leftrightarrow HCO_3^{-} \leftrightarrow CO_3^{--}$ (carbon dioxide, bi-carbonate and carbonate) which are only dependant on acidity (Fig. 3). The carbonate-bicarbonate reaction is important due to its effect on the dissolution or the precipitation of calcium, magnesium and iron-manganese into carbonate reservoir. This controls availability of adsorption sites.

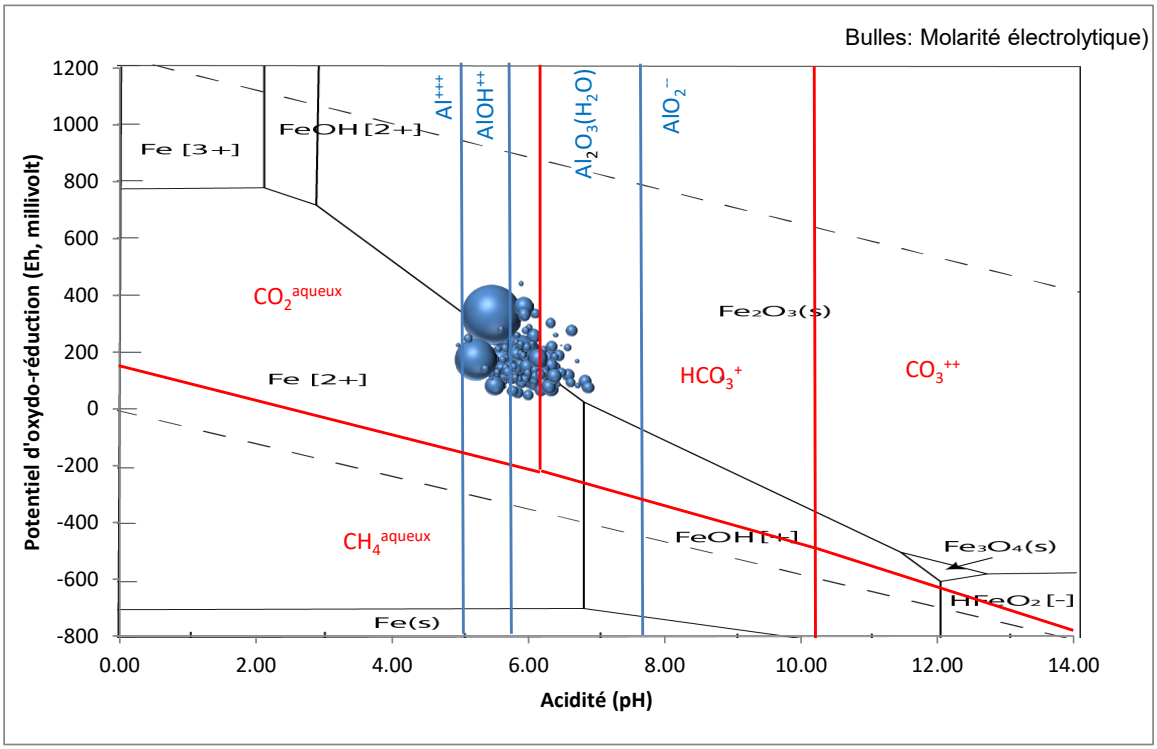


Figure 3. *Acidity and ORP in lake bottom sediments plotted on iron, carbon and aluminium Pourbaix diagrams. The system is invariant anchored on $Fe^{+2} \leftrightarrow F_2O_3$ and $Al^{+3} \leftrightarrow AlOH^{+2}$ buffers and bounded by the bicarbonate reaction.*

Metal abundances in regards of acidity is non-linear discontinuous function dependant on aforementioned reversible buffer reactions (Fig. 4). Each range of acidity between these reactions must be corrected individually, and metal concentrations shall be quantized or binned. Since each metal reacts differently to acidity (Fig. 5), quantized corrections cannot be universally applied, and shall be empirically calculated for each metal individually. Large sets of analyses are required. Corrections for acidity must be compound to the CEC standardization (Fig. 6). The compound effect of these corrections can reach up to an order of magnitude. It is very efficient at correcting results from mild leaching methods, such as MMI, MIG or Ionic Leach, or more conventional sodium pyrophosphate, hydroxylamine or magnesium chloride leaching. Effect of this correction

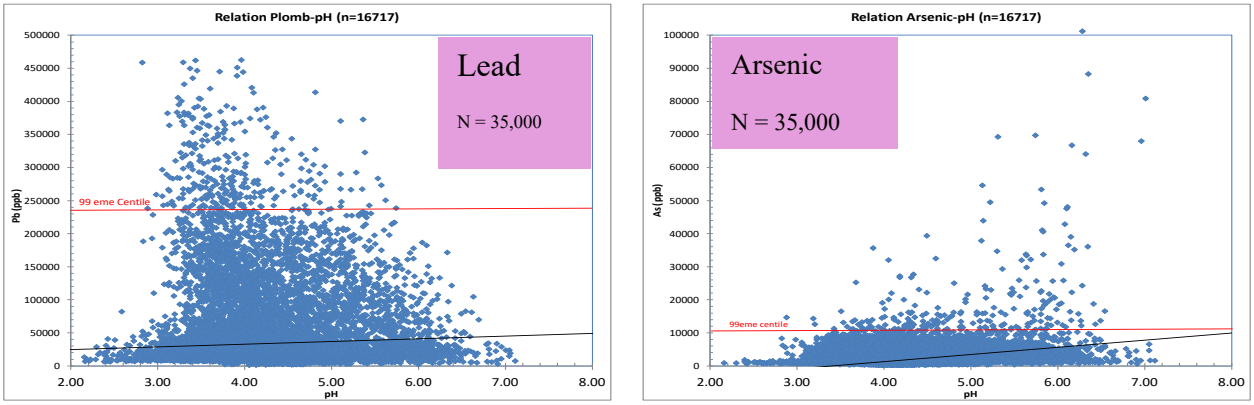


Figure 4. *Distribution of lead (left) and arsenic (right) in humic soil against acidity. Breaks in the distribution are noticeable, with lead enriched in acidic soil and arsenic enriched in neutral soils. Breaks in the distribution are induced by different speciation under different pH ranges.*

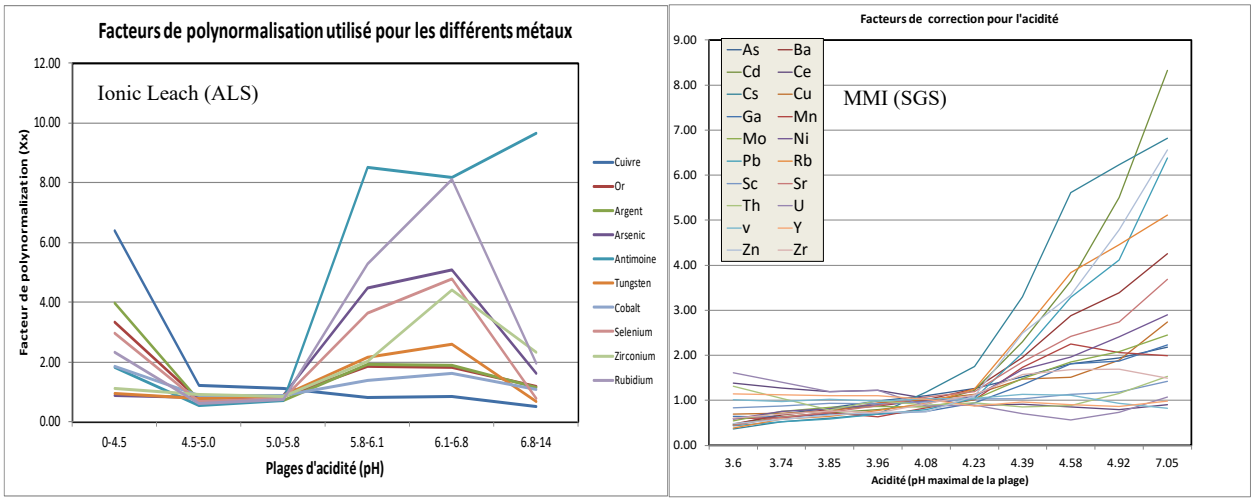


Figure 5. *Standardization factors for various metals according to acidity ranges for Ionic Leach ® and MMI ® partial leach analyses.*

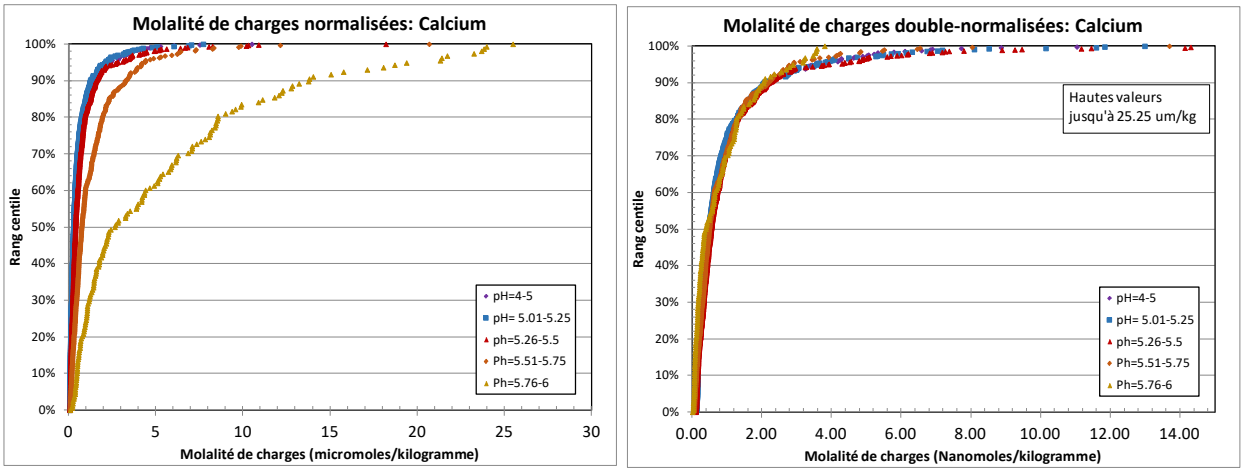


Figure 6. *Charge molarity standardized for CEC of calcium under different acidity ranges (left), and standardized for each acidity ranges (right).*

is however limited for aggressive digestions, such as *aqua regia*, *aqua fortis* or multi acids, where the ionic signal is masked by mineral signal.

NCR Transform

Geochemical data are not normally distributed. They are limited between 0 and 1 (0 to 100%) and tends to be heavily skewed when close to zero (*e.g.*, trace elements) or e to one (*e.g.*, SiO_2 in quartzite). They represent a logit-normal distribution, which can be estimated by a log-normal distribution for trace elements or a normal distribution for abundant elements (major oxides). Most statistical estimators (average, variance, kurtosis, *etc.*) are related to normally distributed data and prone to generate erroneous estimations when applied to highly asymmetrical distribution. This can be noted by the divergence between the median and the average, or by a leptokurtic distribution.

Central limit theorem states that the summation of different random populations (not necessarily normal) tends toward normality. Similarly, the compound effect of different random variables (or summation of their logarithms) leads to a log-normal distribution. So, distributions of trace metal abundances in a regional background is expected to closely follow a log-normal distribution.

To enable modelling of the data distribution, it is necessary to normalize them, and hence transforming their distribution into a normal distribution. For trace elements, this is achieved by computing their logarithm (base 10) and using these logarithms for interpetation or modelling. Furthermore, to enable comparison between different metals, variables or surveys, data shall be converted into Z-scores, which have centered (average of 0) and reduced (standard deviation of 1) distribution $Z_{log} = (x_{log} - \mu_{log})/\sigma_{log}$. The NCR transform can be applied to the raw datas, standardized data, quantilized data or even residuals (Fig. 7).

True or False Anomaly: The Stochastic Modelling

The goal of geochemical exploration is to discriminate locally anomalous metal sources from an ubiquitous background signal. The background signal is random but ruled by probability laws.

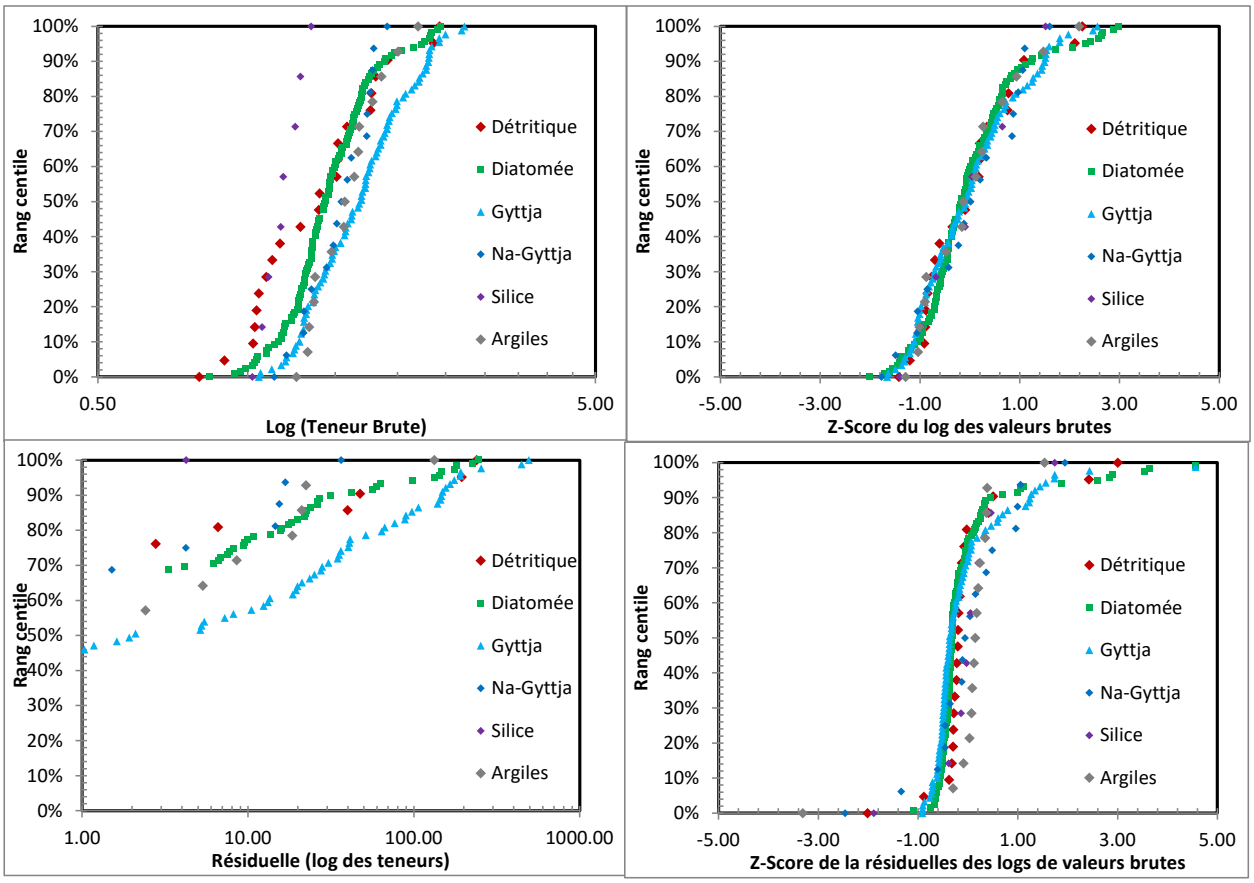


Figure 7. *Cumulative diagram of copper abundance (Fig. 2) in the different type of lake bottom sediments Significant differences are noted for the raw analyses (upper-left), which can be removed through standardization independently for each group of samples (upper-right). Residuals computed on the logarithm of the values regressed against iron, magnesium, sodium and organic matter (lower-left) shows important differences, which are removed through standardization (lower-right).*

It is prone to generate elevated values that can be misinterpreted as anomalies. In any sample, metal abundances will be the sum of the regional contribution, plus the anomalous contribution from local sources (Fig. 8). Metal abundances in a sample are controlled both by the metal availability, which depends if the signal is from a pervasive background or from local sources, and by local conditions controlling its accumulation. The latter are not dependant on metal abundances or the proximity of a source. Metal abundances in the source rock depend on the lithofacies, each with a specific metal abundance distribution. Central limit theorem indicates that mixing different proportions of various rock types with diverse metal contents ineluctably leads to a log-normal distribution of trace metal abundances. Adding a distinctive contribution from mineralized occurrence is expected to cause drifting from lognormality, which would generate outliers, a bimodal distribution, or more commonly a tail of elevated values. This would be inducing a kurtosis on the distribution. In the latter case, discrimination of the anomalous contribution from the regional contribution is fastidious and requires modelling.

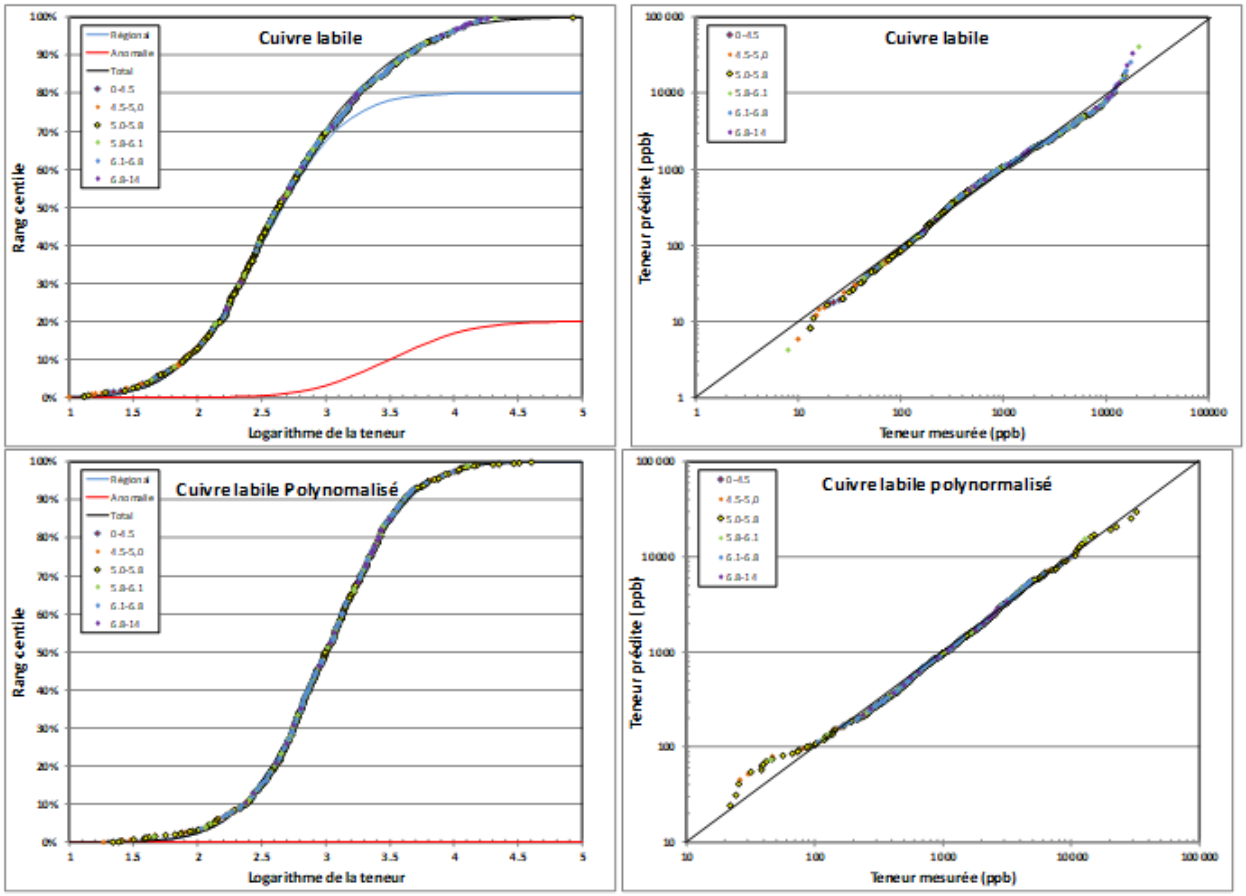


Figure 8. *Cumulative diagram of copper with the cumulative probability functions best fitting the population (upper left). The addition of an anomalous population is needed to fit the data, which represent false anomalies. QQ-plot of the centile distribution* versus *the calculated probabilities where the anomalous population is evident. If data are standardized for CEC and acidity, the cumulative distribution fits the cumulative probability function (lower-left), suggestive of the absence of anomalies (lower-right).*

If the distribution of metal abundances follows a probability function, it means that each metal abundance, either as ppm, log of ppm or Z-score, is attached to a probability of occurring. This can be computed. For example, in a dataset of 100 samples, a sample shall have a probability of 84% to have a Z-score of 1 or less (*e.g.*, one standard deviation), 97.5% for a Z-score of 2, or 99.85% for a Z-score of 3 etc. However, since there are only 100 samples, the probability of having a Z-score of 3 is unlikely, since it represents one sample in 667. By the same logic, the maximum Z-score for a dataset of 100 samples shall be about 2.33. In such event, an additional metal contribution is likely needed, which would relate to a distinct local source (Fig. 9). Hence, that specific sample is deemed undubiously anomalous. Similarly, the second highest sample shall have a maximum Z-score of 2.05. If three (or more) samples equal or exceed such Z-score, it implies that one of these samples is anomalous, although we cannot know which one. It implies that these three samples have about 33% chances of being anomalous. The probability of an anomalous con-

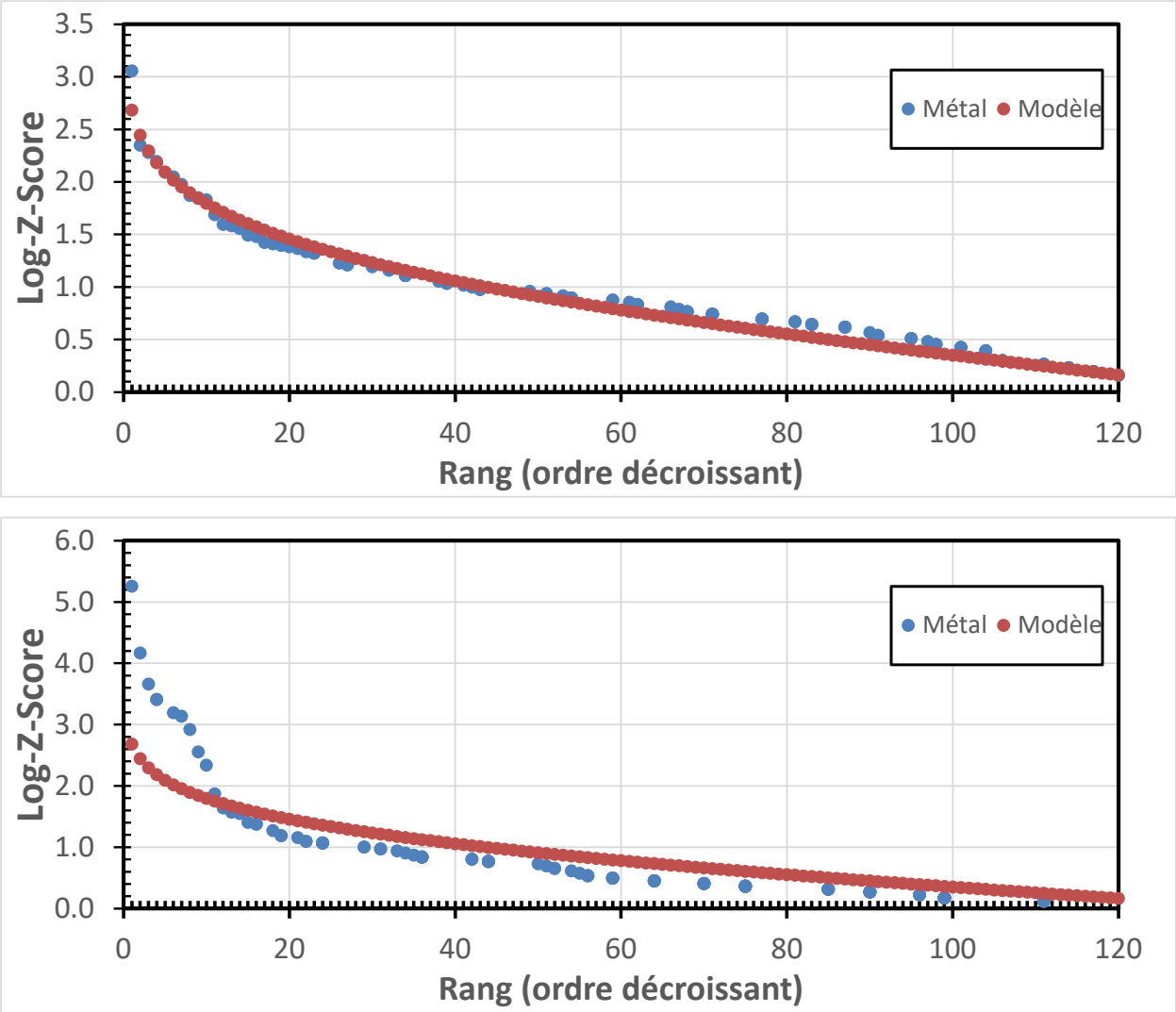


Figure 9. *Log-Z-scores of rubidium (top) and sulphur (bottom) presented in decreasing order, along with the inverted cumulative probability function. The model curve is computed from a centered and reduced log-normal probability distribution. It is noted that rubidium, a ubiquitous metal, closely follows the log-normal distribution, while sulphur has an anomalous population with log-Z-scores indicating unrealistic probabilities for a log-normal distribution of 250 samples.*

tribution to each sample can be computed (Fig. 10) and displayed on an "unlikeliness" map. The process can be applied to raw analyses, standardized data, NCR transformed data or their residuals (Fig. 11).

Grain Counts and Discreet Probabilities

Geochemical analyses generate near continuous data, down to the limit of detection. Grain counts, such as gold grains or kimberlitic indicators, are discreet counts, or real positive integers. They consequently follow a different set of probability laws. The number of grains in a sample is

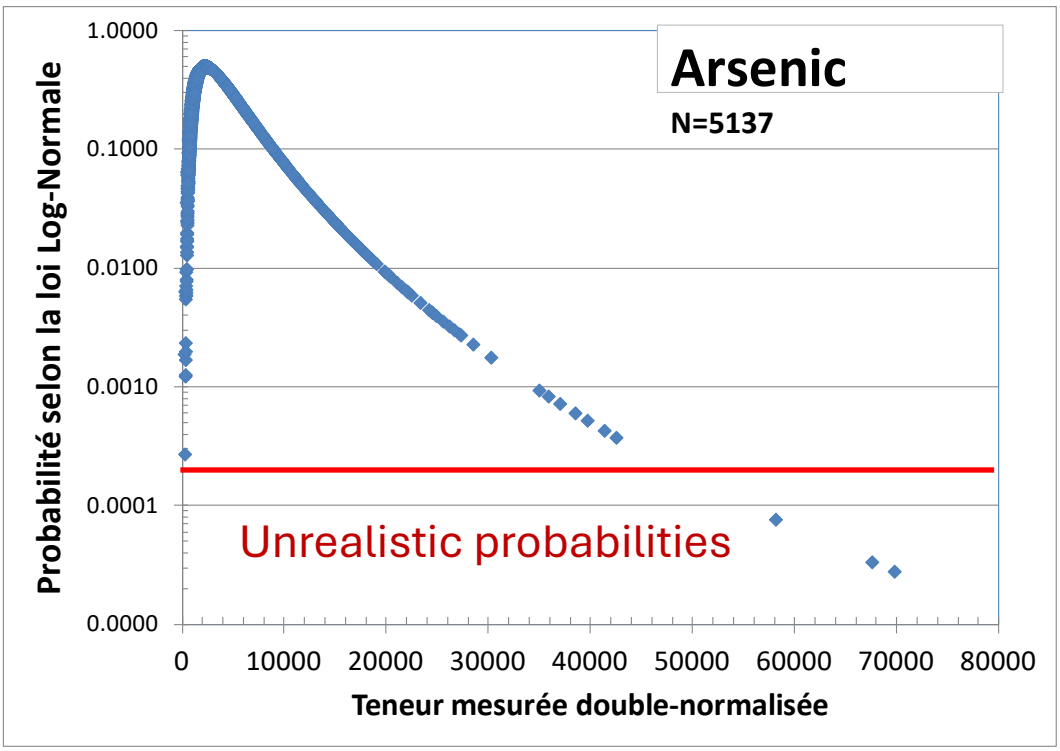


Figure 10. *Computed probability of having a certain abundance (normalized for CEC and acidity, arsenic in humus). In this example, three very riche samples have a probability of occurrence of lesser than 1:5137, meaning they are unlikely to be generated by the background signal.*

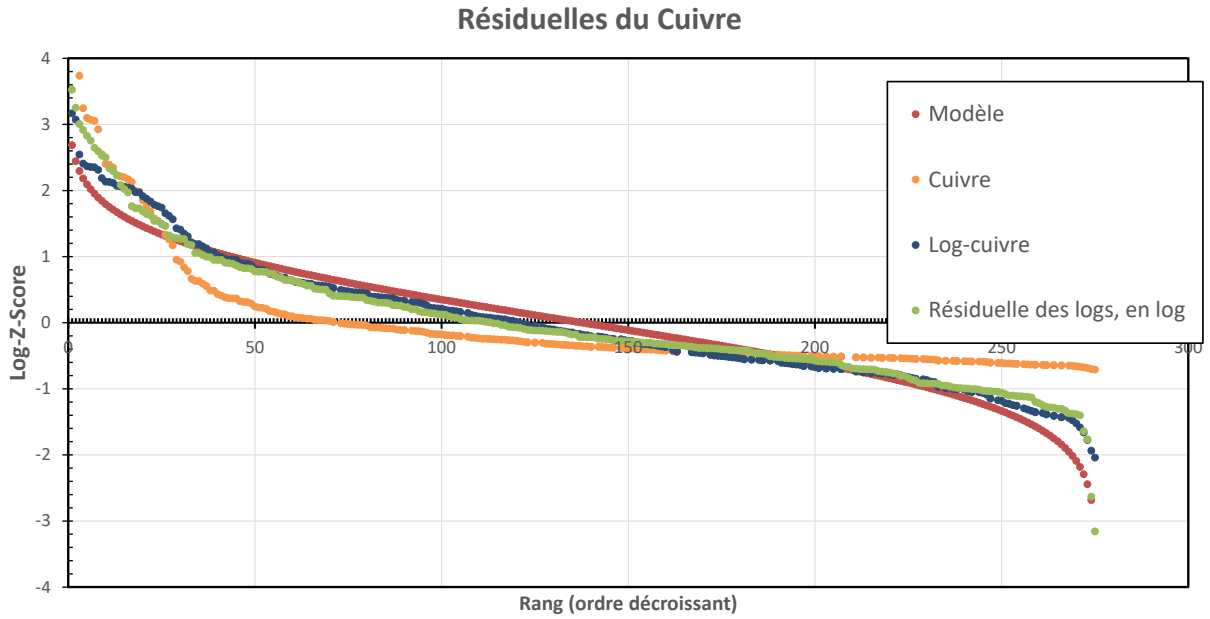


Figure 11. *Log-Z-scores of copper presented in decreasing order, along with the inverted cumulative probability function. The orange curve is calculated on the raw analyses, the blue curve is on logarithm of the analyses, while the green curve is the residuals of a multiple regression on iron, magnesium, sodium and organic matter.*

dictated by a Poisson process. If you take 10 aliquots from an apparently homogeneous sample (or consequently 10 samples from an apparently uniform background), the number of grains in each aliquot will varies according to a Poisson probability function. This means that samples are plagued with intrinsic variability. The Poisson distribution has a few peculiar characteristics, and in particular is an asymmetric function, where its mean value equals its variance. Consequently, it's variation coefficient is equal to 1/mean. This implies that samples with very low counts (a few grains) are unlikely to be replicable, and that a technique, or adequate sample size, that yield high counts is recommendable.

If the material is not thoroughly homogenuous, or having a higher degree of freedom, such as an uneven background signal, the grain abundance distribution will follow a Conway-Maxwell-Poisson (CMP) probability distribution. To reduce variance, it is a common practice to standardize grain counts to a constant weight of the samples. Grain counts are then fractional, or real positive numbers, and quasi-continuous. The CMP distribution becomes an Erlang probability function, which is a special case of the Gamma function, where shape factors (degree of freedoms) are integers. Regional background signal is expected to be uniform, and the distribution will have a small degree of freedom, Inversely, anomalous population of local origin hare expected to be teratogenous with elevated degree of freedom (Fig. 12) The probability of occurrences related to each sample can be computed, yielding a probability of anomalous source contribution and the aforementioned "unlikeliness" map.

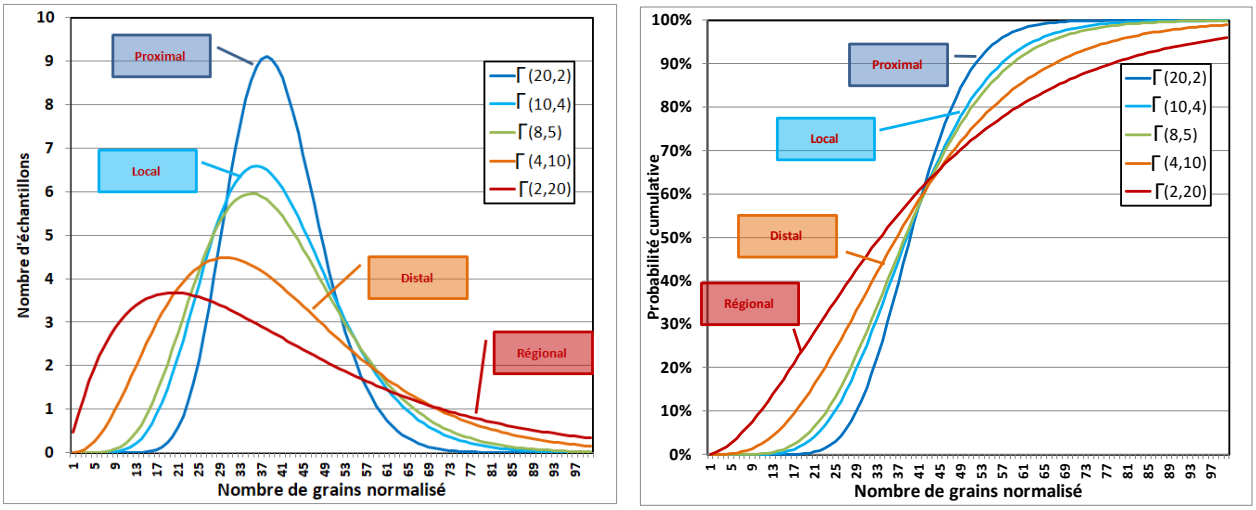


Figure 12. *Erlang density function (left) and cumulative function (right) representing the probability of having a certain number of gold grain in a sample. Regional signal is expected to be homogeneous, and with a low degree of freedom (shape factor), while anomalous localized populations are expected to be heterogenous and with elevated degree of freedom. Average number of grains is the same (40) for all populations.*

Conclusions

The current concepts have numerous outcomes on exploration strategies:

- Eliminates most statistical aberrations;
- Discriminates if an outlying result is anomalous, or merely an elevated expression of the background signal (false positive);
- The various corrections on the data significantly reduce the variance of the dataset, enhancing the contrast between anomalous and background signal;
- Enables detection of feeble anomalous samples hidden among the background signal;
- Provides a probability of success/failure of the follow-up program, enabling rigorous decision making and enhancing discovery rates and lowering risks;
- In most instances, it eliminates the need for contiguity of elevated samples to certify an anomaly, reducing the required sampling density to obtain similar certainties, and hence reducing surveys cost.

The Paradox of Pyrite

Lyndsay Moore
Geological Survey of Canada, 601 Booth Street, Ottawa, ON, K1A 0E8

Introduction

With a formerly glaciated terrain with abundant lakes, rivers, and streams, indicator mineral methods are an important exploration tool in Canada. Recovery and interpretation of indicator mineral data requires a strong working knowledge of the surficial environment being sampled; the underlying bedrock; and heavy mineral concentrate separation techniques. Over the past five decades, indicator mineral studies in Canada have focused on gold, kimberlite indicator minerals (KIMs), and porphyry indicator minerals (PIMs), but have expanded to various deposit types in the last decade or so (*e.g.*, Averill, 2011; McClenaghan *et al.*, 2019a; b).

As one of the most abundant sulphide minerals in the lithosphere, pyrite and its minor and trace element concentrations have been studied as both a petrogenetic indicator and an indicator of deposit fertility and prospectivity for several decades (*e.g.*, Large *et al.*, 2009; Genna and Gaboury, 2015; Large and Maslennikov, 2020; Krushnisky *et al.*, 2022). It is a ubiquitous type 1 indicator mineral found in a number of mineralizing systems such as various gold (*e.g.*, orogenic, epithermal, skarn), intrusion-related Sn–W, magmatic Ni–Cu–PGE, porphyry Cu–Au–Mo, volcanogenic massive sulphide (VMS) and sediment-hosted Zn–Pb deposits (McClenaghan *et al.*, 2020; Beckett-Brown and McClenaghan, 2024). With a specific gravity of approximately 5.0 g/cm^3, it is the perfect density for heavy mineral concentrations. However, despite this wide distribution and wealth of geochemical data, pyrite remains an underutilized indicator mineral. The following is an overview of pyrite as an exploration tool, including its known limitations and where its use could be expanded upon.

Pyrite Formation and Morphology

Pyrite forms under a multitude of physicochemical conditions and is found in numerous tectonic, mineralizing, and depositional settings. Morphologies typically observed include (but are

not limited to) euhedral forms such as cubes and polyhedrons; porous and spongy textures; atoll, colloform and zoned forms; and framboidal clusters, among others. These forms can be directly related to the environment of formation but can also be a reflection of later growth in either the host or secondary mineral environment. Euhedral cubic and polyhedral forms are typically found in metamorphosed terrains, hydrothermal and magmatic deposits, and in vein systems (*e.g.*, Maslennikov *et al.*, 2009). Spongy and porous textures are also found in hydrothermal mineralizing systems, and in epithermal and porphyry deposits (*e.g.*, Steadman *et al.*, 2021). Atoll and colloform morphologies are typically found in sediment-hosted deposits (Jefferson *et al.*, 2023), along with framboidal textures. However, caution should be exercised in interpreting these textures as they are found in a number of modern sedimentary environments and multiple overlapping textures can be found in altered and deformed terrains. Fig. 1 shows examples of different pyrite morphologies present in massive and semi-massive to stringer zones of the Horne and Quemont VMS deposits in the Abitibi greenstone belt, Québec, Canada.

Preservation in the Secondary Mineral Environment

Once pyrite is mobilized from bedrock, through mechanical and chemical weathering processes such as glaciation and in hydrological settings, it enters the secondary mineral environment. In this environment, pyrite is subjected to abrasion, fracturing, and most importantly, oxidation. During the oxidation process, pyrite undergoes a complex transformation involving chemical and biological events and converts into ferrihydrites, oxyhydroxides and other products, including hematite and goethite (*e.g.*, Ramos Arroyo and Siebe, 2007; Gu *et al.*, 2020). These processes, further assisted by the surrounding biosphere, progress from the surface and fractures of liberated grains toward the interior, resulting in a mixture of textures, different mineral phases within one grain, and can produce a variety of pseudomorphs (*e.g.*, Gu *et al.*, 2020). Despite these challenges, pyrite can still be sufficiently preserved in glacial till samples and stream sediments, and used as an effective indicator mineral.

Glacial Till

Duran *et al.* (2019) demonstrated the preservation potential of pyrite and chalcopyrite in till samples collected from a regional sampling campaign completed by the Ministere de Ressources

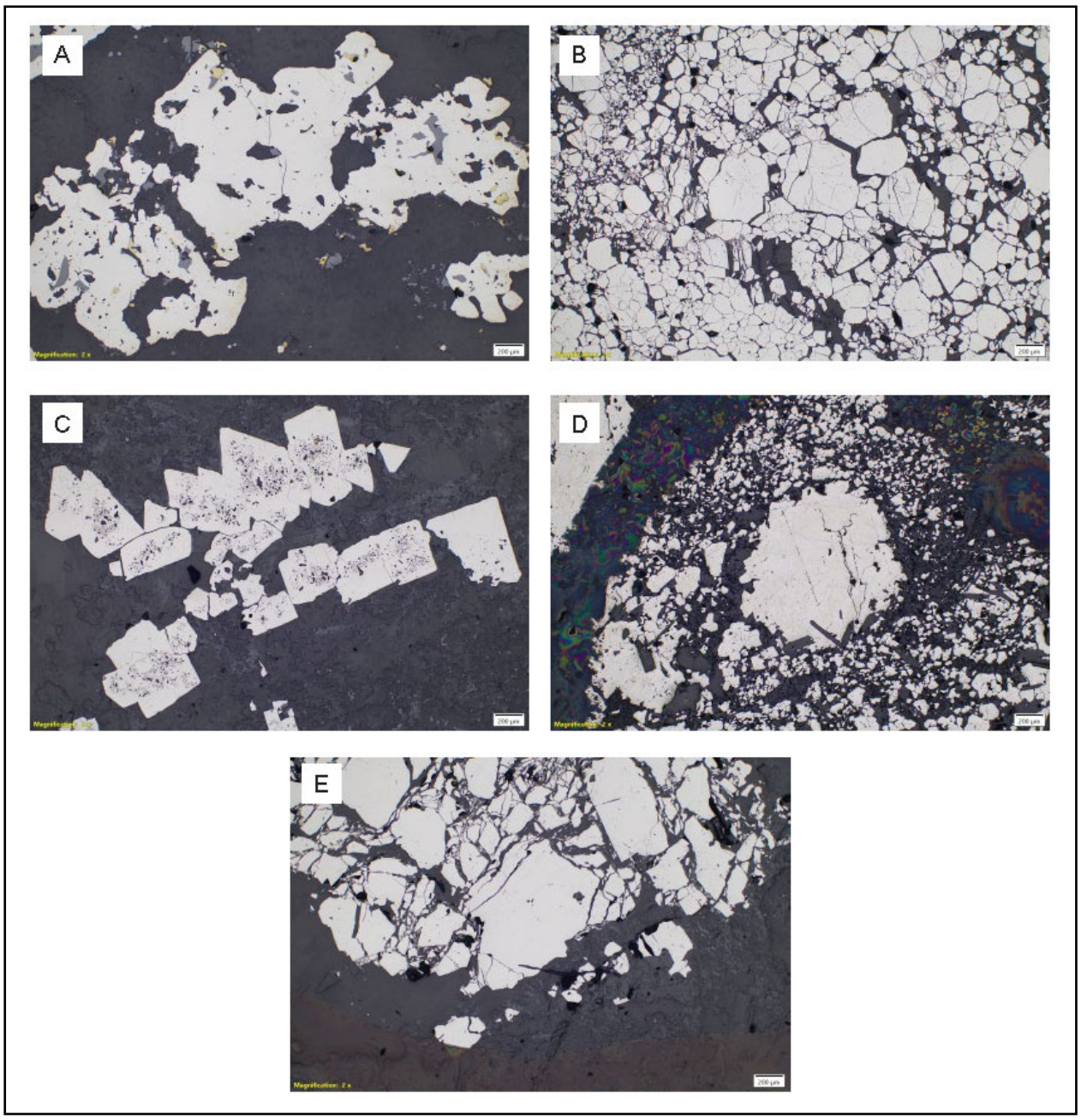


Figure 3. *Pyrite morphology in the Horne-Quemont VMS deposit. A) Anhedral and embayed pyrite with inclusions; B) Subhedral and sub-rounded pyrite with minimal inclusions; C) Euhedral pyrite with spongy core texture; D) Glomerocrystic pyrite exhibiting a snowflake-like morphology; E) Subhedral pyrite with minimal inclusions and brittle fracturing (L. Moore, unpublished).*

Naturelles et Faune (MRNF) in the Churchill province of Québec, Canada. The region was targeted for its variety and abundance of mineralization and its relatively thick cover of glacial sediments, including till and esker facies (Dubé-Loubert *et al.*, 2016). Over 600 samples were collected across a region covered by two NTS map sheets between 2012 and 2015, and early results from heavy mineral concentrates showed relatively significant abundances of pyrite, chalcopyrite, and minor

sulpharsenide grains in 301 samples. Numerous pyrite (and sulphide) morphologies are observed in the preserved grains and many exhibit varying degrees of oxidation along margins (as rims) and along fractures. It is estimated that these sulphide phases were transported over a distance of several tens of kilometres (Duran *et al.*, 2019).

McClenaghan *et al.* (2020) also documented the preservation of pyrite in heavy mineral concentrates from till samples in investigating the use of till sampling in the Sudbury mining district. A total of 118 till samples were collected in the region of the Broken Hammer deposit situated in the North Range of the Sudbury Structure, Ontario, Canada. At the time, limited studies had focused on indicator minerals associated with Ni–Cu–PGE deposits in glaciated terrains and heavy mineral concentrates (McClenaghan *et al.*, 2020). Pyrite, in addition to gold and other sulphide and arnsenide phases such as chalcopyrite, pyrrhotite, and sperrylite, were found to be the most significant indicator minerals recovered from the collected till samples. A typical background abundance of tens to over a hundred grains was reported by the study authors at distances between 10 and 300 m down-ice of mineralization exposed at the surface. Oxidation was present on the surface of numerous pyrite grains, but euhedral forms were distinctly preserved (McClenaghan *et al.*, 2020).

Stream Sediment

In a study conducted in eastern Alaska, where the terrain is covered by thick glacial and other surficial materials, Kelley *et al.* (2022), showed the effective recovery of pyrite from a stream sediment sampling program targeting PIMs. Stream sediment samples were collected from 47 stream sites in and around the Taurus and Bluff porphyry Cu–Mo systems located in the Yukon-Tanana upland region. Indicator minerals recovered from heavy mineral concentrates contain sulphide phases such as pyrite, chalcopyrite, bornite, and pyrrhotite, along with other typical PIM phases including apatite, rutile, jarosite, and tourmaline (Kelley *et al.*, 2022). Pyrite is present in all but four samples and ranges in abundance from 3 to 25,390 grains. Although not the focus of the study, pyrite dispersal in stream sediments was closely related to dispersal of jarosite – a particularly useful PIM in the region (Kelley *et al.*, 2011).

Pyrite Trace Element Chemistry

Pyrite forms under various conditions and throughout stages of petrogenesis, metamorphism, deformation, alteration, and diagenesis. As a result, trace element concentrations in pyrite can vary significantly, allowing for its effective use as a fingerprinting and vectoring tool (*e.g.*, Large *et al.*, 2009; Genna and Gaboury, 2015; Duran *et al.*, 2019; Taivalkoski *et al.*, 2024). For example, through the work of Maslennikov *et al.* (2009) in their study of pyrite trace element geochemistry hosted in fossil black smoker chimneys, a hierarchy for trace element behaviour across a range of temperatures was established: 1) high temperature group (>300°C; Co, Ni, Cu, Se, Te, Bi); 2) mid temperature group (200–300°C; Zn, As, Sb, Sn); low temperature group (150–200°C; Pb, Sb, Ag, Bi, Au, Tl, Mn); 4) seawater group (< 150°C; U, V, Mo, Ni). With the advent of microanalytical techniques such as laser-ablation inductively coupled mass spectrometry (LA-ICP-MS) in the mid- to late- 2000's (*e.g.*, Cook *et al.*, 2016), pyrite has become one of the most studied sulphide phases in terms of its trace element chemistry, with hundreds to thousands of peer reviewed papers published on the topic. For the purposes of this review, publications focused on pyrite chemistry of specific deposit types and studies investigating analysis of pyrite collected from glacial and stream sediments will be briefly discussed.

Deposit Scale

Epithermal, Porphyry and IOCG Deposits

Steadman *et al.* (2021) examined trace element behaviour in pyrite from magmatic-hydrothermal systems (porphyry Cu–Au–Mo, epithermal Au–Ag, and iron oxide copper–gold [IOCG] deposits) across nine study sites in Australia and Zambia. Although trace element behaviours are complex, commonalities and trends were observable across deposit types. In porphyry and IOCG deposits, mid to high temperature group elements such as Co, Ni, Se, and As exhibit oscillatory or sector zonation in pyrite phases, and elements such as Cu, Au, Ag, Pb, Sb, Bi, and Te, are typically found as inclusions in pre-existing pyrites (Steadman *et al.*, 2021). Pyrite in IOCG deposits have characteristically higher concentrations of Co in comparison to phases found in porphyry and epithermal deposits; and epithermal pyrite phases have typically higher concentrations of As and lattice-hosted Au.

Orogenic Gold Deposits

In a recent meta-analysis of pyrite trace element geochemical data from 67 global orogenic gold deposits, Cao *et al.* (2023) used principal component analysis to divide pyrite phases into four distinct groups (I–IV) based on trace element correlations. Typical trace element analysis of orogenic gold related pyrite focuses on varying concentrations of Co, Ni, Sb, As, Se, Au, Te, Ag, Pb, Cu, and Bi, and as such, the defined groups are associated with behaviours of those elements. Group I pyrite is characteristically enriched in Au and As, whereas Group II pyrites exhibit a distinct correlation between Sb and Cu (due to their likely coupled substitution). Group III pyrites have a correlation between Ag, Pb, and Bi concentrations, likely as inclusions; and Group IV pyrites have a distinct relationship among Co, Ni, Te, Se, and Mo concentrations (Cao *et al.*, 2023).

Volcanogenic Massive Sulphide Deposits

A recent contribution from Sun *et al.* (2023) examined the trace element behaviour in pyrite from massive sulphide and stockwork/vein horizons of the Honghai VMS deposit in the Kalatag district, China. A number of distinct pyrite types are observed across the deposit, with four typical pyrite types (M-Py 1–4) in the massive sulphide horizons of the deposit and three types present in the stockwork/vein horizons (V-Py 1–3). Groups M-Py 1–3 are characteristically enriched in Au, Ag, Cu, Zn, Pb, Sb, and Tl, and depleted in Co, Se, Te, Ti, and Sn concentrations in comparison to M-Py4, which is enriched in Te, Ti, and Sn, with a high Co/Ni ratio. Within the stockwork/vein horizon, pyrite types V-Py 1–3 are enriched in Co, Se, Te, and Ti concentrations with high Co/Ni ratios, but have depleted Au, Ag, Cu, Zn, Pb, Sb, and Tl concentrations (Sun *et al.*, 2023).

Pyrite Classification

Duran *et al.* (2015) established a binary discrimination diagram for hydrothermal and magmatic pyrite phases based on Co, Sb, Se, and As concentrations after noting significant distinction in Se/As *vs*. Co/Sb ratios in pyrite phases from the Lac des Iles Pd deposit. Pyrite geochemical data from other deposit types was added to the diagram as well and distinct clustering and segregation is visible for VMS, Cu porphyry, orogenic gold and other Ni–Cu–PGE deposits. In plotting pyrite data from the Horne-Quemont VMS complex (Fig. 2), samples plot across both

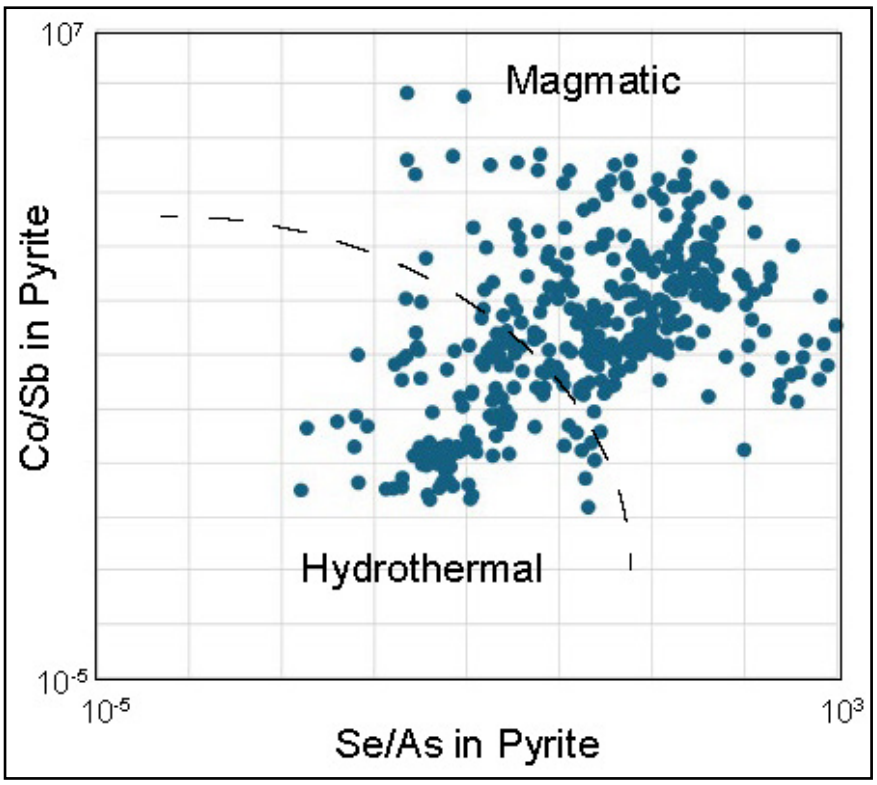


Figure 2. *Binary pyrite discrimenation diagram after Duran* et al. *(2015). Trace element concentrations vary noticeably between magmatic and hydrothermal deposits. Data from pyrite phases of the Horne-Quemont VMS system in Rouyn-Noranda, Quebec (L. Moore, unpublished), plot across both magmatic and hydrothermal fields demonstrating the complex behaviour of trace elements in pyrite in VMS deposits.*

hydrothermal and magmatic fields, demonstrating the mobility and complexity of trace element exchange in pyrite in different mineralizing systems.

Regional Sediment Sampling

In their LA-ICP-MS analysis of sulphide grains from heavy mineral concentrates recovered from till and esker deposits in the Churchill Province, Duran *et al.* (2019) found pyrite with trace element signatures provided fingerprinting of specific deposit types, namely VMS, orogenic gold and copper porphyry and magmatic deposits. Multielement maps of pyrite grains also corroborated the visual observation of thin oxidation rims with enriched concentrations of Ti, V, Mn, Cu, Zn, Ag, Sn, Ba, La, Yb, Hg, Tl, and Pb. The presence of these elements in oxidated rims is a function of their mobility and likely associated with alteration and oxidation following liberation from their bedrock source (Duran *et al.*, 2019).

Taivalkoski *et al.* (2024), in a targeted study in the Petäjäselkä region in Central Lapland, Finland (known for its orogenic gold occurrences), recovered pyrite in heavy mineral concentrates from a total of 218 till and weathered bedrock samples collected between 2006 and 2008. Four distinct pyrite morphologies were identified from photomicrographs of weathered bedrock samples and recovered pyrite grains. Pyrite A has a colloform morphology, with Pyrite B characterized by polygonal to euhedral forms. Pyrite C has a typical spongy appearance with subhedral margins, and Pyrite D shares common characteristics with Pyrite B and C, but is hosted in graphitic cherts. Different pyrite phases recovered from heavy mineral concentrates were most easily distinguished by their Co/As and Ni/As ratios (Taivalkoski *et al.*, 2024).

Conclusions and Implications for Mineral Exploration

Canada is significantly covered by glacial and other surficial deposits and future mineral exploration discoveries will rely on tools applied in covered terrains. Over the past several decades, the researchers in the country have established themselves as leaders in the fields of indicator mineral and mineral chemistry. Despite substantial advances and abundant literature, there is still room for improvement when it comes to the use of pyrite as an effective indicator mineral.

Limitations

The two biggest barriers in recovering pyrite from heavy mineral concentrates are the cost of processing samples (hundreds to thousands of dollars) and the required time (weeks to months). Detailed mineralogical and geochemical studies in addition to this are often beyond timelines and budgets for many exploration companies. Complicating recovery is the preservation potential of pyrite in the oxidative host environments (such as conditions found in till horizons and stream environments), along with the fact pyrite is so ubiquitous in the crust that samples can be inundated with tens of thousands of grains from various deposit types in substantially mineralized terrains. Finally, an abundance of literature on pyrite geochemical analysis for different deposit types and settings is overwhelming, but a lack of studies focused on pyrite in surficial sediments hinders effective application of mineral chemistry to the understanding of whether pyrite is a potentially useful indicator mineral.

Potential and Progress

The volume of literature pertaining to trace element concentrations of pyrite across a multitude of deposit types allows for fingerprinting and vectoring to specific types of mineralization. When combined with detailed petrological examinations and imaging, along with representative sampling, primary or key mineralizing phases can be characterized, along with the constraint of timing, identification of facies, and longevity of the mineralizing system. With an overriding knowledge of potential types of mineralization in the region highlighted for exploration, targeted sampling and processing techniques can be applied to optimize the use of pyrite.

In conclusion, pyrite is best used as part of a suite of indicator minerals, as opposed to a lone exploration tool. In almost all mineralizing systems, there are additional (and preferred) indicator minerals, and the morphological and geochemical characteristics of pyrite can add to solidifying a mineral exploration strategy.

References

Averill, S. A., 2011: Viable indicator minerals in surficial sediments for two major base metal deposit types: Ni-Cu-PGE and porphyry Cu. Geochemistry: Exploration, Environment, Analysis, Volume 11, pages 279–291.

Beckett-Brown, C.E. and McClenaghan, M.B., 2024: Till geochemistry and indicator mineral laboratory methods. *In* Till Geochemistry and Indicator Mineral Methods for Exploration in Glaciated Terrains. *Edited by* R.C. Paulen and M.B. McClenaghan. Geological Survey of Canada, Open File 9210.

Cao, G., Zhang, Y., Zhao, H., Cheng, J., Hao, J., Lei, J. and two others, 2023: Trace element variations of pyrite in orogenic gold deposits: Constraints from big data and machine learning. Ore Geology Reviews, Volume 157, Article 105447.

Cook, N., Ciobanu, C.L., George, L., Zhu, Z.-Y., Wade, B. and Ehrig, K., 2016: Trace element analysis of minerals in magmatic-hydrothermal ores by laser ablation inductively-coupled plasma mass spectrometry: Approaches and opportunities. Minerals, Volume 6, pages 1–34.

Dubé-Loubert, H., Daubois, V. and Roy, M., 2016: Géologie des dépôts de surface de la régeion du lac Henrietta (24H). Ministère de l'Énergie et des Ressources naturelles, Québec (RP-2016-01).

Duran, C.J., Barnes, S.-J. and Corkery, J.T., 2015: Chalcophile and platinum-group element distribution in pyrites from the sulfide-rich pods of the Lac des Iles Pd deposits, Western Ontario, Canada: Implications for post-cumulus re-equilibration of the ore and the use of pyrite compositions in exploration. Journal of Geochemical Exploration, Volume 158, pages 223–242.

Duran, C.J., Dubé-Loubert, H., Pagé, P., Barnes, S.-J., Roy, M., Savard, D. and three others, 2019: Applications of trace element chemistry of pyrite and chalcopyrite in glacial sediments to mineral exploration targeting: Example from the Churchill Province, northern Québec, Canada. Journal of Geochemical Exploration, Volume 196, pages 105–130.

Genna, D. and Gaboury, D., 2015: Deciphering the hydrothermal evolution of a VMS system by LA-ICP-MS using trace elements in pyrite: An example from the Bracemac-McLeod deposits, Abitibi, Canada, and implications for exploration. Economic Geology, Volume 110, pages 2087–2108.

Gu, X., Heaney, P.J., Aarao Reis, F.D.A. and Brantley, S.L., 2020: Deep abiotic weathering of pyrite. Science, Volume 370, Article 6515.

Jefferson, M., Yenial-Arslan, U., Evans, C., Curtis-Morar, C., O'Donnell, R., Parbhakar-Fox, A. and one other, 2023: Effect of pyrite textures and composition on flotation performance: A review. Minerals Engineering, Volume 201, Article 108234.

Kelley, K.D., Eppinger, R.G., Lang, J., Smith, S.M. and Fey, D.L., 2011: Porphyry Cu indicator minerals in till as an exploration tool: Example from the giant Pebble porphyry Cu-Au-Mo deposit, Alaska, USA. Geochemistry: Exploration, Environment, Analysis, Volume 11, pages 321–334.

Kelley, K.D., Graham, G.E., Pfaff, K., Lowers, H. and Koenig, A.E., 2022: Indicator mineral analyses of stream-sediment samples using automated mineralogy and mineral chemistry: Applicability to exploration in covered terranes in eastern Alaska, USA. Ore Geology Reviews, Volume 148, Article 105021.

Krushnisky, A., Mercier-Langevin, P., Ross, P.-S., Goutier, J., McNicoll, V., Moore, L. and five others, 2022: Geology and controls on gold enrichment at the Horne 5 deposit and implications for architecture of the gold-rich Horne volcanogenic massive sulfide complex, Abitibi greenstone belt, Canada. Economic Geology, Volume 118, pages 285–318.

Large, R.R., Danyushevsky, L., Hollit, C., Maslennikov, V., Meffre, S., Gilbert, S. and six others, 2009: Gold and trace element zonation in pyrite using a laser imaging technique: Implications for the timing of gold in orogenic and Carlin-style sediment-hosted deposits. Economic Geology, Volume 104, pages 635–668.

Large, R.R. and Maslennikov, V.V., 2020: Invisible gold paragenesis and geochemistry in pyrite from orogenic and sediment-hosted gold deposits. Minerals, Volume 10, pages 339–360.

Maslennikov, V.V., Maslennikov, S.P., Large, R.R. and Danyushevsky, L.V., 2009: Study of trace element zonation in vent chimneys from the Silurian Yaman-Kasy volcanic-hosted massive sulfide deposit (Southern Urals, Russia) using laser ablation-inductively coupled plasma mass spectrometry (LA-ICP-MS). Economic Geology, Volume 104, pages 1111–1141.

McClenaghan, M.B., Ames, D.E. and Cabri, L.J., 2019: Indicator mineral and till geochemical signatures of the Broken Hammer Cu-Ni-PGE-Au deposit, North Range, Sudbury Structure, Ontario, Canada. Geochemistry: Exploration, Environment, Analysis, Volume 20, pages 337–356.

McClenaghan, M.B., Paulen, R.C. and Kjarsgaard, 2019: Rare metal indicator minerals in bedrock and till at the Strange Lake peralkaline complex, Québec and Labrador, Canada. Canadian Journal of Earth Sciences, Volume 56, pages 857–869.

McClenaghan, M.B., Spirito, W.A., Plouffe, A., McMartin, I., Campbell, J.E., Paulen, R.C. and four others, 2020: Geological Survey of Canada till-sampling and analytical protocols: From field to archive, 2020 update. Geological Survey of Canada, Open File 8591, 73 pages.

Ramos Arroyo, Y.R. and Siebe, C., 2007: Weathering of sulphide minerals and trace element speciation in tailings of various ages in the Guanajuato mining district, Mexico. Catena, Volume 71, pages 497–506.

Steadman, J.A., Large, R.R., Olin, P.H., Danyushevsky, L.V., Meffre, S., Huston, D., Fabris, A. and two others, 2021: Pyrite trace element behaviour in magmatic-hydrothermal environments: An LA-ICP-MS imaging study. Ore Geology Reviews, Volume 128, Article 103878.

Sun, Z., Deng, X. and Pirajno, F., 2023: Textures, trace element compositions, and sulfur isotopes of pyrite from the Honghai volcanogenic massive sulfide deposit: Implications for ore genesis and mineral exploration. Science China Earth Sciences, Volume 66, pages 738–764.

Taivalkoski, A., Ranta, J.-P., Sarala, P., Nikkola, P., Liu, X., Kalubowila, C. and three others, 2024: Mineral exploration using trace element composition of pyrite grains from till: A case study from the Petäjäselkä Au occurrence, northern Finland. Journal of Geochemical Exploration, Volume 257, pages 107359.